ERDC/CHL TR-10-12

Coastal and Hydraulics Laboratory

US Army Corps of Engineers®
Engineer Research and Development Center

Seabrook Fish Larval Transport Study

Jennifer N. Tate, Tahirih C. Lackey, and Tate O. McAlpin

December 2010

Approved for public release; distribution is unlimited.

ERDC/CHL TR-10-12
December 2010

Seabrook Fish Larval Transport Study

Jennifer N. Tate, Tahirih C. Lackey, and Tate O. McAlpin

Coastal and Hydraulics Laboratory
U.S. Army Engineer Research and Development Center
3909 Halls Ferry Road
Vicksburg, MS 39180-6199

Final report

Approved for public release; distribution is unlimited.

Prepared for U.S. Army Corps of Engineers
New Orleans District, Hurricane Protection Office
7400 Leake Ave., Rm 184
New Orleans, LA 70118

Abstract: The U.S. Army Engineer Hurricane Protection Office (HPO) requested that the USACE Engineer Research and Development Center (ERDC) perform a numerical modeling study for the purpose of analyzing the impacts of proposed hurricane and storm damage risk reduction system (HSDRRS) measures to be placed in the Gulf Intracoastal Waterway (GIWW) and the Mississippi River Gulf Outlet (MRGO) on the larval fish transport in the area. This study was requested in addition to separate navigation studies to analyze the impacts the protection measures have on the hydrodynamics and vessel traffic. It is known that larval fish migrate from the Gulf of Mexico into Lake Pontchartrain. A particle tracking simulation can be performed such that the particles are given basic larval fish transport behaviors and released at various locations in the area. The hydrodynamic processes move these particles within the system and the changes to the transport due to the planned changes to the system can be analyzed. The model is validated with field data from 2008 of water surface elevation, discharge, and velocity. Four plan simulations are modeled in addition to the base condition. Transport of particles within the system is dominated by the hydrodynamics of the system. The tidal intensity and regularity of the tidal signal are a main factor of transport. Particles released during stronger events may be recruited at a greater rate than a less intense flow condition. However that is additionally affected by the larval fish characteristic transport behaviors.

DISCLAIMER: The contents of this report are not to be used for advertising, publication, or promotional purposes. Citation of trade names does not constitute an official endorsement or approval of the use of such commercial products. All product names and trademarks cited are the property of their respective owners. The findings of this report are not to be construed as an official Department of the Army position unless so designated by other authorized documents.

DESTROY THIS REPORT WHEN NO LONGER NEEDED. DO NOT RETURN IT TO THE ORIGINATOR.

Contents

Figures and Tables v

Preface xii

Executive Summary xiii

Unit Conversion Factors xviii

1 Introduction 1
Background 1
Technical Approach 3
Hydrodynamic Modeling 3
Particle Tracking Model for Fish Larval Transport 5

2 Hydrodynamic Model Development 7
Model Description 7
Mesh Development 7
Boundary Conditions 9

3 Hydrodynamic Model Verification 14
Model/Field Comparisons 16
Sensitivity Analysis 33
Summary 42

4 Design Alternatives 44

5 Larval Fish Transport 50
Background 50
Method 51
Particle Velocity 54
Anchoring 55
Limitations 56
Simulation Details and Model Input 57
Source Input 58
Recruitment Regions 62

6 Hydrodynamic Results 64
Velocity Magnitudes 64
Water Surface Analysis 80
Circulation Analysis 99
Summary 102

7 Particle Tracking Results 103
Case 1 103

Case 2 104
Case 3 120

8 Particle Tracking Results – Anchoring Effects and Final Plan 126
Case 1 128
Case 3 128
Case 4 130
Incoming Tide- West 130
Incoming Tide- East 137

9 Conclusions 152

References 154

Acknowledgements 155

Appendix A : Hydrodynamic Sensitivity Simulations 156

Appendix B: Description of the Adaptive Hydraulics Model (ADH) 184

Appendix C: Description of the Particle Tracking Model Processes and Algorithms 189

Report Documentation Page

Figures and Tables

Figures

Figure 1-1. Vicinity map. 2
Figure 1-2. Project area map. 3
Figure 2-1. Model domain and bathymetry. 8
Figure 2-2. Manning's Roughness Values. 9
Figure 2-3. Location of river inflows. 10
Figure 2-4. River inflow discharges for 2008. 11
Figure 2-5. Gage locations for development of tidal boundary (NOOA map). 11
Figure 2-6. End points and mid point of tidal boundary. 12
Figure 2-7. Location of New Orleans International Airport wind gage. 13
Figure 2-8. Wind speed and direction (0° is East and 90° is North). 13
Figure 3-1. Water surface elevation field data locations. 14
Figure 3-2. Discharge field measurement transects for Seabrook. 15
Figure 3-3. Discharge field measurement transects for GIWW/MRGO area. 16
Figure 3-4. Mississippi Sound at Grand Pass water surface elevation . 17
Figure 3-5. Rigolets water surface elevation . 17
Figure 3-6. Chef Menteur water surface elevation . 18
Figure 3-7. Paris Road water surface elevation 18
Figure 3-8. IHNC South Lock water surface elevation . 19
Figure 3-9. Bayou Bienvenue East water surface elevation . 19
Figure 3-10. Bonnet Carre water surface elevation . 20
Figure 3-11. West End water surface elevation . 20
Figure 3-12. Lakefront Airport water surface elevation 21
Figure 3-13. Tidal constituent comparison of amplitude at Grand Pass 23
Figure 3-14. Tidal constituent comparison of amplitude at Paris Road . 24
Figure 3-15. Tidal constituent comparison of amplitude at Chef Menteur. 24
Figure 3-16. Tidal constituent comparison of amplitude at West End . 25
Figure 3-17. GIWW/MRGO discharge for lines 6 and 8. 26
Figure 3-18. GIWW/MRGO discharge for lines 4 and 5. 27
Figure 3-19. GIWW/MRGO discharge for lines 1, 2, and 3. 27
Figure 3-20. IHNC Seabrook discharge 28
Figure 3-21. IHNC Seabrook model velocity on October 16, 2008 at 15:33. 29
Figure 3-22. IHNC Seabrook model velocity on October 17, 2008 at 06:30. 30
Figure 3-23. IHNC Seabrook model velocity on October 17, 2008 at 09:05. 31
Figure 3-24. IHNC Seabrook model velocity on October 17, 2008 at 13:29. 32
Figure 3-25. GIWW/MRGO velocity on July 31, 2008 at 10:30. 34

Figure 3-26. GIWW/MRGO velocity on July 31, 2008 at 14:30. 35
Figure 3-27. GIWW/MRGO velocity on July 31, 2008 at 16:00. 36
Figure 3-28. GIWW/MRGO velocity on August 13, 2008 at 9:00. 37
Figure 3-29. GIWW/MRGO velocity on August 13, 2008 at 13:00. 38
Figure 3-30. GIWW/MRGO velocity on August 14, 2008 at 16:00. 39
Figure 3-31. GIWW/MRGO velocity on August 14, 2008 at 6:00. 40
Figure 3-32. GIWW/MRGO velocity on August 14, 2008 at 9:00. 41
Figure 3-33. Sensitivity analysis results. 43
Figure 3-34. Flow area calculations. 43
Figure 4-1. Base configuration: no closures, no structures 44
Figure 4-2. Plan 1 configuration: close the MRGO at La Loutre 45
Figure 4-3. Plan 2 configuration: includes Plan 1 and the Borgne alignment 46
Figure 4-4. Plan 3 configuration: includes Plan 1, Plan 2 and a 95 ft X 16 ft structure at Seabrook. 47
Figure 4-5. Plan 3 Final configuration: includes Plan 1, Plan 2 and a 95 ft X 20 ft sector gate with two side 50 ft X 16 ft auxiliary gates at Seabrook 48
Figure 4-6. Tide signal for both four week analysis periods. 48
Figure 4-7. Wind signal for both four week analysis periods. 49
Figure 5-1. Description of the Particle Tracking Modeling input and output. 52
Figure 5-2. Case 1 initial positions are designated by the red circle. 60
Figure 5-3. Locations of areas in which larvae are initiated for case 2. Yellow colored rectangles represent the locations of initial positions. 61
Figure 5-4. Location of areas in which larvae are initiated for case 3. Orange colored region represents the location of initial positions. 62
Figure 5-5 Location of area in which larvae are initiated in case 4. Yellow colored rectangle represents the location of initial positions. 62
Figure 5-6. Locations of larval fish recruitment regions. Larvae that reach these areas are considered recruited. 63
Figure 6-1. Hydrodynamic analysis locations – Seabrook. 65
Figure 6-2. Hydrodynamic analysis locations – Bayou Bienvenue Structure, GIWW Sector Gate, and GIWW Barge Gate. 65
Figure 6-3. Velocity average for September (positive). 66
Figure 6-4. Velocity average for September (negative). 66
Figure 6-5. Velocity maximum for September (positive). 67
Figure 6-6. Velocity minimum for September (negative). 67
Figure 6-7. Velocity average for March (positive). 68
Figure 6-8. Velocity average for March (negative). 68
Figure 6-9. Velocity maximum for March (positive). 69
Figure 6-10. Velocity minimum for March (negative). 69
Figure 6-11. Percent less than of velocity magnitude analysis locations. 71
Figure 6-12. Bayou Bienvenue percent less than plot for September. 71
Figure 6-13. GIWW Sector Gate percent less than plot for September. 72

Figure 6-14. GIWW Barge Gate percent less than plot for September. 72
Figure 6-15. Seabrook percent less than plot for September. 73
Figure 6-16. Chef Menteur percent less than plot for September. 73
Figure 6-17. Rigolets percent less than plot for September. 74
Figure 6-18. Lake Pontchartrain percent less than plot for September. 74
Figure 6-19. Lake Borgne percent less than plot for September. 75
Figure 6-20. Bayou Bienvenue percent less than plot for March. 75
Figure 6-21. GIWW Sector Gate percent less than plot for March. 76
Figure 6-22. GIWW Barge Gate percent less than plot for March. 76
Figure 6-23. Seabrook percent less than plot for March. 77
Figure 6-24. Chef Menteur percent less than plot for March. 77
Figure 6-25. Rigolets percent less than plot for March. 78
Figure 6-26. Lake Pontchartrain percent less than plot for March. 78
Figure 6-27. Lake Borgne percent less than plot for March. 79
Figure 6-28. Location map for water surface analysis. 81
Figure 6-29. Inset for water surface analysis location map. 81
Figure 6-30. Water surface elevation north of MRGO closure at La Loutre. 82
Figure 6-31. Water surface elevation south of MRGO closure at La Loutre. 82
Figure 6-32. Water surface elevation north of MRGO closure at Bayou Bienvenue. 83
Figure 6-33. Water surface elevation south of MRGO closure at Bayou Bienvenue 83
Figure 6-34. Water surface elevation west of Bayou Bienvenue structure 84
Figure 6-35. Water surface elevation east of Bayou Bienvenue structure. 84
Figure 6-36. Water surface elevation west of GIWW structures 85
Figure 6-37. Water surface elevation east of GIWW structures 85
Figure 6-38. Water surface elevation north of Seabrook structure 86
Figure 6-39. Water surface elevation south of Seabrook structure. 86
Figure 6-40. Water surface elevation in GIWW at IHNC. 87
Figure 6-41. Water surface elevation in Chef Menteur 87
Figure 6-42. Water surface elevation north in Rigolets 88
Figure 6-43. Water surface elevation at Lake Borgne perimeter 88
Figure 6-44. Water surface elevation at Lake Borgne center. 89
Figure 6-45. Water surface elevation at Lake Pontchartrain. 89
Figure 6-46. Water surface elevation north of MRGO closure at La Loutre. 90
Figure 6-47. Water surface elevation south of MRGO closure at La Loutre. 90
Figure 6-48. Water surface elevation north of MRGO closure at Bayou Bienvenue. 91
Figure 6-49. Water surface elevation south of MRGO closure at Bayou Bienvenue. 91
Figure 6-50. Water surface elevation west of Bayou Bienvenue structure. 92
Figure 6-51. Water surface elevation east of Bayou Bienvenue structure. 92
Figure 6-52. Water surface elevation west of GIWW structures. 93
Figure 6-53. Water surface elevation east of GIWW structures. 93

Figure 6-54. Water surface elevation north of Seabrook structure 94
Figure 6-55. Water surface elevation south of MRGO Seabrook structure 94
Figure 6-56. Water surface elevation in GIWW at IHNC 95
Figure 6-57. Water surface elevation in Chef Menteur 95
Figure 6-58. Water surface elevation in Rigolets 96
Figure 6-59. Water surface elevation at Lake Borgne perimeter 96
Figure 6-60. Water surface elevation at Lake Borgne center 97
Figure 6-61. Water surface elevation in Lake Pontchartrain 97
Figure 6-62. Direction of flow for incoming tide in Base case. 100
Figure 6-63. Direction of flow for incoming tide for Plan 1, Plan 2, Plan 3, and Plan 3 Final.... 100
Figure 6-64. GIWW velocity analysis locations.... 101
Figure 6-65. Velocity signal in the GIWW west of MRGO, velocities west of the Borgne alignment on the GIWW decrease with the closure of the MRGO at La Loutre. 101
Figure 6-66. Velocity signal in the GIWW east of MRGO, velocities east of the Borgne alignment on the GIWW increase with the closure of the MRGO at La Loutre.... 102
Figure 7-1. Location and transport path for larvae initiated for Case 2. The red circle represents the approximate location of the initial positions.... 103
Figure 7-2 September, Base condition larvae positions after a) 1 day, b) 1 week, c) 4 weeks. Red particles are initiated on the GIWW and yellow particles are initiated on the MRGO.... 105
Figure 7-3 September, Plan 1 condition larvae positions after a) 1 day, b) 1 week, c) 4 weeks. Red particles are initiated on the GIWW and yellow particles are initiated on the MRGO.... 106
Figure 7-4 September, Plan 2 condition larvae positions after a) 1 day, b) 1 week, c) 4 weeks. Red particles are initiated on the GIWW and yellow particles are initiated on the MRGO....107
Figure 7-5. September, Plan 3 condition larvae positions after a) 1 day, b) 1 week, c) 4 weeks. Red particles are initiated on the GIWW and yellow particles are initiated on the MRGO.... 108
Figure 7-6 March, Base condition larvae positions after a) 1 day, b) 1 week, c) 4 weeks. Red particles are initiated on the GIWW and yellow particles are initiated on the MRGO.... 112
Figure 7-7. March, Plan 1 condition larvae positions after a) 1 day, b) 1 week, c) 4 weeks. Red particles are initiated on the GIWW and yellow particles are initiated on the MRGO.... 113
Figure 7-8. March, Plan 2 condition larvae positions after a) 1 day, b) 1 week, c) 4 weeks. Red particles are initiated on the GIWW and yellow particles are initiated on the MRGO.... 114
Figure 7-9. March, Plan 3 condition larvae positions after a) 1 day, b) 1 week, c) 4 weeks. Red particles are initiated on the GIWW and yellow particles are initiated on the MRGO.... 115
Figure 7-10. Time series of the number of larvae recruited with time for Base, Plan1, Plan2, and Plan3 configurations using September 2007 hydrodynamics. 4800 particles total. 116
Figure 7-11. Time series of the number of larvae recruited with time for Base, Plan1, Plan2, and Plan3 configurations using March 2008 hydrodynamics. 4800 particles total. 116
Figure 7-12 Time series of the number of larvae recruited with time for Base, Plan1, Plan2, and Plan3 configurations using March 2008 hydrodynamics for GIWW source only (2195 particles total).... 118

Figure 7-13. Time series of the number of larvae recruited with time for Base, Plan1, Plan2, and Plan3 configurations using March 2008 hydrodynamics for GIWW source only (2195 particles total). 118

Figure 7-14 Comparison of Larvae Recruitment Time Series for the March 2008 Hydrodynamic, Base configuration. 119

Figure 7-15 Percentage of larvae recruited at Seabrook (blue) and Chef Menteur (red) for Base, Plan1, Plan2, and Plan3 configurations using September 2007 hydrodynamics. 122

Figure 7-16 Percentage of larvae recruited at Seabrook (blue) and Chef Menteur (red) for Base, Plan1, Plan2, and Plan3 configurations using the March 2008 hydrodynamics. 123

Figure 7-17. March, base condition larvae positions after a) 1 day, b) 1 week, c) 4 weeks. Particles initiated in Lake Borgne. 124

Figure 8-1 Circulation Diagram of flow direction for incoming tide for all configurations 127

Figure 8-2. March, Base condition larvae positions after a) 1 day, b) 1 week, c) 4 weeks. Particles initiated in Lake Borgne. 129

Figure 8-3 September, Base condition larvae positions after a) 1 day, b) 1 week, c) 4 weeks. Particles anchored based on incoming tide to the west and are color coded based on behavior. 131

Figure 8-4 September, Final plan condition larvae positions after a) 1 day, b) 1 week, c) 4 weeks. Particles anchored based on incoming tide to the west and color coded based on behavior. 132

Figure 8-5 March, Base condition larvae positions after a) 1 day, b) 1 week, c) 4 weeks. Particles anchored based on incoming tide to the west. and color coded based on behavior. 133

Figure 8-6 March, Final plan condition larvae positions after a) 1 day, b) 1 week, c) 4 weeks. Particles anchored based on i ncoming tide to the west. and color coded based on behavior. 134

Figure 8-7 Comparison of Larvae Recruitment Time Series for the September 2007 Hydrodynamics, larval fish preferred path to the west. Particles anchored based on incoming tide to the west. 136

Figure 8-8 Comparison of Larvae Recruitment Time Series for the March 2008 Hydrodynamic, larval fish preferred path to the west. Particles anchored based on incoming tide to the west. 136

Figure 8-9 Percentage of larvae recruited at Seabrook (blue) and Chef Menteur (red) for Base, Plan1, Plan2, and Plan3 configurations using September 2007 hydrodynamics, larval fish preferred path to the west. Particles anchored based on incoming tide to the west. 138

Figure 8-10 Percentage of larvae recruited at Seabrook (blue) and Chef Menteur (red) for Base, Plan1, Plan2, and Plan3 configurations using March 2008 hydrodynamics, larval fish preferred path to the west. Particles anchored based on incoming tide to the west. 140

Figure 8-11 September, Base condition larvae positions after a) 1 day, b) 1 week, c) 4 weeks. Particles anchored based on incoming tide to the east and color coded based on behavior. 142

Figure 8-12 September, Final plan condition larvae positions after a) 1 day, b) 1 week, c) 4 weeks. Particles anchored based on incoming tide to the east and color coded based on behavior. 143

Figure 8-13 March, Base condition larvae positions after a) 1 day, b) 1 week, c) 4 weeks. Particles anchored based on incoming tide to the east and color coded based on behavior. 144

Figure 8-14 March, Final plan condition larvae positions after a) 1 day, b) 1 week, c) 4 weeks. Particles anchored based on incoming tide to the east and color coded based on behavior. 145

Figure 8-15 Comparison of Larvae Recruitment Time Series for the September 2007 Hydrodynamic, larval fish preferred path to the east. Particles anchored based on incoming tide to the east. 146

Figure 8-16 Comparison of Larvae Recruitment Time Series for the March 2008 Hydrodynamic, larval fish preferred path to the east. Particles anchored based on incoming tide to the east. 146

Figure 8-17 Percentage of larvae recruited at Seabrook (blue) and Chef Menteur (red) for Base, Plan1, Plan2, and Plan3 configurations using September 2007 hydrodynamics, larval fish preferred path to the east. Particles anchored based on incoming tide to the east. 148

Figure 8-18 Percentage of larvae recruited at Seabrook (blue) and Chef Menteur (red) for Base, Plan1, Plan2, and Plan3 configurations using March 2008 hydrodynamics, larval fish preferred path to the east. Particles anchored based on incoming tide to the east. 150

Figure A1. Hydrodynamic analysis locations – Seabrook. 157

Figure A2. Hydrodynamic analysis locations – Bayou Bienvenue Structure, GIWW Sector Gate, and GIWW Barge Gate. 158

Figure A3. Velocity average for September (positive). 159

Figure A4. Velocity average for September (negative). 159

Figure A5. Velocity maximum for September (positive). 160

Figure A6. Velocity minimum for September (negative). 160

Figure A7. Velocity average for March (positive). 161

Figure A8. Velocity average for March (negative). 161

Figure A9. Velocity maximum for March (positive). 162

Figure A10. Velocity minimum for March (negative.). 162

Figure A11. Velocity less than at the GIWW sector gate for September. 163

Figure A12. Velocity less than at the GIWW sector gate for March. 163

Figure A13. Velocity less than at the Seabrook structure for September. 164

Figure A14. Velocity less than at the Seabrook structure for March. 164

Figure A15. Water surface analysis arc and location reference in 1000 ft increments. 165

Figure A16. Water surface elevation along arc for Base and all plans for August 27, 2007. 166

Figure A17. Water surface elevation along arc for Base and all plans for March 3, 2008. 166

Figure A18. Water surface elevation through GIWW sector gate (August). 167

Figure A19. Water surface elevation through GIWW sector gate (March). 167

Figure A20. Water surface elevation through IHNC and Seabrook structure (August). 168

Figure A21. Water surface elevation through IHNC and Seabrook structure (March). 168

Figure A22. Seabrook analysis locations for cofferdam simulation. 169

Figure A23. Velocity average for September with cofferdam (positive). 170

Figure A24. Velocity average for September with cofferdam (negative). 170

Figure A25. Velocity maximum for September with cofferdam (positive). 171

Figure A26. Velocity minimum for September with cofferdam (negative). 171

Figure A27. Velocity average for March with cofferdam (positive). 172
Figure A28. Velocity average for March with cofferdam (negative). 172
Figure A29. Velocity maximum for March with cofferdam (positive). 173
Figure A30. Velocity minimum for March with cofferdam (negative). 173
Figure A31. Velocity magnitude and direction at the cofferdam for a high flood flow in March. 174
Figure A32. Velocity magnitude and direction at the cofferdam for a high ebb flow in March. 175
Figure A33. Plan 3 geometry configuration (95 X 16 ft Seabrook structure) with bridge piers. 177
Figure A34. Velocity average for September (positive). 177
Figure A35. Velocity average for September (negative). 178
Figure A36. Velocity maximum for September (positive). 178
Figure A37. Velocity minimum for September (negative). 179
Figure A38. Velocity average for March (positive). 179
Figure A39. Velocity average for March (negative). 180
Figure A40. Velocity maximum for March (positive). 180
Figure A41. Velocity minimum for March (negative). 181
Figure A42. Velocity magnitude and direction with bridge piers for a high flood flow in March 182
Figure A43. Velocity magnitude and direction with bridge piers for a high ebb flow in March 183

Tables

Table 3-1. Tidal Constituents. 23
Table 3-2. Tidal Constituent Amplitude Comparisons (ft). 25
Table 5-1. List of species and representative behavior. 57
Table 5-2. Locations of polygon boundaries for initial particle positions for each case. 59
Table 7-1 Percentage of larvae recruited for each construction phase for simulations in which particles are initiated in the MRGO and GIWW. 111
Table 7-2 Percentage of larvae recruited for each construction phase for simulations in which particles are initiated in Lake Borgne. 125
Table 8-1 Recruitment Percentages for Case 3 particles – Incoming Tide to the West 130
Table 8-2 Recruitment Percentages for Case 3 particles – Incoming Tide to the East 130
Table 8-3 Percentage of larvae recruited for each construction phase for simulations in which particles are anchored based on incoming tide to the west 137
Table 8-4 Percentage of larvae recruited for each construction phase for simulations in which particles are anchored based on incoming tide to the east 147

Preface

The model investigation presented in this report was authorized and funded by the U.S. Army Corps of Engineers Hurricane Protection Office (HPO), New Orleans in effort to support the environmental impacts analysis completed as part of the approved Alternative Arrangement provisions of the Council of Environmental Quality Regulations for Implementing the National Environmental Policy Act (40 CFR 1506.11). This modeling effort will be documented in Individual Environmental Report #11 Tier 2 Pontchartrain for the improved protection of the Inner Harbor Navigation Canal. This fish larval transport study into Lake Pontchartrain through Seabrook, including the Mississippi River Gulf Outlet and the Gulf Intercoastal Waterway was conducted by Jennifer Tate, Dr. Tahirih Lackey, Tate McAlpin, and Cassandra Ross.

This work was conducted at the Coastal and Hydraulics Laboratory (CHL) of the U.S. Army Engineer Research and Development Center (ERDC) during the period of November 2008 to March 2009 under the direction of Thomas W. Richardson, Director of the CHL; Dr. Rose Kress, Chief of the Navigation Division, CHL; Bruce Ebersole, Chief of the Flood and Storm Protection Division, CHL; Ty V. Wamsley, Chief of the Coastal Processes Branch, CHL; Dr. Robert McAdory, Chief of the Estuarine Engineering Branch, CHL.

COL Gary E. Johnston was Commander and Executive Director
Dr. Jeffery P. Holland was Director of ERDC.

Executive Summary

Background

The U.S. Army Engineer Hurricane Protection Office (HPO) requested that the USACE Engineer Research and Development Center (ERDC) at Waterways Experiment Station perform a numerical modeling study for the purpose of analyzing the impacts of proposed hurricane and storm damage risk reduction system (HSDRRS) measures to be placed in the Gulf Intracoastal Waterway (GIWW) and the Mississippi River Gulf Outlet (MRGO) on the larval fish transport in the area. This study was requested in addition to separate navigation studies to analyze the impacts the protection measures have on the hydrodynamics and vessel traffic.

The MRGO Canal is a 66-mile-long deepwater channel that extends northwest from deep water in the Gulf of Mexico to New Orleans, LA (Figures 1-1 and 1-2). The MRGO merges with the GIWW and continues 5 miles further to the west where it joins the Inner Harbor Navigation Canal (IHNC). The IHNC extends another approximately 3 miles north from its intersection with the GIWW to connect with Lake Pontchartrain at Seabrook. To the East of the connection of the GIWW with the MRGO, the GIWW extends northeast approximately 6 miles to its first connection with Lake Borgne via Chef Menteur and 20 miles with its connection via the Rigolets.

It is known that larval fish migrate from the Gulf of Mexico into Lake Pontchartrain. A particle tracking simulation is performed such that the particles are given basic larval fish transport behaviors and released at various locations in the area. The characteristic larval fish transport behaviors are provided by an interagency team composed of representatives from various state and federal regulatory agencies. The hydrodynamic processes move these particles within the system and the alterations to the transport due to the planned changes to the system are analyzed.

Hydrodynamic Numerical Model

The hydrodynamic code used in this study is Adaptive Hydraulics (ADH). ADH is a finite element code that can simulate three-dimensional groundwater, three-dimensional navier-stokes, and two- and three-

dimensional shallow water equations. This study utilizes the 2-dimensional shallow water equations of ADH. The model is simulated on high performance computing machines to obtain quick results. Further details on the ADH model and its equations can be found in Appendix B and several publications are available at https://adh.usace.army.mil.

The model is validated with water surface elevation, discharge, and velocity field data from 2008 of water surface elevation, discharge, and velocity. Current bathymetry data were collected by ERDC-CHL in the IHNC, GIWW, and northern MRGO to approximately channel mile 56. The model boundary conditions include tidal elevations, river inflows, and wind forcings.

Model Scenarios

Four plan simulations are modeled in addition to the base condition. The conditions are given below.

- Base – includes the fully open MRGO, GIWW, and IHNC
- Plan 1 – close the MRGO at La Loutre
- Plan 2 – close the MRGO at La Loutre, include the Borgne alignment (close the MRGO south of Bayou Bienvenue, 56 ft X 8 ft gate on Bayou Bienvenue, two 150 ft X 16 ft gates on GIWW)
- Plan 3 – close the MRGO at La Loutre, include the Borgne alignment, include the Seabrook structure with southern scour hole filled (95 ft X 16 ft gate)
- Plan 3 Final - close the MRGO at La Loutre, include the Borgne alignment, include the 95 ft X 20 ft sector gate at Seabrook with two flanking 50 ft X 16 ft auxiliary gates with southern scour hole filled

The Base and four scenarios are modeled according to the validation conditions requested by HPO and the hydrodynamic results are used to drive the particle tracking simulations. Details and analysis of additional hydrodynamic simulations requested by HPO are provided in Appendix A.

Particle Tracking Model Larval Fish Transport

Larval fish transport for this project is simulated using the particle tracking model (PTM) which is a Lagrangian transport model. PTM is an ERDC-developed model designed specifically to track the fate of point-

source constituents (sediment, chemicals, debris, biologicals, etc) released from local sources (outfalls, dredges, etc) in complex hydrodynamic and wave environments (McDonald et al. 2006, Lackey and McDonald 2007, Lackey and Smith 2008). Characteristic larval fish transport behaviors as defined by the Interagency team are:

- Tidal Lateral (particles move to center of the channel during incoming tide)
- Tidal Vertical (particles move up during incoming tide)
- Bottom Movers (particles remain within 25 cm from bottom)
- Passive or particles that move only with the water (as a default)

In addition, the capability of an "anchoring" behavior was added to tidal lateral, tidal vertical, and bottom movers. This behavior allows particles to have a method of preventing themselves from being transported away from recruitment regions during the outgoing tide. As the tide comes in, a particle moves upward in the water column (to the top for tidal vertical movers, between 0.5 and 25cm from the bed for bottom movers). As the tide goes out, particles move towards the bottom. When a particle reaches the bottom it remains stationary until the next incoming tide.

Particle Tracking Simulations

Four cases were simulated using the PTM for each of the model scenarios. Cases were differentiated based on initial positions of representative larval fish particles.

- Case 1 – initiated in MRGO at La Loutre
- Case 2 – initiated in MRGO at Bayou Bienvenue and GIWW at constriction
- Case 3 – initiated in Lake Borgne
- Case 4 – initiated in GIWW at constriction

Particles are introduced into the system and tracked until they are "recruited." In this case the term "recruited" refers to particles reaching a position in which they are considered in or near their optimum environmental area where they can then develop into adults. There are two recruitment positions within this system in Lake Pontchartrain at Seabrook and Chef Menteur.

Results are presented as time dependent particle positions, recruitment time series, and percentage of recruited particles relative to the previously described characteristic larval fish behaviors.

Conclusions

The results of the hydrodynamic simulations show that by cutting off the MRGO at La Loutre, as in Plan 1, the entire circulation pattern within the GIWW/MRGO system changes. A percent exceedence analysis of the velocities is used to show the range of the velocities at a given location as well as the percentage of time that a given velocity is experienced. This analysis illustrates that although there are some extreme velocity magnitudes through the structures, these values are not typical and occur a small fraction of the time, typically under strong storm circumstances. “Strong” is defined here as a short lived event with flows and winds speeds of larger magnitudes than those at other times. At these times transport can be high due to the high speed of the flow. The transport, however, is also dependent of the behavior of the species and not only on the flow speed or direction.

Transport of particles within the system is dominated by the hydrodynamics of the system. The tidal intensity and regularity of the tidal signal are a main factor of transport. Particles released during stronger events may be recruited at a greater rate than those released during less intense flow conditions. However that is additionally affected by the larval fish characteristic transport behaviors as defined by the Interagency team.

Analysis of simulation results shows that the rate of particle recruitment is affected by the plan configuration for Cases 2-4. The Base configuration shows the highest recruitment values and Plan 3 configuration shows the lowest recruitment values. The Plan 3 Final configuration shows a decrease of particles reaching recruitment areas in comparison to the Base design, Plan 1, and Plan 2. However recruitment values for the simulations using the Plan 3 Final geometry increase with respect to Plan 3. This is most likely due to the increase of cross sectional area at Seabrook shown in Plan 3 Final due to the three gate structure in comparison to Plan 3, which is only a single gate structure. Results indicate an approximate 10-15 percent recruitment decrease between Plan 1 and Plan 3 Final.

Case 3 results, particles released in Lake Borgne, show that there is no real difference between the transport pathways from Lake Borgne to Lake

Pontchartrain via Chef Menteur with respect to the plans. The Base case generally has a slightly higher value of recruited particles. Recruitment rates among Plans 1-3 and Plan 3 Final differ by amounts less than 5 percent.

Characteristic fish behavior affects the recruitment rate of particles. When the transport mechanism of anchoring is added to particle transport behavior, recruitment occurs at a much faster rate than without the mechanism. Generally passive particles had the lowest recruitment values, followed by tidal lateral behavior, bottom movers, and finally tidal vertical movers.

Unit Conversion Factors

Multiply	By	To Obtain
acres	4,046.873	square meters
acre-feet	1,233.5	cubic meters
cubic feet	0.02831685	cubic meters
cubic inches	1.6387064 E-05	cubic meters
cubic yards	0.7645549	cubic meters
degrees (angle)	0.01745329	radians
degrees Fahrenheit	(F-32)/1.8	degrees Celsius
fathoms	1.8288	meters
feet	0.3048	meters
foot-pounds force	1.355818	joules
inches	0.0254	meters
inch-pounds (force)	0.1129848	newton meters
knots	0.5144444	meters per second
microns	1.0 E-06	meters
miles (nautical)	1,852	meters
miles (U.S. statute)	1,609.347	meters
slugs	14.59390	kilograms
square feet	0.09290304	square meters
square yards	0.8361274	square meters
yards	0.9144	meters

1 Introduction

Background

The U.S. Army Corps of Engineers (USACE) Hurricane Protection Office (HPO) is authorized to provide New Orleans with a risk reduction system for the one percent annual change of exceedance flooding event (HSDRRS). The purpose and need for the proposed action is to provide, in a timely manner, the 100-year level of risk reduction from flood damage to the areas surrounding the IHNC due to flooding from hurricanes and other severe storm events. The term "100-year level of risk reduction," as it is used throughout this document, refers to a level of risk reduction that reduces the chance of storm surge and wave-driven flooding in the New Orleans Metropolitan Area to a one percent chance in any given year. The elevations of the existing Lake Pontchartrain and Vicinity (LPV) HSDRRS in the project area were below those needed to achieve the desired level of risk reduction. The proposed action resulted from a defined need to reduce flood risk and storm damage to residences, businesses, and other infrastructure from hurricanes and other high water events. The completed HSDRRS would lower the risk of harm to citizens and damage to infrastructure during a storm event. The safety of people in the region is the highest priority of the USACE.

This is being accomplished through the construction of a comprehensive system of levees, gates, and drainage structures. Several planned structures (to be located along the levee system) allow for continued navigation in the Inner Harbor Navigational Canal (IHNC), Bayou Bienvenue, and on the Gulf Intracoastal Waterway (GIWW). The IHNC Seabrook, Bayou Bienvenue, and GIWW gate structures are designed to remain open during normal tidal conditions with the ability to close during surge events. However, navigation results may require a change in the operation procedures.

With the construction of this levee system, it is important to consider the biological effects that will occur due to these proposed projects. To model juvenile and fully grown fish, an equation must be available to define their swimming behavior. At this point, there has not been enough research to fully model the fish that inhabit this area. Larval fish behave in a much simpler manner and therefore can be modeled as particles with certain

native tendencies. This type of modeling is being performed using the Particle Tracking Model (PTM). PTM (McDonald et al. 2006, Lackey and McDonald 2007, Lackey and Smith 2008) is an Engineering Research and Development Center (ERDC)-developed model designed specifically to track the fate of user defined particles (sediment, chemical, debris, biological particles, etc) released from locations within complex hydrodynamic and wave environments. HPO has requested that ERDC, Coastal and Hydraulics Lab (CHL) perform a model study to determine the effect of the proposed HSDRRS system on the passage of larval fish within the system at Seabrook. PTM is utilized to transport discrete passive particles which have been modified with characteristic larval fish transport behaviors through the hydrodynamic system. This effect will be approximate due to the limitation of the modeling tool to only transport larval fish with specified characteristics. This work will not address the effects on adult fish or behavior patterns that are not included. Figure 1-1 shows the project vicinity. Figure 1-2 shows a more detailed project area.

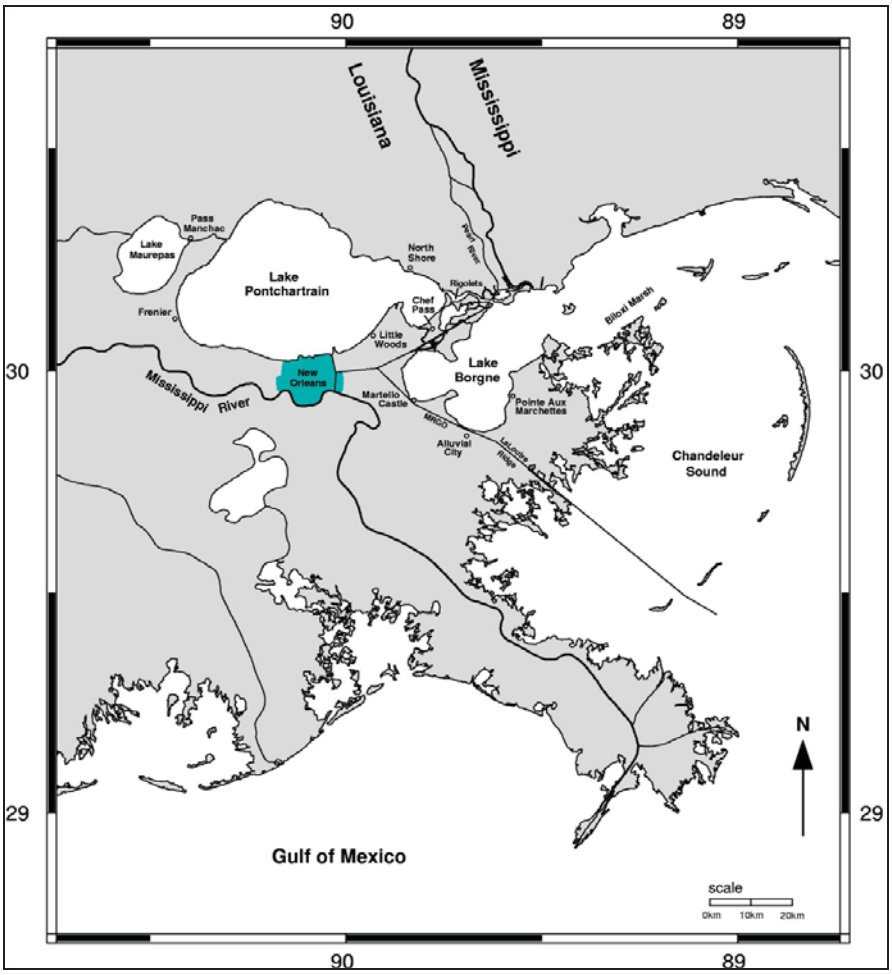

Figure 1-1. Vicinity map.

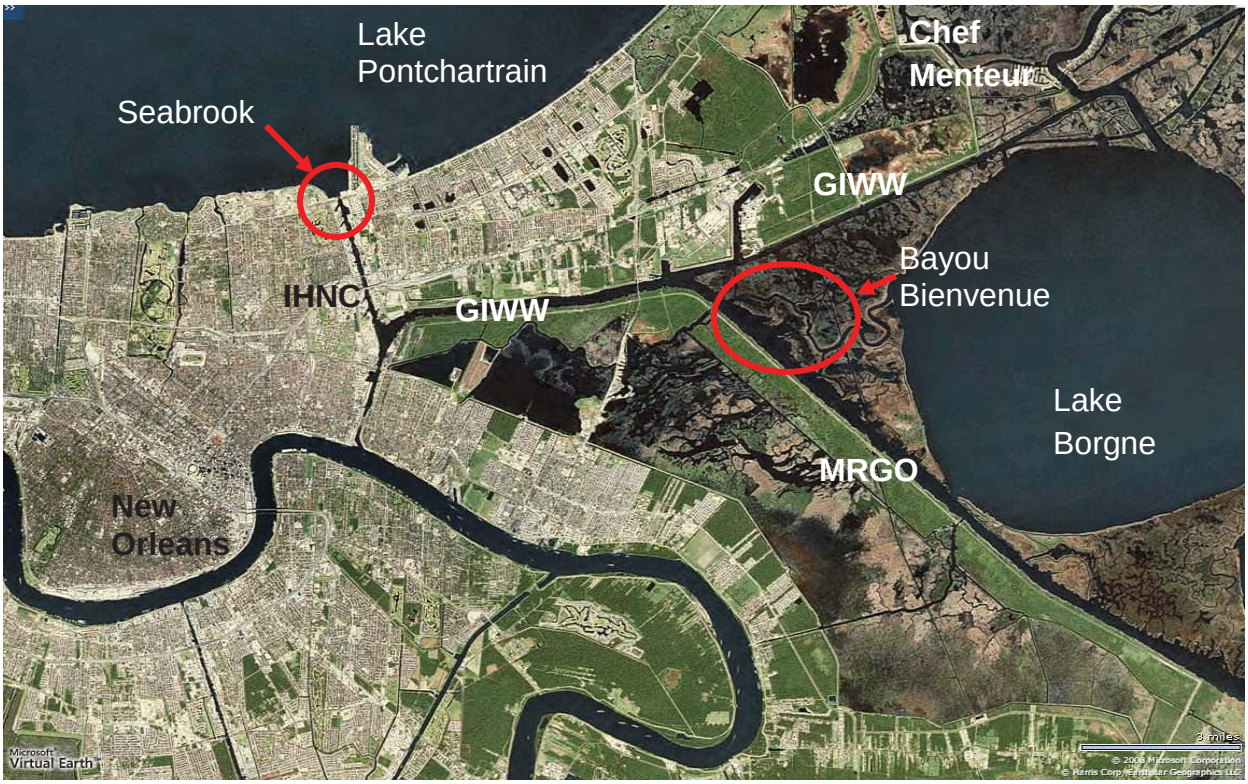

Figure 1-2. Project area map.

Technical Approach

The modeling for this study considers hydrodynamic movement using the Adaptive Hydraulics (ADH) code in two-dimensions (2D) and the fish larval movement using PTM. Velocities are compared with data in hand. As discussed above, this study is designed to determine the approximate effects, only, of planned flood control works on the movement of larvae. Also, since the structures will only be closed a very small percentage of the time, this analysis considers a structure either open or closed for the entire time of a simulation.

The tasks discussed below can be separated into two sections, hydrodynamic modeling and fish larval modeling.

Hydrodynamic Modeling

Grid Modifications

A previous ADH model for this area was developed to model navigational effects in the GIWW area under the Lake Borgne Surge Barrier Navigation study directed by HPO (Martin et al. in review). The IHNC area near

Seabrook is crudely represented in the existing model and, using data subsequently collected, is updated for bank lines and bathymetry. This recently collected data provides improved representation for this fish passage work and also benefits the current navigational study being performed.

Boundary Condition Development

To perform a proper comparison between observed results and model results, the same conditions (time period) will be used for the validation model run. Therefore a boundary condition file is created to model the time period during which the calculations are made. The boundary condition file consists of the river inflows, wind forcings, and tidal conditions for Jan 1, 2008 to October 21, 2008. An additional boundary condition file will be developed that includes the August and September 2007 conditions for the plan alternative simulations.

Validation to Observed Data

Although the previous Lake Borgne Surge Barrier model was validated to water surface elevation data, this study made additional comparisons to observed velocity data and water surface data. The validation indicates that the model only requires minor modifications to obtain satisfactory model results. For the purpose of this study, the flow directions are very important. Field discharge measurements are used to ensure that the flow patterns are represented correctly.

Base and Plan simulations

The base (existing conditions) and four additional plan configurations are simulated and the hydrodynamic results are then used in the PTM modeling effort. The scenarios modeled are:

- Base – includes the fully open MRGO, GIWW, and IHNC
- Plan 1 – close the MRGO at La Loutre (see Figure 1-1)
- Plan 2 – close the MRGO at La Loutre, include the Borgne alignment (close the MRGO south of Bayou Bienvenue, 56 ft X 8 ft gate on Bayou Bienvenue, two 150 ft X 16 ft gates on GIWW)
- Plan 3 – close the MRGO at La Loutre, include the Borgne alignment, include the Seabrook structure with southern scour hole filled (95 ft X 16 ft gate)

- Plan 3 Final - close the MRGO at La Loutre, include the Borgne alignment, include the 95 ft X 20 ft sector gate at Seabrook with two flanking 50 ft X 16 ft auxiliary gates with southern scour hole filled

Initially, two different two-week periods were to be simulated as specified by HPO for PTM analysis. These two periods are the final two weeks of March 2008 and the first two weeks of September 2007. These time periods were selected by the interagency team, made up of representatives from National Marine Fisheries Service, U.S. Fish and Wildlife Service, Louisiana Department of Natural Resources, Louisiana Department of Wildlife and Fisheries, Louisiana Department of Environmental Quality, U.S. Environmental Protection Agency and the USACE, and they were based on flow and wind conditions best suited for larval fish transport. After initial PTM model testing, the simulation periods were extended to four weeks to include the two weeks prior to those requested by the interagency team. The periods included for these simulations are August 15 – September 15, 2007 and March 1-31, 2008. A total of six weeks was simulated with the hydrodynamic model to include two weeks for model "spin-up" prior to the four week analysis periods.

Particle Tracking Model for Fish Larval Transport

Fish Larval Behavior Development

The interagency team provided CHL with the larval fish behavior characteristics portrayed by the local fish population. The interagency team noted eight dominant species with three general behavior characteristics. A more detailed explanation of PTM modeling is given within Chapter 5 and in Appendix C. However it should be mentioned that all particles in PTM move within a prescribed 3D flowfield. When the hydrodynamic field provided is determined by the 2D shallow water equations, as is the case for this work, the vertical profile is taken to be logarithmic. This allows particle equations to be solved in all coordinates (x,y, and z). The behaviors listed below are included in the PTM modeling.

1. Tidal Lateral (move to center of the channel during incoming tide)
2. Tidal Vertical (move up during incoming tide)
3. Bottom Movers (25 cm from bottom)
4. Passive or particles that move only with the water (as a default)

In addition to the four behaviors, particles also display an additional "anchoring" behavior in which particles remain motionless as flow pushes them away from a prescribed direction. Since the PTM model will not transport species differently, it would be misleading to divide a behavior type into various species. The statistics of how each species moves within the system would be misrepresented since the model sees no difference in species having the same behavior.

PTM Source Input

The Particle Tracking Model is dependent on user defined sources. In this case, those sources represent characteristic larval fish transport behavior. Initial start locations were provided by the interagency team based on typical conditions for the species being modeled as discussed above, and particles were released over a specified period of time. A recruitment location is defined approximately one mile into Lake Pontchartrain from the Seabrook structure. An additional recruitment area is placed at the entrance of Chef Menteur to Lake Pontchartrain to account for particles that reach the lake through this waterway. Once particles reach these areas they are considered recruited and are no longer part of the system.

Base and Plan PTM Model Runs

All five of the previously mentioned scenarios are modeled in PTM and the results provided to the interagency team. The same ADH simulation periods used in the hydrodynamic tasks are used in this task. For each configuration and flow condition, the four behavior types are modeled. Analyses consist of fish recruitment statistics as well as particle path analyses.

2 Hydrodynamic Model Development

Model Description

ADH is the modeling tool used for the simulations in this study. ADH is a finite element model that is capable of simulating three-dimensional (3D) Navier Stokes equations, two and three-dimensional shallow water equations, and groundwater equations. It can be used in a serial or multi-processor mode on personal computers, UNIX, Silicon Graphics, and CRAY operating systems. The uniqueness of ADH is its ability to dynamically refine the domain mesh in areas where more resolution is needed at certain times due to changes in the flow conditions. ADH can simulate the transport of conservative constituents, such as dye clouds, as well as sediment transport that is coupled to bed and hydrodynamic changes. The ability of ADH to allow the domain to wet and dry within the marsh areas as the tide changes is suitable for the shallow marsh environment. This tool is a product of the System Wide Water Resources Program (SWWRP) at ERDC and has been used to model sediment transport in sections of the Mississippi River, tidal conditions in southern California, and vessel traffic in the Houston Ship Channel, among other sites.

For this study, the two-dimensional shallow water module of ADH is used for all simulations. This tool solves for depth and depth averaged velocity throughout the model domain. In this case, density effects due to salinity or other factors are ignored and therefore their effects on the flow are not included in these simulations and results. More details of the two-dimensional shallow water module of ADH and its computational philosophy and equations can be found in Appendix B or at https://adh.usace.army.mil.

Mesh Development

The computational model domain is given in Figure 2-1. This is the same model domain as in previous studies of this area as described in McAnally et al. 1997 and Tate et al. 2002. This mesh has since been modified to include more recent bathymetry, post Katrina updates, and additional marsh storage (representing the Central Wetlands Area to the southwest of the MRGO) and flow pathways for the navigation study of the Borgne alignment. The domain extends east of the Chandeleur Islands into the Gulf of

Mexico, follows the coastline of Mississippi and Louisiana on the north, follows the MRGO on the south, and includes Lake Pontchartrain and Lake Maurepas. The actual mesh was taken from that used in the navigation study and modified to fit the ADH format of linear, triangular elements. Bathymetry data were collected by ERDC-CHL in the IHNC, GIWW, Bayou Bienvenue and northern MRGO in November 2008. These data were incorporated into the mesh. Mesh boundaries were also better defined along the IHNC, GIWW, and Bayou Bienvenue. The vertical datum for this mesh is NAVD 88 (2004.65). The computational model domain for the base condition contained 32,087 elements and 17,796 nodes with elements ranging in area from 1000 ft^2 to 100 million ft^2, the largest located in the Gulf of Mexico.

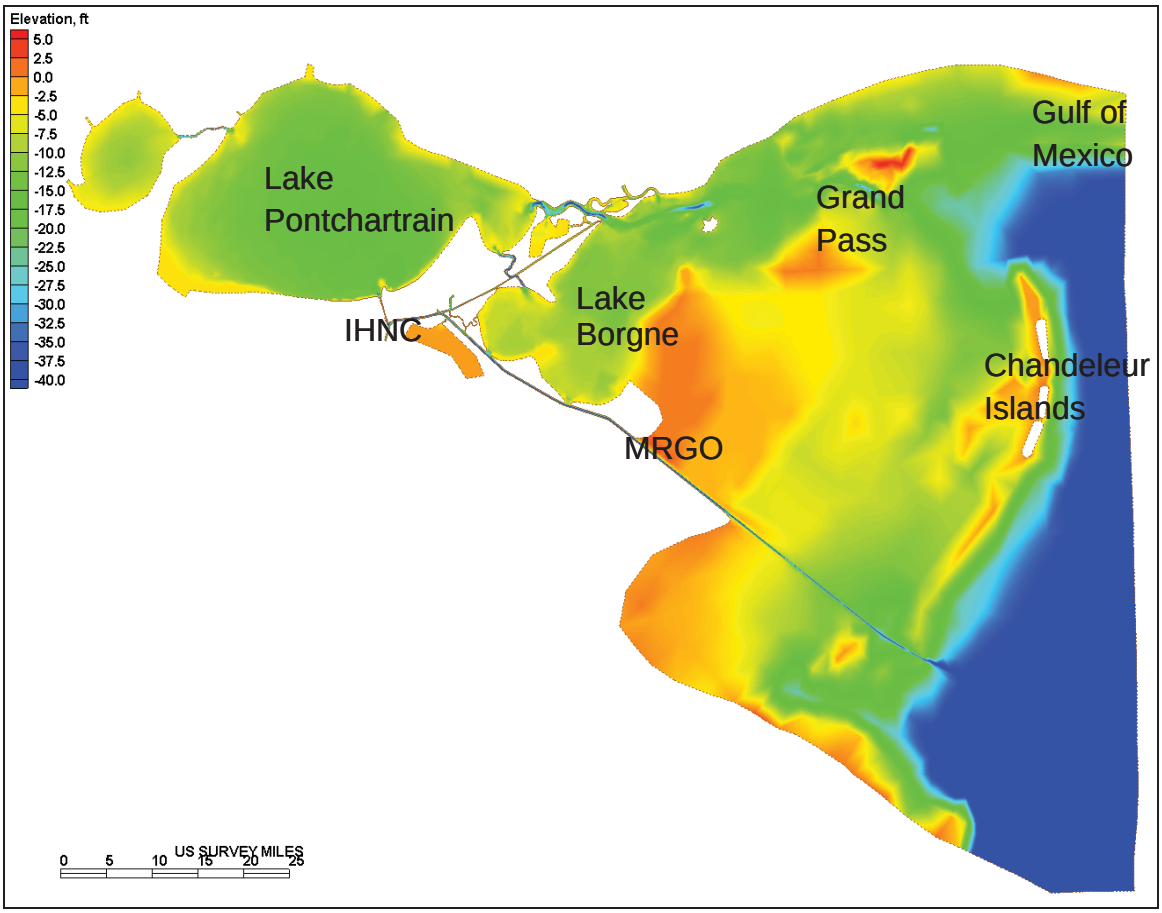

Figure 2-1. Model domain and bathymetry.

The friction on the bed is described using a Manning's approach and varies spatially over the domain. Figure 2-2 shows the spatial variation of the roughness parameters. Eight different Manning's roughness parameters are used for this domain and were defined by typical values for these types of

locations and adjusted during the validation process to determine the best values to represent reality. In the shallow areas, the model is more sensitive to these roughness parameters than in the deeper, channelized regions. ADH uses a roughness algorithm that equates the Manning's roughness value to an estimated roughness height of the bed. By doing this, ADH is able to represent any changes in roughness effects due to the depth of the water on a physical basis, as opposed to other methods that apply an additional algorithm requiring user input to make these adjustments.

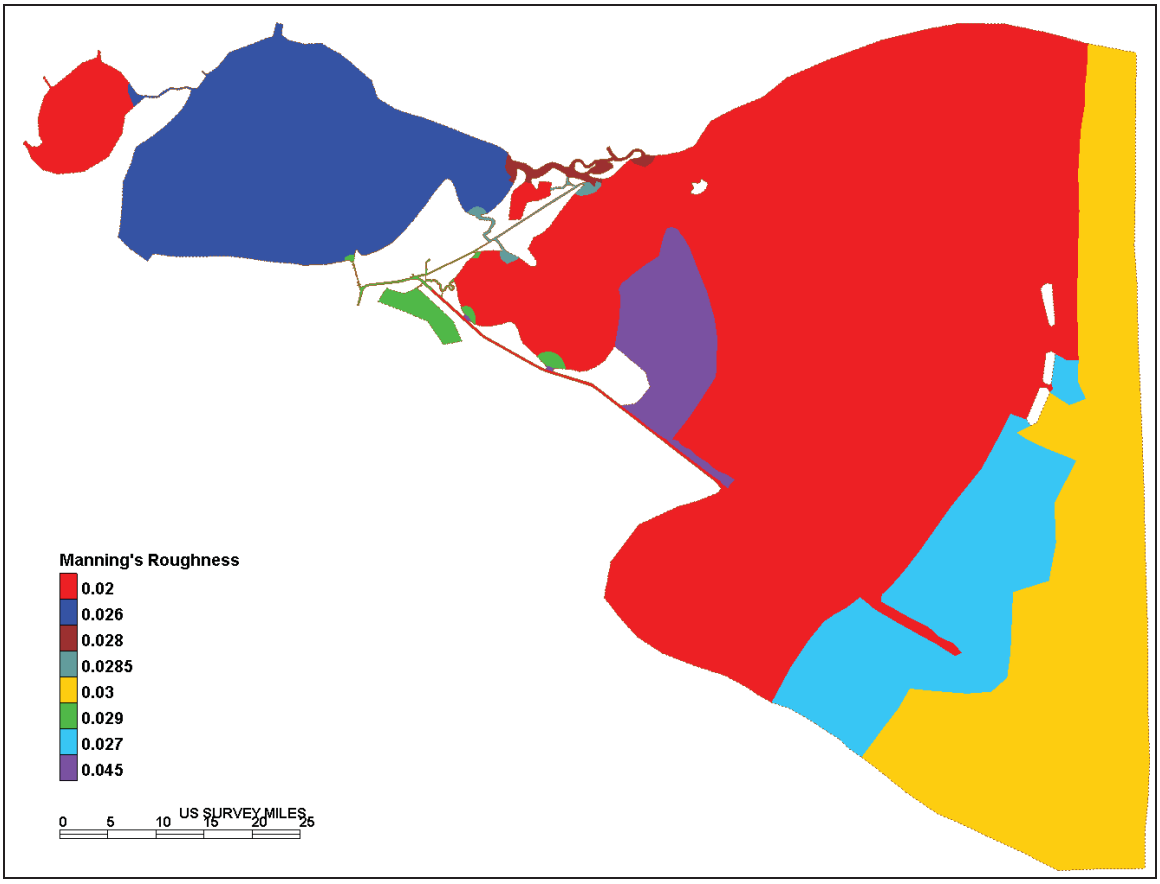

Figure 2-2. Manning's Roughness Values.

Boundary Conditions

Boundary conditions for this model include river inflows, tidal water surface elevations, and wind forcings. This information is needed for August 2007 through October 2008 to perform the analyses and the model validation. The validation period is January through October 2008. The data used for validation were obtained from several sources.

The river inflows to the model domain are taken from the U.S. Geologic Survey streamflow database. Daily average values are applied to the model at six locations: the Pearl River, the Amite River, the Blind River, the Tchefuncte River, the Tickfaw River, and the Tangipahoa River. The locations of these rivers are shown in Figure 2-3. Flow from the Mississippi River into the Gulf of Mexico is accounted for in the tidal boundary condition since it does not enter directly into the model domain. Ungaged flows are not factored into the model, which includes any flow through the wetland areas along the Mississippi River. The 2008 flows for each of the rivers are shown in Figure 2-4. The Blind River was not included on the plot as it was a constant flow of 216 cfs as determined from previous work (McAnally et al. 1997). Time 0 corresponds to 12:00 AM on January 1 for all figures, unless otherwise stated.

The tidal forcings for the hydrodynamic model are generated using 2008 NOAA gage data from Gulfport Harbor (gage #8745557) and Pilots Station East, SW Pass (gage #8760922). Figure 2-5 shows the location of these points as the red dots. This figure was taken from NOAA. The time series for the endpoints of the tidal boundary are shown in Figure 2-6 along with the tide boundary condition at a location at the boundary midpoint. The harmonic constituents and the nonpredicted, or subtidal, signal (the difference between the predicted value based on tidal constituents and the observed value which includes winds and other factors) for each station are used to generate a tidal forcing or water surface elevation at each node along the tidal boundary over the time of the simulation. The values for each node are determined by performing a linear interpolation of the amplitude and phase for each tidal constituent as well as for the nonpredicted signal. The tide is then reconstituted at each location along the boundary using these interpolated parameters.

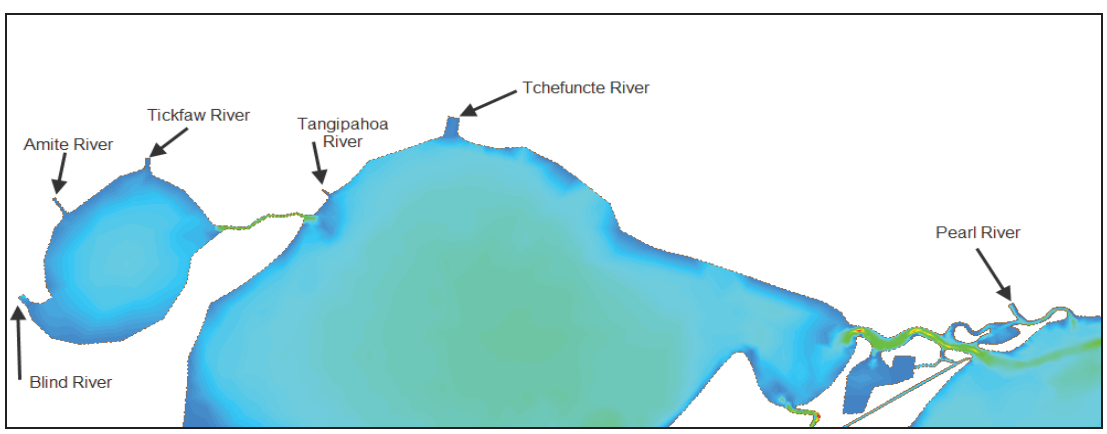

Figure 2-3. Location of river inflows.

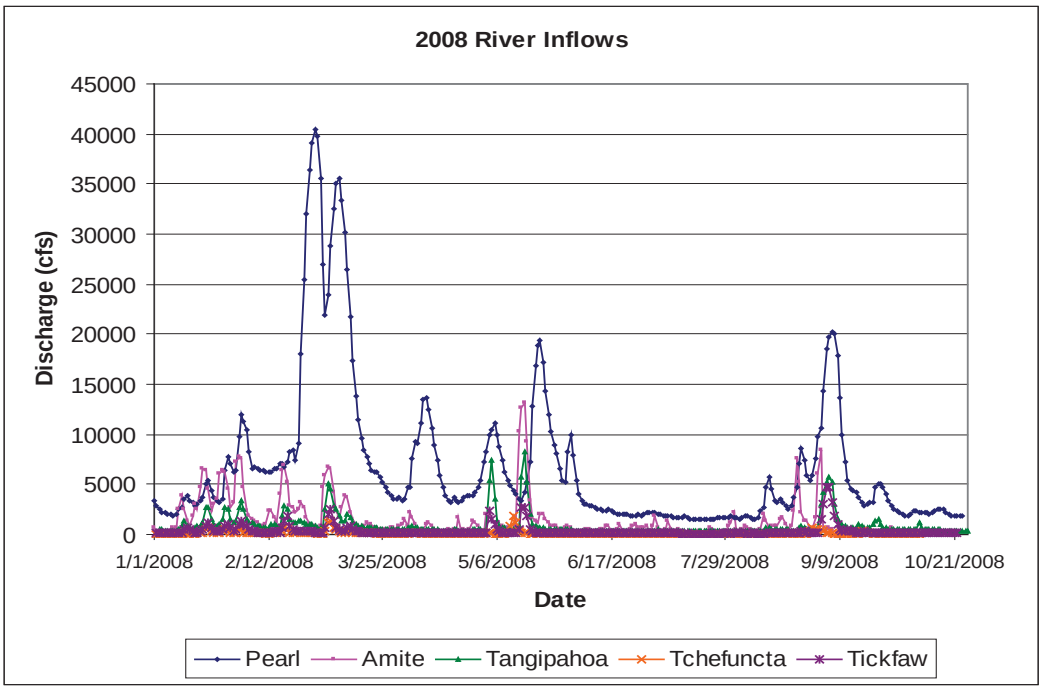

Figure 2-4. River inflow discharges for 2008.

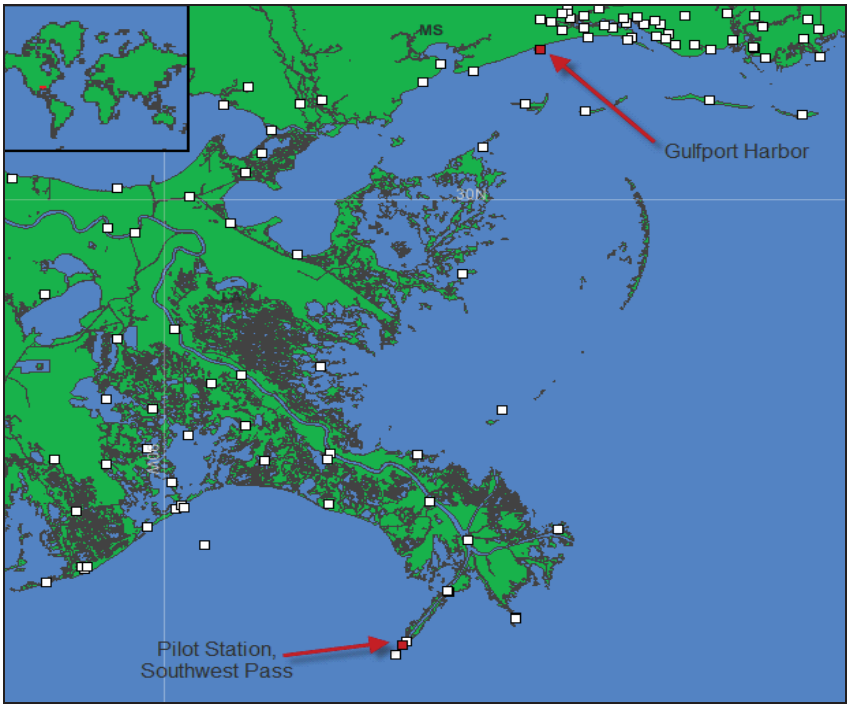

Figure 2-5. Gage locations for development of tidal boundary (NOOA map).

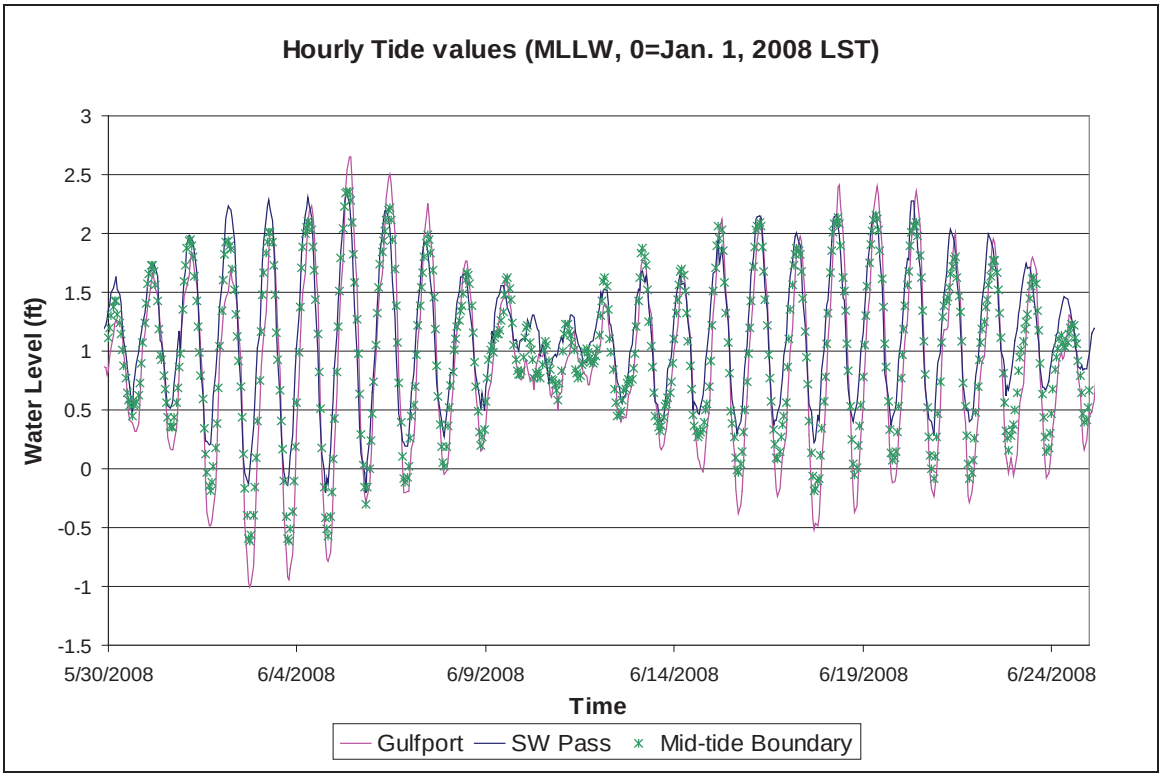

Figure 2-6. End points and mid point of tidal boundary.

The wind data used were obtained from the Joint Air Force and Army Weather Information Network and the Air Force Combat Climatology Center in Ashville, NC. These data are hourly surface winds at the New Orleans International Airport (Station 722310 – KMSY). The wind signal is interpolated using a polynomial interpolation for the wind signal components to fill any data gaps. Generally, these gaps in the wind data are only on the order of 2 hours; however, there is a 25 hour gap due to machine malfunction during the September analysis period and a 7 hour data gap during the March period. ADH requires that the wind be applied to the model as a shear stress and there are several options for this calculation. The wind speed and direction for this study were converted to wind shear stress using the Wu formulation (Wu 1969). During 2008 the wind speeds rarely exceed 20 mph, although there are several storm events that increase the wind speed, especially during hurricane season. Figure 2-7 shows the location of the wind gage and Figure 2-8 shows the time varying wind speed and direction toward which it is blowing for 2008.

Figure 2-7. Location of New Orleans International Airport wind gage.

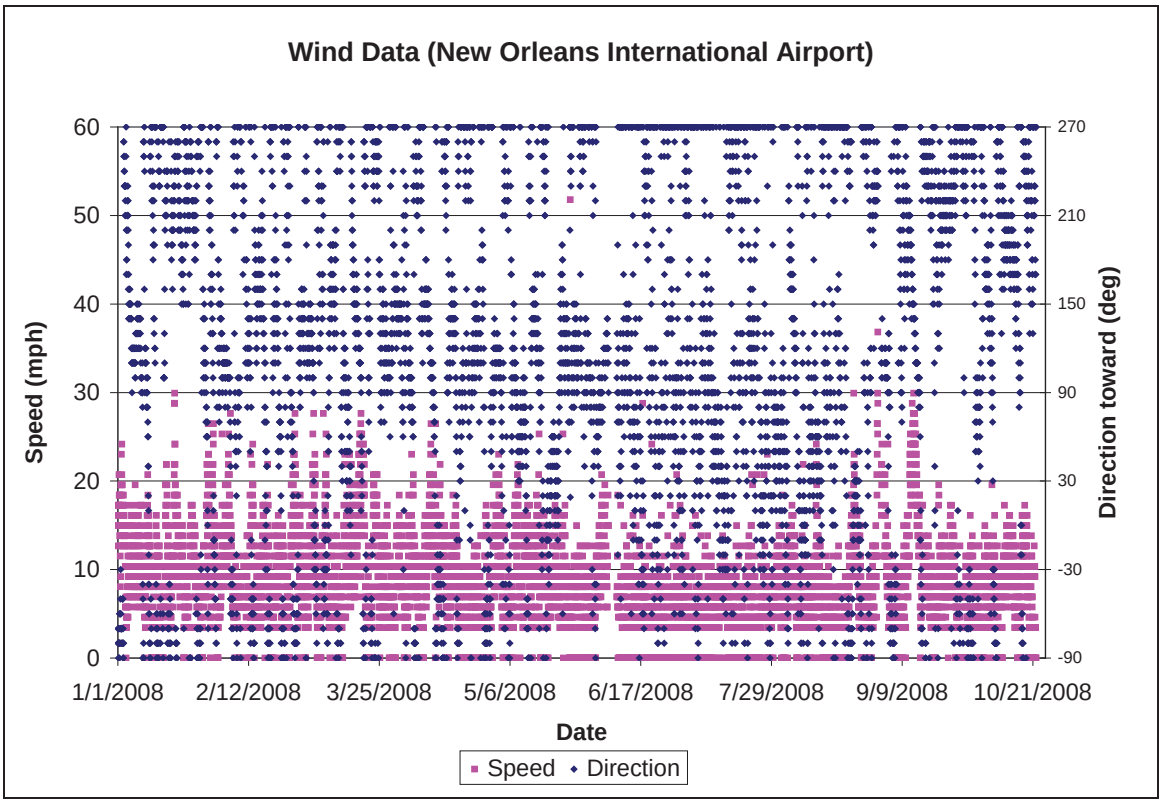

Figure 2-8. Wind speed and direction (0° is East and 90° is North).

3 Hydrodynamic Model Verification

The ADH model verification is performed using field data from several collection efforts and sources during calendar year 2008. The model results for water surface elevation, velocity, and flow direction are compared to the field data at nine locations. See data points 1 through 9 in Figure 3-1.

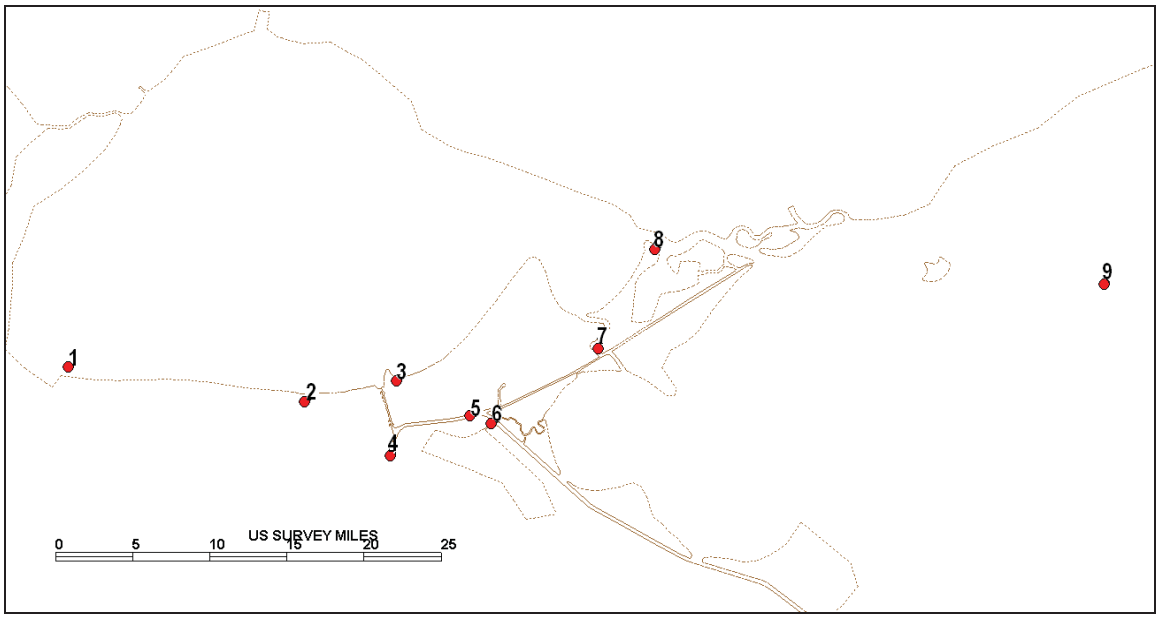

1	Lake Pontchartrain at Bonnet Carre Spillway (85555)
2	Lake Pontchartrain at West End (85625)
3	Lake Pontchartrain at Lakefront Airport (85670)
4	Inner Harbor Navigation Canal at South Lock (USGS) (76160)
5	Gulf Intracoastal Waterway at Paris Road (USGS) (073802338)
6	Bayou Bienvenue Floodgate East (76025)
7	Chef Menteur Pass near Lake Borgne (85750)
8	Rigolets near Lake Pontchartrain (85700)
9	Mississippi Sound at Grand Pass (3007220891501)

Figure 3-1. Water surface elevation field data locations.

Water surface elevations were obtained from www.RiverGages.com which is maintained by the Corps of Engineers. Additional water levels were provided by the U.S Geological Survey (USGS). Figure 3-1 shows the locations of the water surface elevation gages used for model/field comparisons. The gage numbers are given in parentheses. ADCP discharge

and velocity measurements around the intersection of the GIWW and MRGO were collected by ERDC-CHL during 31 July and 13-14 August, 2008. Another collection of ADCP discharges and velocity data was made along the IHNC near Seabrook during 16-17 October 2008. The red lines in Figures 3-2 and 3-3 give the locations of the flow data obtained by ERDC-CHL during these collection efforts. The IHNC collection at Seabrook included 12 passes at each transect over a 25 hour period. The July data collection along the MRGO and GIWW included 4 passes along each transect over a 7 hour period and the August data collection included 9 or 10 passes at each transect over a 25 hour period.

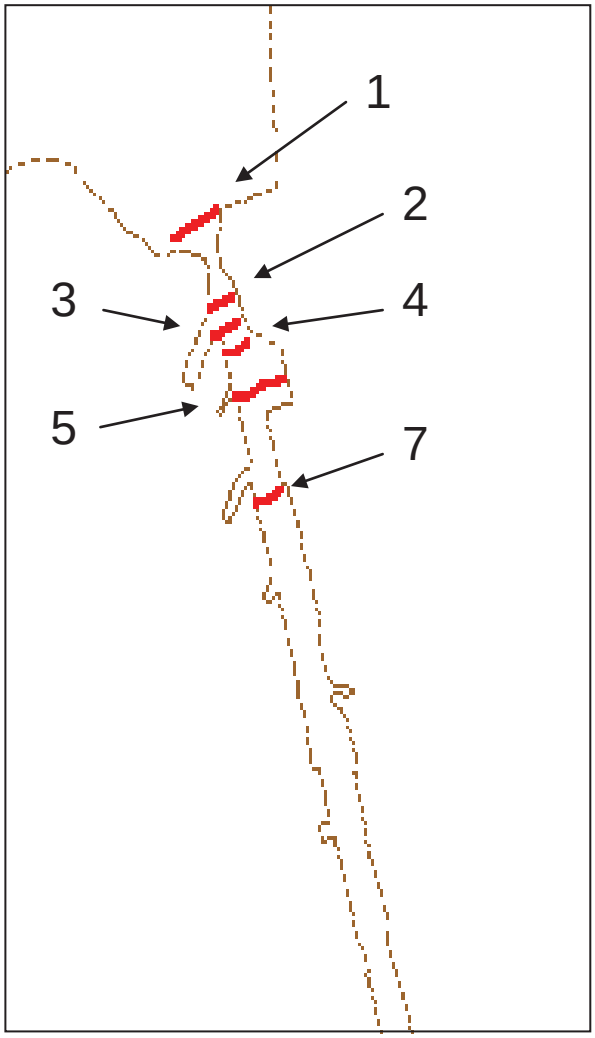

Figure 3-2. Discharge field measurement transects for Seabrook.

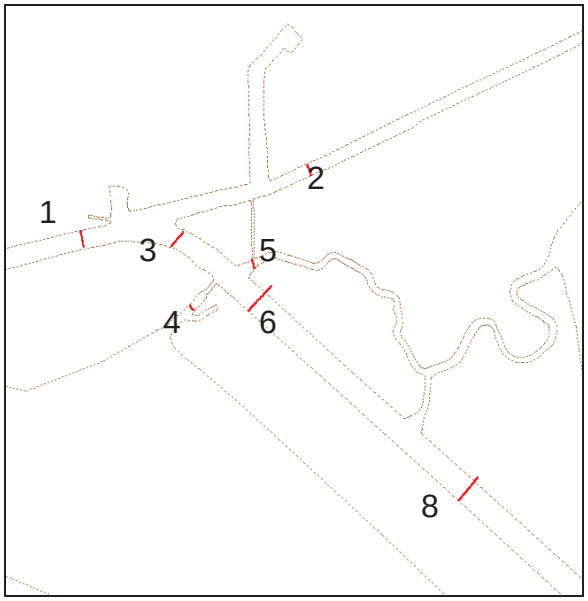

Figure 3-3. Discharge field measurement transects for GIWW/MRGO area.

Model/Field Comparisons

Figures 3-4 through 3-12 show the field water surface elevations in blue and the model predicted results in pink. The comparisons shown here are taken for a specific period during the entire year-long simulation (Jan. 23 – Mar. 30, 2008). Although only this subset is shown, the model/field comparisons are made for the entire data set. The vertical scale is set to a constant range from -1 to 3 ft and the only differing horizontal scale is the gage at Grand Pass due to data only being available late in the year. See Figure 3-1 for the location of the Grand Pass gage.

The model is driven with a tidal elevation along the Gulf boundary and wind shears from data obtained at New Orleans International airport. Although there are river inflows, the tidal boundary is the dominant driving force. The comparison at Grand Pass is important for ensuring that the signal is being properly applied to and propagated into the model. Figure 3-4 shows the comparison of the water level at this location (point 9 in Figure 3-1). On approximately October 9, 2008 there is a shift in the gage datum. Upon inspection, the model continues to reproduce the pattern of the water surface elevation and the signal would have to be shifted at this time to show a realistic comparison.

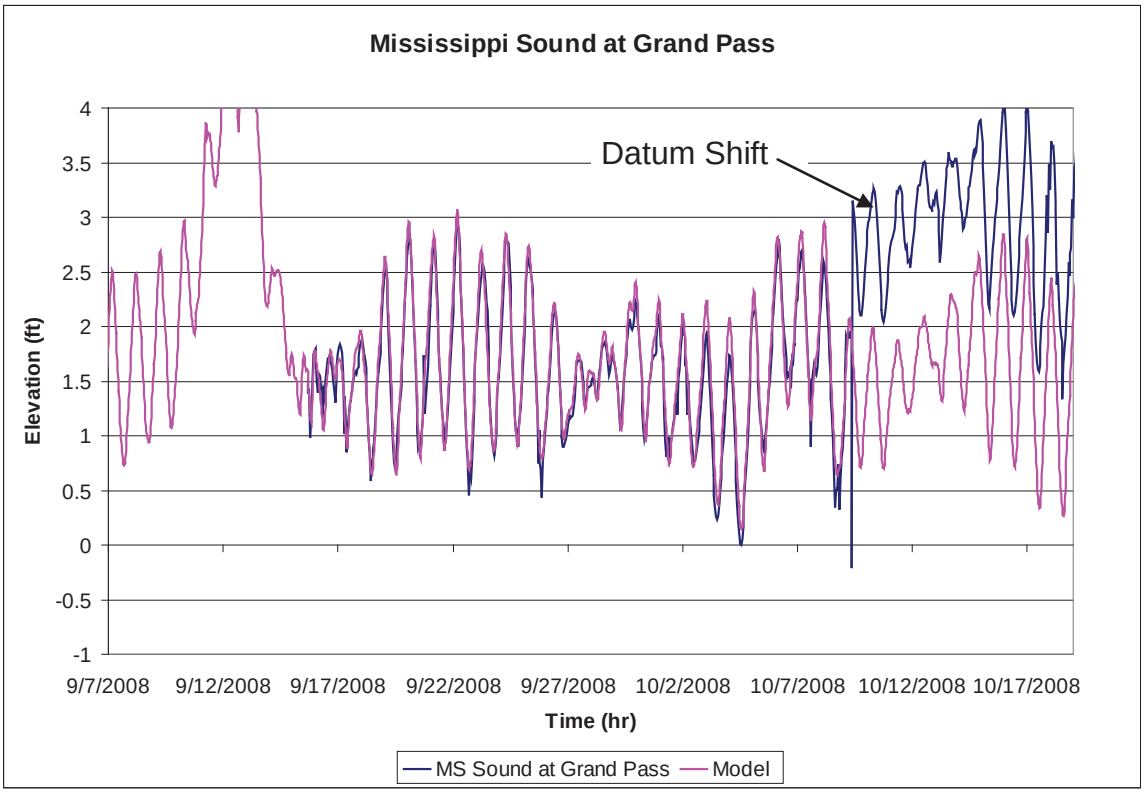

Figure 3-4. Mississippi Sound at Grand Pass water surface elevation (point 9 on Fig. 3-1).

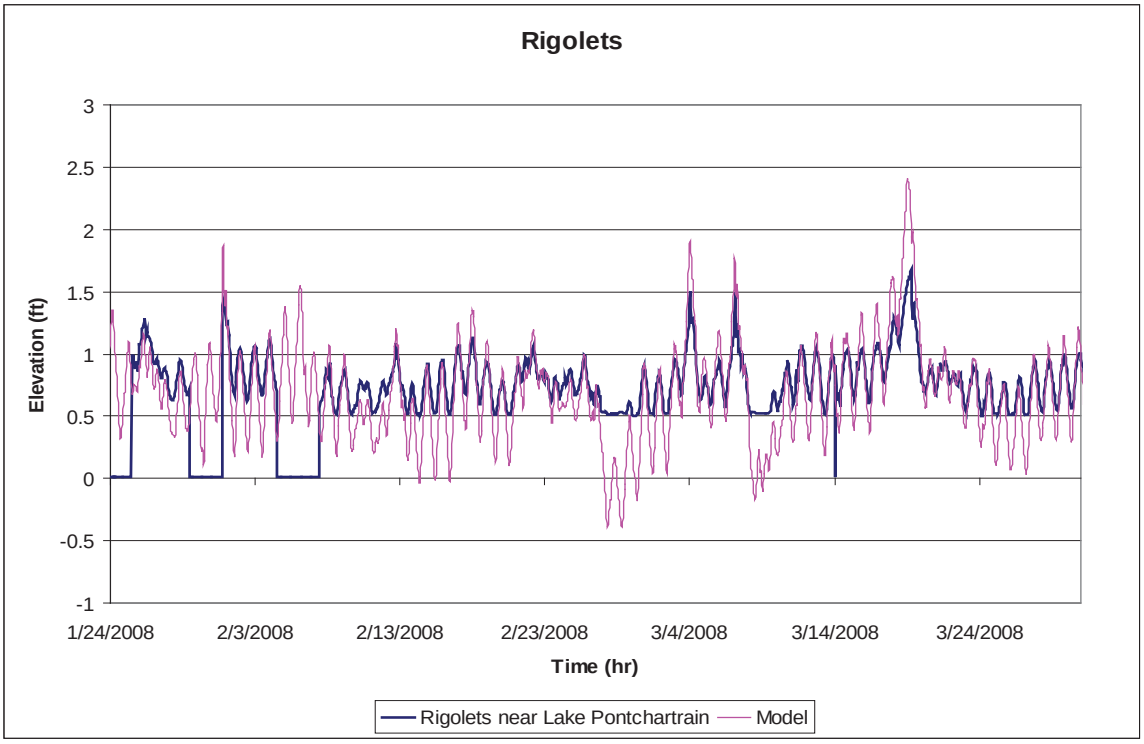

Figure 3-5. Rigolets water surface elevation (point 8 on Fig. 3-1).

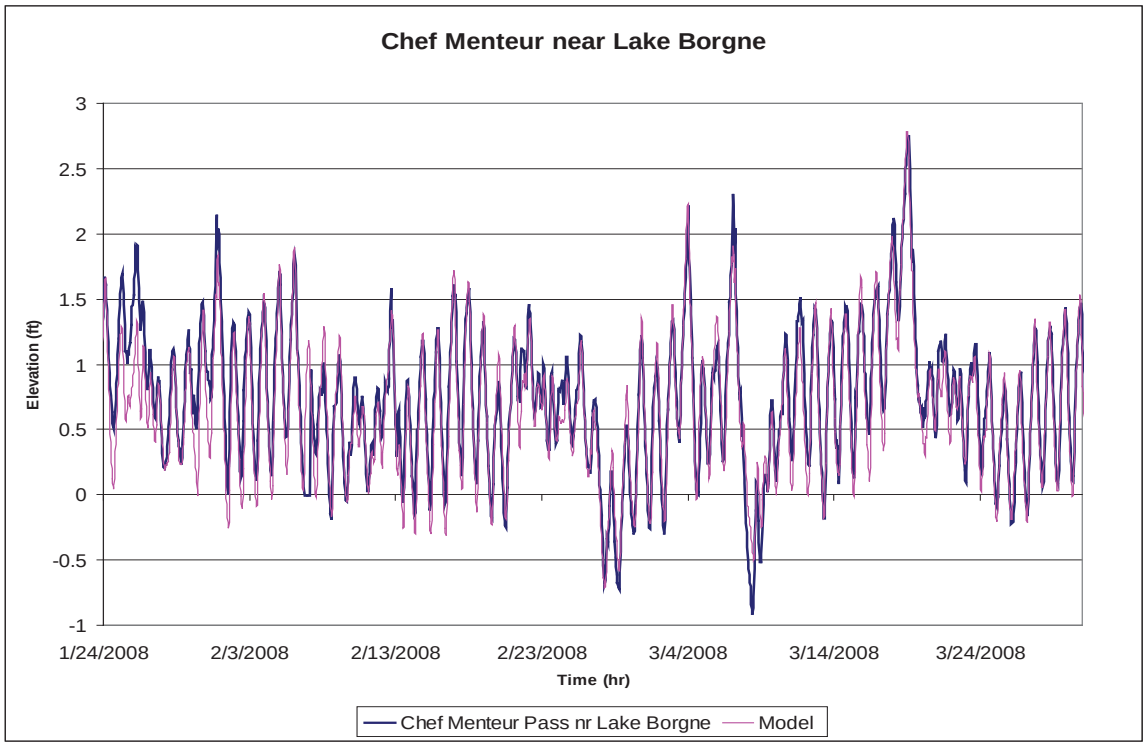

Figure 3-6. Chef Menteur water surface elevation (point 7 on Fig. 3-1).

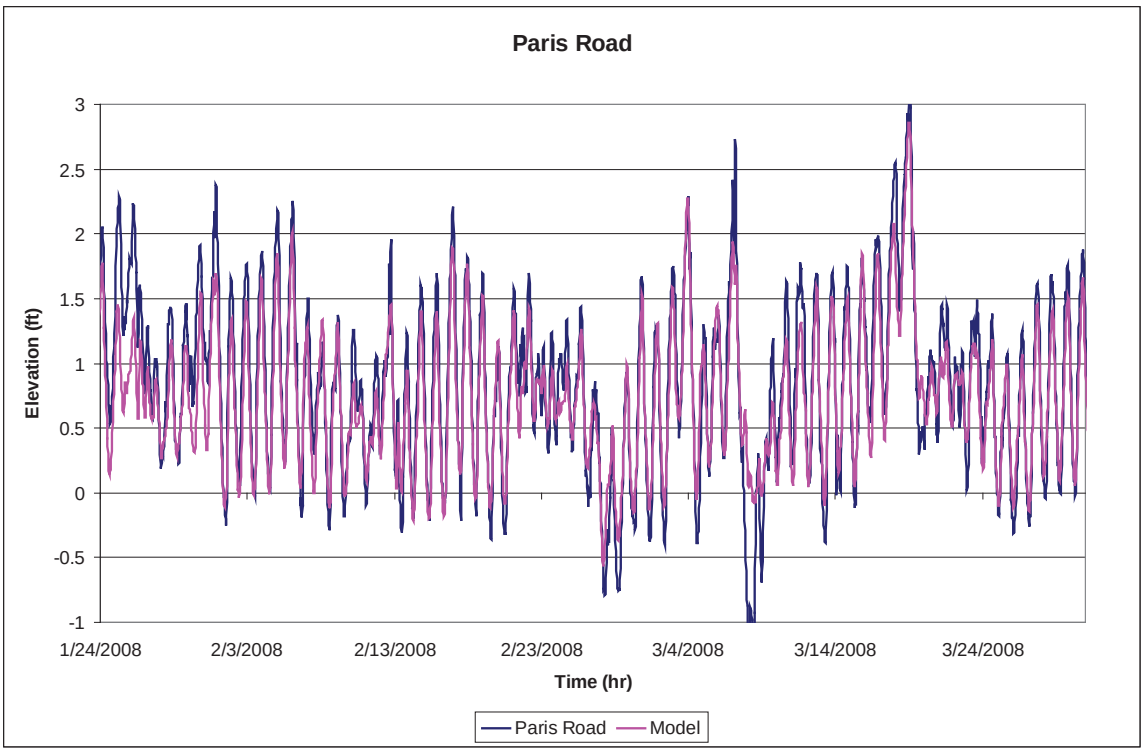

Figure 3-7. Paris Road water surface elevation (point 5 on Fig. 3-1).

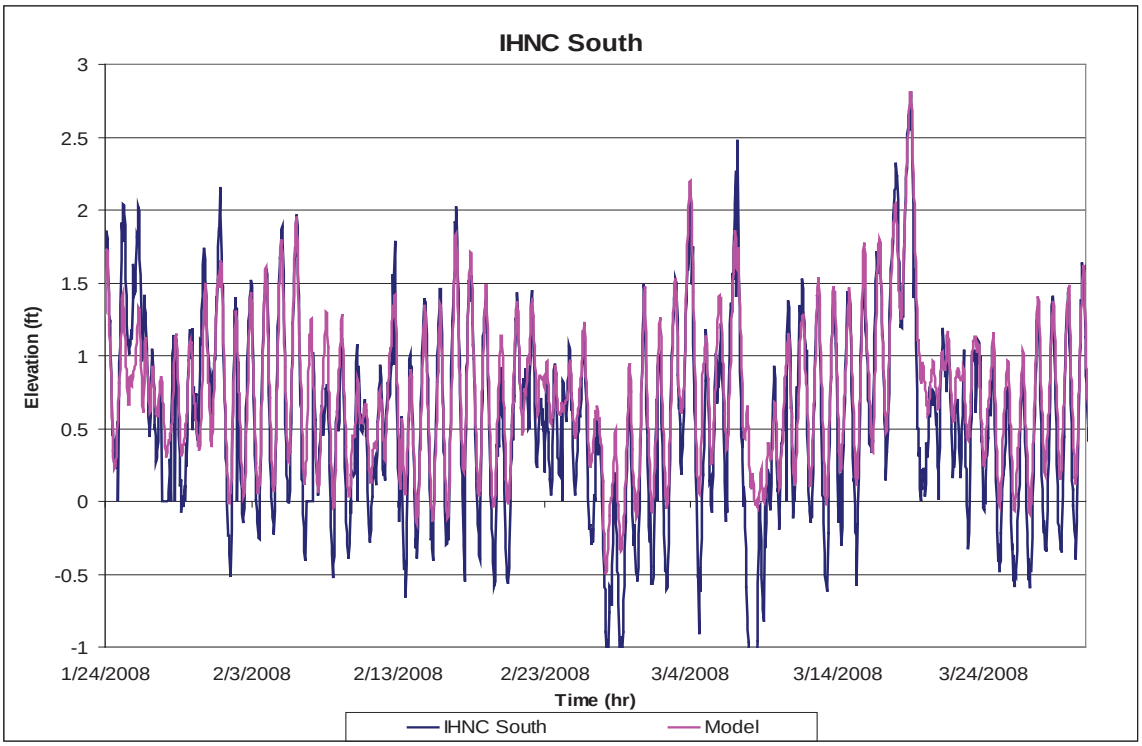

Figure 3-8. IHNC South Lock water surface elevation (point 4 on Fig. 3-1).

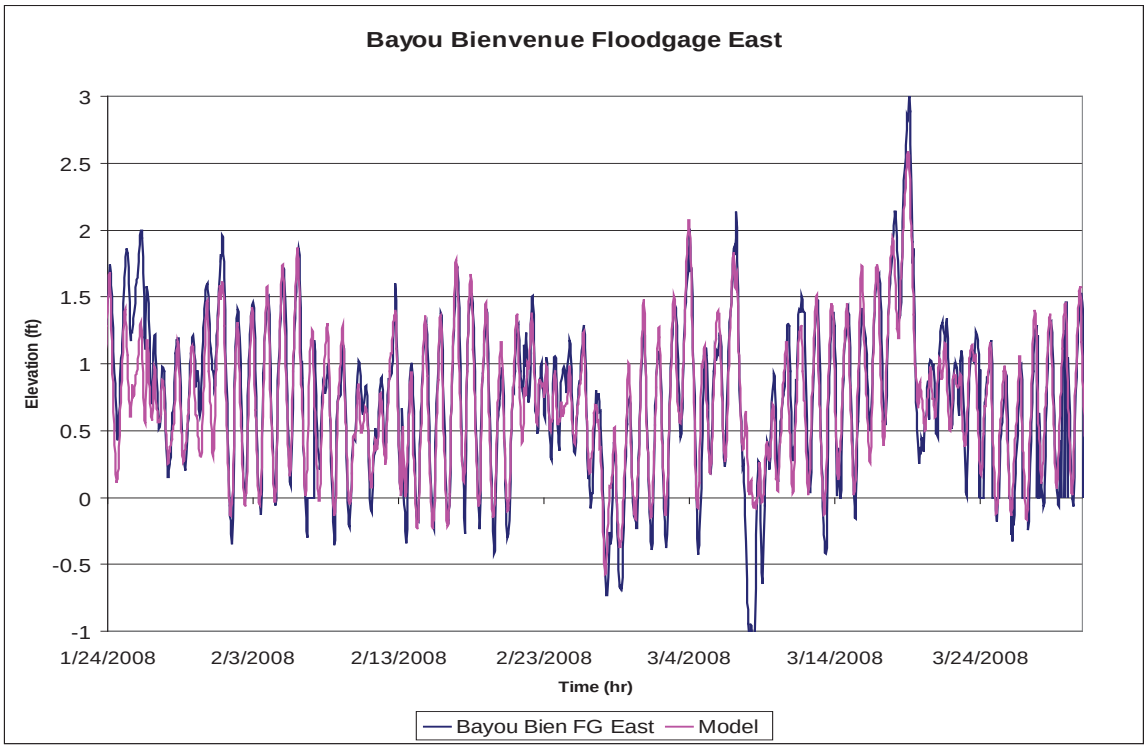

Figure 3-9. Bayou Bienvenue East water surface elevation (point 6 on Fig. 3-1).

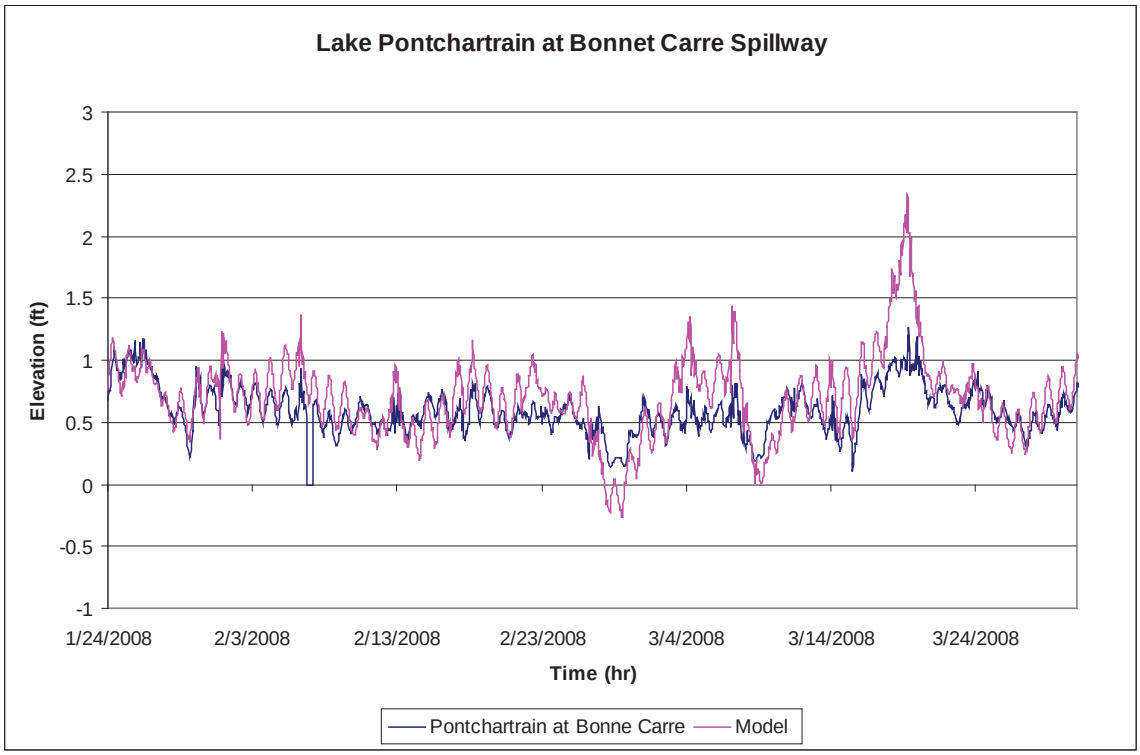

Figure 3-10. Bonnet Carre water surface elevation (point 1 on Fig. 3-1).

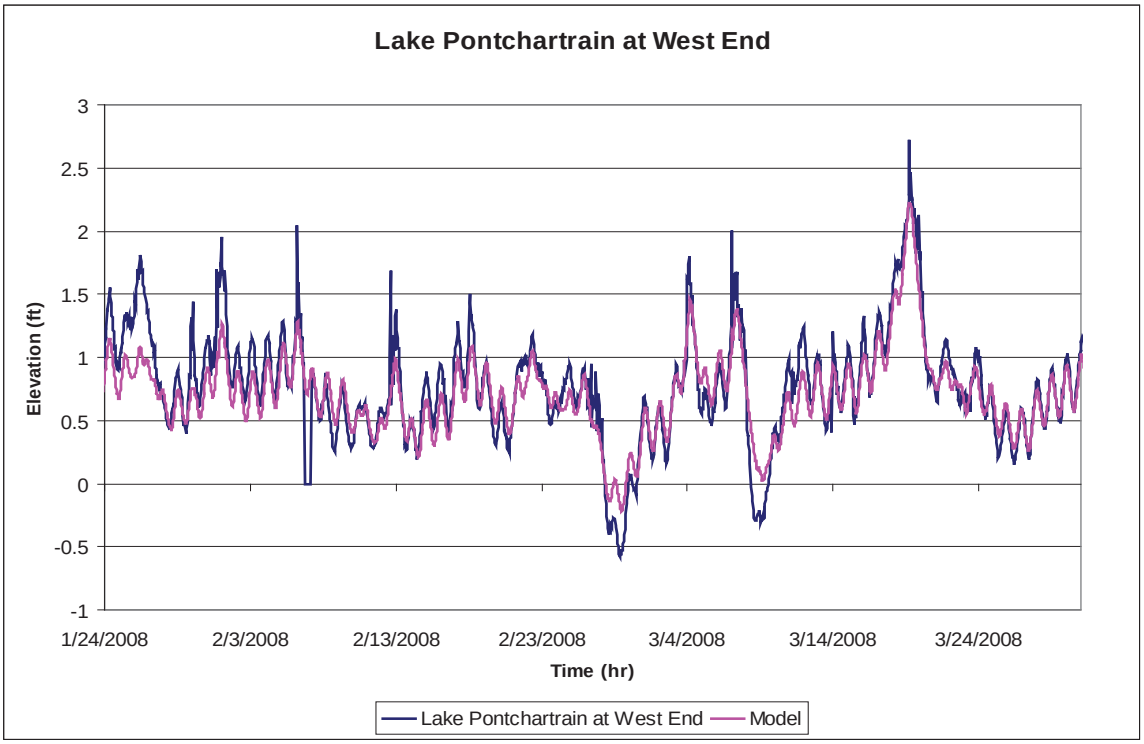

Figure 3-11. West End water surface elevation (point 2 on Fig. 3-1).

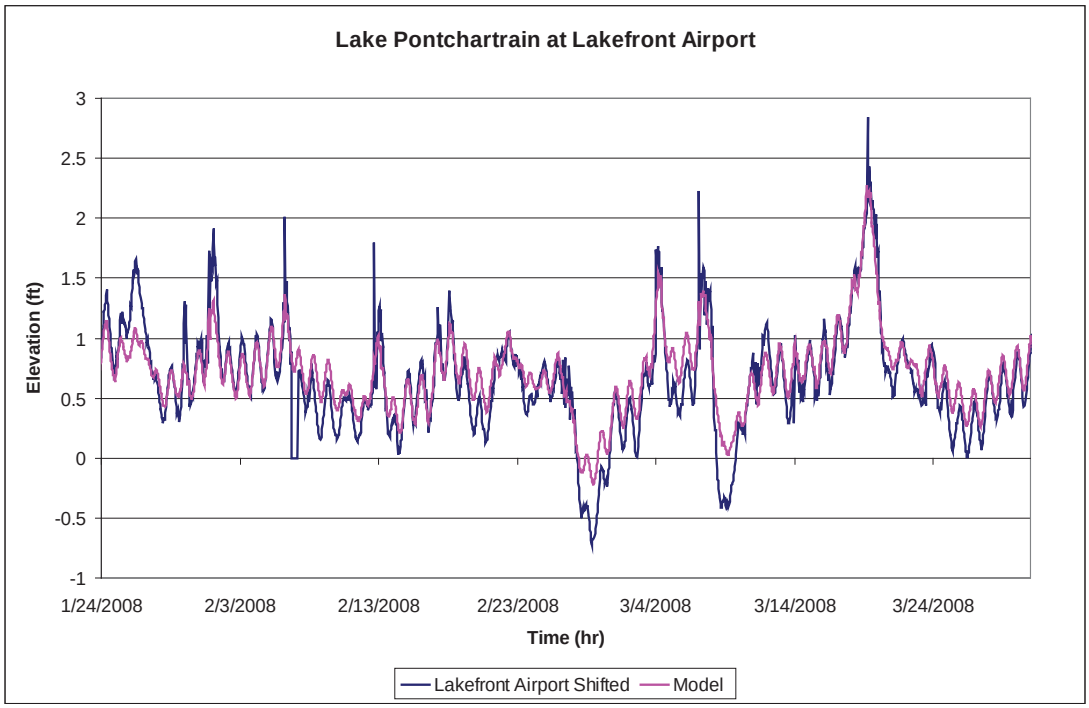

Figure 3-12. Lakefront Airport water surface elevation (point 3 on Fig. 3-1).

Progressing further into the system, the gages at the Rigolets (Figure 3-5) and at Chef Menteur (Figure 3-6) are analyzed. The model predicts larger water surface elevation changes at the Rigolets than those observed in the field. This gage is actually located in a small waterway that extends from the main channel that is not included in the mesh domain. The model data shown here are those for the channel center. It is not surprising that the data at the actual gage location are different from that obtained from the model due to these differences. The model/field comparison at Chef Menteur, however, is very good, with the model accurately representing the tide range.

The gage at Paris Road is located in the GIWW just west of its connection to the MRGO (point 5 on Figure 3-1). This comparison is given in Figure 3-7. Although some of the low range amplitudes are not reproduced, the overall comparison is very good at this location. The extreme low at around 3/10/08 is shown in the data for the Chef Menteur, Paris Road, IHNC South Lock, Bayou Bieuvenue (points 7, 5, 4, and 6, respectively) and to a lesser extent at Lake Pontchartrain at West End and Lakefront Airport (points 2 and 3). These set downs are likely due to a local weather event affecting most strongly MRGO and not captured well in the New Orleans airport wind data. The low range amplitudes missed in the model at the IHNC gage located at the lock on the southern end of the IHNC (point 4 on Figure 3-1)

as seen in Figure 3-8 also illustrate a limitation of the model. Due to the lock closure and the ADH model not including the details of this structure, reflections and 3D effects can be produced in the field that are not captured in a 2D depth averaged model which have an effect on the water levels. The pattern of the water level changes is matched and the higher level amplitudes are better captured in the model.

One gage exists within the model domain at Bayou Bienvenue on the west side of the MRGO (point 6 on Figure 3-1). This comparison is given in Figure 3-9. In the model, this marsh area west of the MRGO (typically known as the Central Wetlands) is described as a storage area and is not detailed due to there being no available bathymetry data for the area. The gage at this location shows that the model is replicating the exchange into this area which is important in the transport of particles for which this study is intended.

The final water surface elevation gages available to compare with model results are located in Lake Pontchartrain (points 1, 2, and 3 on Figure 3-1). Figure 3-10 shows the elevations at the Bonnet Carre Spillway, Figure 3-11 shows those at West End, and Figure 3-12 shows them at Lakefront Airport. The overall amplitude of the water surface elevations is lower in the lake than elsewhere. As with the gage at the Rigolets, the gages at West End and Lakefront Airport are not located within the model domain. To get a comparison, data from the model was taken just within the domain at these locations. Therefore, the model/field comparison analysis should consider this difference in the comparison locations. Overall the comparisons for eastern Lake Pontchartrain are good. There are events when the highs or lows are not reproduced fully, but the comparison is acceptable for the intent of this project.

A second comparison is made on the water surface elevation computations at selected stations. This comparison is performed on the amplitudes of the major tidal constituents. The constituents chosen for the comparison are those used in ADCIRC modeling simulations – M2, S2, N2, K2, O1, K1, Q1, M4, and M6. These constituents describe different influences on the tide, such as the lunar (M2, N2, O1, K1, Q1) or solar (S2) components or semi-diurnal (M2, S2, N2, K2) or diurnal (O1, K1, Q1) components. Shallow water overtides are included in the M4 and M6 components. A complete descripttion of the tidal constituents can be found at http://co-ops.nos.noaa.gov/harmonic_cons_defs.html. The periods of these signals are

given in Table 3-1. The stations where these comparisons are made are Grand Pass, Paris Road, Chef Menteur, and Lake Pontchartrain at West End. See Figure 3-1 for the location of each station. Figures 3-13 through 3-16 show the amplitude comparison for the field and model water surface signals. Table 3-2 gives a summary of amplitude values for the field and model as well as a percent difference between the two. The most significant components are O1 and K1 for all locations. The maximum difference for these constituents is 16.5%. An occasional difference of 15-20% falls within an acceptable range for the project's intent. There are larger differences in constituents that contribute much less to the overall tidal signal. Although some constituents compare better than others, the overall replication is good.

Table 3-1. Tidal Constituents.

Constituent	Period (hr)
M2	12.4206
S2	12
N2	12.65835
K2	11.96723
O1	25.81934
K1	23.93447
Q1	26.86836
M4	6.2103
M6	4.1402

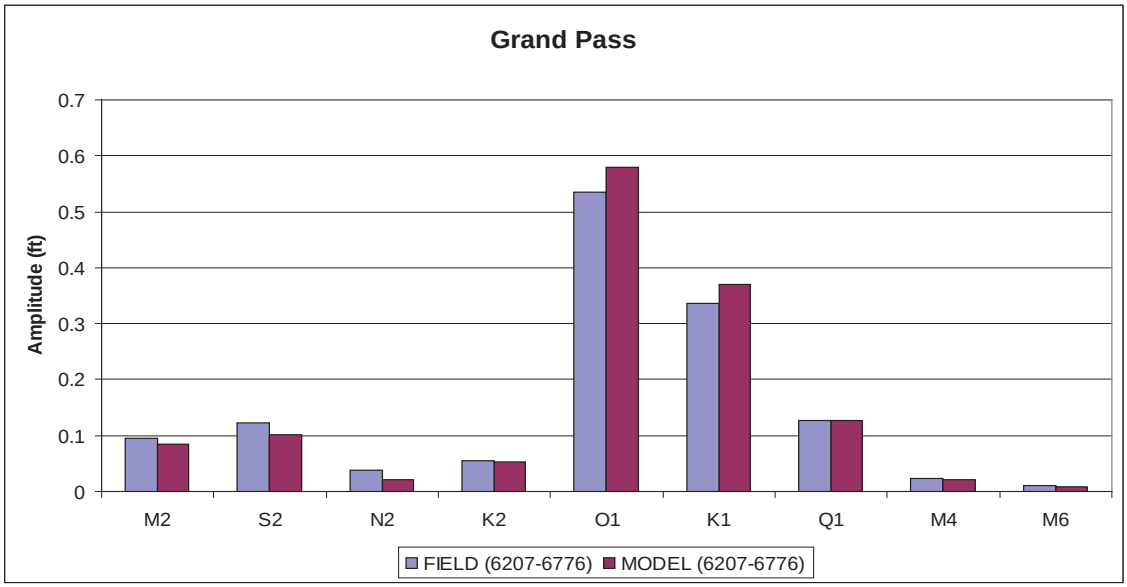

Figure 3-13. Tidal constituent comparison of amplitude at Grand Pass (point 9 in Fig. 3-1).

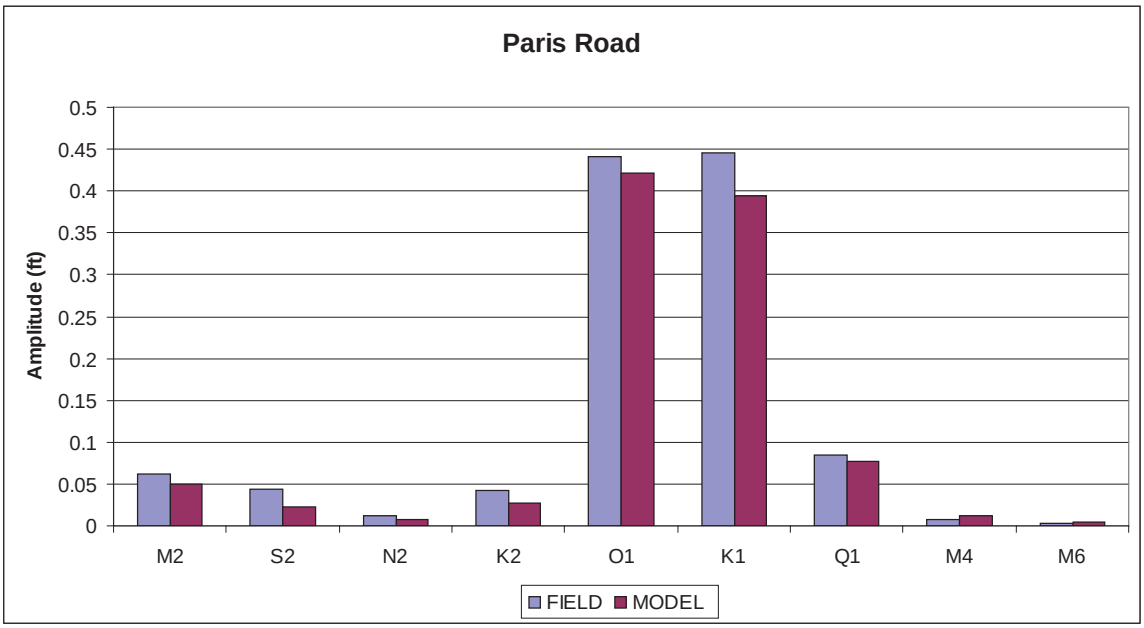

Figure 3-14. Tidal constituent comparison of amplitude at Paris Road (point 5 in Fig. 3-1).

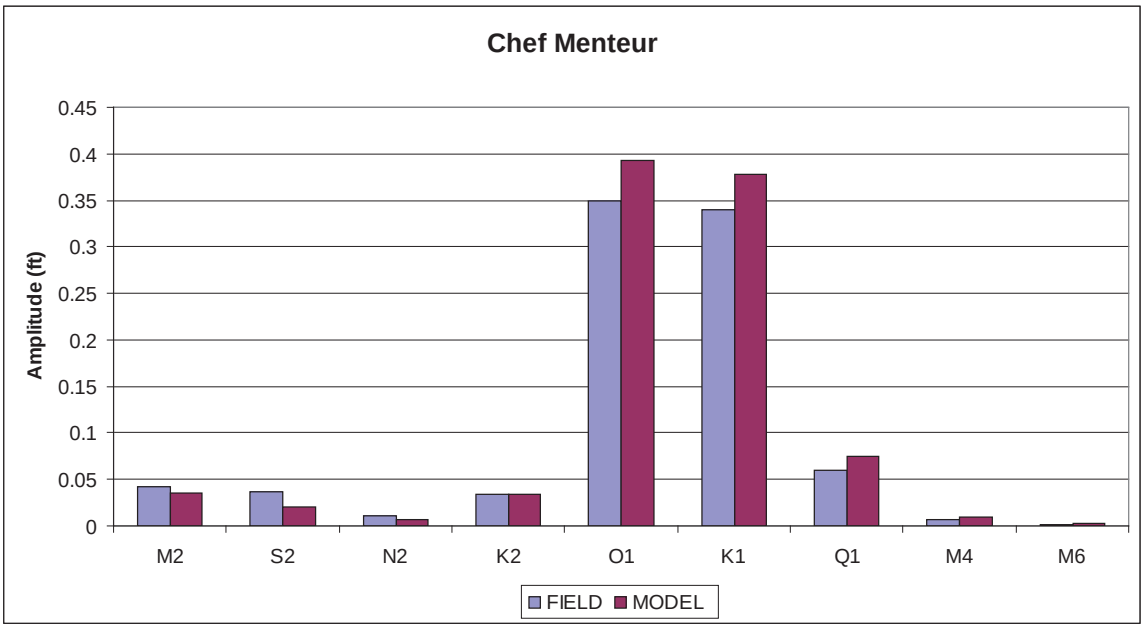

Figure 3-15. Tidal constituent comparison of amplitude at Chef Menteur (point 7 in Fig. 3-1).

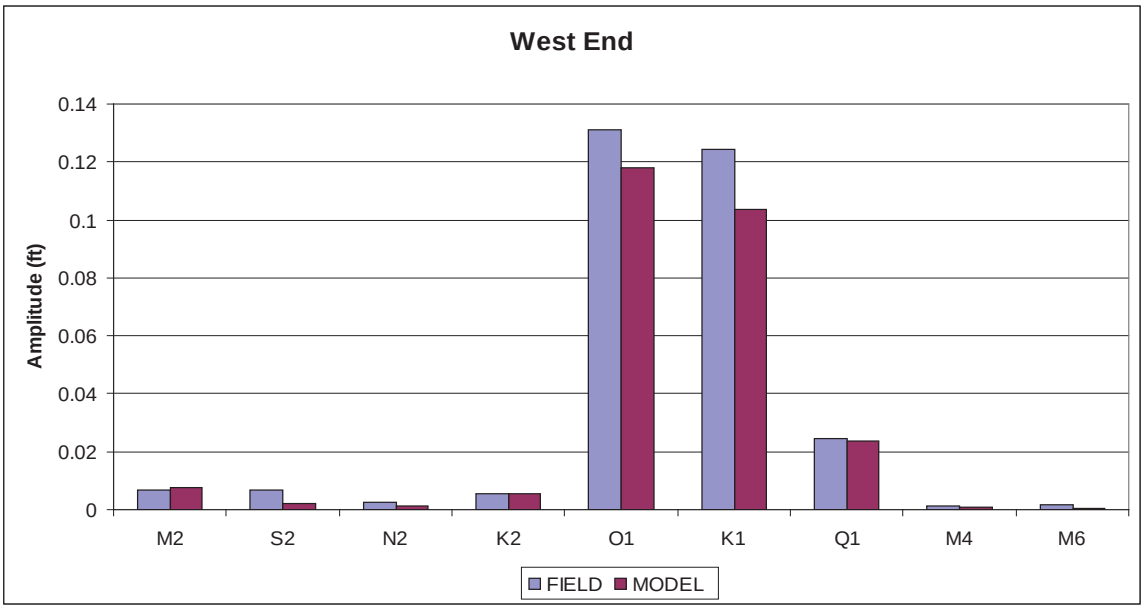

Figure 3-16. Tidal constituent comparison of amplitude at West End (point 2 in Fig. 3-1).

Table 3-2. Tidal Constituent Amplitude Comparisons (ft).

	Grand Pass			Paris Rd.			Chef Menteur			West End		
Constituent	Field	Model	% Diff	Field	Model	% Diff	Field	Model	% Diff	Field	Model	% Diff
M2	0.312	0.274	-12.07	0.205	0.161	-21.17	0.138	0.114	-17.78	0.023	0.025	9.52
S2	0.403	0.333	-17.27	0.145	0.076	-47.55	0.121	0.065	-45.97	0.023	0.007	-67.77
N2	0.127	0.066	-47.86	0.037	0.025	-32.27	0.036	0.022	-39.33	0.009	0.004	-60.15
K2	0.179	0.173	-3.53	0.140	0.091	-35.27	0.111	0.113	1.35	0.018	0.018	3.16
O1	1.757	1.902	8.23	1.445	1.381	-4.43	1.146	1.290	12.55	0.431	0.387	-10.06
K1	1.106	1.217	10.04	1.464	1.295	-11.53	1.116	1.241	11.14	0.407	0.340	-16.49
Q1	0.413	0.416	0.54	0.277	0.255	-7.86	0.198	0.244	23.36	0.081	0.077	-4.40
M4	0.076	0.067	-12.40	0.027	0.041	49.90	0.023	0.033	39.44	0.004	0.002	-47.34
M6	0.036	0.025	-30.06	0.011	0.014	23.52	0.003	0.007	146.42	0.006	0.002	-67.48

The discharge comparisons are made for the transects shown in Figures 3-2 and 3-3. Figures 3-17 through 3-19 give the field value (points) of the total flow passing each transect as well as the model results over time (lines) of the transects from Figure 3-3. Flow is positive when moving towards the north or east and negative when moving towards the south or west. The ADH model is reasonably accurate in reproducing the circulation direction and general percentage flow split between the GIWW and MRGO. Field discharge measurements are affected by many things such as instrument-

ation limits as well as the limitations caused by the physical nature of where the data are being collected. Although recent bathymetry data were collected upstream of the locations on the MRGO, the bathymetry data at these locations is slightly older and the channel boundaries are used as model boundaries. It is likely also that the flow at these locations is not as clear-cut as it is depicted in the model due to the marsh conditions in much of this area. The goal of this analysis is to get the trends and direction of the flow as accurate as possible. There is a variation in the comparison over the limited field samples.

Figure 3-17 gives the model comparison to the field for transects 6 and 8 which are located along the MRGO. The model shows good agreement to the discharge magnitude and direction at these locations. Figure 3-18 shows the comparison at lines 4 and 5. These transects cross side channels and are low in flow magnitude. Due to Bayou Bienvenue (line 5 in Figure 3-3) flowing through a very marshy area which is not fully detailed in the model, this area is artificially widened in the model so that the flow passage will include any water filtering in from the surrounding marsh. The model is able to reproduce the flow through these sections as shown in Figure 3-18, although the flow through Bayou Bienvenue is not as accurate as desired. Figure 3-19 shows the same comparisons at lines 1 and 2 along the GIWW

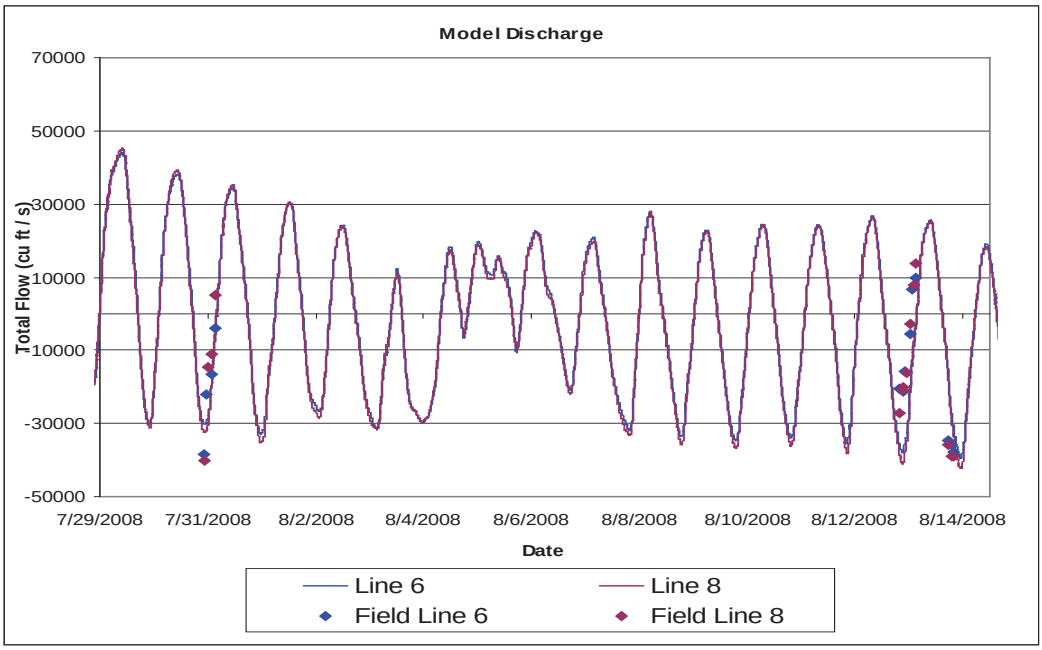

Figure 3-17. GIWW/MRGO discharge for lines 6 and 8.

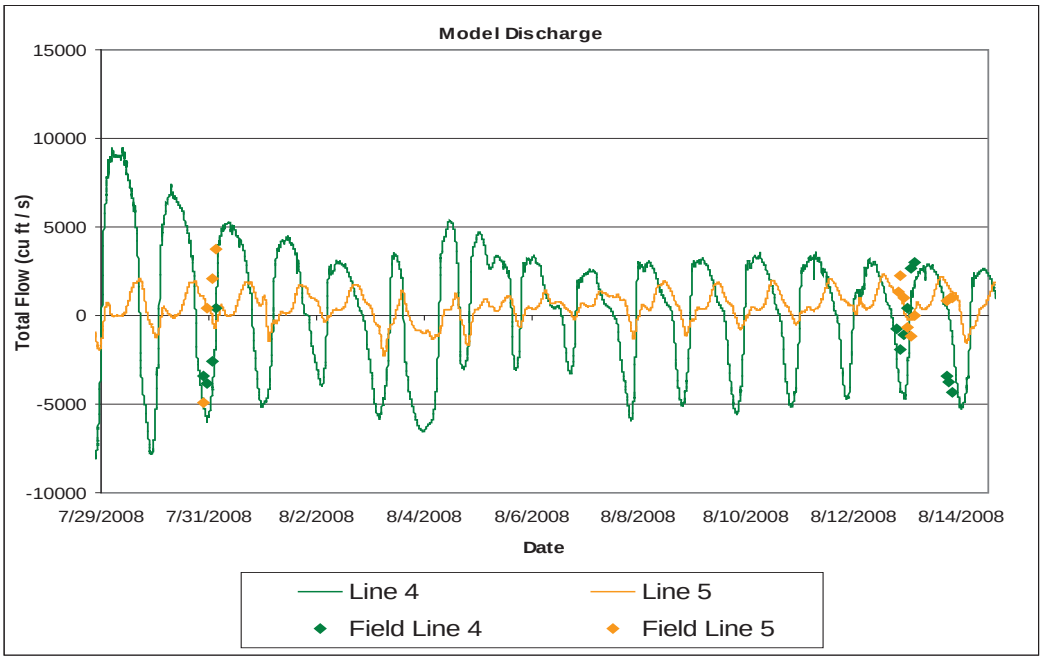

Figure 3-18. GIWW/MRGO discharge for lines 4 and 5.

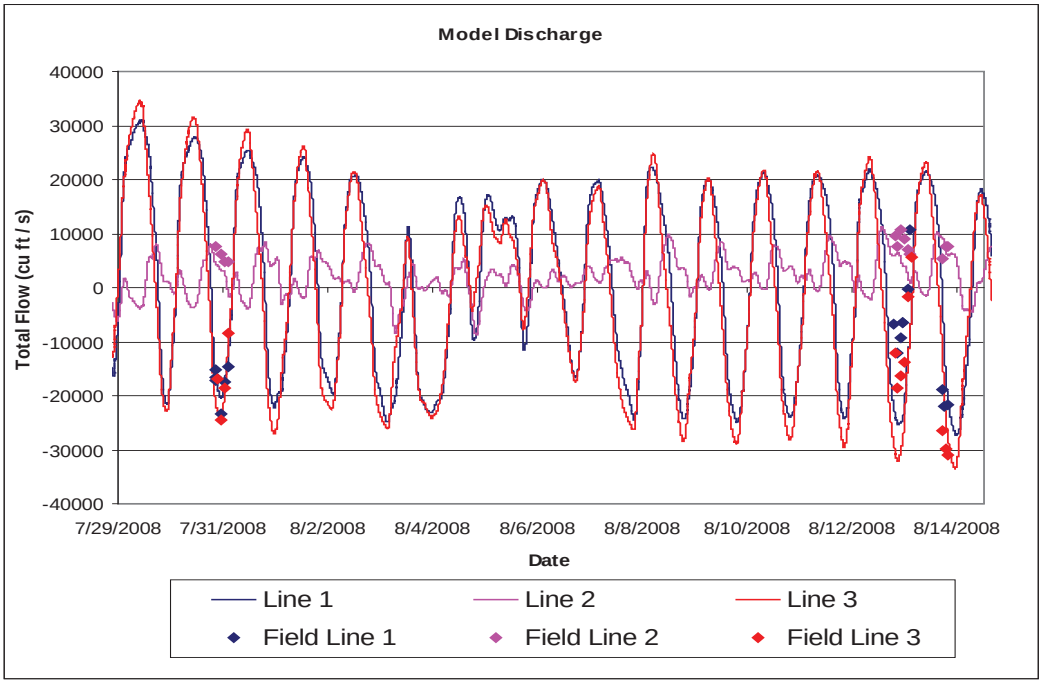

Figure 3-19. GIWW/MRGO discharge for lines 1, 2, and 3.

and at line 3 at the north end of the MRGO. The flow split at this location is such that the flows passing lines 2 and 3 should equal the flow passing line 1. This is reproduced in the model as shown in Figure 3-19. It is in this area that the direction of flow becomes very important. The model is good at maintaining the overall magnitude and direction of the flow.

Discharge and velocity comparisons are also performed in the Seabrook area of the IHNC. These transects are shown in Figure 3-2. Figure 3-20 shows the total flow comparison of the model to the field values. Unfortunately no data were collected during the peak flow conditions and data were also only collected during times when the velocity direction was towards the south (positive values in Figure 3-20). Due to instrument limitations, field conditions, and assumptions that are made when obtaining discharge data, model to field comparisons within 20% are typically deemed acceptable, although dependent on the intended use of the model. The model produces flows in this area that are slightly higher than those found in the field but the comparison is within the generally accepted range and is therefore considered good. The velocity comparisons at these transects at various times are shown in Figures 3-21 through 3-24. The black arrows represent the model predicted velocity vectors and the red arrows represent the field data. Both sets of vectors are scaled so that the length of the arrows gives the magnitude of the flow. The direction of the flow and the location of eddies is reproduced well in the model, especially when the magnitude of the flows is large. Such an eddy is located in the off channel area on the east in Figure 3-21. At higher flow magnitudes, transport occurs more easily and the ultimate intent of this work is to model larval fish transport. Therefore, accuracy of magnitude and direction at higher flows is important. Judging from Figures 3-20 through 3-24, the flows through the Seabrook-IHNC vicinity appear adequate for the larval tracking work.

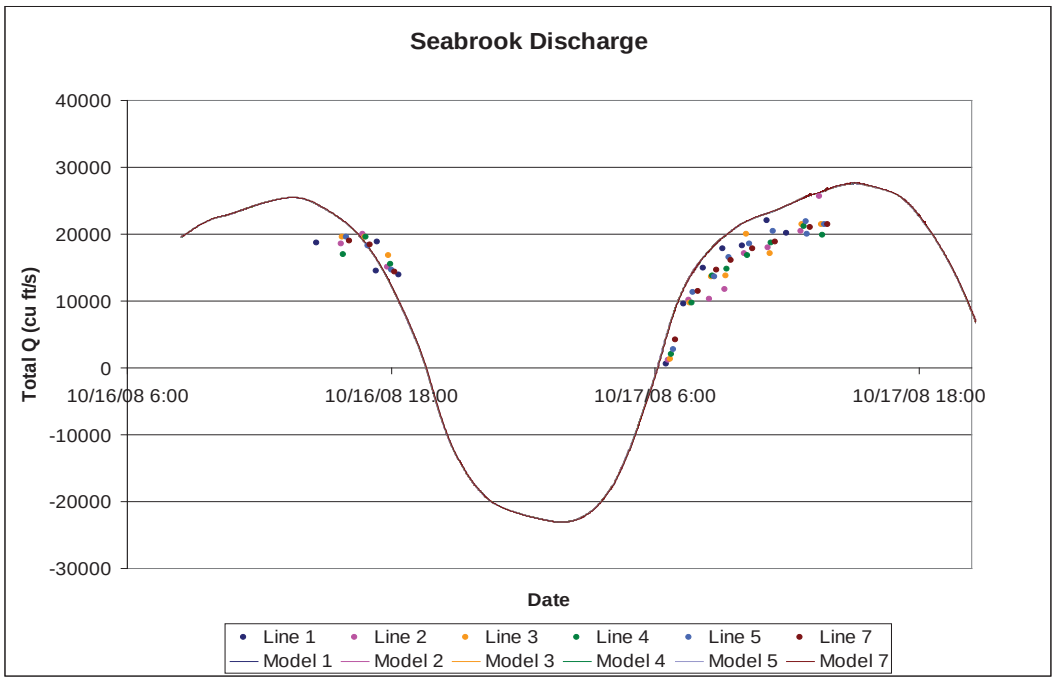

Figure 3-20. IHNC Seabrook discharge (all model results trace the same curve in this figure).

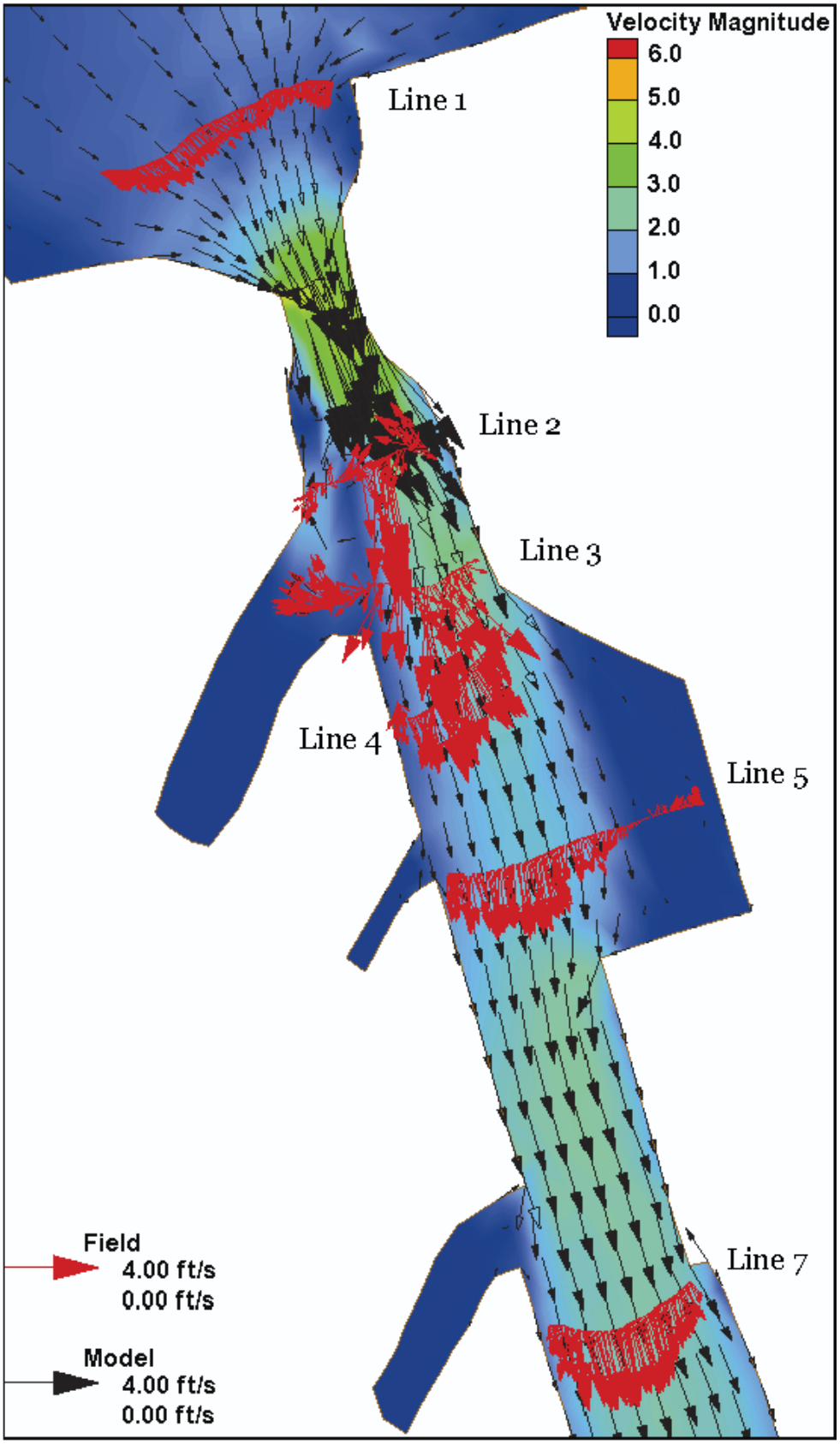

Figure 3-21. IHNC Seabrook model velocity on October 16, 2008 at 15:33.

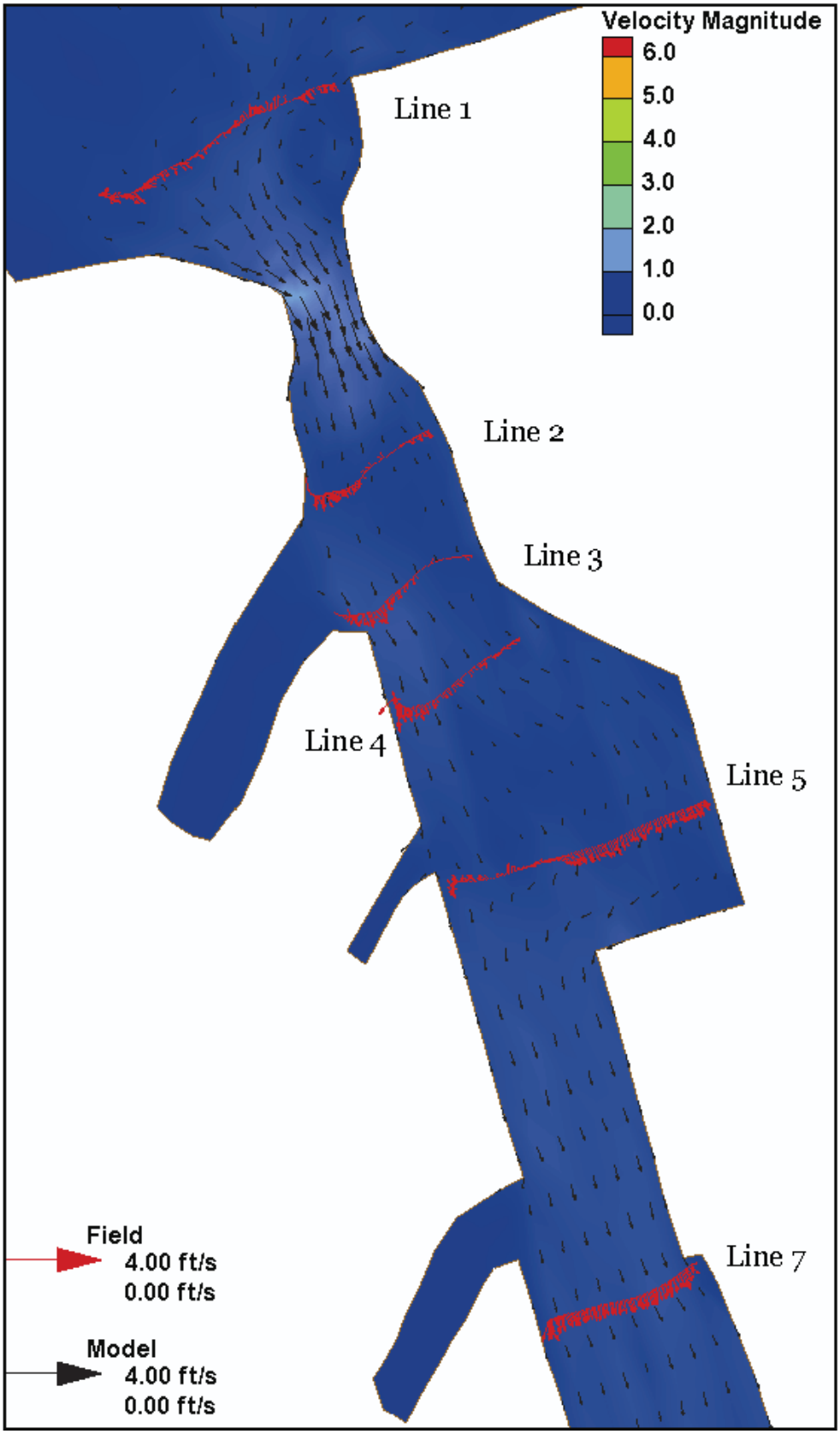

Figure 3-22. IHNC Seabrook model velocity on October 17, 2008 at 06:30.

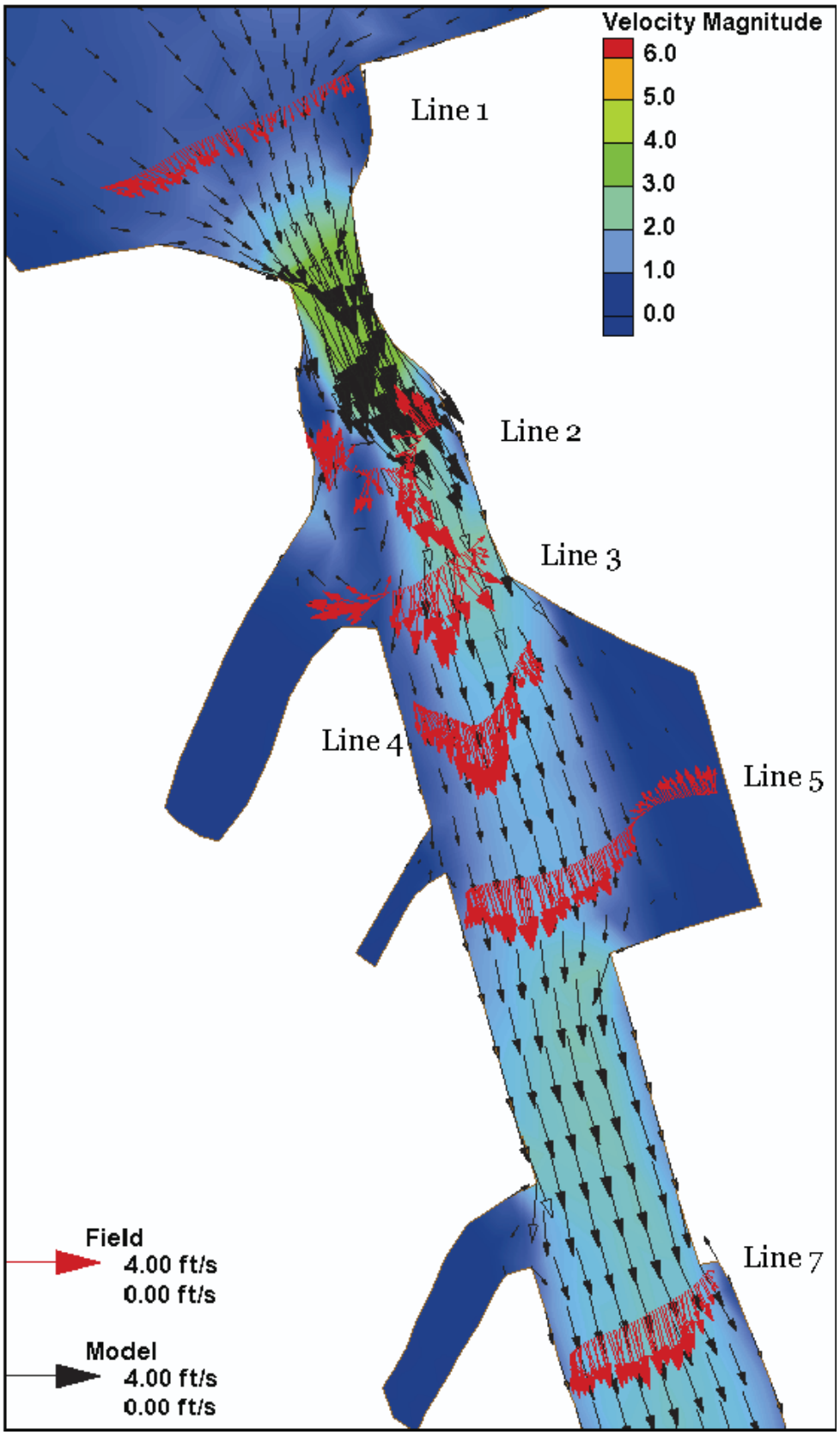

Figure 3-23. IHNC Seabrook model velocity on October 17, 2008 at 09:05.

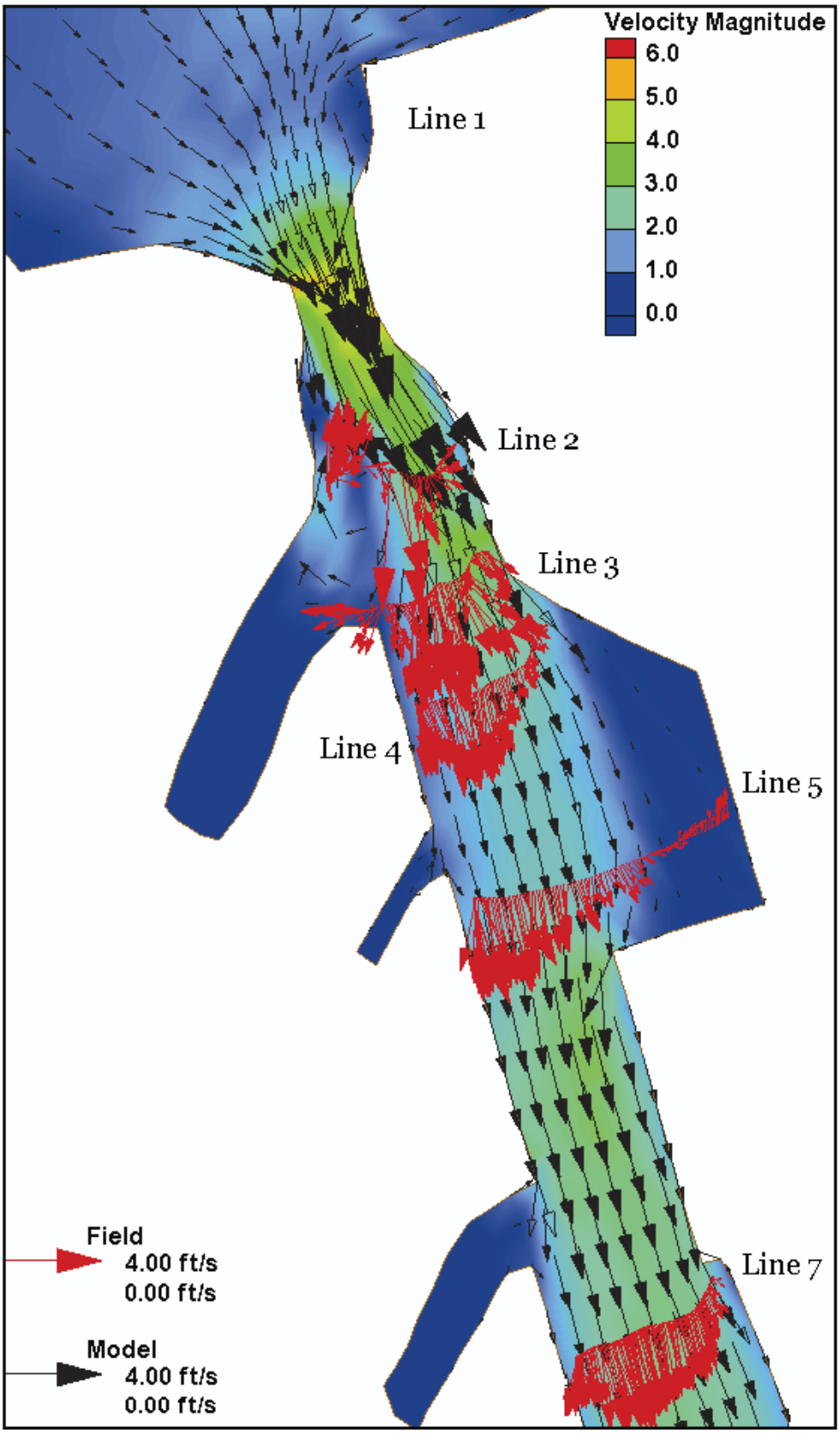

Figure 3-24. IHNC Seabrook model velocity on October 17, 2008 at 13:29.

Depth averaged velocity comparison during the time of the discharge comparisons in the GIWW/MRGO area are shown in Figures 3-25 through 3-32. The velocity magnitude is contoured according to the legend on the upper right. The length of the vectors in these figures is defined in the vector legend on the bottom left. The scale shows the length of a vector representing 4.0 ft/s. The model time closest to the field data collection time is used for the data comparison. The general flow patterns are replicated in the model. The timing of the change in direction at locations 4 and 5 does lag the field slightly. However, the discharges are being reproduced. Due to having no further data to compare to and other locations in the area producing good comparisons to the field, these differences in the model will be accepted.

It is apparent that some of the flow peaks and exact timings are not captured by the model due to various limitations mentioned in this section, including the use of only one wind station and the simple depiction of the very complex and fragmented marsh areas. A closer comparison of the model results to the field data could be performed if more time were available for the task. However, these differences do not adversely impact the results necessary for the study's intended purpose and the model validation was accepted. The aim of this study is to determine how the proposed new works will affect the circulation and, thus, the movement of larvae, as modeled in the PTM. The hydrodynamic model adequately reproduces the main features of the basic circulation of the system and is thus deemed appropriate for use as a base for judging the changes in circulation when the proposed works are implemented in the model.

Sensitivity Analysis

Before leaving the subject of hydrodynamic model validation, the results of a sensitivity analysis are presented. Such an analysis is important to understand the extent to which unknowns and uncertainties, such as in the wind forcings, are important. Thus, basic sensitivity analyses were performed, focusing in the area of the GIWW. These sensitivity tests include effects of the wind speed as well as mesh boundary depths along the navigable waterways.

It is known that wind speeds and directions vary throughout the model domain. Since a single wind station is used for this simulation, local affects due to varying wind conditions might not be reproduced exactly. A simulation is performed in which the wind speed is increased by 50%. The

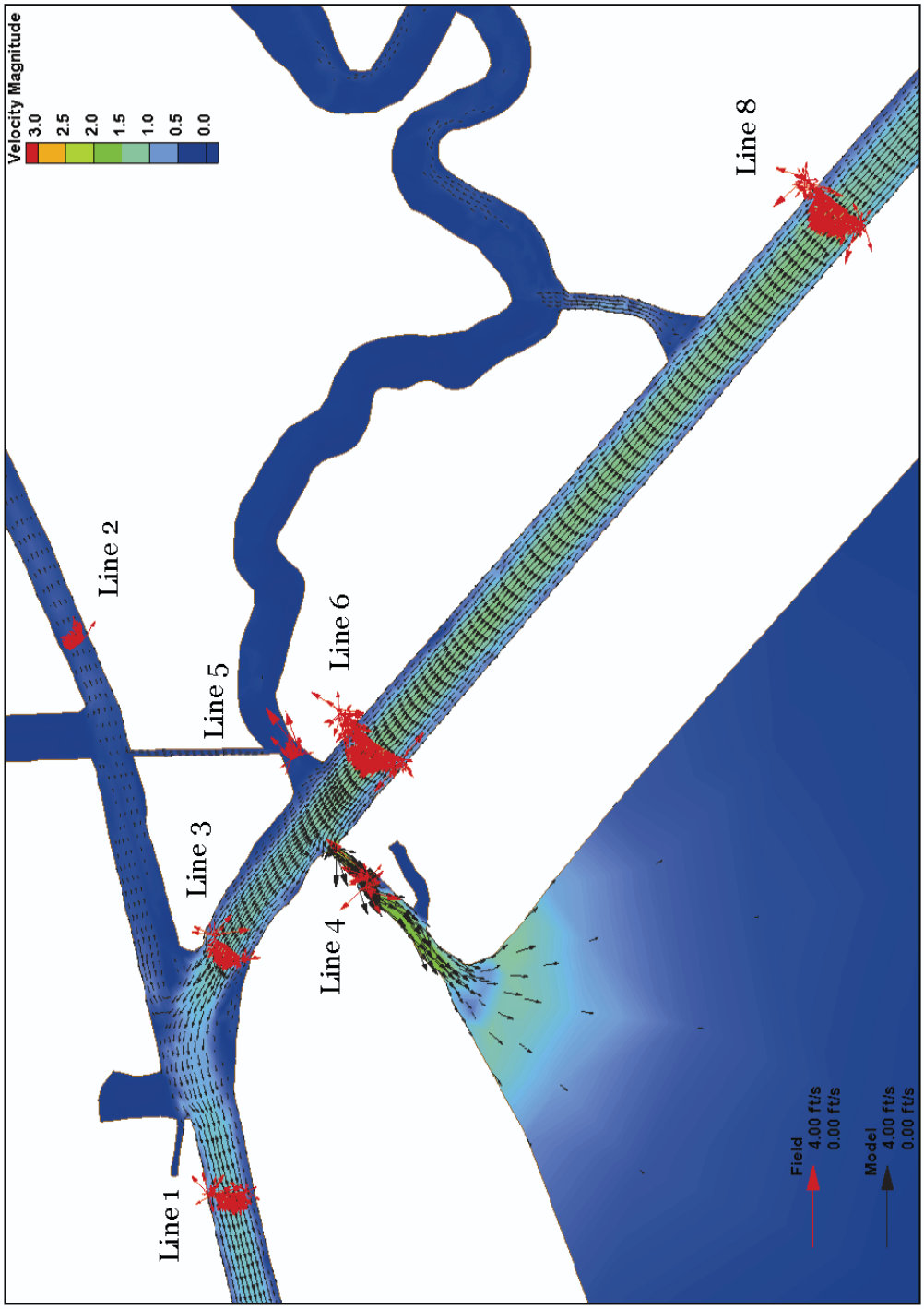

Figure 3-25. GIWW/MRGO velocity on July 31, 2008 at 10:30.

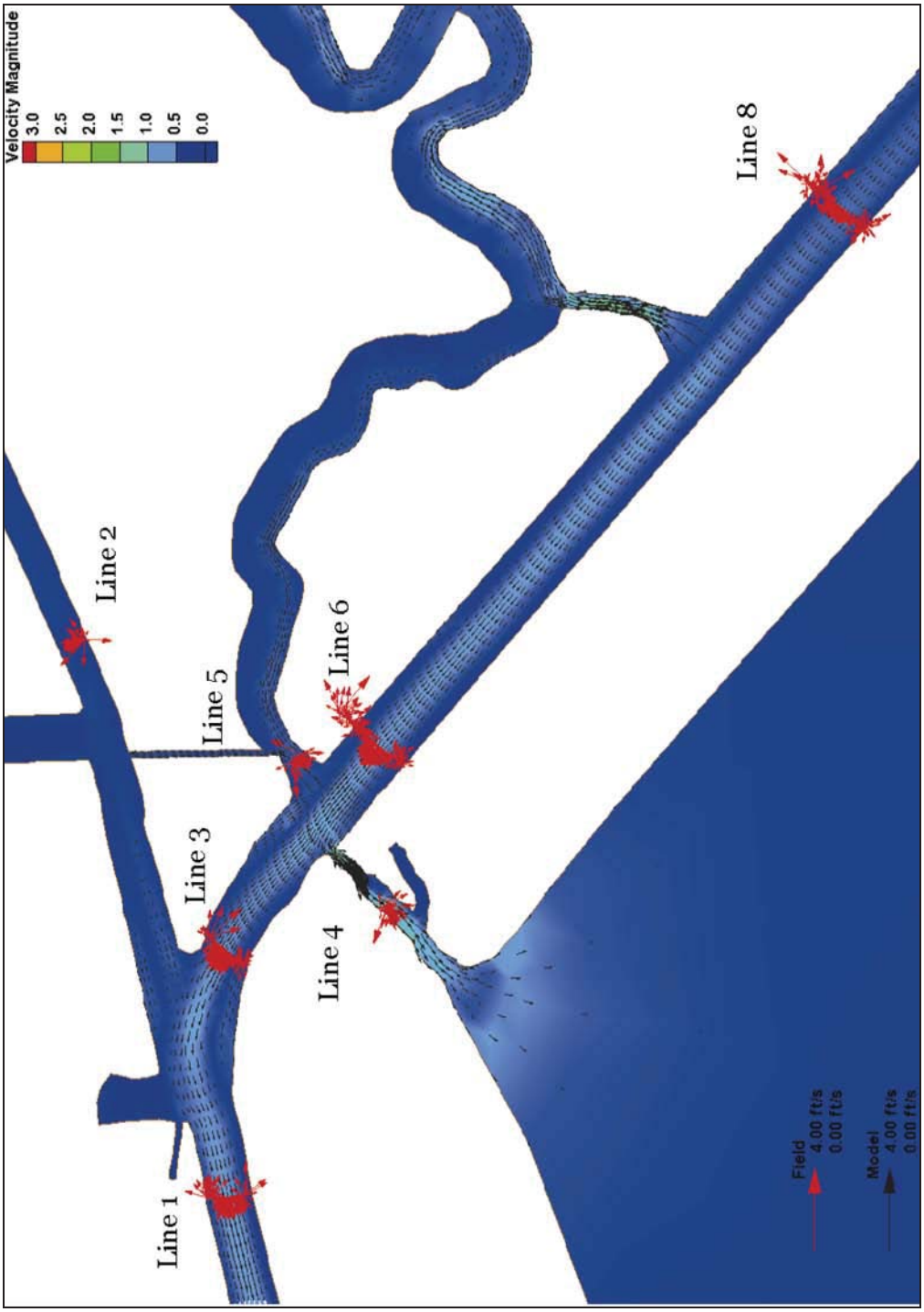

Figure 3-26. GIWW/MRGO velocity on July 31, 2008 at 14:30.

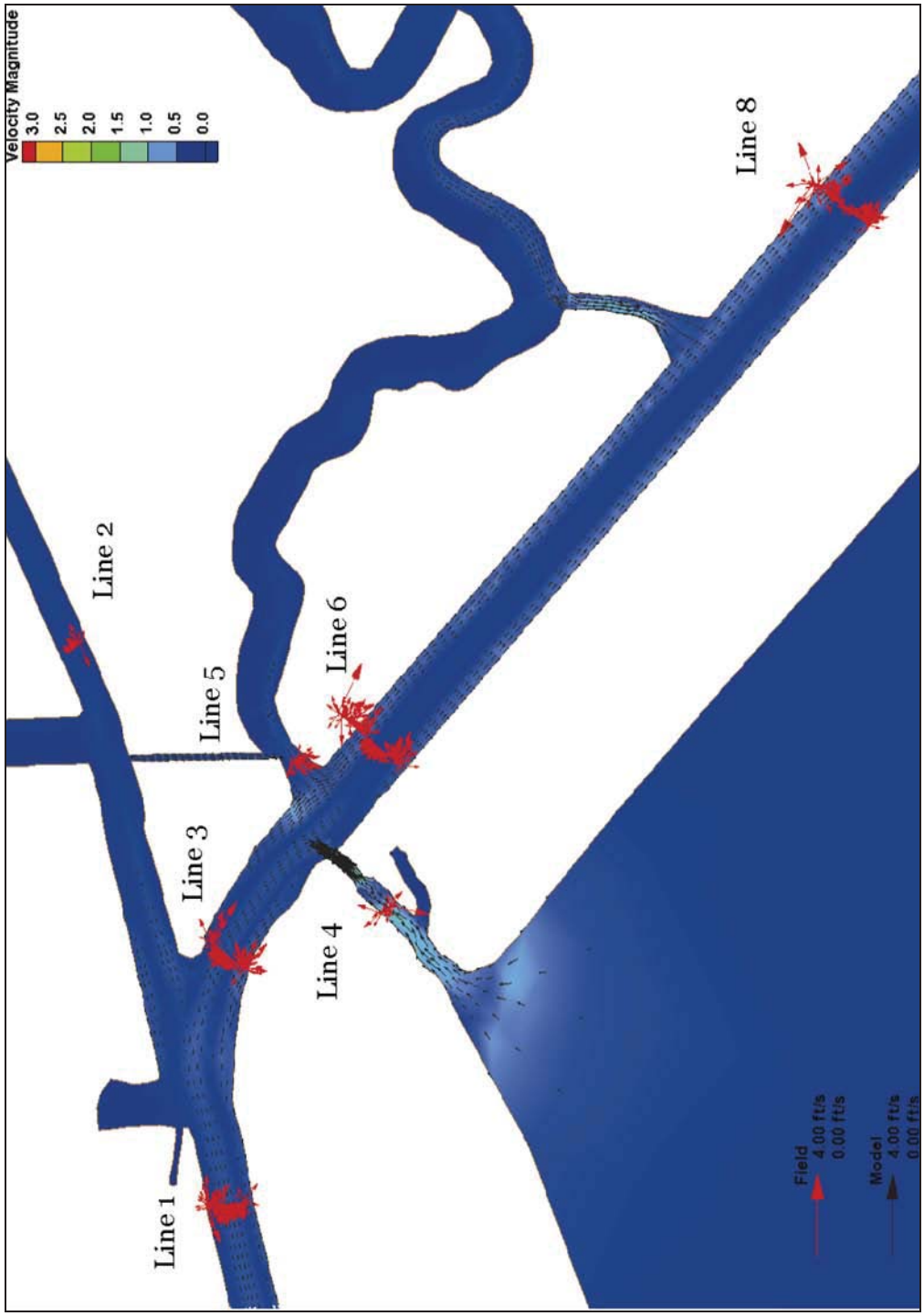

Figure 3-27. GIWW/MRGO velocity on July 31, 2008 at 16:00.

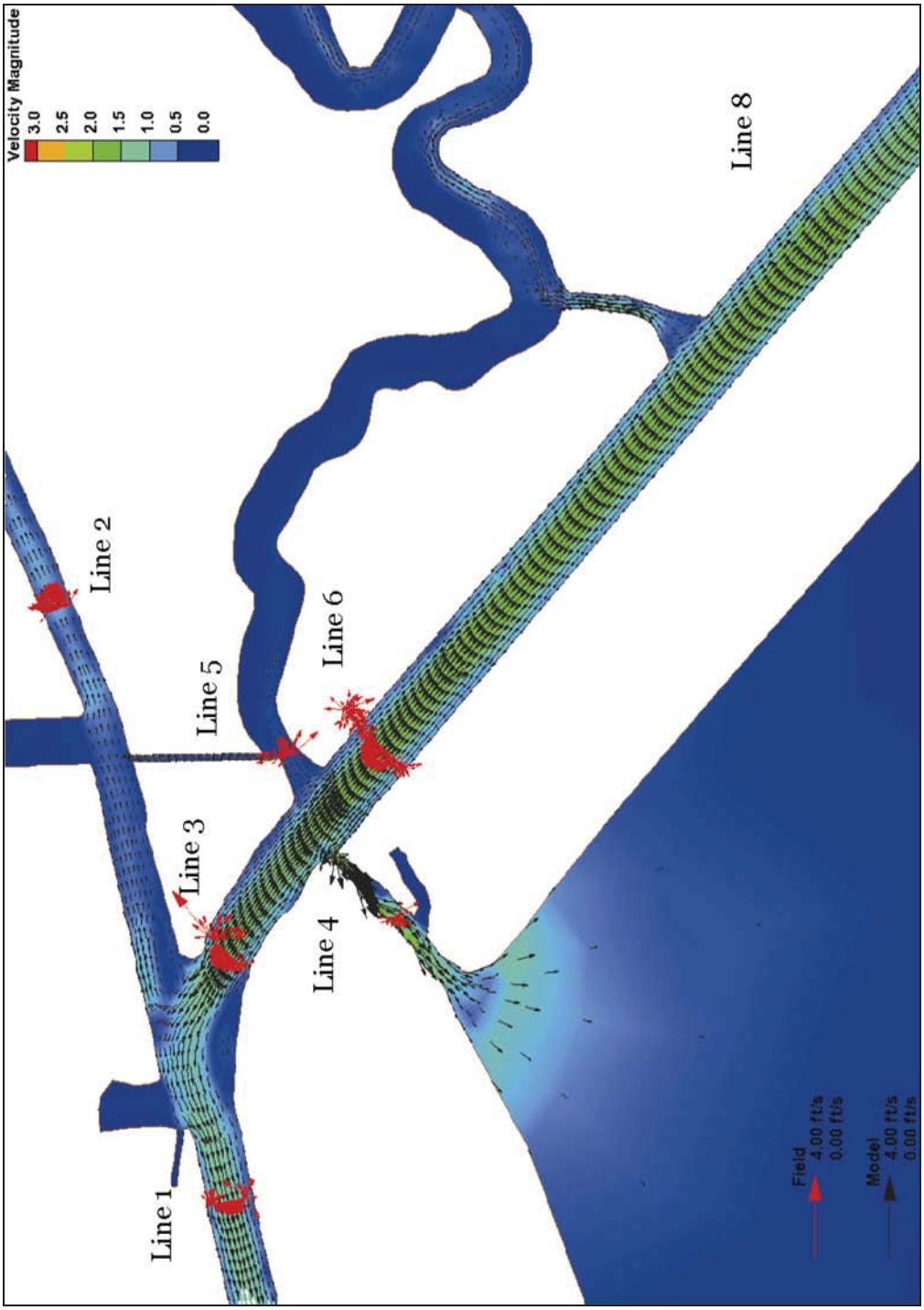

Figure 3-28. GIWW/MRGO velocity on August 13, 2008 at 9:00.

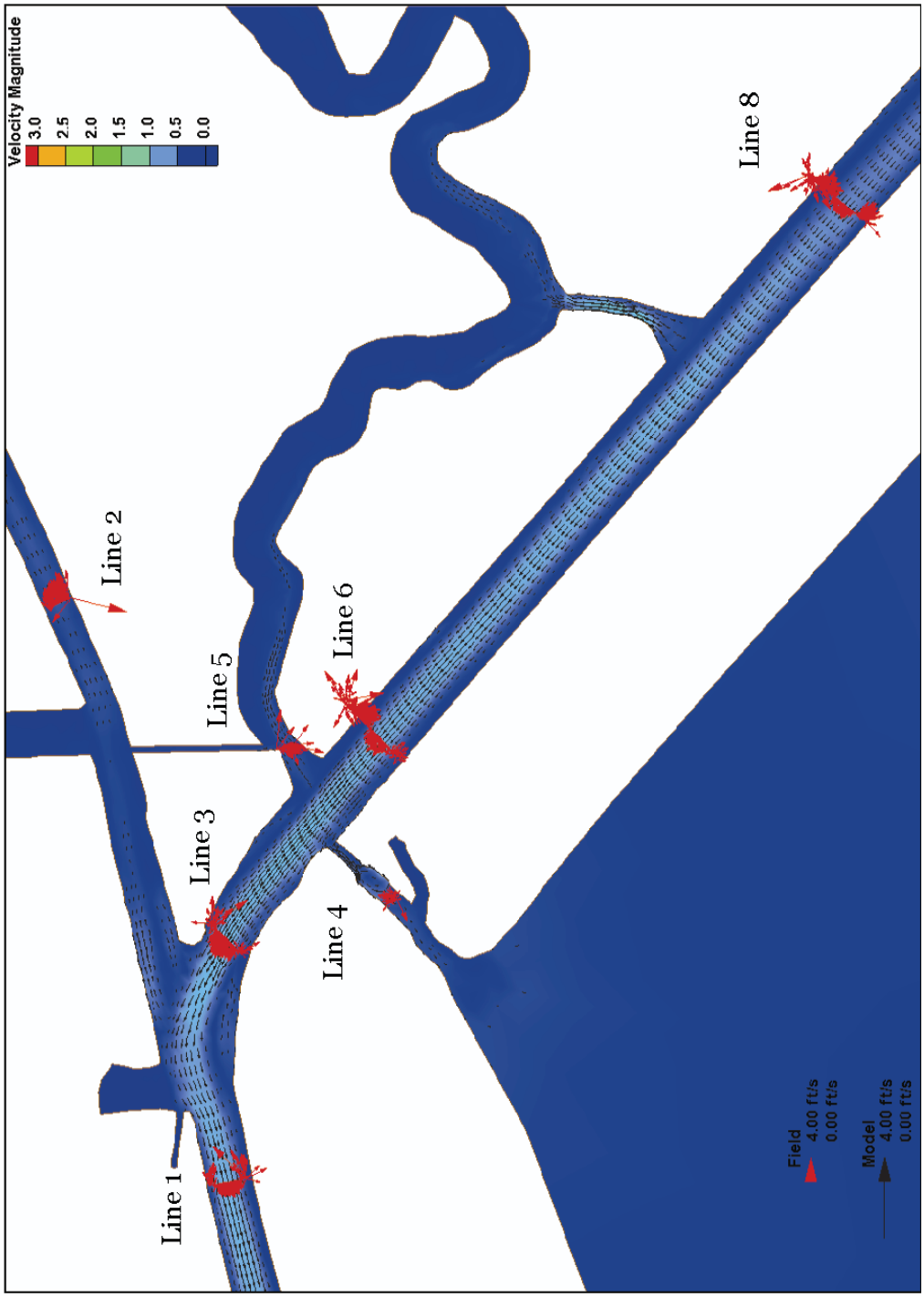

Figure 3-29. GIWW/MRGO velocity on August 13, 2008 at 13:00.

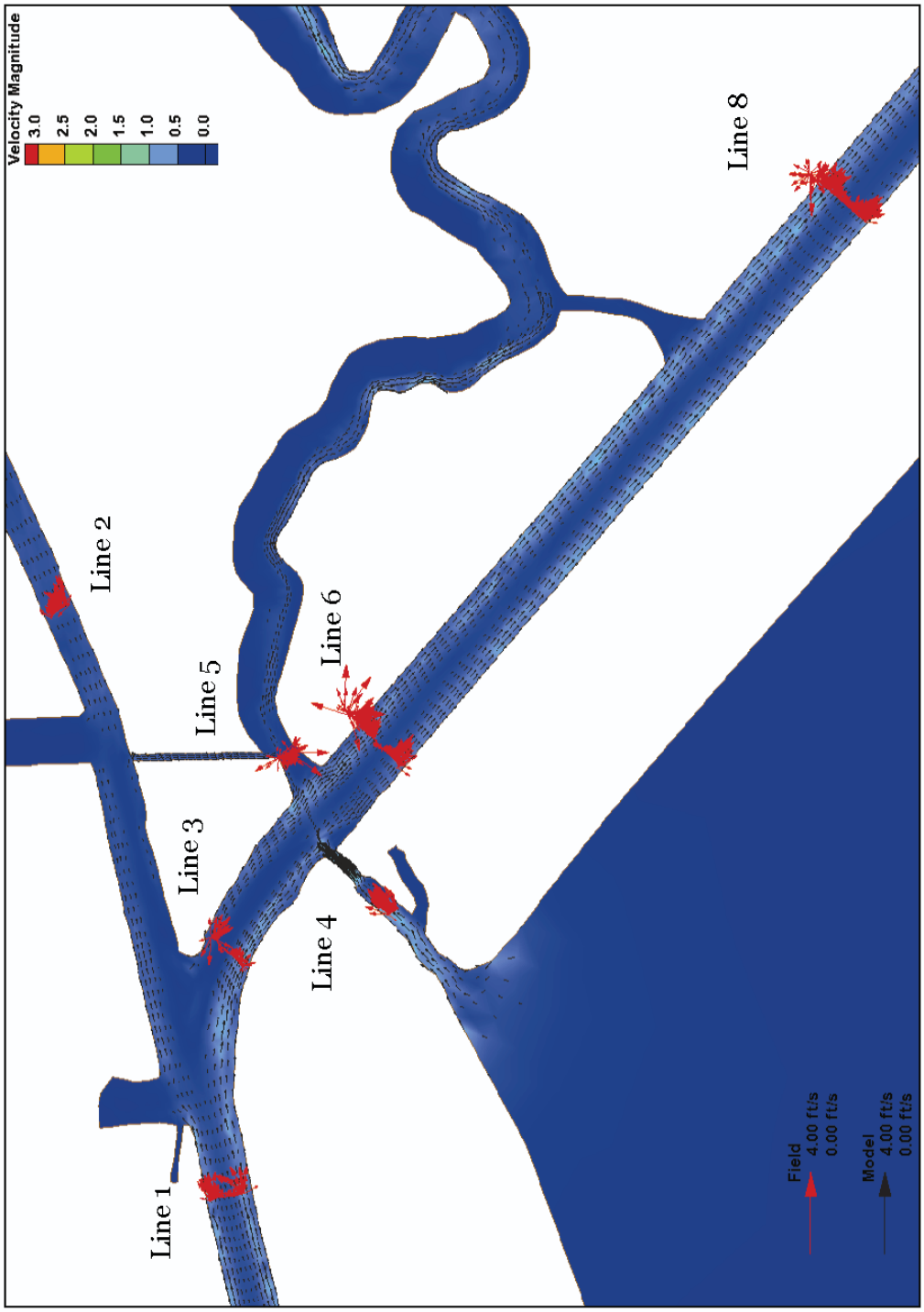

Figure 3-30. GIWW/MRGO velocity on August 14, 2008 at 16:00.

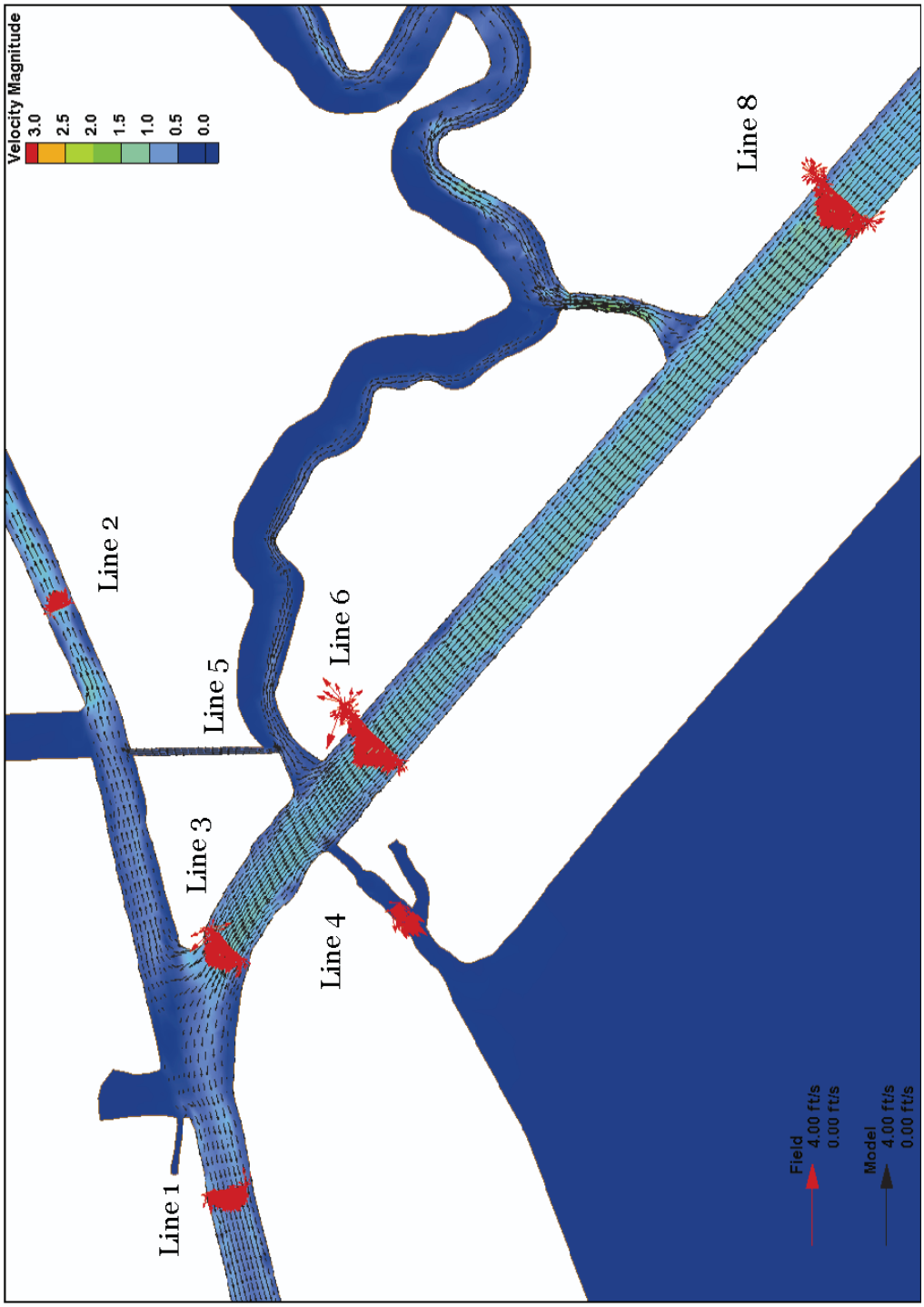

Figure 3-31. GIWW/MRGO velocity on August 14, 2008 at 6:00.

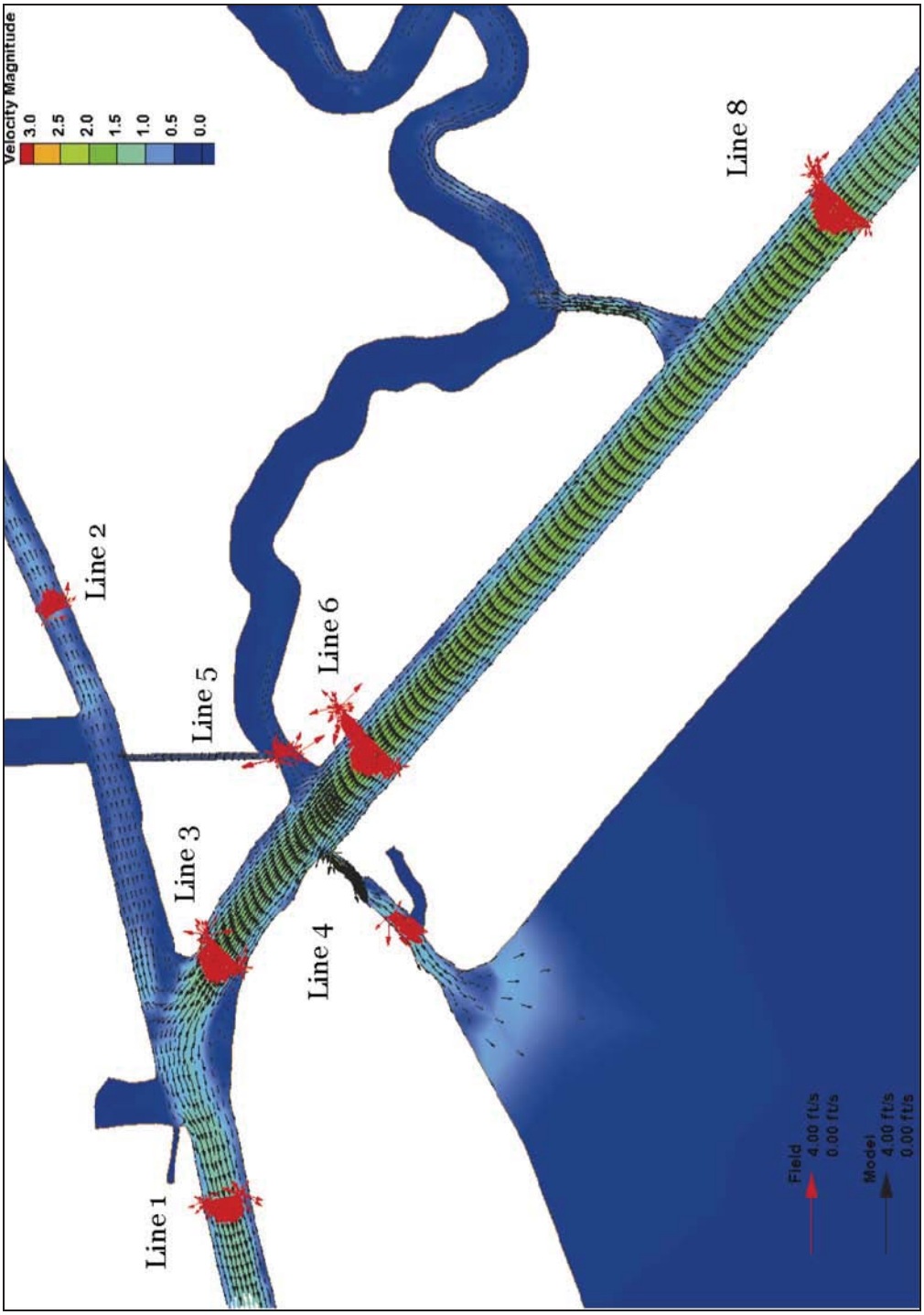

Figure 3-32. GIWW/MRGO velocity on August 14, 2008 at 9:00.

result of this simulation is given in the blue line in Figure 3-33. The details of the discharges through line 2 from Figure 3-3 change with this test, but the overall behavior does not.

A second test is performed in which the mesh boundaries along the banks of the GIWW are deepened to -8 ft. See Figure 3-34 for an illustration of this concept. If the model boundary is set at the intersection of the dashed line and the red line, the area in “A” is not accounted for. By deepening the model boundary, the area in “B” gets added to the model to account for that lost from “A”. If these depths are not selected carefully, the flow area can be misrepresented in the model. The green line in Figure 3-33 shows these results. The pink line is the base model results at line 2 (see Figure 3-3). Again, the details of the discharges through line 2 change with this test, but the overall behavior does not. The resilience of the model to these uncertainties in wind forcing and channel bathymetry, for example, thus supports its use in determining the way circulation will change when the new works, as described in the plans, are considered.

Summary

The validation of the model described above includes comparisons of model output to field data measurements for water surface elevation, discharge, and velocity at various locations within the study area. These comparisons were obtained after much testing of roughness parameters and checking of geometry, bathymetry, and boundary conditions. Given the available information of the system and the historically accepted range of roughness parameters, the parameter set used to generate the comparisons shown represents the best overall agreement to the field data. Now that the geometry and model parameters have been adjusted to give the best representation of the system, plan simulations and base/plan comparisons can be made using the validated model. For this project, hydrodynamic information will be used to drive a particle tracking model to simulate the movement of larval fish into the Lake Pontchartrain area with and without the planned hurricane protection measures.

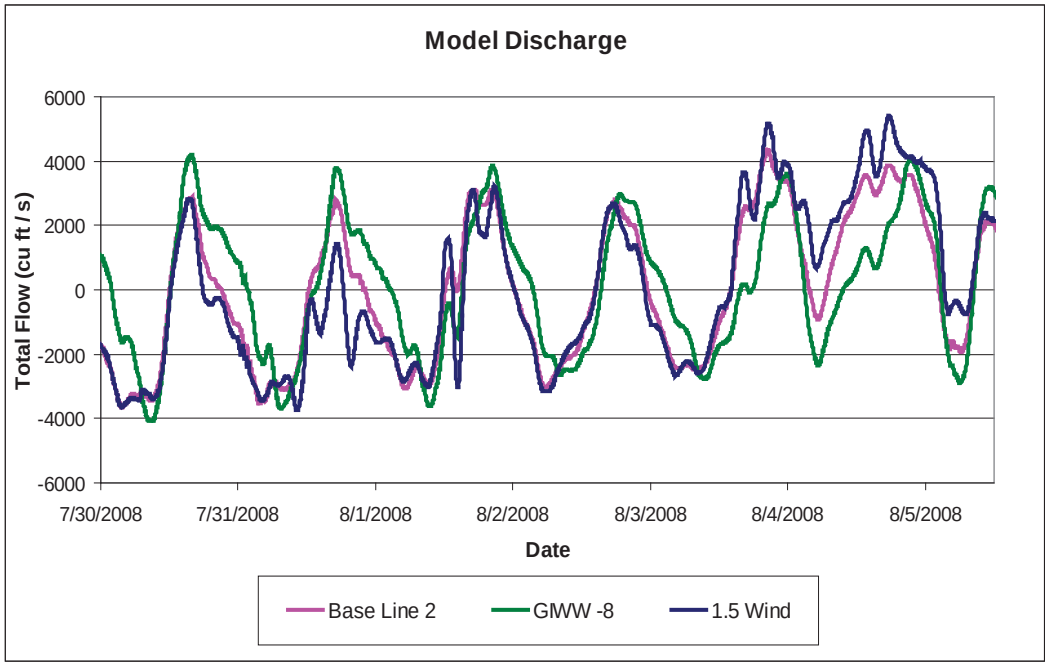

Figure 3-33. Sensitivity analysis results.

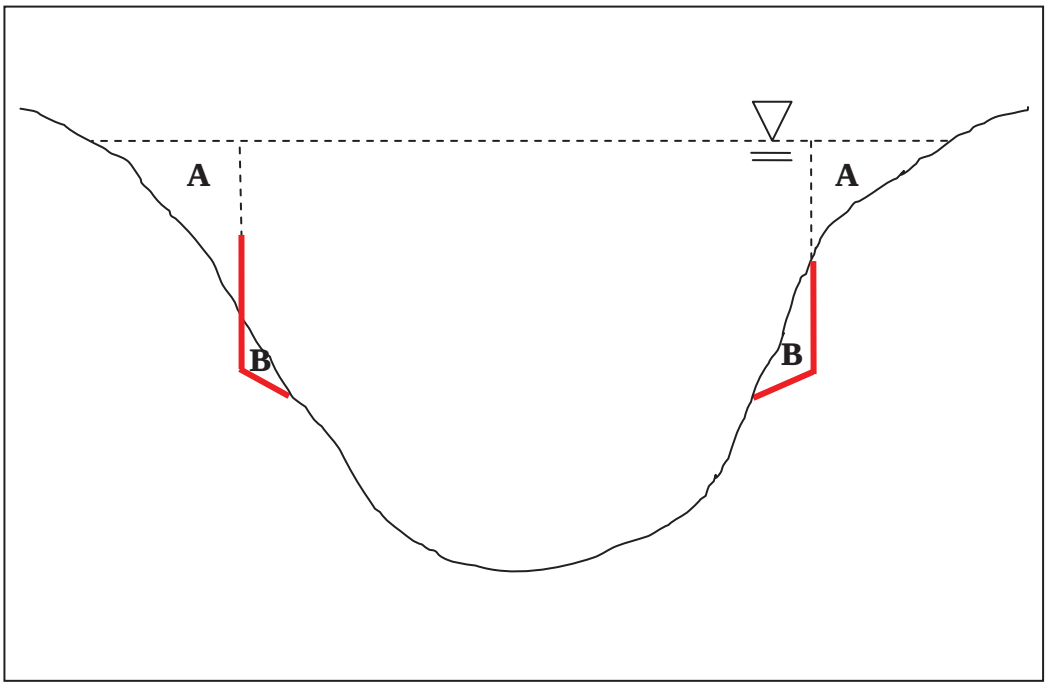

Figure 3-34. Flow area calculations.

4 Design Alternatives

The design alternatives are developed with the aim to reduce flooding in the region due to storm passage. The effect that these alternatives have on the larval fish then becomes a question of concern. Four alternatives and the base condition were chosen for testing with the particle tracking model. Much of the design process has focused on the effects of the plans on navigation and not with their effects on larval fish transport. These design alternatives are chosen based on previously planned navigation structures and changes to the system. They are organized into four plans as described below. For all structures, the sill elevation is -16 ft.

- Base - condition includes the fully open MRGO, GIWW, and IHNC (Figure 4-1)
- Plan 1 – close the MRGO at La Loutre (Figure 4-2)

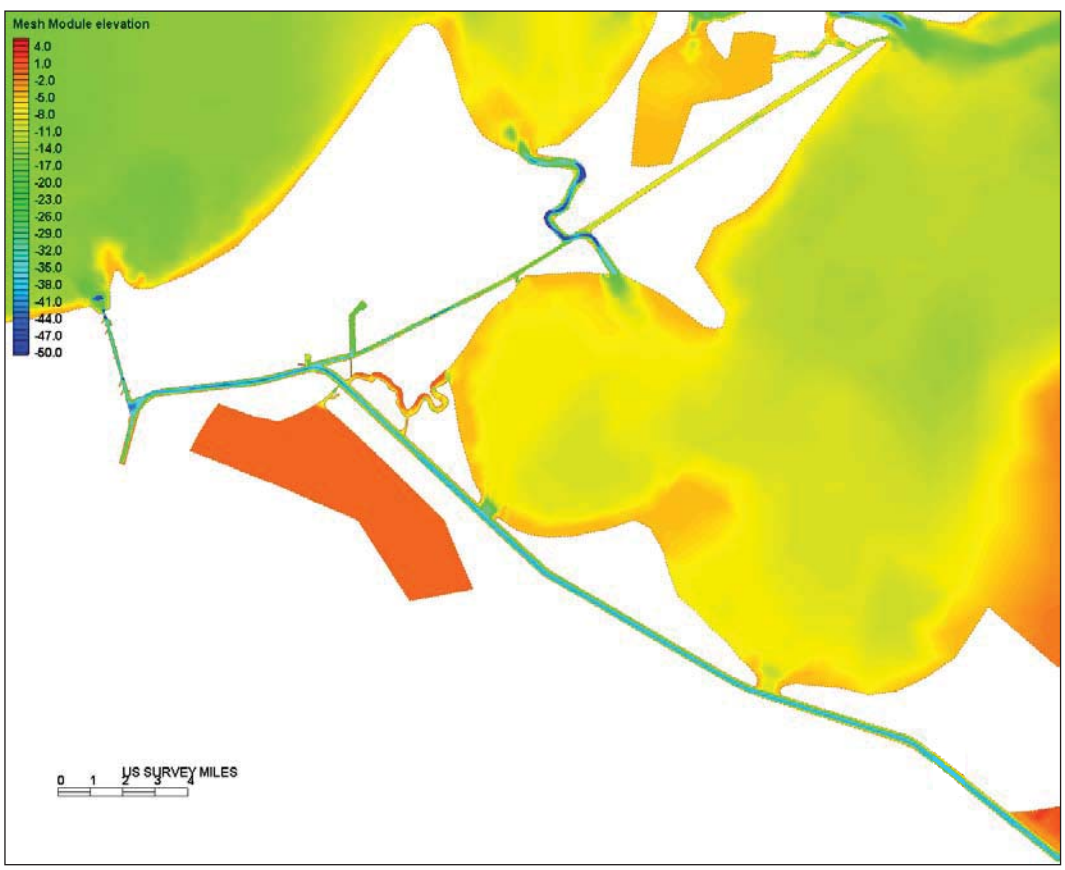

Figure 4-1. Base configuration: no closures, no structures (showing bathymetry where 0 equals NAVD88, 2004.65).

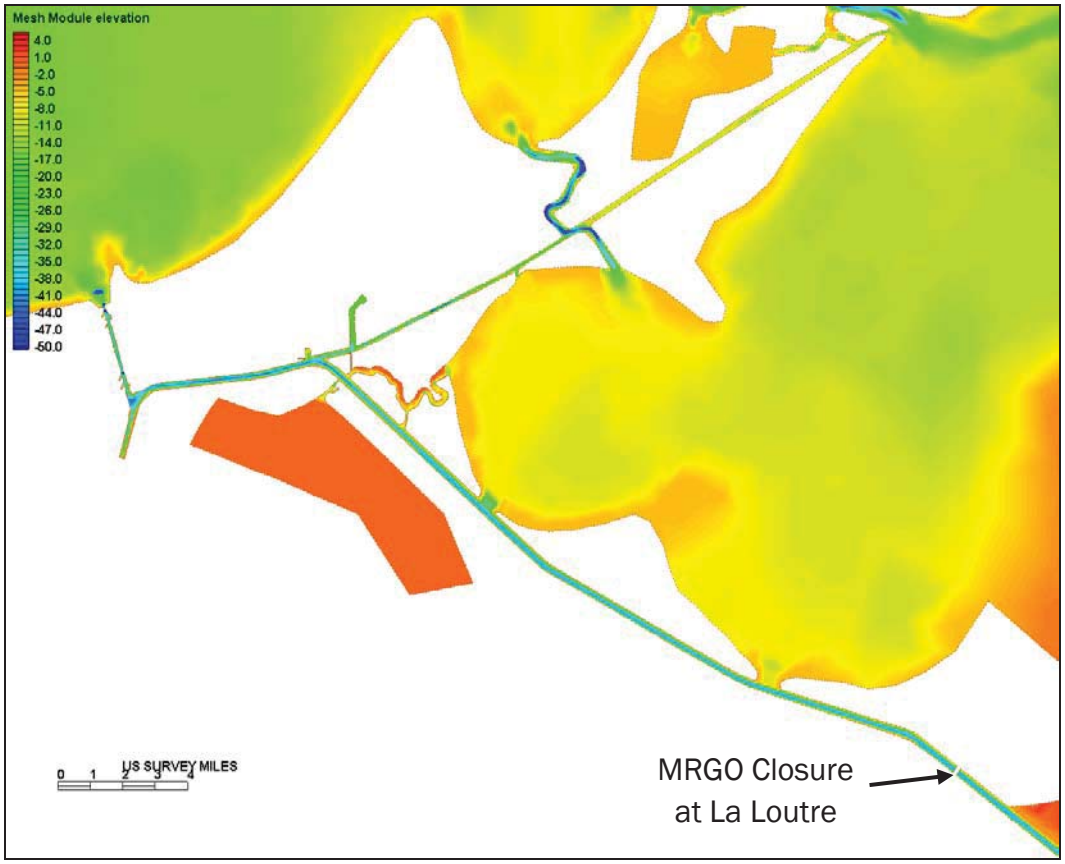

Figure 4-2. Plan 1 configuration: close the MRGO at La Loutre (showing bathymetry where 0 equals NAVD88, 2004.65).

- Plan 2 – close the MRGO at La Loutre, include the Borgne alignment (close the MRGO south of Bayou Bienvenue, 56 ft X 8 ft gate on Bayou Bienvenue, two 150 ft X 16 ft gates on GIWW) (Figure 4-3)
- Plan 3 – close the MRGO at La Loutre, include the Borgne alignment, include the 95 ft X 16 ft gate at Seabrook structure with southern scour hole filled (Figure 4-4)
- Plan 3 Final - close the MRGO at La Loutre, include the Borgne alignment, include the 95 ft X 20 ft sector gate at Seabrook with two flanking 50 ft X 16 ft auxiliary gates with southern scour hole filled (Figure 4-5)

The hydrodynamic and particle tracking simulations for the base condition and four plans are run for two different time periods. The analysis period was initially 2 weeks but extended to 4 weeks to get better, more representative results from the PTM simulations. A two week spin-up period is included in the hydrodynamic simulations prior to the analysis period such that a six week period is simulated with each model run. The two analysis time periods used for this study are August 15 – September 15, 2007

(labeled as September) and March 1 – 31, 2008. A general picture of the tidal signal near the Gulf boundary for these two time periods is shown in Figure 4-6 and the wind speeds at the New Orleans International Airport for these periods are given in Figure 4-7. It is apparent in these figures that the March winds and tide are indicative of the spring season when conditions are more erratic due to front passages and rain events. The September period shows lower wind speeds and a more typical diurnal tide signal which is expected in the Gulf of Mexico.

The proposed channel changes were incorporated in the computational mesh. After the hydrodynamic model was run for the two time periods using the tide, wind, and fresh water flows for the two simulation periods, the results were provided to the PTM effort. Additional hydrodynamic simulations were performed during the design process to test alternatives and analyze model sensitivities. These simulations and results are documented in Appendix A.

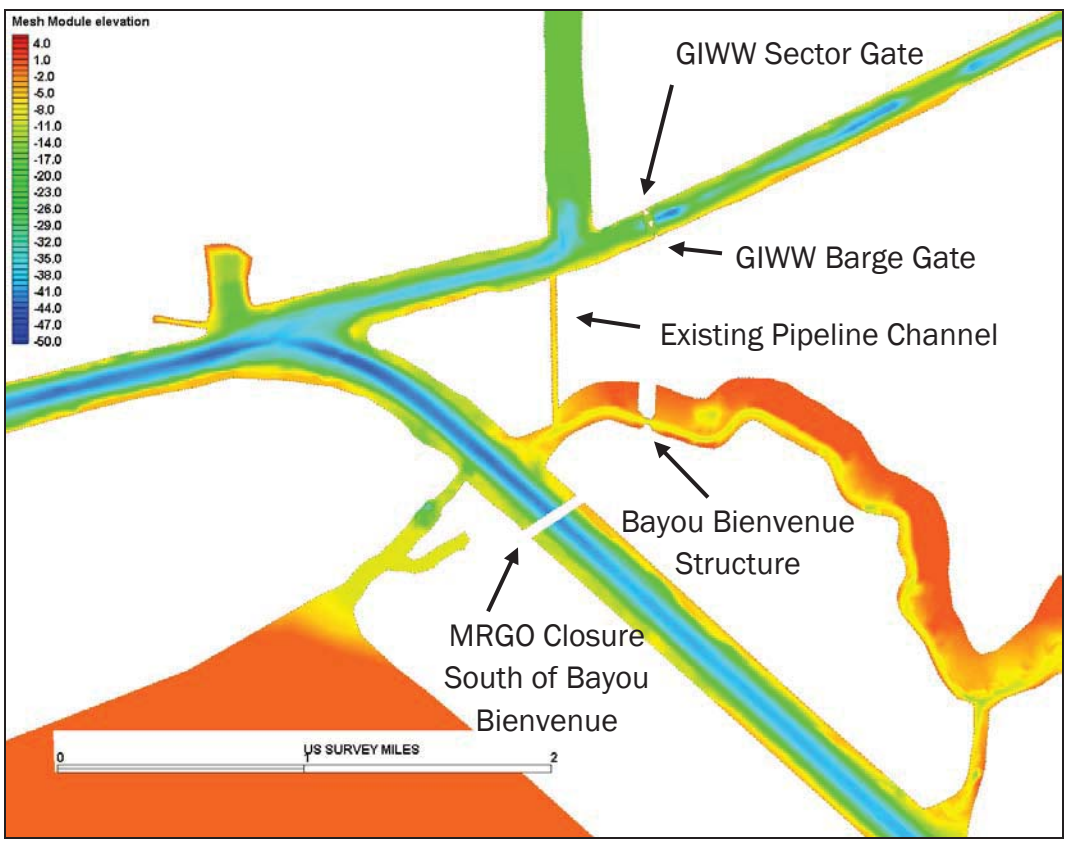

Figure 4-3. Plan 2 configuration: includes Plan 1 and the Borgne alignment (56 ft X 8 ft gate on Bayou Bienvenue, and two 150 ft X 16 ft gates on GIWW) (showing bathymetry where 0 equals NAVD88, 2004.65).

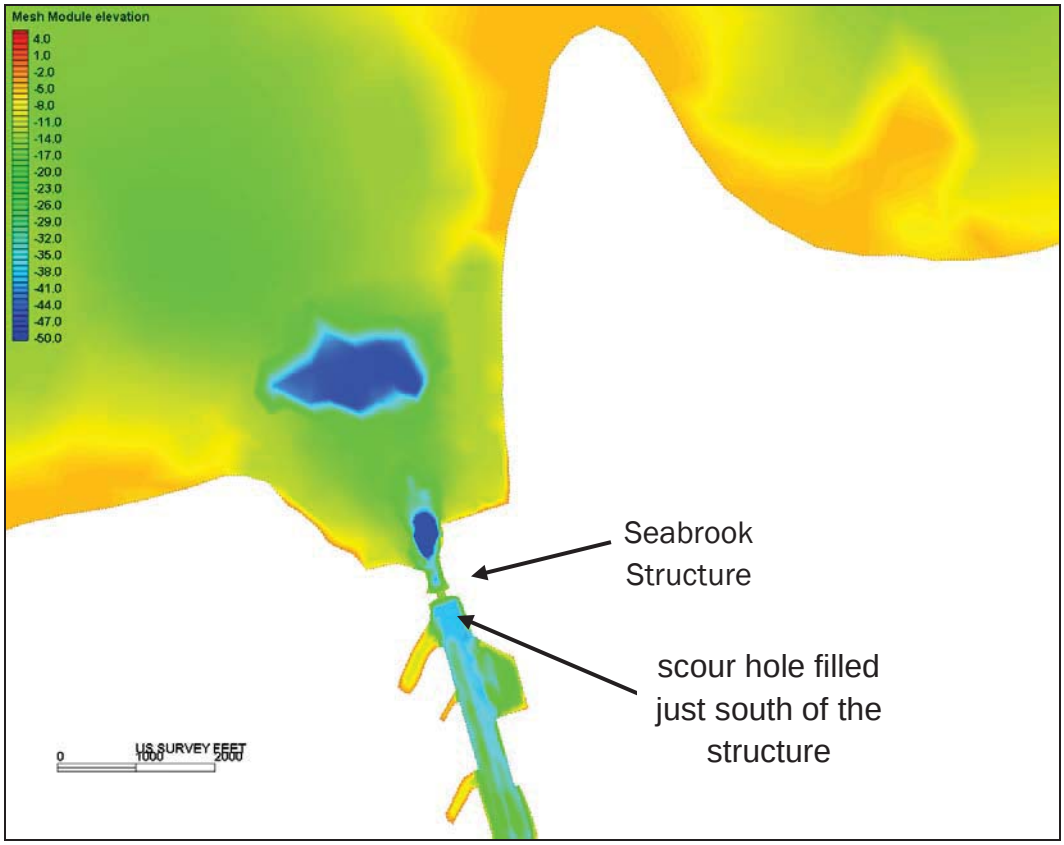

Figure 4-4. Plan 3 configuration: includes Plan 1, Plan 2 and a 95 ft X 16 ft structure at Seabrook (showing bathymetry where 0 equals NAVD88, 2004.65).

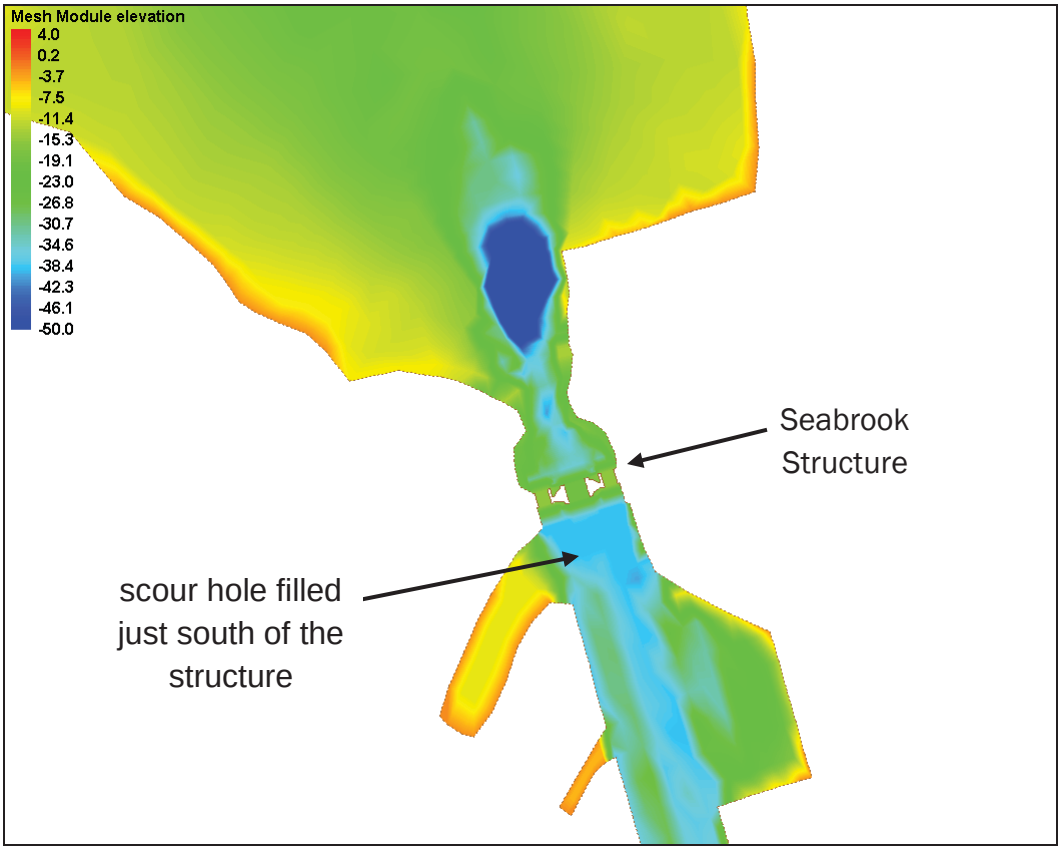

Figure 4-5. Plan 3 Final configuration: includes Plan 1, Plan 2 and a 95 ft X 20 ft sector gate with two side 50 ft X 16 ft auxiliary gates at Seabrook (showing bathymetry where 0 equals NAVD88, 2004.65).

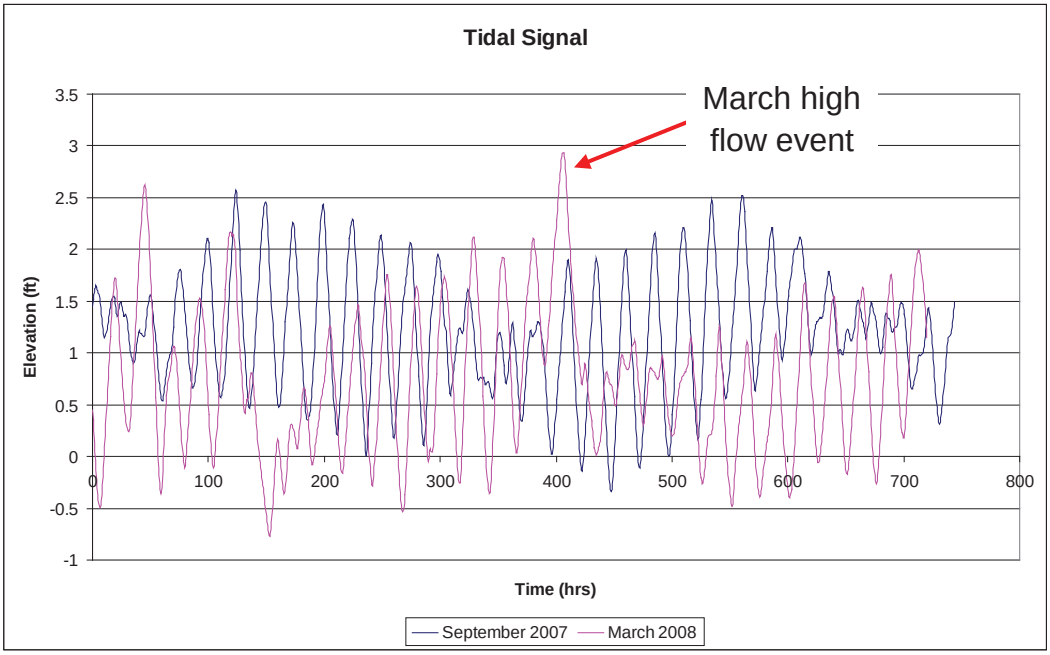

Figure 4-6. Tide signal for both four week analysis periods.

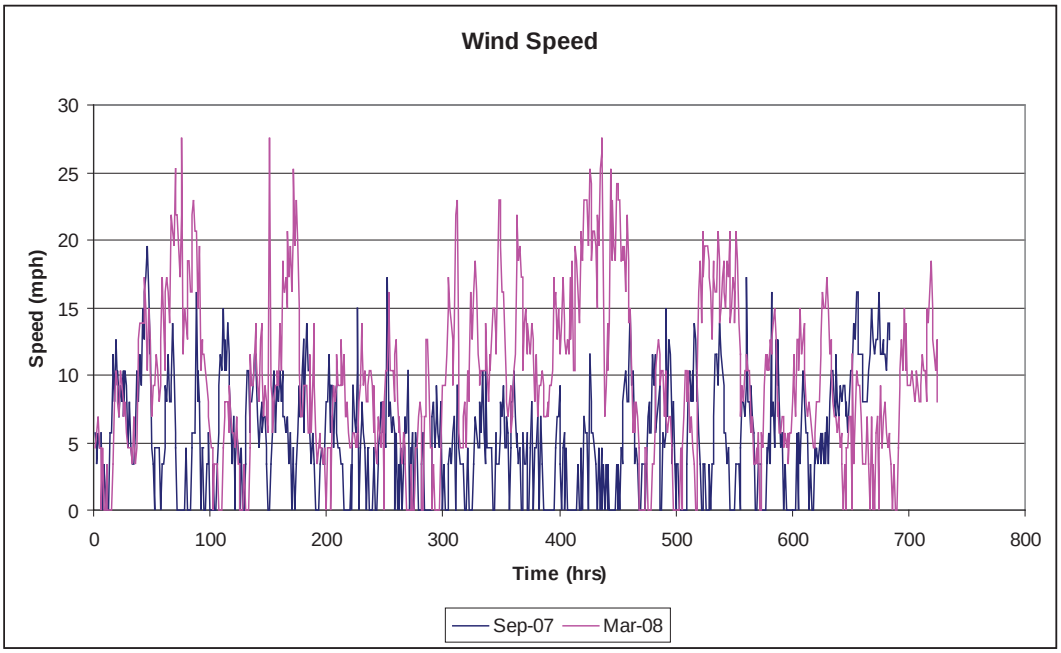

Figure 4-7. Wind signal for both four week analysis periods.

5 Larval Fish Transport

Larval fish transport for this project is simulated using the particle tracking model (PTM). This section gives a general background into PTM and discusses the algorithms added to PTM which pertain to larval fish transport. In addition, it gives the simulation details and all model input data. Simulation results based on these algorithms are shown in Chapters 7 and 8.

Background

PTM is an ERDC-developed model designed specifically to track the fate of point-source constituents (sediment, chemicals, debris, biologicals, etc) released from local sources (outfalls, dredges, etc) in complex hydrodynamic and wave environments (McDonald et al. 2006, Lackey and McDonald 2007, Lackey and Smith 2008). Each local source is defined independently and may have multiple constituents. Therefore, model results include the fate of each constituent from each local source. PTM simulates transport using pre-calculated periodically saved hydrodynamic (and wave) model output. The hydrodynamic model is not coupled to the transport model and therefore can be run once for multiple PTM simulations. Each particle in PTM represents a specific mass (or number of particulates) of one constituent. Total mass is conserved because particles are conserved, that is all particles that are created are accounted for through the simulation. Hydrodynamic output does not need to be conservative, so the user can specify hydrodynamic model output for PTM without concern for conservation of water mass. The ADH code used in this application, however, does conserve water mass. A random walk method is used to represent particle diffusion. PTM simulations can be either 3D or 2D. For 2D mode, the particle algorithms do not take into account the hydrodynamic vertical profile, but instead move vertically based on a centroid method. A detailed explanation of this method is described in McDonald et al. (2006). For the characteristic larval fish transport application, the 3D mode is used. Utilizing this method particles determine vertical flow changes based on given 3D hydrodynamics or if 2D hydrodynamic flowfields are given based on the 2D shallow water equations (as is the case for this work), a logarithmic profile is assumed in the vertical direction.

In addition to the hydrodynamic input (i.e. water surface elevation and velocities) that is used as a forcing for particle dynamics, PTM requires mesh and bathymetry information, and sediment characterization of the native or bed sediment. PTM also needs detailed constituent or source information. The user specifies particle characteristics and processes, including settling, critical stresses, and erosion rates. If processes data are not available, these values may be calculated within the model based on verified theoretical relationships. The specific equations for those processes are discussed in Appendix C and are described in further detail by McDonald et al. (2006). Particles can be positively, neutrally, or negatively buoyant. Positively buoyant, for example, would represent floating debris while neutrally buoyant may represent chemicals and negatively buoyant may represent sediment. In the case of larval fish modeling, particles are considered neutrally buoyant with additional characteristic larval fish behavior specified.

Model output includes time dependent particle positions throughout the domain. Various other attributes such as mass, density, and suspension status are also assigned to each of the output particles. Elevation in the water column is calculated and stored. PTM setup and execution are done within the ERDC-sponsored Surface Water modeling System (SMS) interface (McDonal et al. 2006). SMS includes multiple tools for post-processing PTM output to assess distribution of concentration, deposition, and other results at any time during the simulation. These results are processed for each constituent from each source or for combined constituents or sources.

Method

The particle tracking model is a Lagrangian particle tracker. Like most Lagrangian particle trackers, all transport is in the reference frame of the particle, ultimately solving a classic system of equations:

$$\frac{d\vec{x}}{dt} = \vec{u} \tag{1}$$

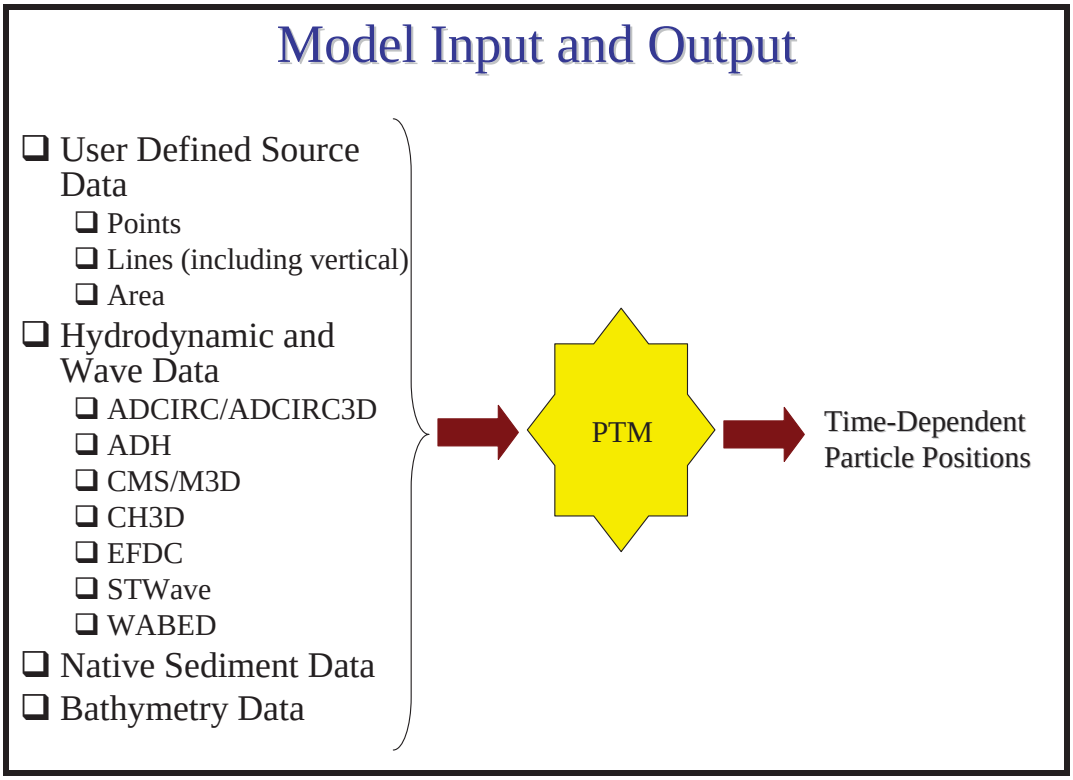

Figure 5-1. Description of the Particle Tracking Modeling input and output.

In this system, **x** is the particle position vector **x**=(x,y,z) and **u** is the flow field velocity vector **u**=(u,v,w). Numerically this system of equations can be discretely solved as:

$$\mathbf{x}^{n+1} = \mathbf{x}^{n} + \Delta t \vec{\mathbf{u}}^{n} \tag{2}$$

That is, the new position of a particle at time *n+1* is equal to the old position of a particle at time *n* added to whatever distance it traveled during a time step Δt. This distance is directly dependent on the velocity of the particle at that point. The solution to Equation (1) is applicable primarily to passive particles which are particles that have no real ability to affect their transport or have no additional transport dependencies such as mass or density effects. For most transport performed utilizing PTM, the equation becomes more complex:

$$\mathbf{x}^{n+1} = \mathbf{x}^{n} + \Delta t \mathbf{F}^{n} \tag{3}$$

where **F** is a function of the flow field velocity, diffusion, and multiple other processes. With regard to sediment, this includes settling, burial, etc.

However, for PTM larval fish modeling **F** is also a function of the expected behavioral characteristic of the larvae.

$$F(u) = u_{advection} + u_{diffusion} + u_{behavior} \tag{4}$$

For every time step, the model calculates for each particle the velocity due to advection, diffusion, and the larval fish velocity assigned to the particle due to the behavioral characteristic applied to the particle. The velocity due to advection is interpolated from the three surrounding mesh nodes of an element to the particle position within the element. The velocity due to diffusion is calculated via a random walk diffusion algorithm (McDonald et al. 2006).

Currently, PTM models transport for the following behaviors:

1. Tidal Lateral
2. Tidal Vertical
3. Diel Vertical
4. Bottom Movers
5. Top Movers
6. Passive

These behaviors were developed based up0n instructions from the Keith Lake fish passage study interagency team, as well as through the Seabrook larval fish transport interagency team.

Tidal Lateral

Tidal lateral behavior describes particles that will move laterally (horizontally) due to changes in the tide. In PTM, this means that, as the model perceives an incoming tide, particles move towards the maximum velocities. In most channels and rivers, this will be towards the center of the channel. During outgoing tide, particles move towards areas of minimum velocity.

Tidal Vertical

Tidal vertical behavior describes particles that will move vertically due to changes in the tide. In PTM this means that as the model perceives an incoming tide, particles move upwards in the water column. Incoming and outgoing tides are as defined in Chapter 7. For general flows that are fairly

uniform over the depth, higher velocities will occur at the top of the water column, and due to the logarithmic velocity profile, the velocities will decay to zero at the bed. During outgoing tide, particles move downwards towards the bed and areas of minimum velocity.

Diel Vertical

Diel Vertical behavior describes particles that will move vertically due to the time of day. Currently, this behavior is described as particles moving upwards during the daytime and downwards at nighttime. Daytime is currently set as 6am-6pm and nighttime is set as 6pm-6am.

Bottom Movers

Bottom movers are particles which stay in the lower 25cm of the water column. Currently, the particles are allowed to move freely by the flow until they move above the 25cm level in the water column. At this point, they are forced lower in the water column.

Top Movers

Top movers are particles which stay in the upper 25cm of the water column. Currently, the particles are allowed to move freely by the flow until they move below the 25cm level in the water column. At this point, they are forced higher in the water column

Passive Movers

Passive movers within the water column are moved only via advection and diffusion. These particles do not have any additional applied behavior.

Particle Velocity

For all particles that have applied behaviors, movement occurs based on a maximum velocity C_{max}. C_{max} is defined as 10mm/s. For Chapter 7 simulations, particle movement occurs at a decaying rate. Particles move towards their goal (i.e. the top or bottom of the water column, etc) at a rate of C_{max} when farthest from the goal. Upon reaching the destination, the velocity becomes zero. So for example, tidal vertical movers have a $u_{behavior}$ which is defined by:

$$u_{behavior} = C_{\max}\left(1 - \frac{P_{height}}{Depth}\right) \tag{5}$$

Here, P_{height} is the height of the particle above the bed and *Depth* is the total depth of the water. So as a particle moves upwards in the water column and P_{height} becomes equal to the total depth of the water column, the velocity contribution from the behavior goes to zero. However if the particle is at the bed, at the lowest percentage of the depth possible, the particle will travel at approximately $C_{max.}$ For Chapter 8 simulations, all particles except tidal lateral movers move at a constant rate C_{max}. Because of their interaction with the channel walls and to accommodate anchoring, tidal lateral particles decay as they reach the side.

Anchoring

Anchoring has been added to three of the particle behavior types for Chapter 8 simulation results: tidal lateral movers, tidal vertical movers, and bottom movers. This behavior allows particles to have a method of preventing themselves from being transported away from recruitment regions during the outgoing tide. As the tide comes in, a particle moves upward in the water column (to the top for tidal vertical movers, between 0.5 and 25cm from the bed for bottom movers). As the tide goes out, particles move towards the bottom. When a particle reaches the bottom it remains stationary until the next incoming tide.

To apply anchoring, an improvement in the implementation of the tidal flag was also needed. Within PTM a flag is required that signals to a particle that the tide is in or out. Originally, this signal was determined by focusing on the boundary condition of the flow coming in from the Gulf. By looking at a single position, the incoming tide was determined when the water surface elevation increased and the outgoing tide was determined as the water surface elevation decreased.

Now the determination of the incoming tide is more localized. Multiple positions have been chosen around the system. As a particle enters into the range of these locations, the particle references the signal (tide in or tide out) at that position. The tidal flag is determined by the circulation in an area. The tide is in when the flow is in the direction of the flow for incoming tide and the tide is out when the flow is in opposite direction. For a complex system, such as one in which the tidal direction is difficult

to establish, this may cause difficulties in accurately simulating the transport of larval fish. In the case of this study, efforts were made to take into account these difficulties by considering alternate tidal directions.

Limitations

PTM has several limitations. Because the model is not coupled with the hydrodynamics, there is an implicit assumption within the model that the particles do not affect the hydrodynamics. Therefore in cases where transported particles affect flow conditions, PTM should not be used or should be used with reservations. For sediment and contaminant transport, PTM does not model each and every individual grain of sand. Instead it models representative parcels. For this type of transport, steps must be taken to determine the number of particles which will sufficiently determine qualitative and quantitative trends.

There are also several limitations to the applied larval fish behaviors. The ultimate goal is to model the behavior of the larvae. However, even if it could be modeled in its entirety, larval behavior is not completely understood. Therefore, PTM is applied with the understanding that it is modeling particles that have the aforementioned characteristics and not actual larvae. That is, these particles do not die or consume or have many of the types of realistic life traits which may or may not affect the transport of living organisms. These particles have simplistic character traits which are suspected to affect transport and recruitment time. Analysis of model results must be addressed accordingly.

Another unknown is the validity of the value $C_{max.}$ The current value of 10mm/s is a best estimate due to knowledge of certain larvae species. A true parameterization of this quantity based on specific species and other conditions may eventually be added to the model.

Because of these limitations, the behavioral aspects of this model are still in development. As further information, algorithms, and behavioral catalysts are determined, larval transport characteristic behaviors will be improved. This means that while the model is useful to larval fish transport studies, these limitations should be taken into account during interpretation of results. There should also be an understanding that it might be impossible to model in its entirety the complex behavior of larval fish. Instead, the goal of this modeling effort is to determine the major

contributors to transport and focus on those characteristics to determine trends and effects.

Simulation Details and Model Input

The simulations for this study are designed to model pathways and recruitment rates for larval fish that migrate from the Gulf of Mexico into Lake Pontchartrain. Bathymetry and hydrodynamic data input have been described in detail within the previous chapters. Ten conditions, obtained from the ADH hydrodynamic computations, were utilized in the simulations. Two months (March 2008 and September 2007) are modeled to reflect the transport variations that can exist due to changes in the seasonal flows as well as five construction phases.

The simulations have been further categorized into four cases. Each case is distinguished by the initial position of the particles (Table 5-2). The details of these cases will be discussed in the following source input section. Four week simulations were run for each of the eight hydrodynamic conditions and cases. Particles are released and transported for a period of two weeks and then transported throughout the system for the remaining two weeks.

Table 5-1. List of species and representative behavior.

Species	Behavior
Blue Crab	Tidal Vertical
Brown Shrimp	Tidal Lateral
White Shrimp	Tidal Lateral
Gulf Menhaden	Tidal Lateral
Bay Anchovy	Tidal Lateral
Atlantic Croaker	Bottom Mover
Red Drum	Tidal Lateral
Spotted Sea Trout	Tidal Vertical

Four behaviors are modeled within the simulations. Three of these behaviors are representative of eight species (Table 5-1) determined to be relevant to the system. In addition, passive particles are also modeled to compare the effect of the behaviors.

Generally, native sediment data are important to sediment particle transport simulations. However, because these particles represent larval

fish behavior and particle-bed interactions are kept to a minimum, native sediment data are irrelevant to these computations.

Source Input

To simulate fish larval sources, PTM requires the following user specified data:

- ❑ Date/Time of source release
- ❑ Initial Positions (x,y,z) of source introduced into the water column
- ❑ Rate of source introduction
- ❑ Characteristic larval fish behavior

The date and time of the particle introduction to the system began at the beginning of each hydrodynamic condition. In this study, three cases are considered based on the initial positions of the particles. In all cases, sources are designed to release particles uniformly for the first two weeks of the four week period. This is at the beginning of the modeled hydrodynamic period (see Figure 4-6). In addition, larval fish behaviors are evenly distributed between the particles. Particles are placed vertically in the water column based on their representative behavior. Particles that represent bottom movers are introduced close to the bed. Particles that move laterally or vertically based on the tidal position, as well as passive movers, are initiated at the average depth of the flow. The rate of source introduction into the system is determined based on total number of particles simulated. For example, if 4800 particles are initiated over the two week time period, then approximately 342 particles are introduced into the flow field per day. The number of particles chosen for the simulations is based on numerical efficiency, statistical necessity, and visual information. Particles of all behaviors are introduced into the system concurrently.

Case 1

For case 1, particles are released to the east of the MRGO closure at La Loutre (Figure 5-2). Approximately 500 particles are released in this position during the first two week period of the four week simulation. Larval fish behaviors are evenly distributed between the particles. Figure 5-2 shows the approximate initial position (red circle) of the particles released in Case 1.

Table 5-2. Locations of polygon boundaries for initial particle positions for each case.

Case	Description of initial starting positions	X coordinate of Polygon in which particles are starting	Ycoordinate of Polygon in which particles are starting
1	Particles initiated in two locations (MRGO @ Bayou Bienevenue and GIWW@ constriction)		
	Location 1	1139268.00	169327.00
		1139315.80	169219.00
		1139458.60	169273.00
		1139405.80	169394.20
	Location 2		
		1137982.00	166224.00
		1138031.00	166125.00
		1138198.70	166269.20
		1138120.00	166362.00
2	Particles initiated in one location (MRGO @ La Loutre)	1170600.00	145890.00
		1170600.00	145690.00
		1170800.00	145600.00
		1170800.00	145780.00
3	Particles initiated in one location (Lake Borgne)	1151870.00	170830.00
		1149610.00	171360.00
		1147090.00	171580.00
		1145130.00	170260.00
		1143820.00	168460.00
		1143370.00	167070.00
		1143480.00	165340.00
		1144270.00	163080.00
		1145510.00	161430.00
		1147200.00	160860.00
		1149570.00	160940.00
		1149570.00	161580.00
		1147730.00	161650.00
		1145890.00	162180.00
		1144680.00	164060.00
		1144040.00	165750.00
		1144460.00	168160.00
		1146490.00	170260.00
		1148290.00	170640.00
		1150550.00	170380.00

Case 2

Due to complexities that will be described in the results section, additional initial conditions were chosen for Case 2 closer to the MRGO Bayou Bienvenue closure and the GIWW constriction (see Figure 5-3). For these simulations 4800 particles are modeled. Particles initiated in the GIWW are placed directly to the northeast of the constriction and particles initiated in the MRGO are placed directly southeast of the 2nd MRGO closure.

Case 3

Case 3 introduces particles within Lake Borgne. These particles are representative of an alternate path (in addition to the MRGO) through which larval fish are expected to enter the system. Approximately 700 particles are introduced into the system. Several different positions within Lake Borgne were considered. Initially, particles were placed very close to the connection between Lake Borgne and the GIWW. It was determined that this skewed the results, suggesting that the preferred pathway between Lake Borgne and the Lake Pontchartrain recruitment regions was that connection. Particles were also initiated in the center of Lake Borgne, but statistically relevant recruitment results were difficult to

Figure 5-2. Case 1 initial positions are designated by the red circle.

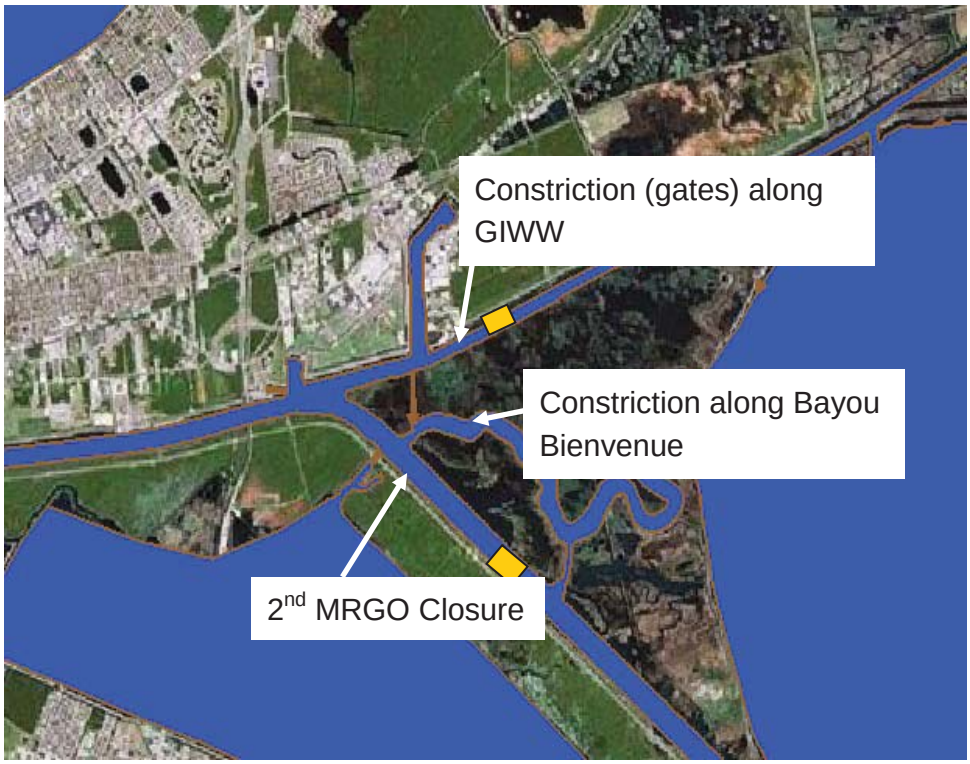

Figure 5-3. Locations of areas in which larvae are initiated for case 2. Yellow colored rectangles represent the locations of initial positions.

attain utilizing those conditions. That is, not enough particles were able to exit Lake Borgne and subsequently be recruited to determine the effect of the construction phases within the simulation time frame. Finally, the conditions seen in Figure 5-4 were developed. Here particles are initiated in a semi circular band along the edges of Lake Borgne, representing the paths that particles would take to exit the lake without skewing the results towards any one specific outlet.

Case 4

The particle source for this case is similar to that of case 2. However, in case 2 there are two source locations. For the case 4 set of simulations, one location (near the 2nd MRGO closure) has been removed (see Figure 5-5). In case 4, approximately 2150 particles are released from the GIWW source over a two week period. Particles are then transported for an additional two weeks. The four behaviors are distributed evenly between the particles. In addition, tidal vertical movers and bottom movers have anchoring. Tidal lateral movers and passive movers have no anchoring.

Figure 5-4. Location of areas in which larvae are initiated for case 3. Orange colored region represents the location of initial positions.

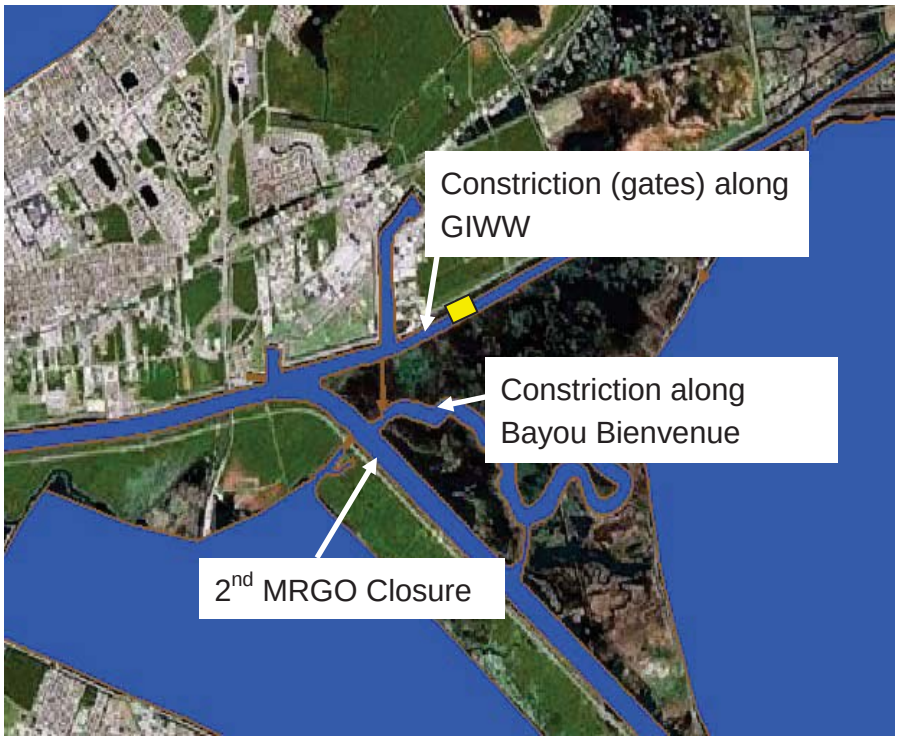

Figure 5-5 Location of area in which larvae are initiated in case 4. Yellow colored rectangle represents the location of initial positions.

Recruitment Regions

A major component of this project is to compare the rate at which larval fish are recruited based on the changes due to the design phase. In this

case the term “recruited” refers to particles reaching a position in which they are considered in or near their optimum environmental area where they can then develop into adults. There are two recruitment positions within this system. As shown in Figure 5-6, the first recruitment position is the Seabrook recruitment area (R1). To reach this zone, the particles have to pass through the Seabrook construction area. The second recruitment position is the Chef Menteur recruitment area (R2).

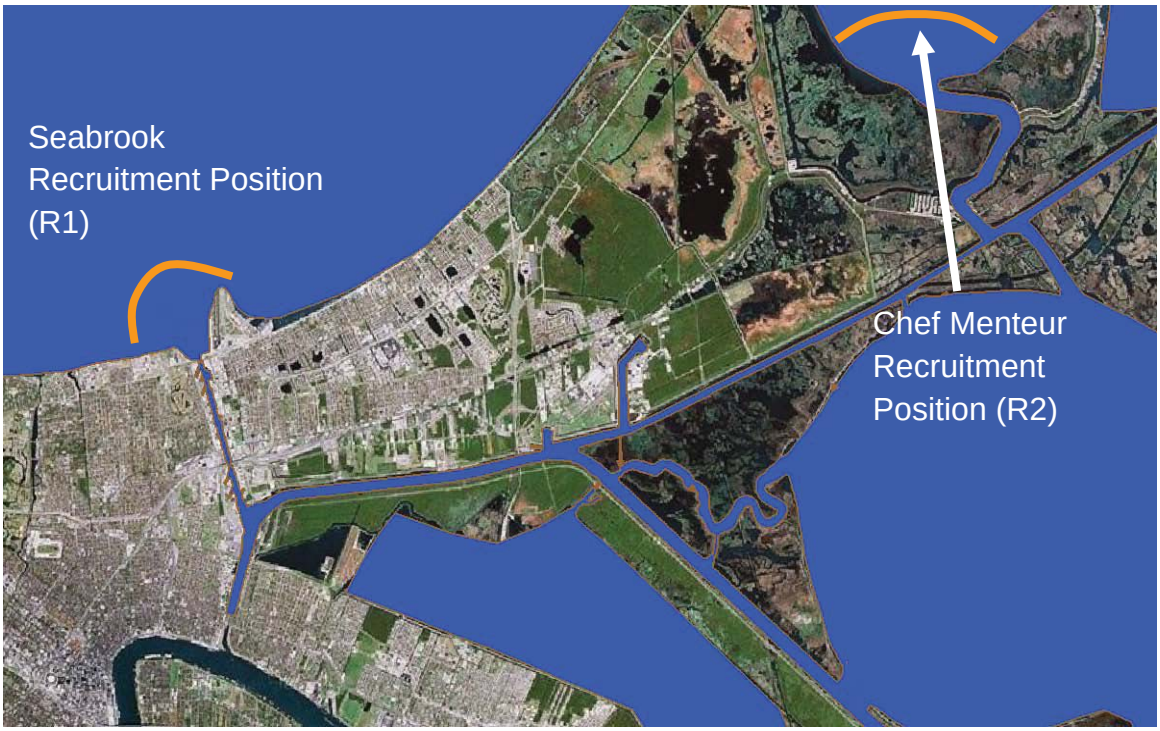

Figure 5-6. Locations of larval fish recruitment regions. Larvae that reach these areas are considered recruited.

PTM models the recruitment areas using a computational trap. Numerically this is a horizontal arc that is then projected downward through the water column. If particles pass through this arc anywhere within the water column, they are considered recruited. For computational efficiency, once a particle is considered recruited it is removed from the calculations and no longer appears visually in particle position results.

6 Hydrodynamic Results

The results of the hydrodynamic simulations are supplied to the particle tracking model to drive the transport. An analysis of how the plan conditions affect the velocities and water surface elevations in the area of the structures is given in this section as is a discussion of the circulation changes that result due to the plan conditions.

Velocity Magnitudes

Velocity data were taken in the location of the structures for the Bayou Bienvenue structure, the GIWW sector gate, the GIWW barge gate, and the Seabrook structure for analysis of how the plan conditions affected the velocities and water surface elevations. Figures 6-1 and 6-2 show these locations. For the base condition and Plans 1 and 2, data are analyzed at a location north of the Seabrook structure location where the velocities are greatest. The analysis for Plan 3 and Plan 3 Final is at the location in each Seabrook structure where the velocity magnitudes are also the greatest. For Plan 3 Final, this location is in the center sector gate. The chosen location of the analysis is the position which yields the velocity maximum for each plan. It is important to keep in mind that velocities will increase when the cross-sectional area is reduced given the same flux due to continuity. Although the changes to the system do change the flux passing through the structures, the ratio of the two fluxes is not constant and therefore, once a structure is in place at these locations, it is not unlikely that the velocity magnitudes will rise within the structure. In other words, the changes to the cross sectional area due to the structures are not the only factor changing in the flux equations.

The average velocities for flood and ebb over the four week analysis period are determined at each location and time period for the base and four plans as are the maximum velocities for all conditions. Since there is a circulation within this system through the GIWW, the definition of flood and ebb can be misleading. For this reason a definition of positive and negative or flood and ebb is necessary. Positive values are defined as those directed predominantly toward the north or east and negative values are defined as those directed predominantly toward the south or west. The

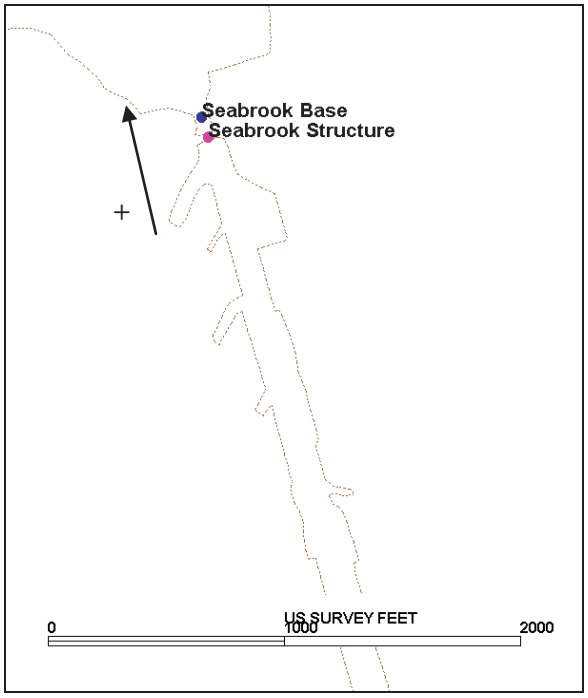

Figure 6-1. Hydrodynamic analysis locations – Seabrook.

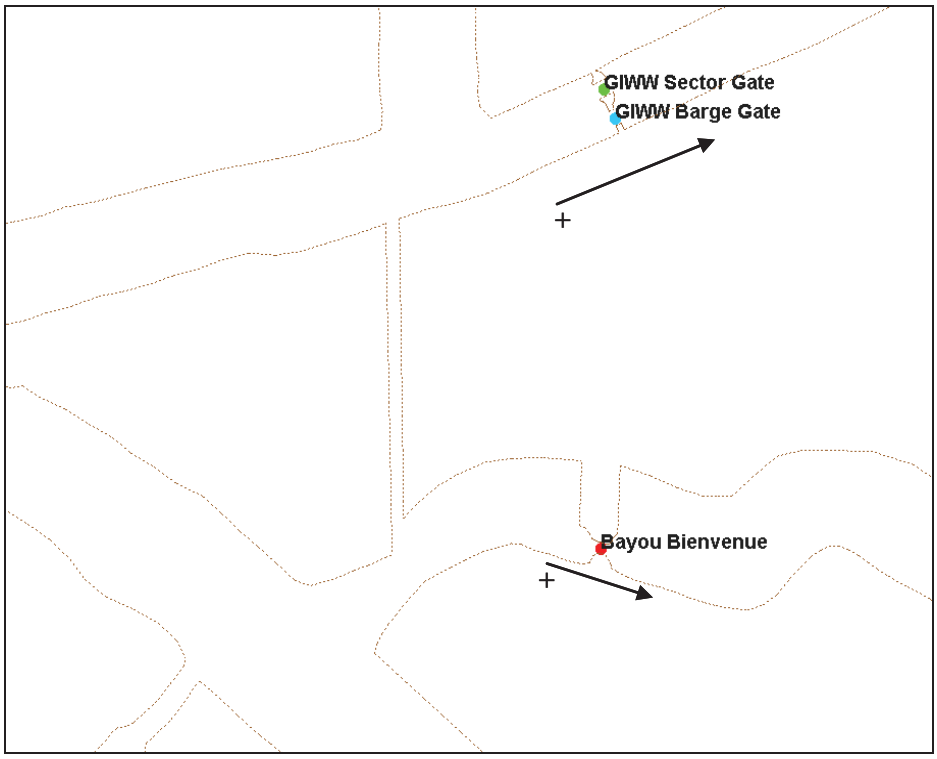

Figure 6-2. Hydrodynamic analysis locations – Bayou Bienvenue Structure, GIWW Sector Gate, and GIWW Barge Gate.

arrows in Figures 6-1 and 6-2 show the positive direction for each location. The results of this analysis are given in Figures 6-3 through 6-10. A direction arrow is included for each location to help define the flow direction.

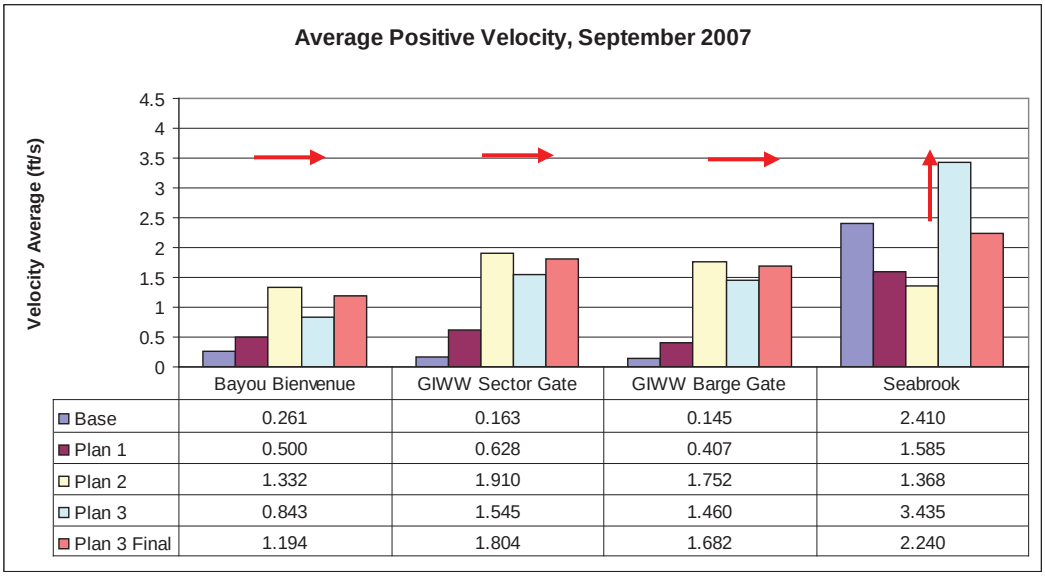

	Bayou Bienvenue	GIWW Sector Gate	GIWW Barge Gate	Seabrook
Base	0.261	0.163	0.145	2.410
Plan 1	0.500	0.628	0.407	1.585
Plan 2	1.332	1.910	1.752	1.368
Plan 3	0.843	1.545	1.460	3.435
Plan 3 Final	1.194	1.804	1.682	2.240

Figure 6-3. Velocity average for September (positive).

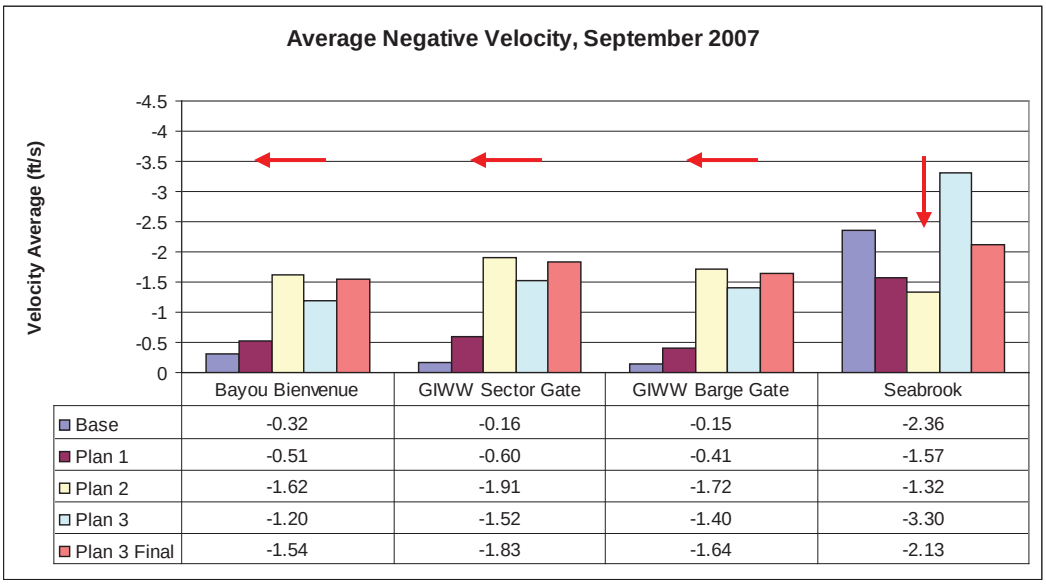

	Bayou Bienvenue	GIWW Sector Gate	GIWW Barge Gate	Seabrook
Base	-0.32	-0.16	-0.15	-2.36
Plan 1	-0.51	-0.60	-0.41	-1.57
Plan 2	-1.62	-1.91	-1.72	-1.32
Plan 3	-1.20	-1.52	-1.40	-3.30
Plan 3 Final	-1.54	-1.83	-1.64	-2.13

Figure 6-4. Velocity average for September (negative).

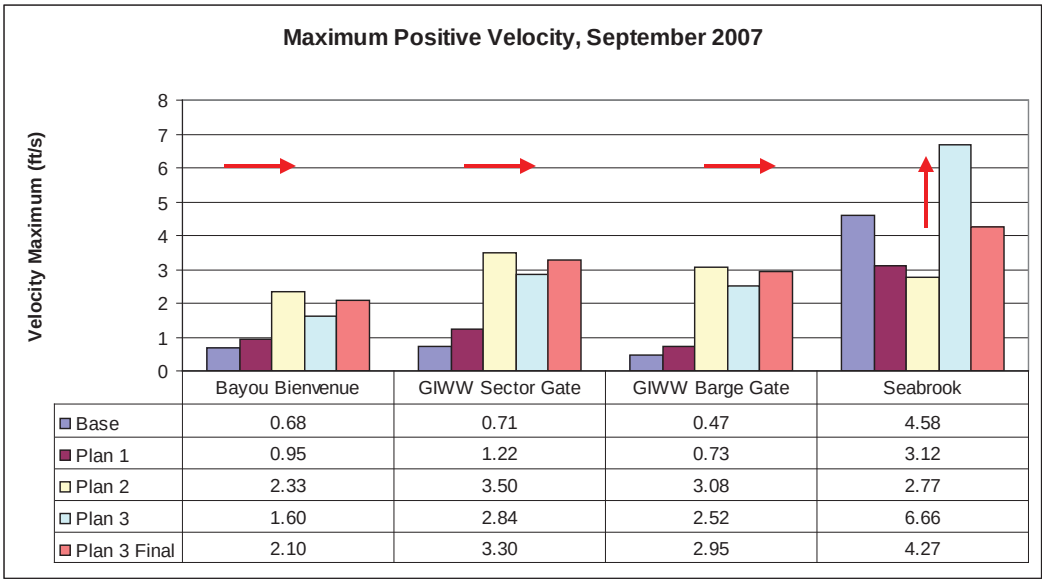

	Bayou Bienvenue	GIWW Sector Gate	GIWW Barge Gate	Seabrook
Base	0.68	0.71	0.47	4.58
Plan 1	0.95	1.22	0.73	3.12
Plan 2	2.33	3.50	3.08	2.77
Plan 3	1.60	2.84	2.52	6.66
Plan 3 Final	2.10	3.30	2.95	4.27

Figure 6-5. Velocity maximum for September (positive).

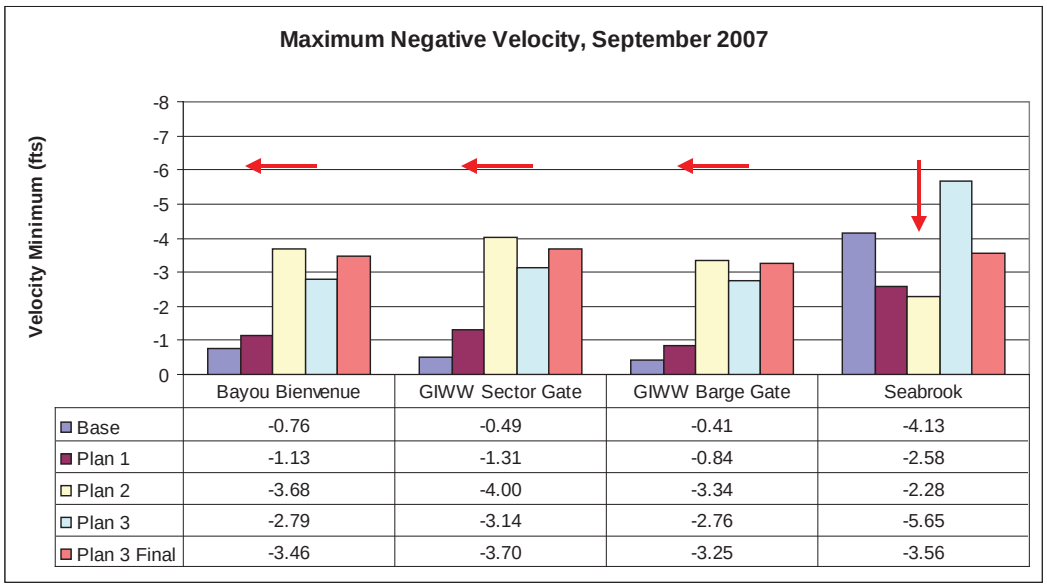

	Bayou Bienvenue	GIWW Sector Gate	GIWW Barge Gate	Seabrook
Base	-0.76	-0.49	-0.41	-4.13
Plan 1	-1.13	-1.31	-0.84	-2.58
Plan 2	-3.68	-4.00	-3.34	-2.28
Plan 3	-2.79	-3.14	-2.76	-5.65
Plan 3 Final	-3.46	-3.70	-3.25	-3.56

Figure 6-6. Velocity minimum for September (negative).

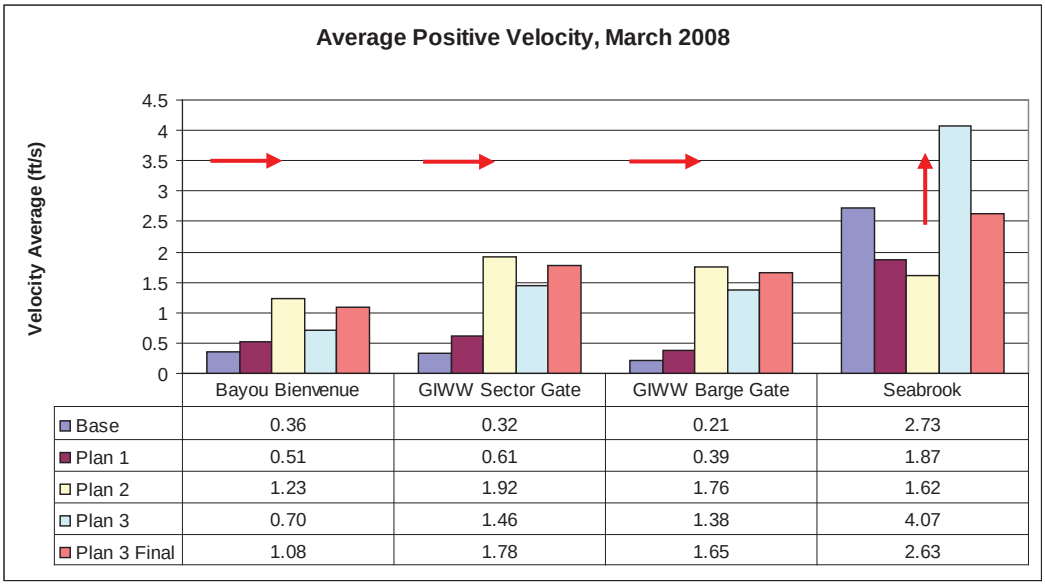

	Bayou Bienvenue	GIWW Sector Gate	GIWW Barge Gate	Seabrook
Base	0.36	0.32	0.21	2.73
Plan 1	0.51	0.61	0.39	1.87
Plan 2	1.23	1.92	1.76	1.62
Plan 3	0.70	1.46	1.38	4.07
Plan 3 Final	1.08	1.78	1.65	2.63

Figure 6-7. Velocity average for March (positive).

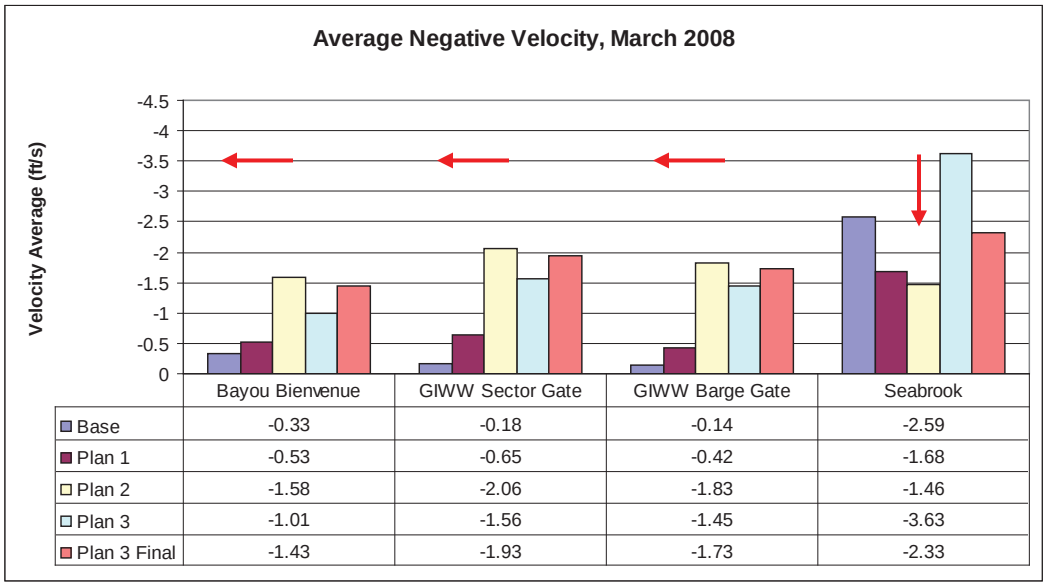

	Bayou Bienvenue	GIWW Sector Gate	GIWW Barge Gate	Seabrook
Base	-0.33	-0.18	-0.14	-2.59
Plan 1	-0.53	-0.65	-0.42	-1.68
Plan 2	-1.58	-2.06	-1.83	-1.46
Plan 3	-1.01	-1.56	-1.45	-3.63
Plan 3 Final	-1.43	-1.93	-1.73	-2.33

Figure 6-8. Velocity average for March (negative).

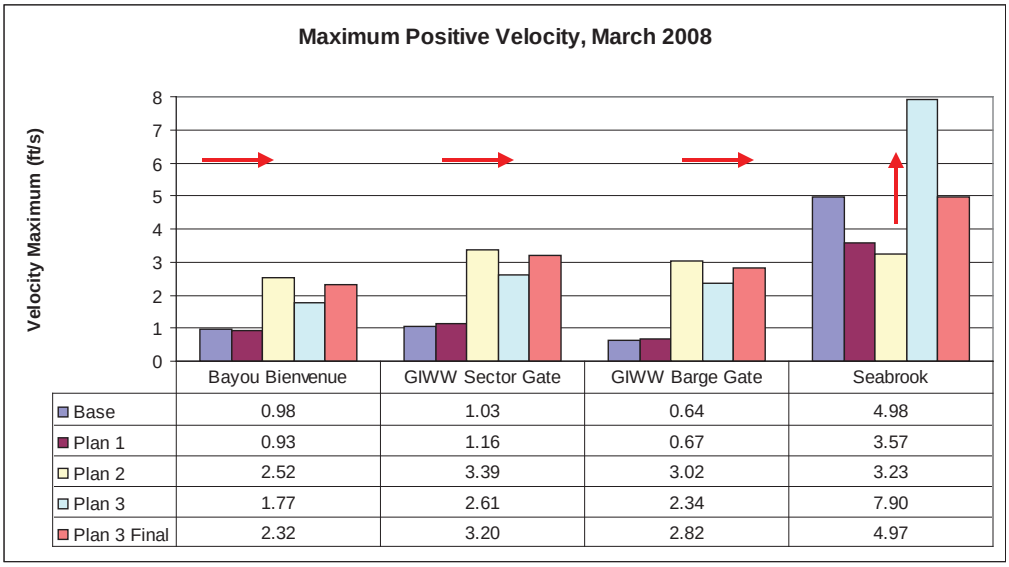

	Bayou Bienvenue	GIWW Sector Gate	GIWW Barge Gate	Seabrook
Base	0.98	1.03	0.64	4.98
Plan 1	0.93	1.16	0.67	3.57
Plan 2	2.52	3.39	3.02	3.23
Plan 3	1.77	2.61	2.34	7.90
Plan 3 Final	2.32	3.20	2.82	4.97

Figure 6-9. Velocity maximum for March (positive).

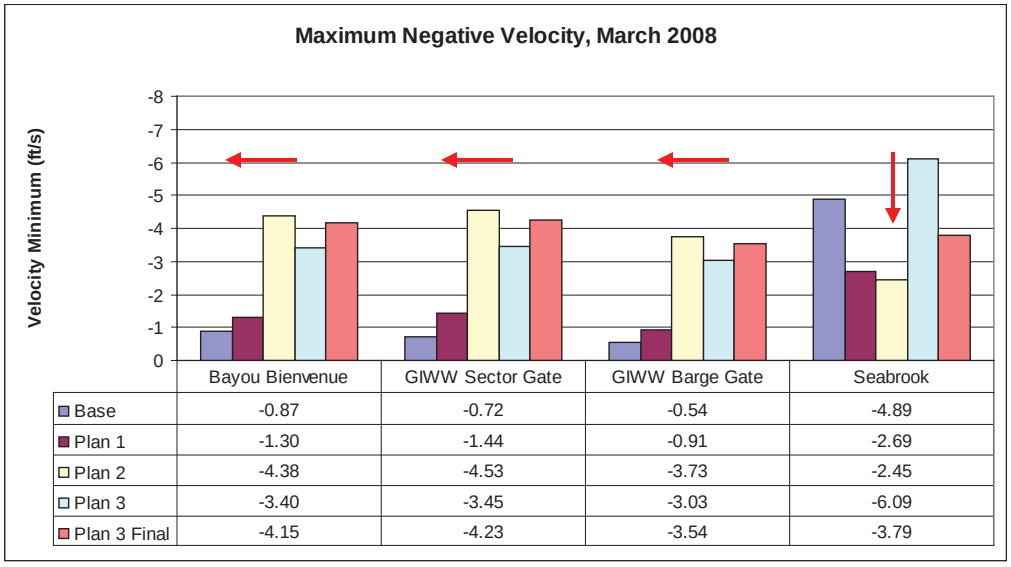

	Bayou Bienvenue	GIWW Sector Gate	GIWW Barge Gate	Seabrook
Base	-0.87	-0.72	-0.54	-4.89
Plan 1	-1.30	-1.44	-0.91	-2.69
Plan 2	-4.38	-4.53	-3.73	-2.45
Plan 3	-3.40	-3.45	-3.03	-6.09
Plan 3 Final	-4.15	-4.23	-3.54	-3.79

Figure 6-10. Velocity minimum for March (negative).

These figures show that the March conditions for the base case generally produce higher velocity magnitudes than the September conditions, although these differences are not great. This is due, primarily, to the strong tides of the March period. Due to the high flow event that occurs around mid-March (see Figure 4-6), the extreme velocity magnitudes will be higher for the March simulations.

In the Plan 1 condition, the MRGO is closed at La Loutre, and the velocity increases in the GIWW and Bayou Bienvenue structure locations as compared to the Base for both September and March. The velocity at the

GIWW and Bayou Bienvenue structure locations increases again with the inclusion of the Plan 2 structures, although by a much greater fraction due to the structures being applied at these locations. The velocities at these locations then drop when the Seabrook structure is included with Plan 3. These structures, individually and collectively, restrict the transport of water in the GIWW, the IHNC, and Bayou Bienvenue. Plan 3 Final allows for increased flows through the GIWW structures for the same reason Plan 3 reduces the flows: the addition of more conveyance area partly undoes the earlier effect of placing a structure at Seabrook. With Plan 3 Final there is more flow area so the exchange through the system of channels is larger when the three structures are included for flow passage instead of the single structure.

For March and September the velocities are highest at Seabrook for both the Base and Plan 3 configurations. The drop in velocity magnitude at Seabrook for Plans 1 and 2 is due primarily to the closure of the MRGO at La Loutre and the decreasing flow volume through the system of channels. With each closure of the MRGO (at La Loutre in Plan 1 and south of Bayou Bienvenue in Plan 2) the velocity drops at Seabrook. Once the Plan 3 structure is in place at Seabrook, these velocities increase simply due to the constriction created by the gate structure and reduction in cross-sectional area at Seabrook. However, Plan 3 Final results increased conveyance due to the increase in cross-sectional area from Plan 3 such that the velocities drop at Seabrook to values below those observed for the base condition.

These extreme velocity magnitudes, however, are simply that – a maximum value at some point during the simulation. They do not occur often during the simulation. A percent exceedance (i.e. percent less than) analysis is performed to determine how often during the four week simulation periods the velocity magnitudes are within certain ranges. Figures 6-12 through 6-28 show the percent less than plots for the locations given in Figure 6-11. These locations are the same as those in the previous velocity analysis (see Figures 6-1 and 6-2) as well as additional locations in Lake Borgne, Lake Pontchartrain, Chef Menteur, and the Rigolets. These plots show velocity magnitude on the x-axis and percentage of time on the y-axis. At the maximum velocity magnitude, the percentage is almost 100 since the velocity is less than this over the length of the simulation. All lines cross zero at 0% since the velocity magnitude is always greater than zero. Where each line crosses 50% the velocity is greater half the time and less half the time over the 4 week analysis period.

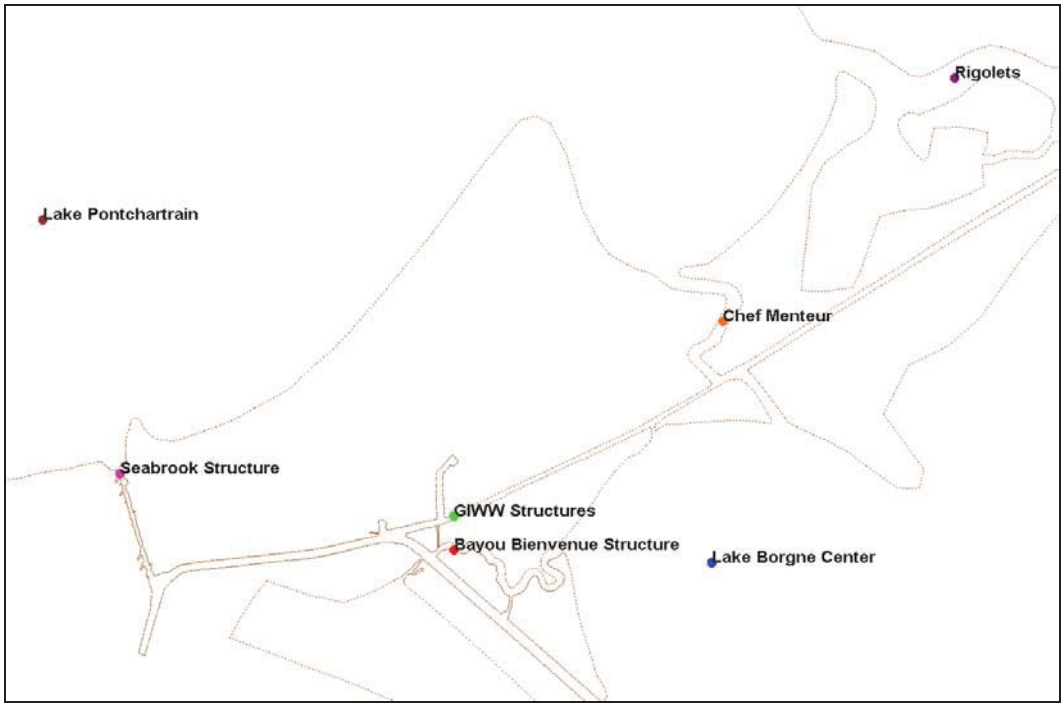

Figure 6-11. Percent less than of velocity magnitude analysis locations.

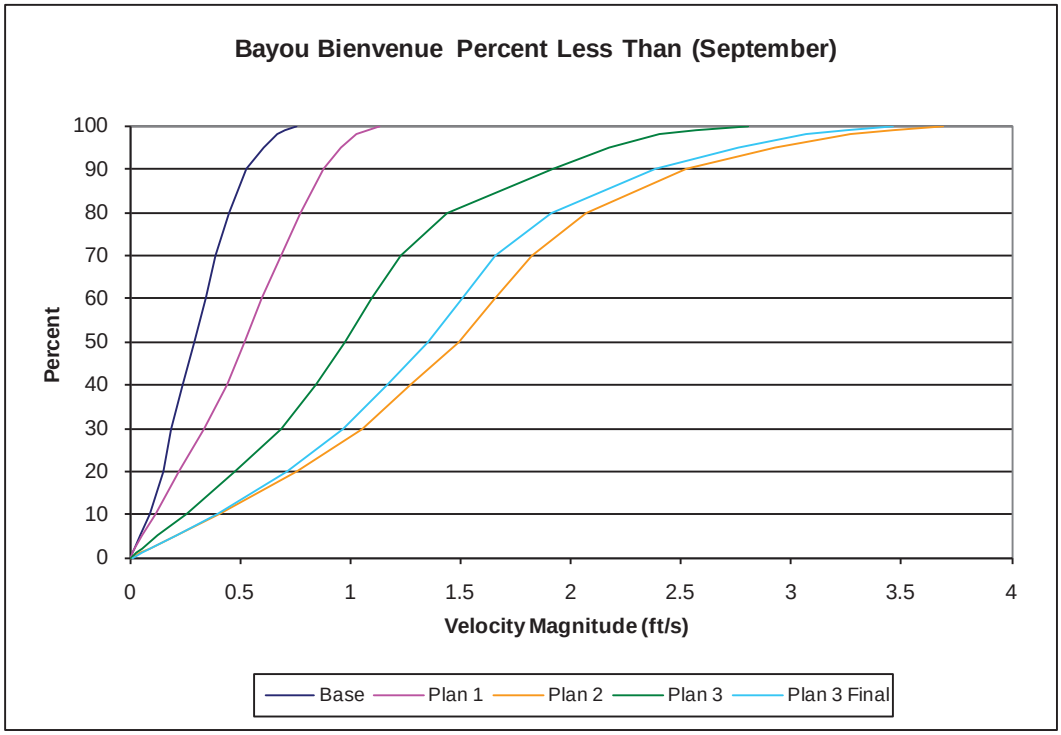

Figure 6-12. Bayou Bienvenue percent less than plot for September.

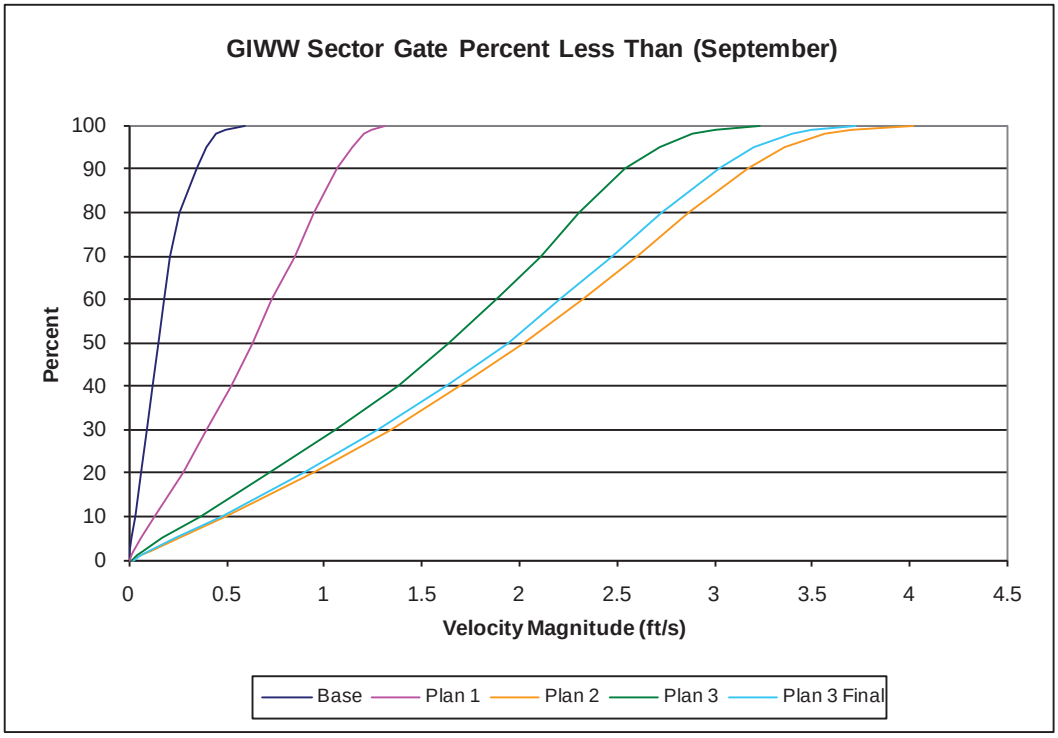

Figure 6-13. GIWW Sector Gate percent less than plot for September.

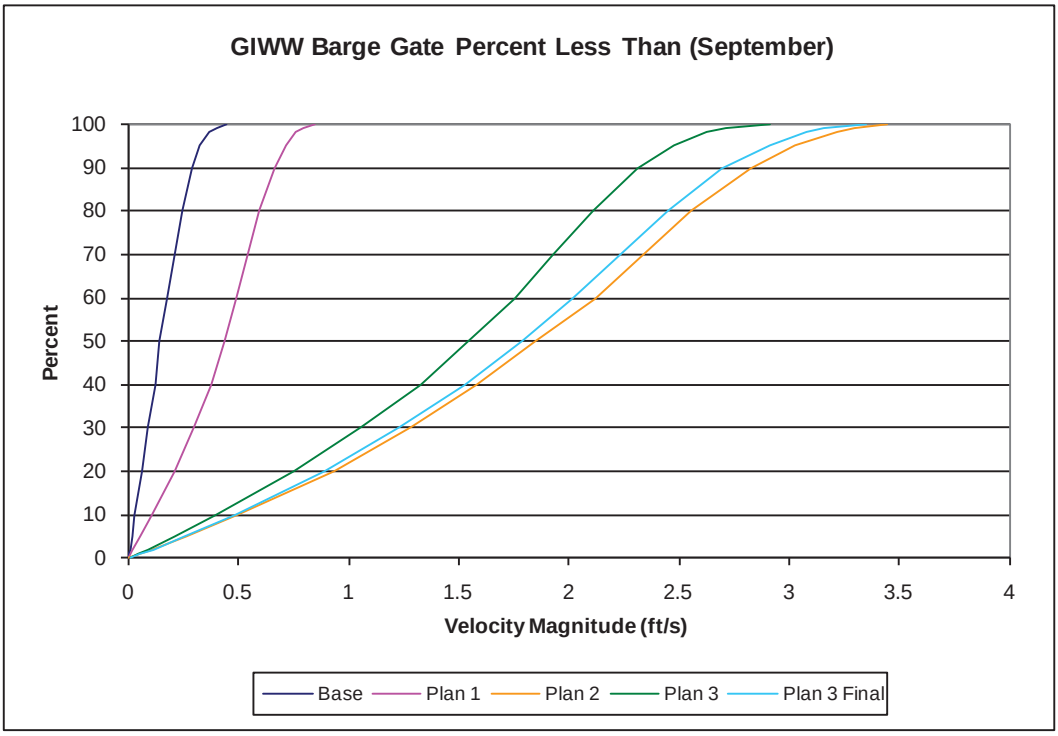

Figure 6-14. GIWW Barge Gate percent less than plot for September.

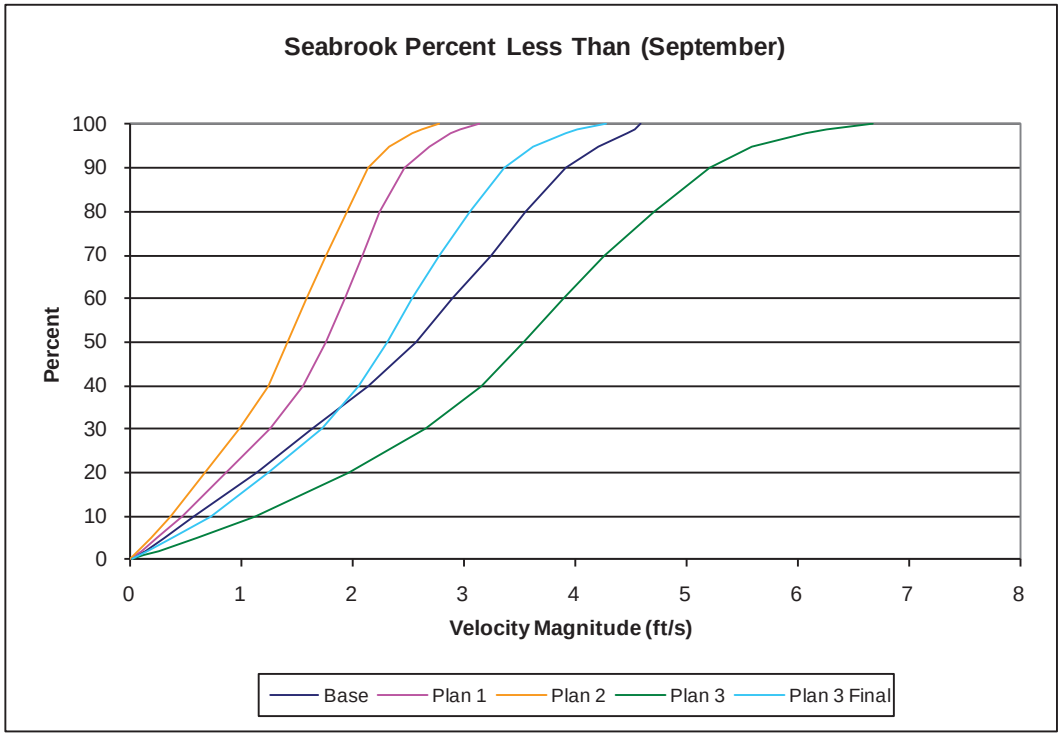

Figure 6-15. Seabrook percent less than plot for September.

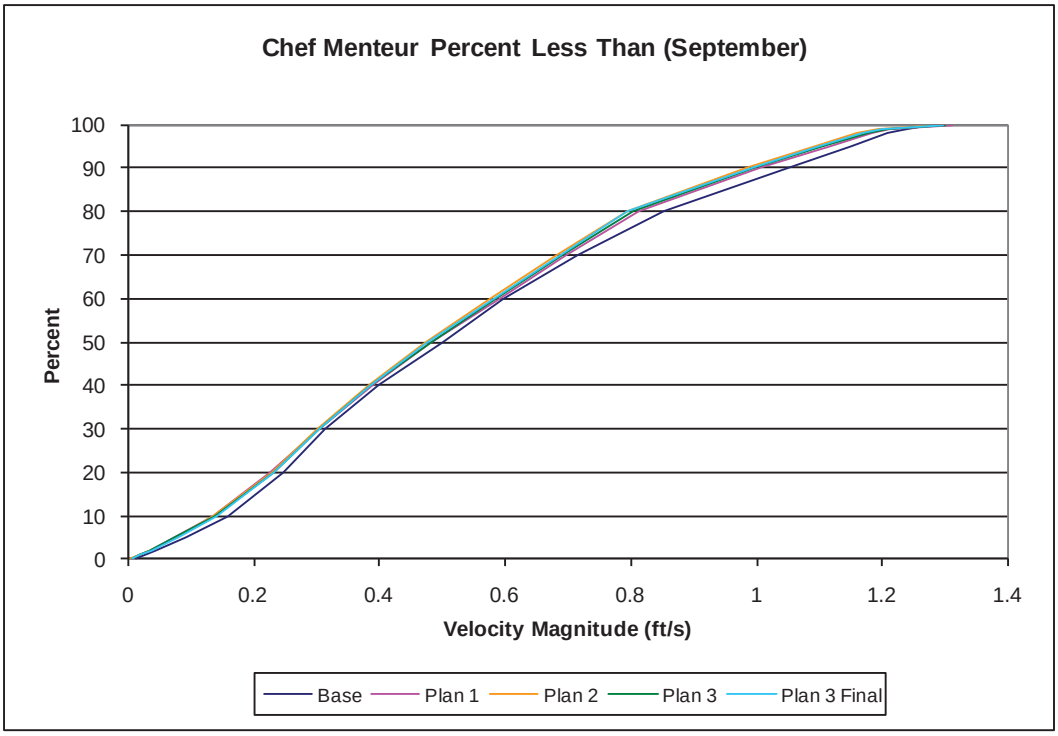

Figure 6-16. Chef Menteur percent less than plot for September.

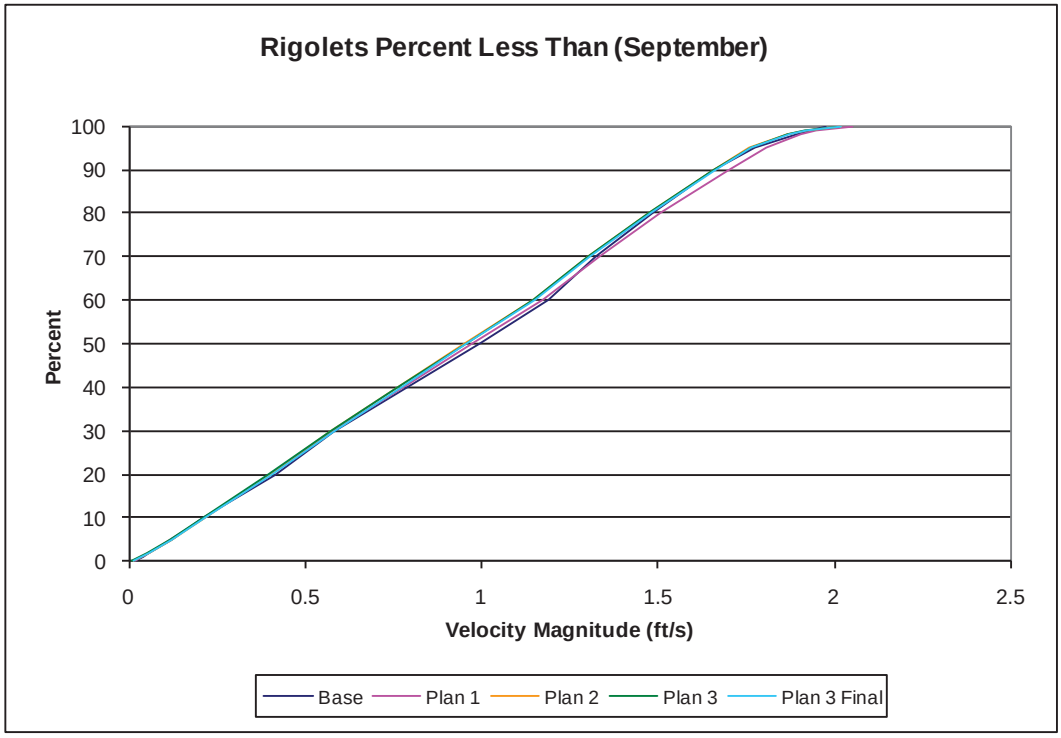

Figure 6-17. Rigolets percent less than plot for September.

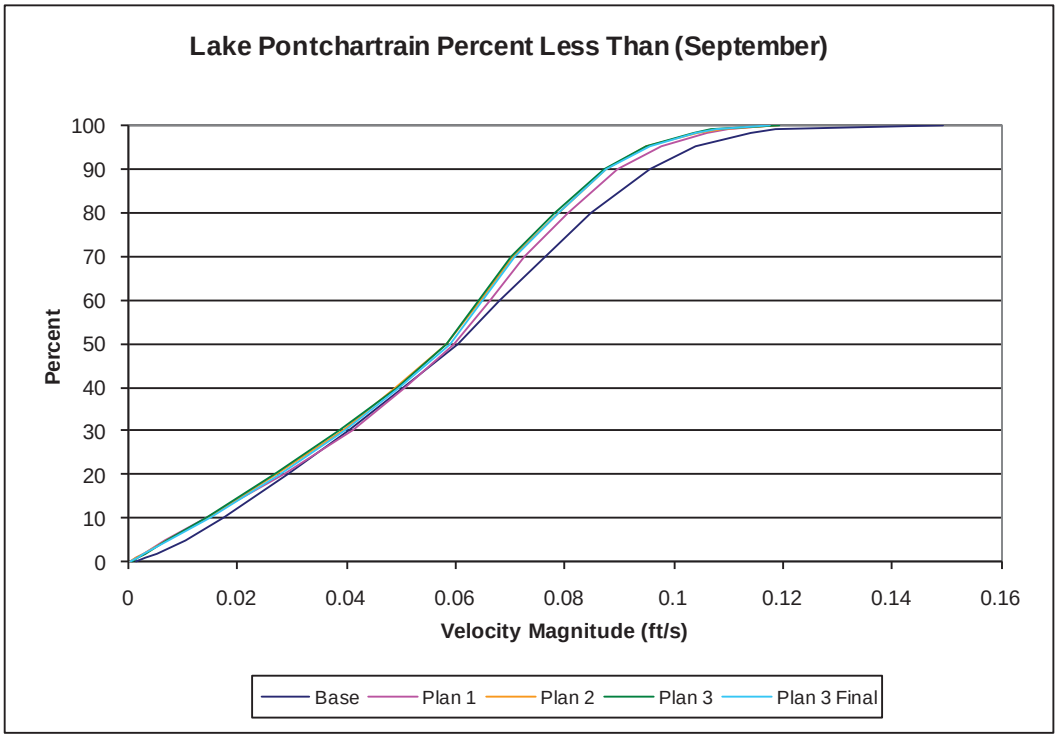

Figure 6-18. Lake Pontchartrain percent less than plot for September.

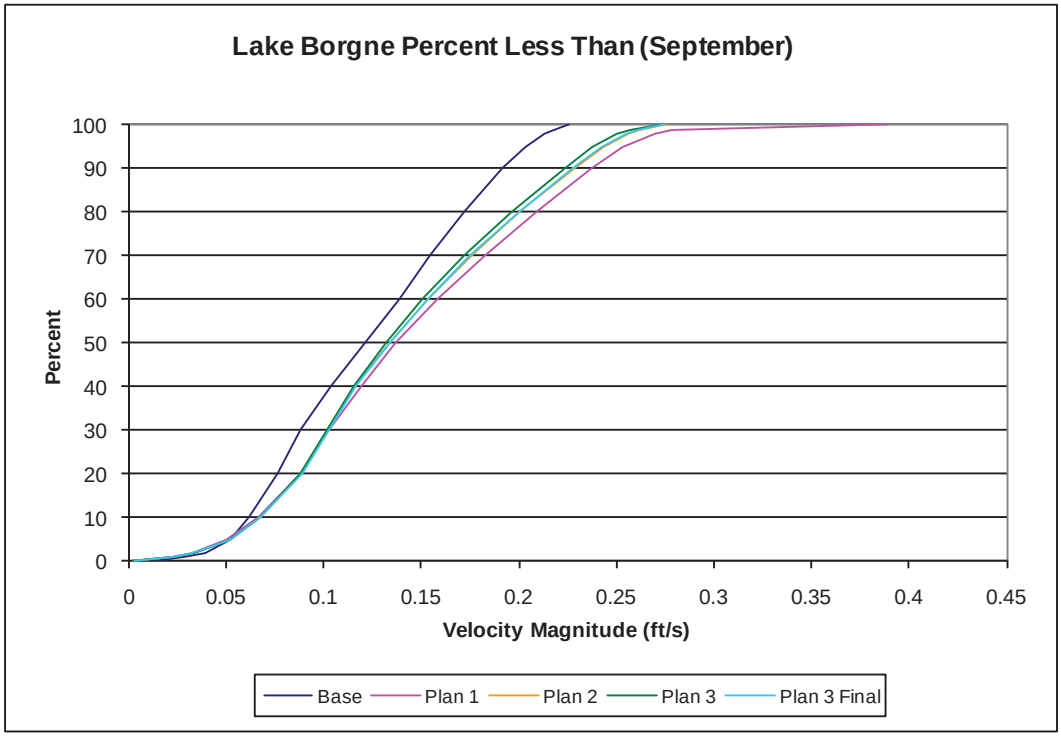

Figure 6-19. Lake Borgne percent less than plot for September.

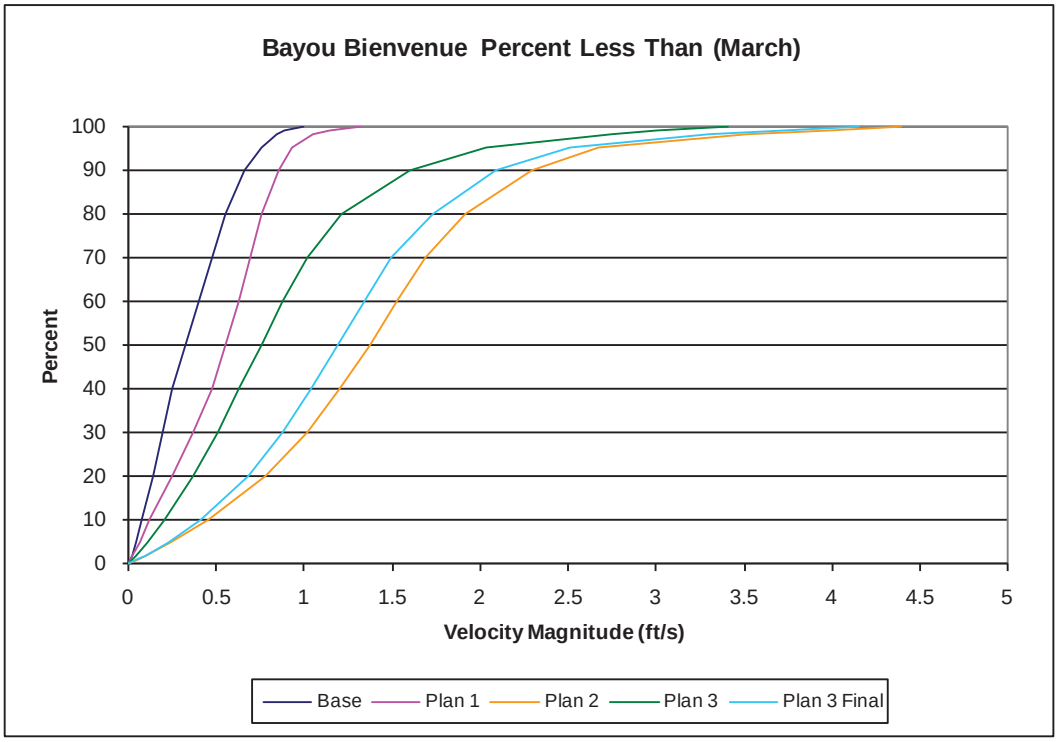

Figure 6-20. Bayou Bienvenue percent less than plot for March.

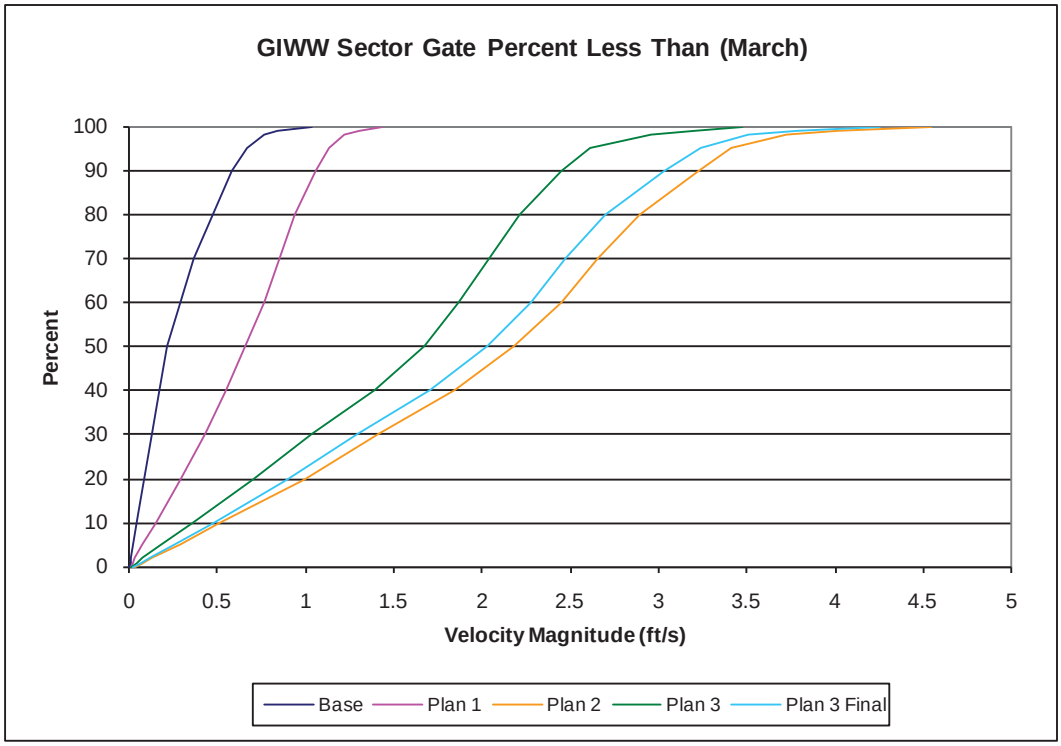

Figure 6-21. GIWW Sector Gate percent less than plot for March.

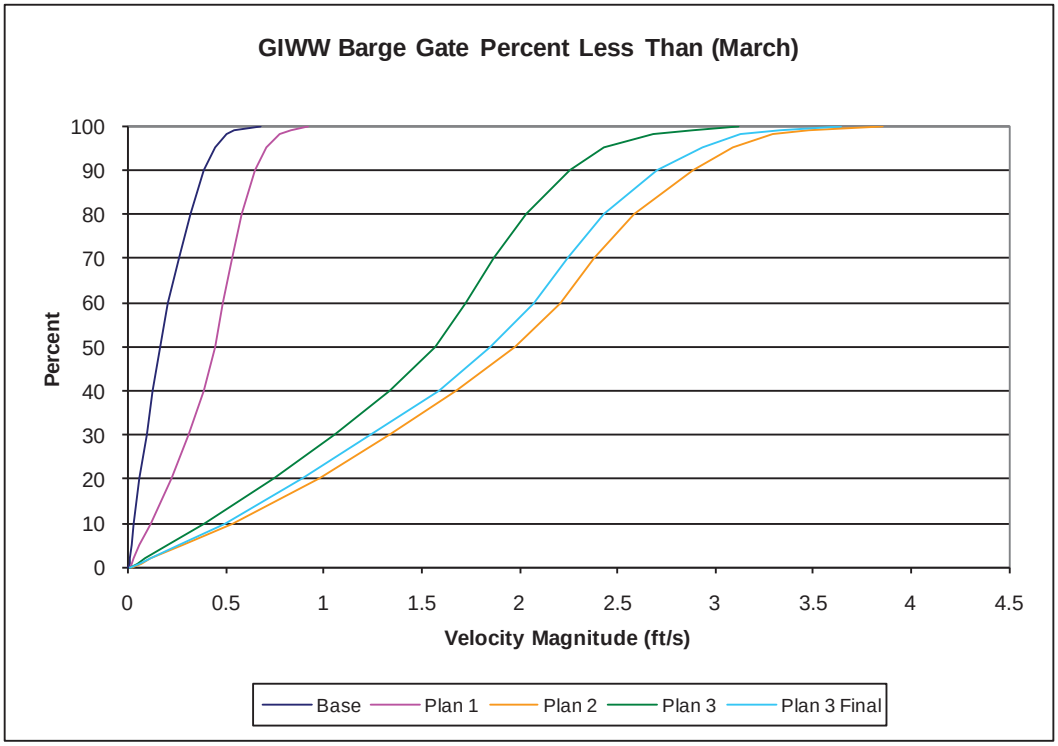

Figure 6-22. GIWW Barge Gate percent less than plot for March.

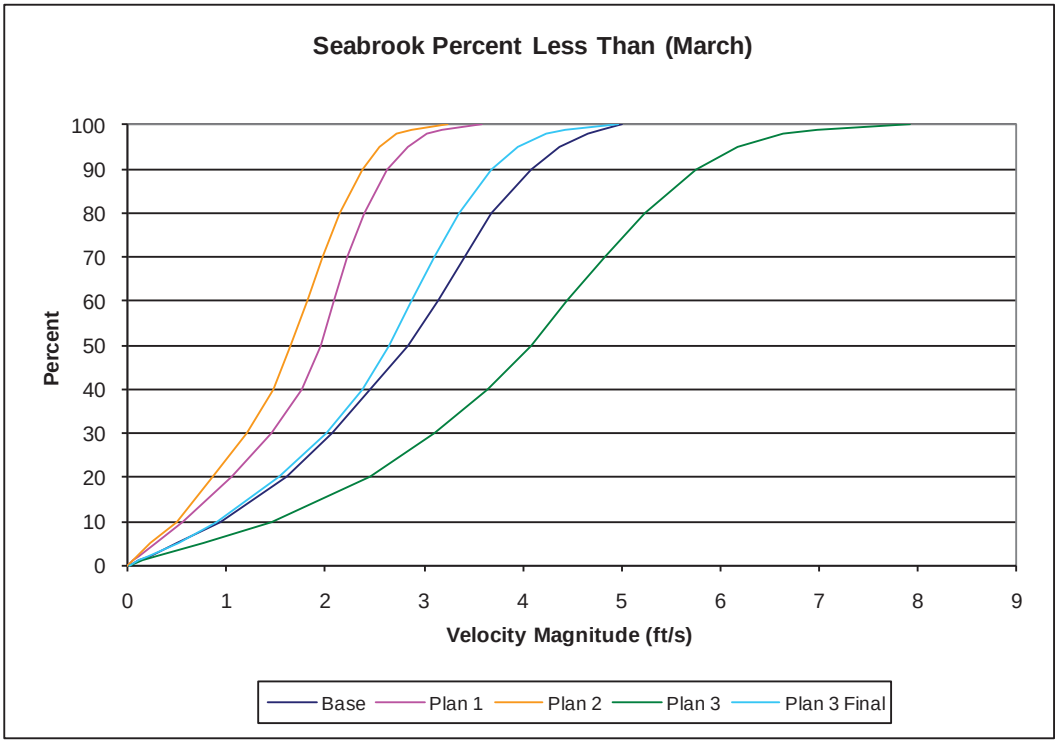

Figure 6-23. Seabrook percent less than plot for March.

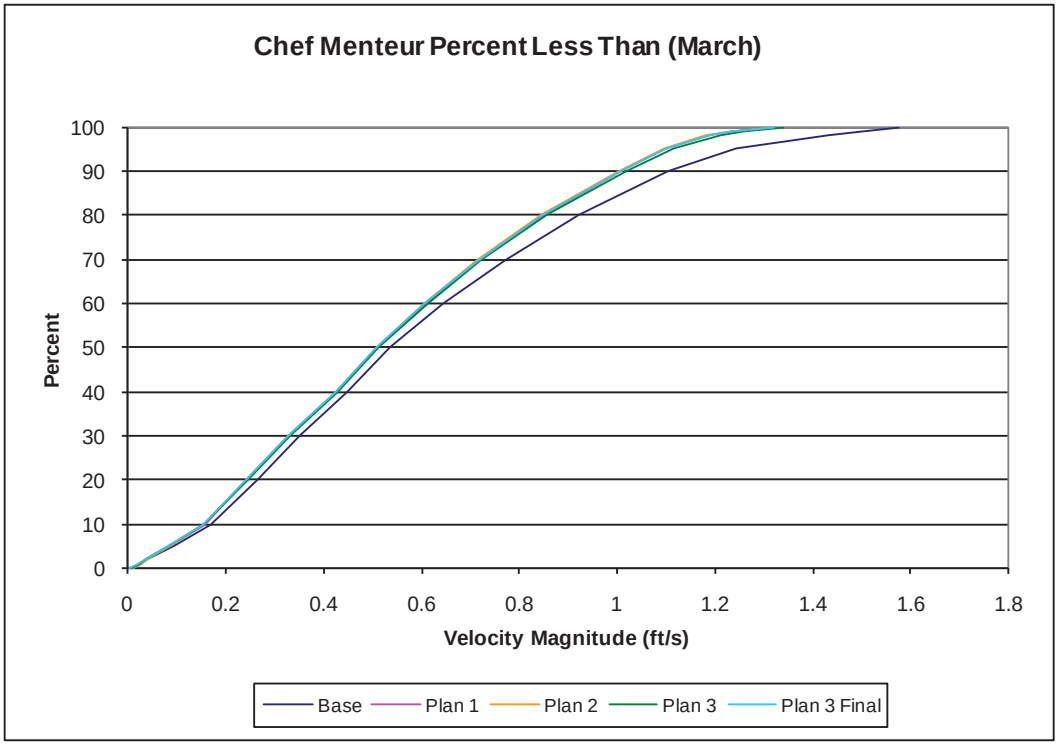

Figure 6-24. Chef Menteur percent less than plot for March.

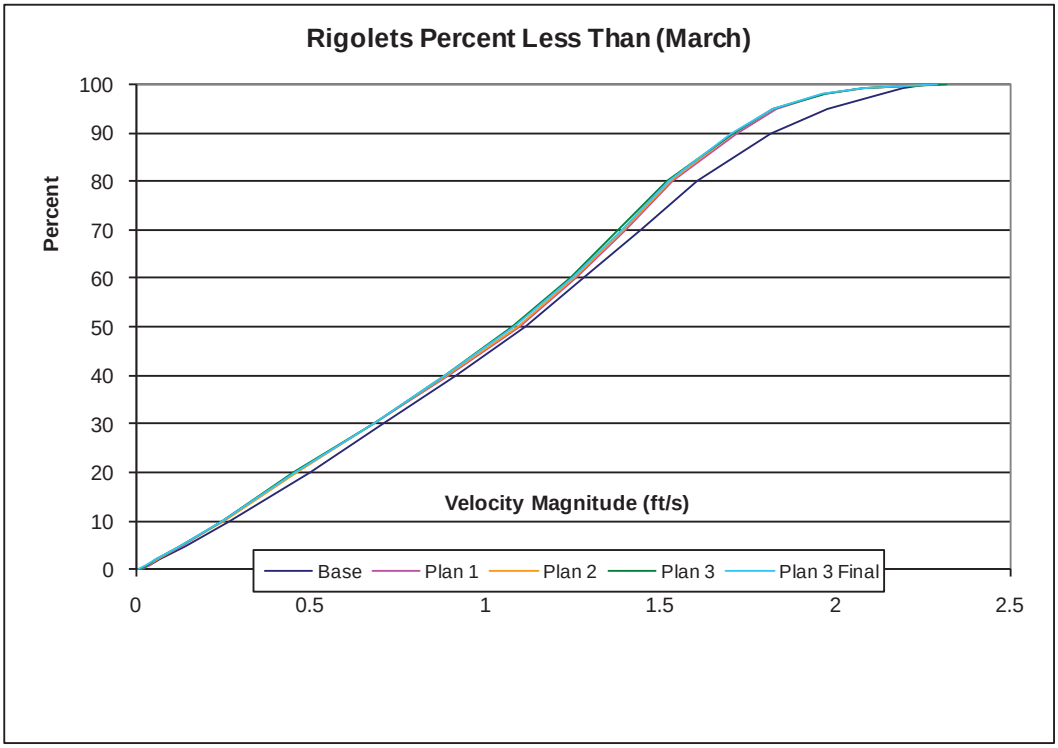

Figure 6-25. Rigolets percent less than plot for March.

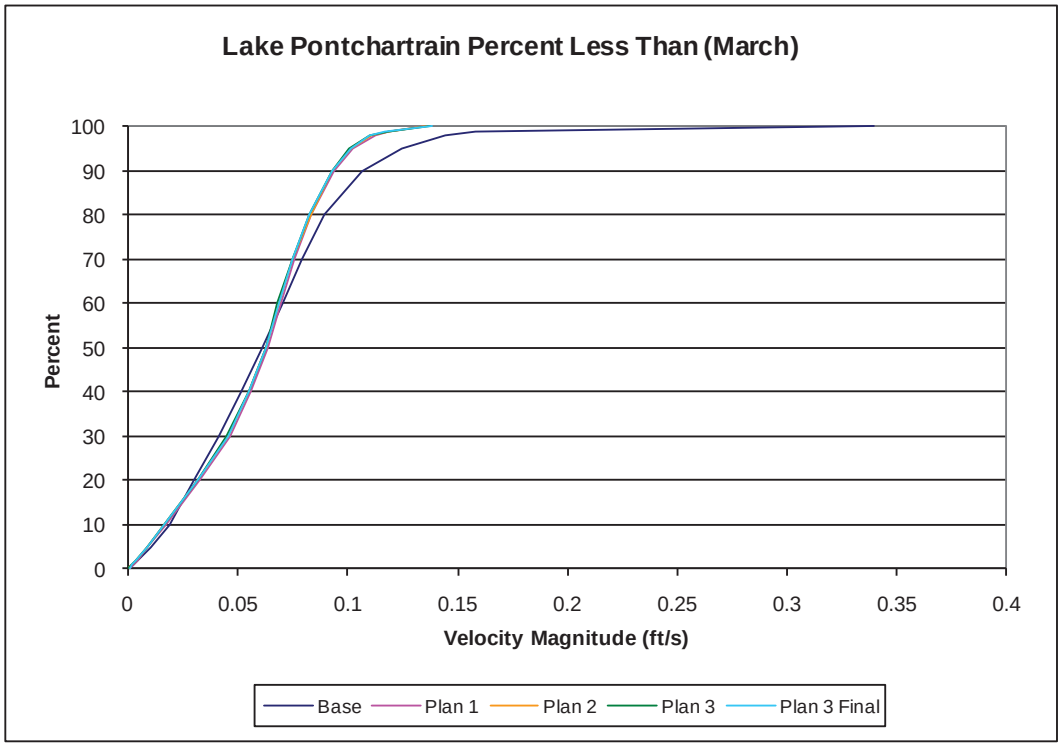

Figure 6-26. Lake Pontchartrain percent less than plot for March.

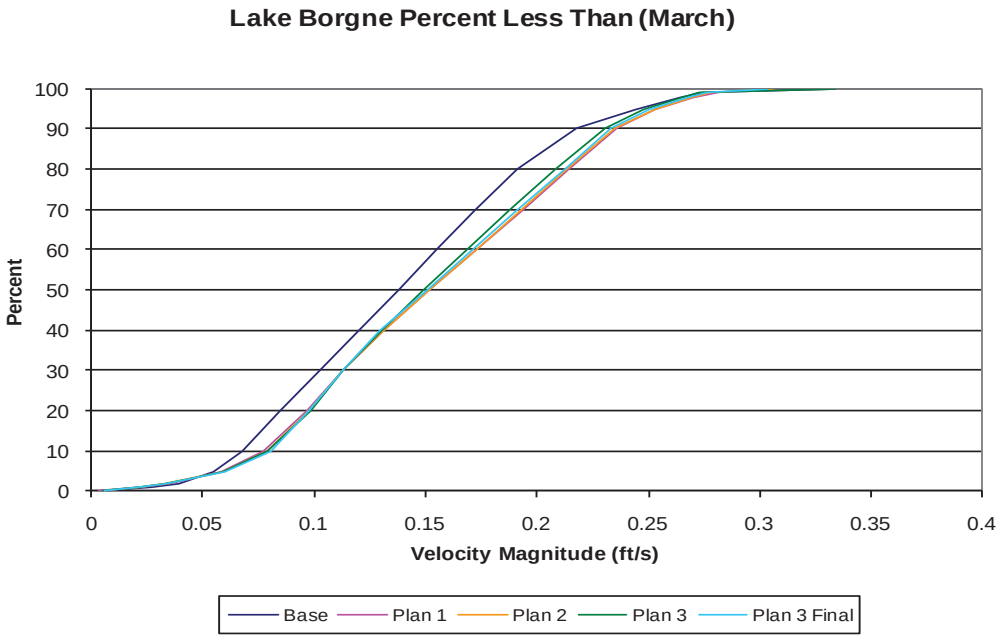

Figure 6-27. Lake Borgne percent less than plot for March.

Figures 6-12 through 6-27 show that the velocity differences between the base and plan conditions are significant in the location of the structures. Not only are the maximum flood and ebb values larger for the plans but so are the values in general. For the locations in the structures, the velocity patterns are the same as those seen in the previous figures (Figures 6-12 through 6-27). At the Bayou Bienvenue and GIWW structures, Plan 1 velocities are higher than the Base in most cases and continue to increase with Plan 2 but then reduce when the Seabrook structure is included. Plan 3 reduces velocities in the structures more than Plan 3 Final since it has a cross-sectional area about half that of Plan 3 Final. The velocities at the Seabrook structure, however, are lower for Plan 1 and Plan 2, as compared with the base condition, due to the reduction in flow from the MRGO and then increase once the structure is in place. In the Seabrook structure, velocities increase with Plan 3 but Plan 3 Final produces a drop in velocity to values comparable with the Base condition. Again, this is due to changes in conveyance area. These patterns are observed for both the September and March flow conditions.

The percent less than plots for Chef Menteur and the Rigolets show that the velocity values, and therefore fluxes, are affected very little when the plan conditions are in place. At Chef Menteur there is a slight reduction in the velocity magnitudes and the frequency of these magnitudes. This trend is more obvious in March but seen in September as well. At the Rigolets

this trend is less noticeable. It appears to occur in March but the September conditions produce little change.

The final two analysis locations are in the center of Lake Borgne and Lake Pontchartrain. These locations are further away from the plan modifications so their analysis can help understand how the flow patterns are changed with each plan alternative. The velocity magnitudes in these two locations are very small. Maximum values are less than 0.4 ft/s for both September and March. In Lake Borgne, the velocities increase once the MRGO is cut off from the Gulf of Mexico with Plan 1. This result is reasonable since the flow that previously traveled the MRGO is now forced into Lake Borgne. In Lake Pontchartrain there is a reduction in velocity magnitude. This result is due to the reduction of total flow into the lake since the MRGO was a large transport mechanism for flow into Lake Pontchartrain. However, the drop in velocity magnitude is very small overall since the Rigolets and Chef Menteur remain open and continue to allow flow into this area.

Water Surface Analysis

A water surface elevation analysis is performed at a total of 16 points within the model domain. The initial locations are set at 250 ft to each side of a proposed structure. Six additional locations are chosen so that an overall response to the system due to the plan alternatives can be observed. Figures 6-28 and 6-29 show the analysis locations. Locations for each side of a structure are shown as a single point. This analysis is performed on both the September and March flow conditions. The water surface elevation for each location and alternative is shown in Figures 6-30 to 6-61. These figures display 12.5 days of a particular simulation period (August 22 – September 3, 2007; March 9 - 21, 2008).

The water surface elevation changes due to the plan conditions are most noticeable at the location where the MRGO is being cut off from the Gulf of Mexico. South of the closure at La Loutre, there is very little change for the September condition and slightly more for the March condition when flows are larger and the blockage of the MRGO creates reflections of the wave that affect the amplitude, although the effects here are much less than those at the other analysis locations. However, north of this closure there is a large difference in the phasing and tidal amplitude, approximately a 2.5 hour lag from the Base to Plan 1 results due to the closure at La Loutre and a 4-5 hour lag from the Base to Plan 2/Plan 3/Plan 3 Final results due to the addition of the Borgne alignment (defined in Chapter 4). The wave that

previously reached this location through the MRGO now travels through Lake Borgne before reaching this point. This greater distance to travel equates to a longer travel time as well as lower range due to the blockage offlow volume. At the MRGO closure south of Bayou Bienvenue, there is also a reduction in elevation range due to these closures as well as a phase shift on both sides of the closure.

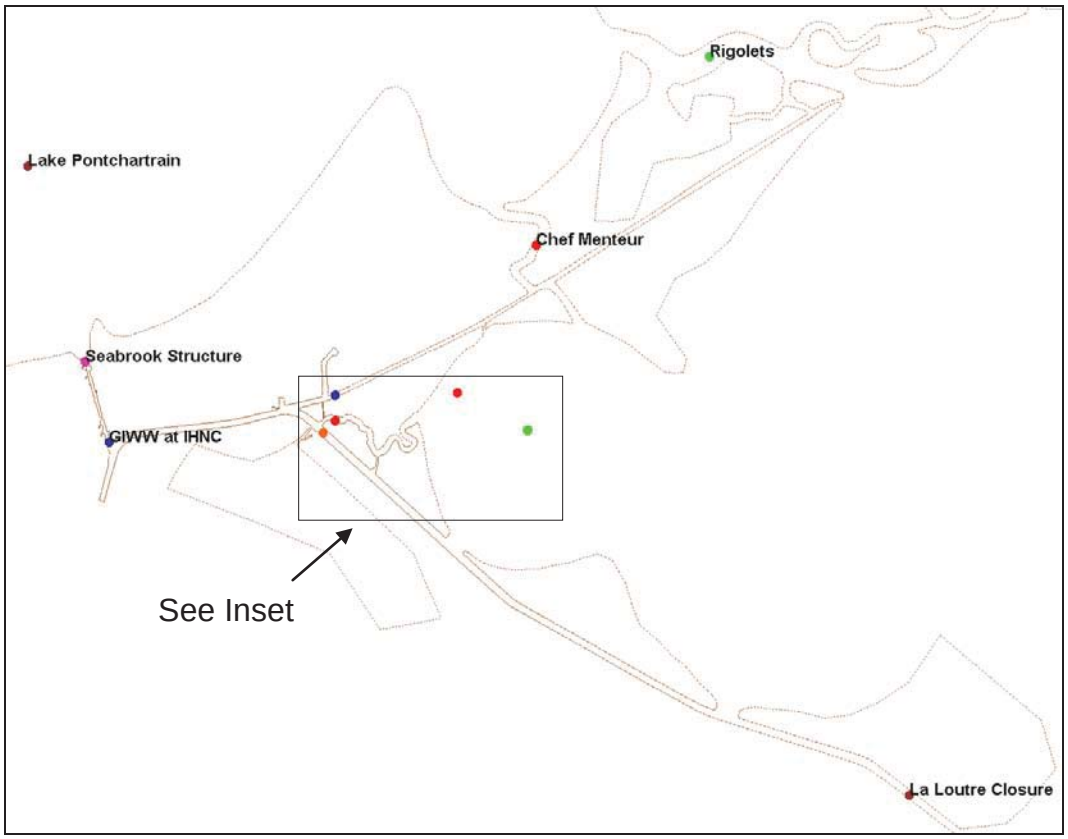

Figure 6-28. Location map for water surface analysis.

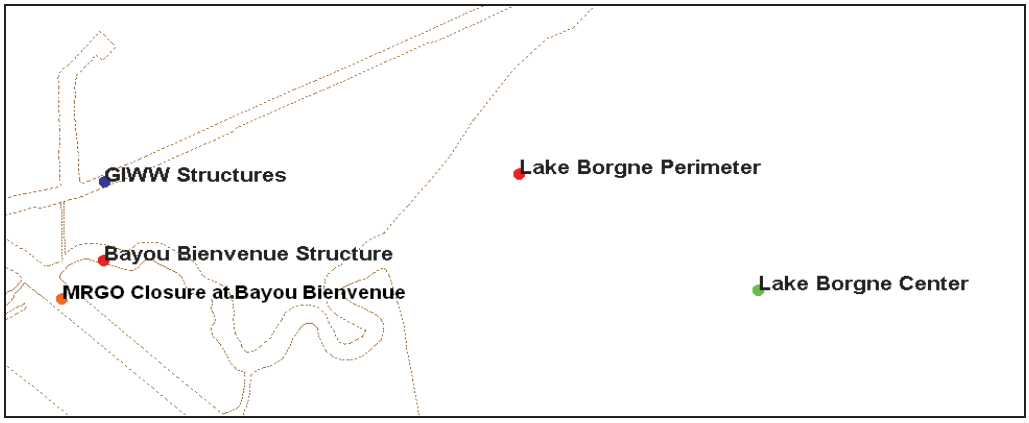

Figure 6-29. Inset for water surface analysis location map.

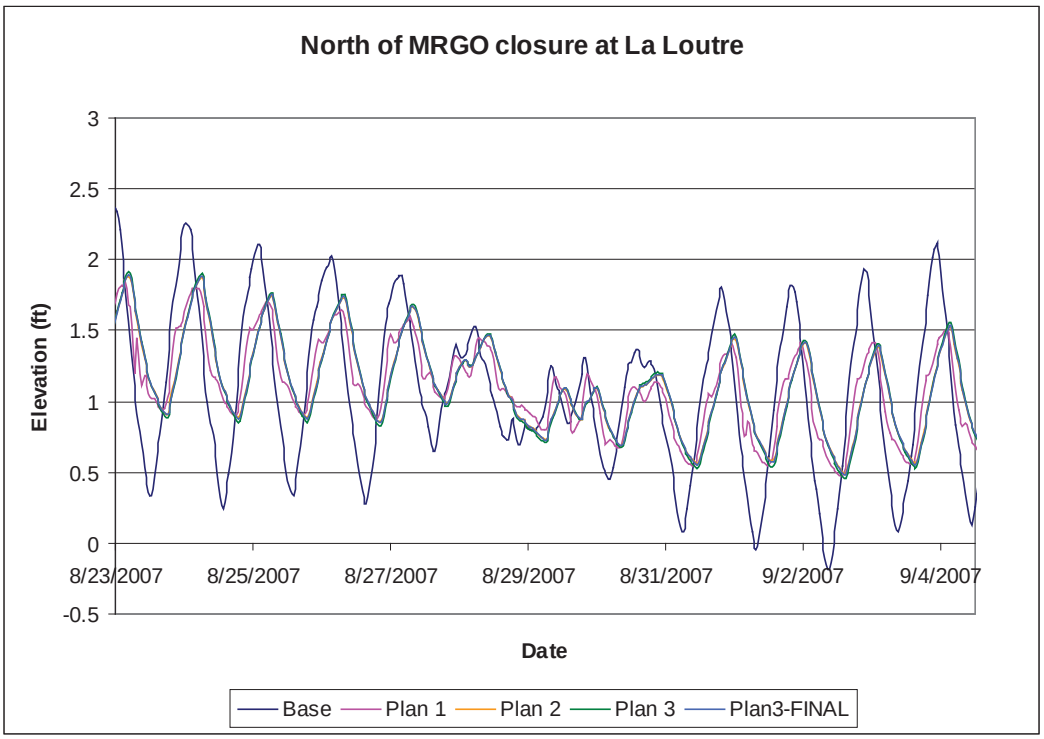

Figure 6-30. Water surface elevation north of MRGO closure at La Loutre (September).

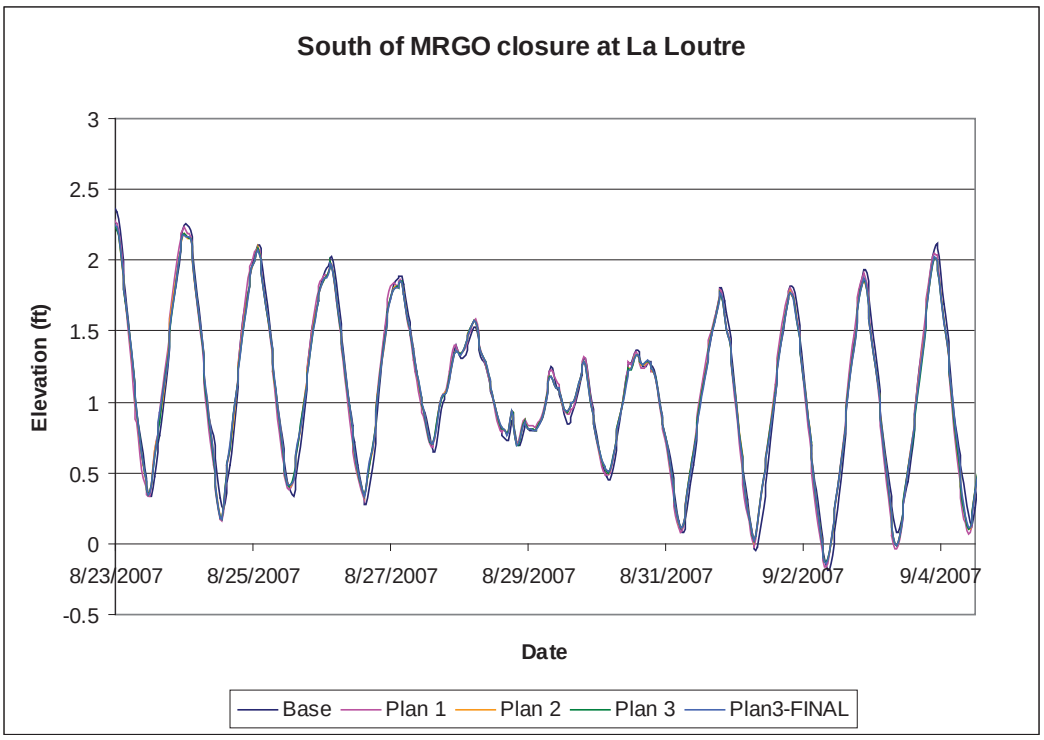

Figure 6-31. Water surface elevation south of MRGO closure at La Loutre (September).

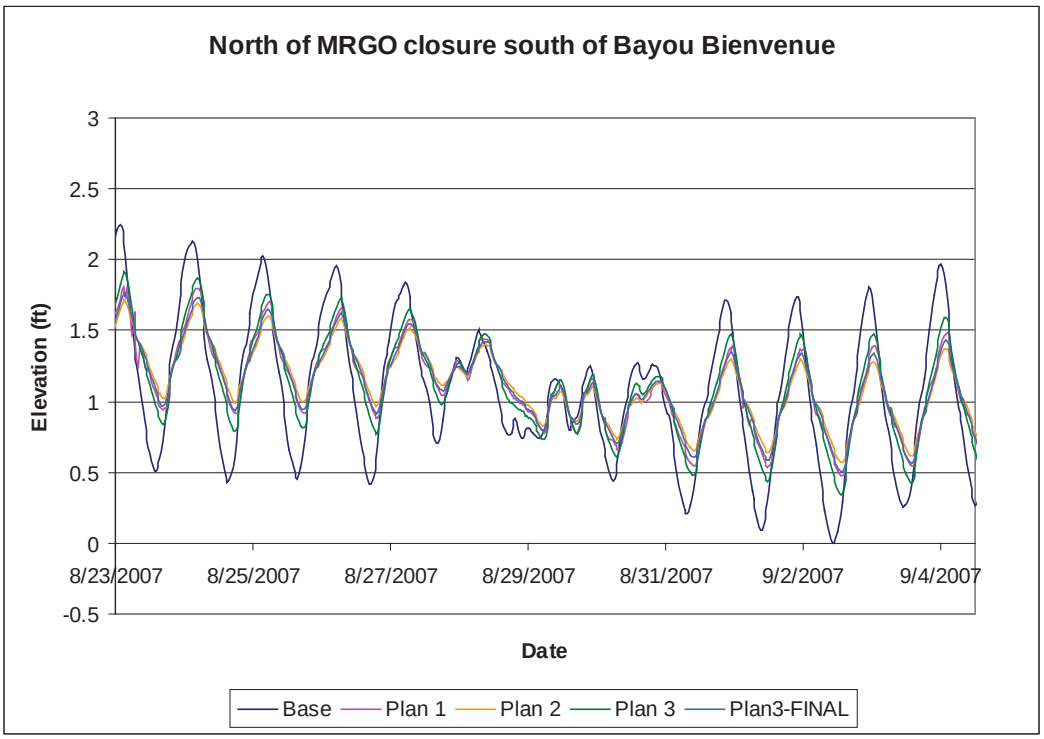

Figure 6-32. Water surface elevation north of MRGO closure at Bayou Bienvenue (September).

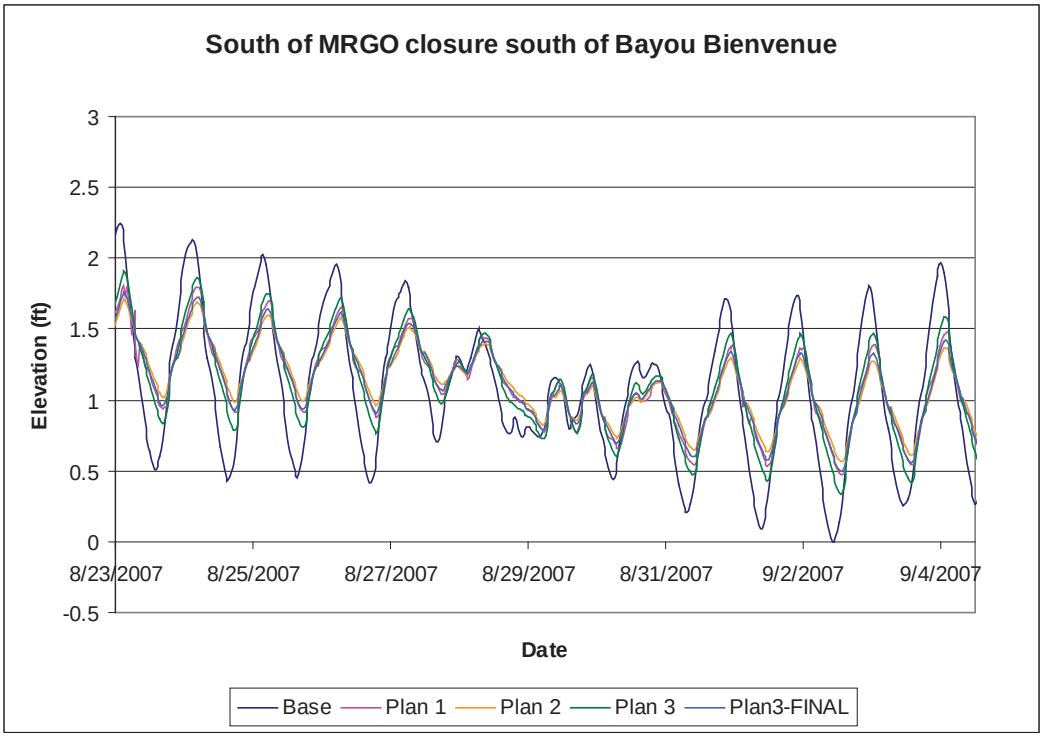

Figure 6-33. Water surface elevation south of MRGO closure at Bayou Bienvenue (September).

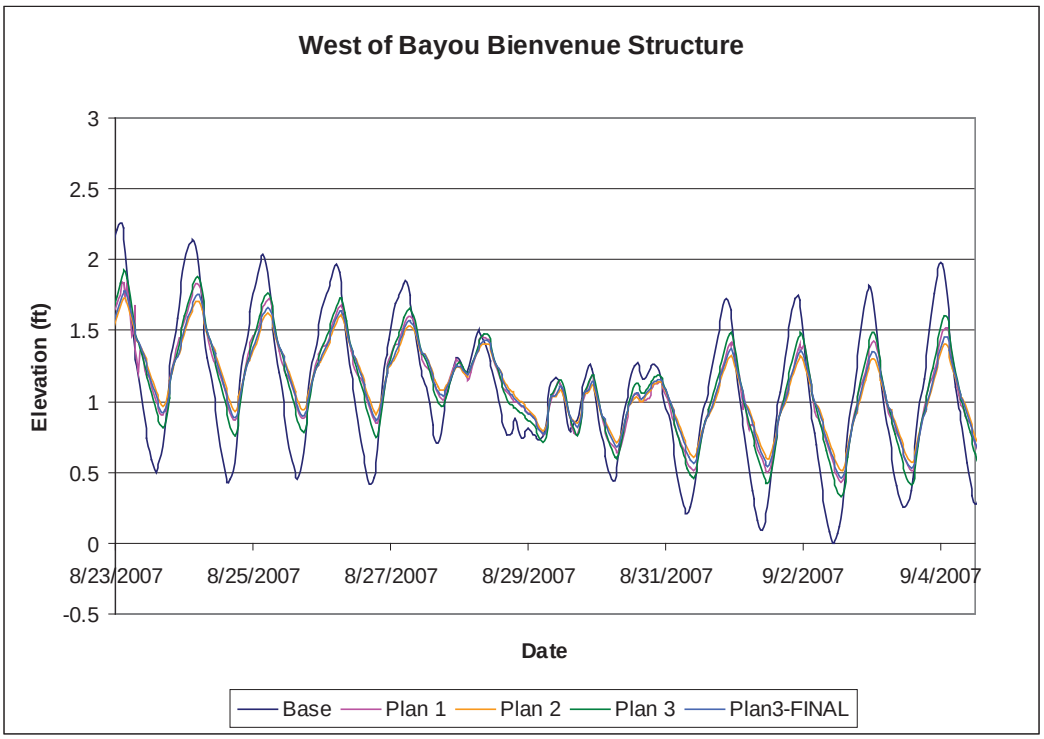

Figure 6-34. Water surface elevation west of Bayou Bienvenue structure (September).

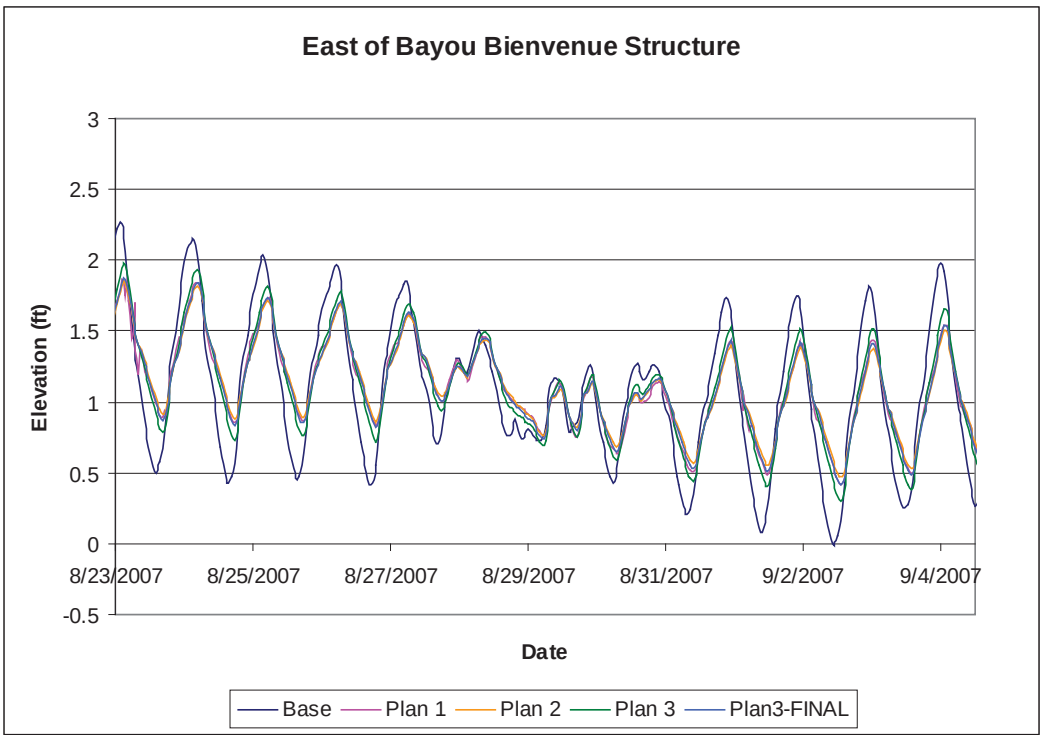

Figure 6-35. Water surface elevation east of Bayou Bienvenue structure (September).

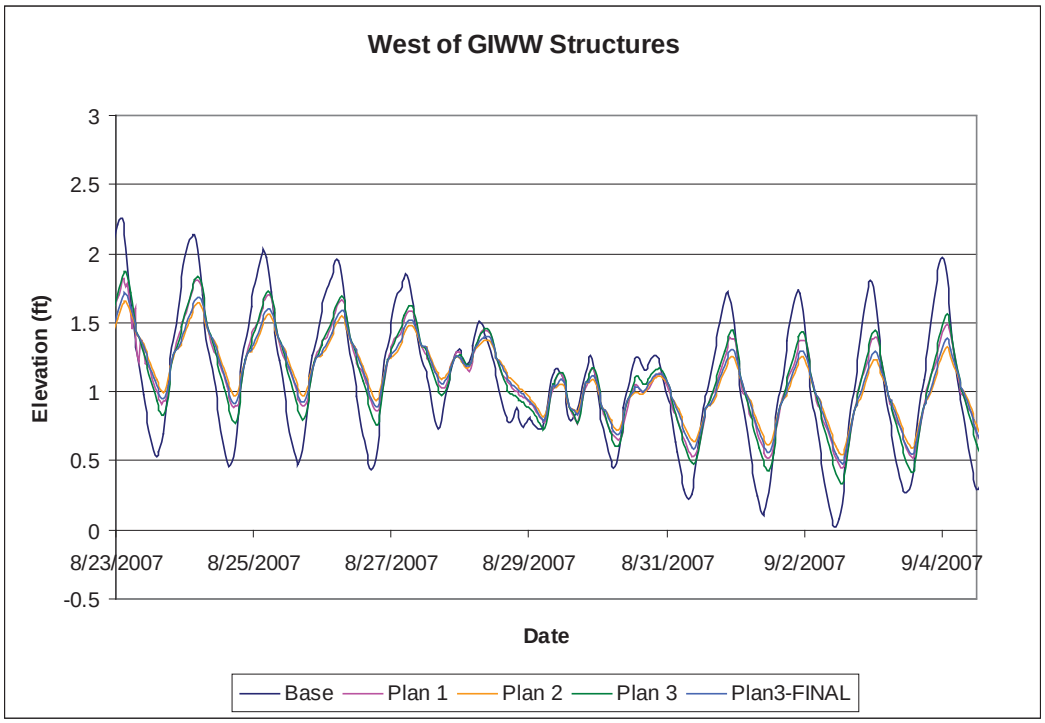

Figure 6-36. Water surface elevation west of GIWW structures (September).

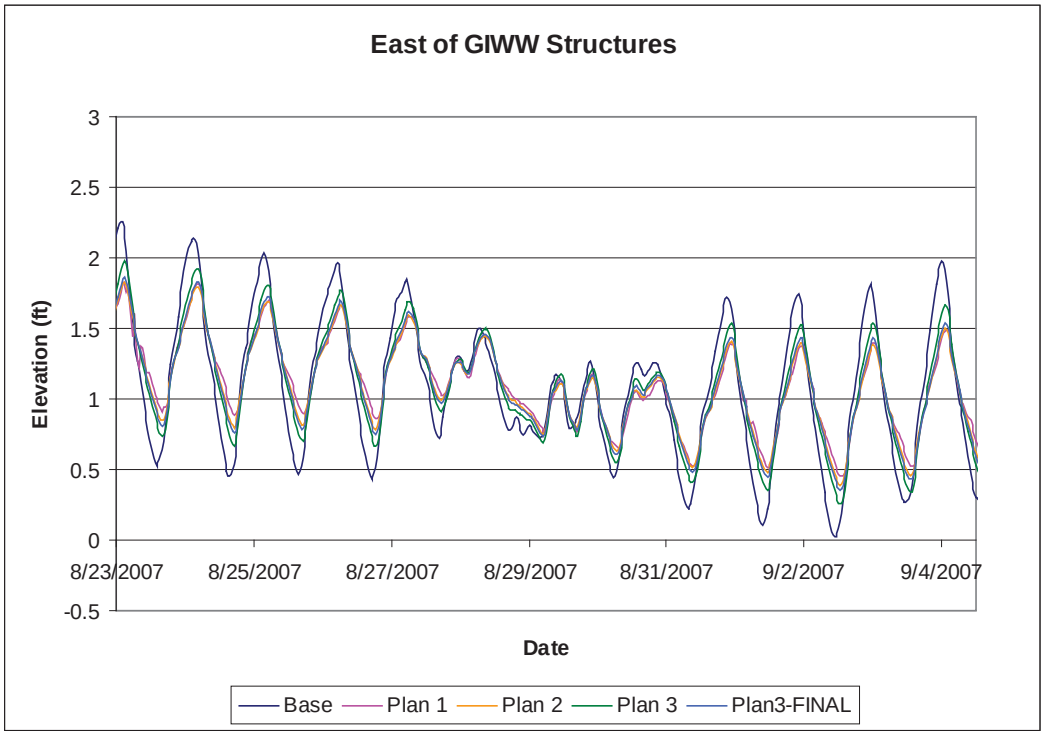

Figure 6-37. Water surface elevation east of GIWW structures (September).

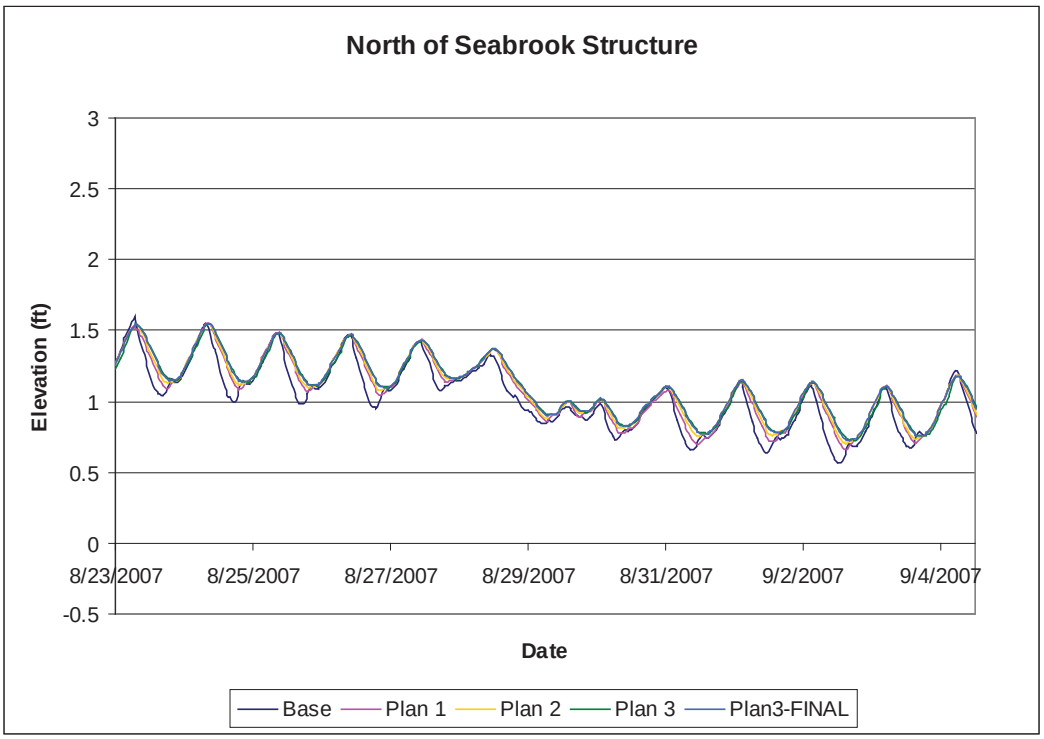

Figure 6-38. Water surface elevation north of Seabrook structure (September).

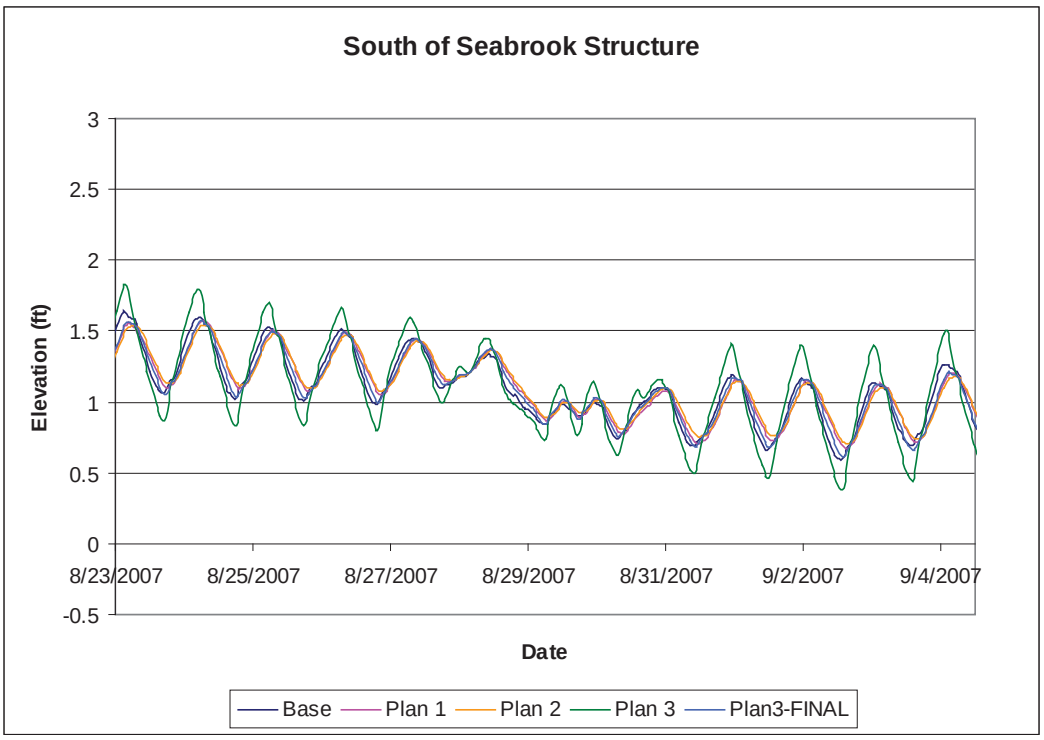

Figure 6-39. Water surface elevation south of Seabrook structure (September).

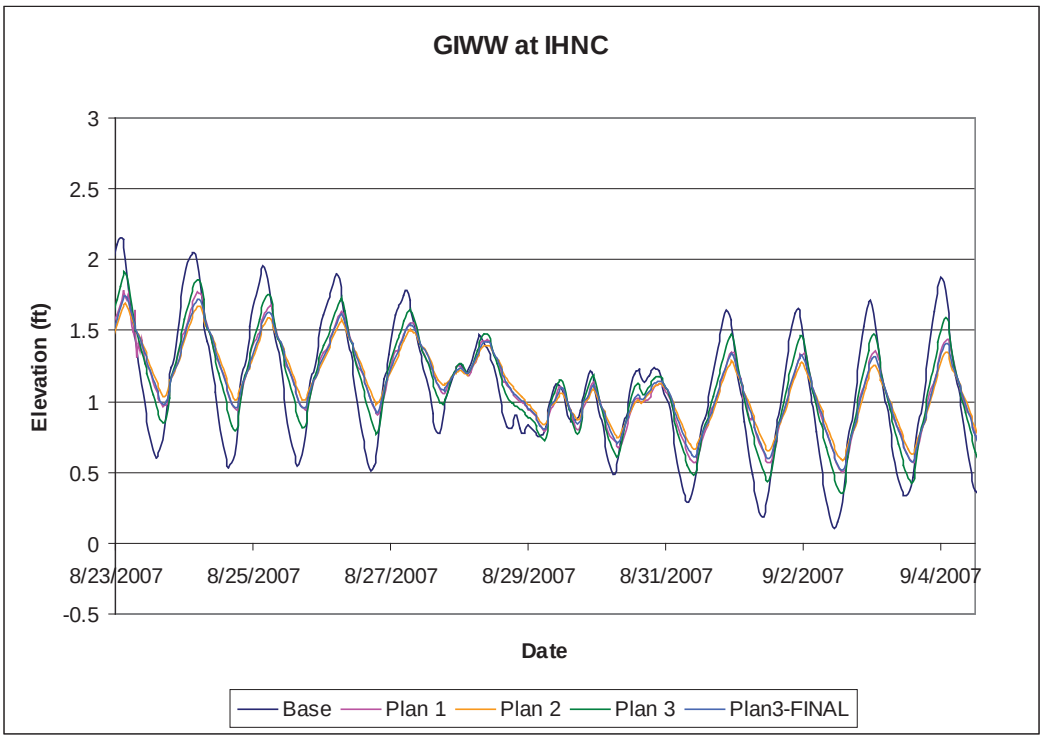

Figure 6-40. Water surface elevation in GIWW at IHNC (September).

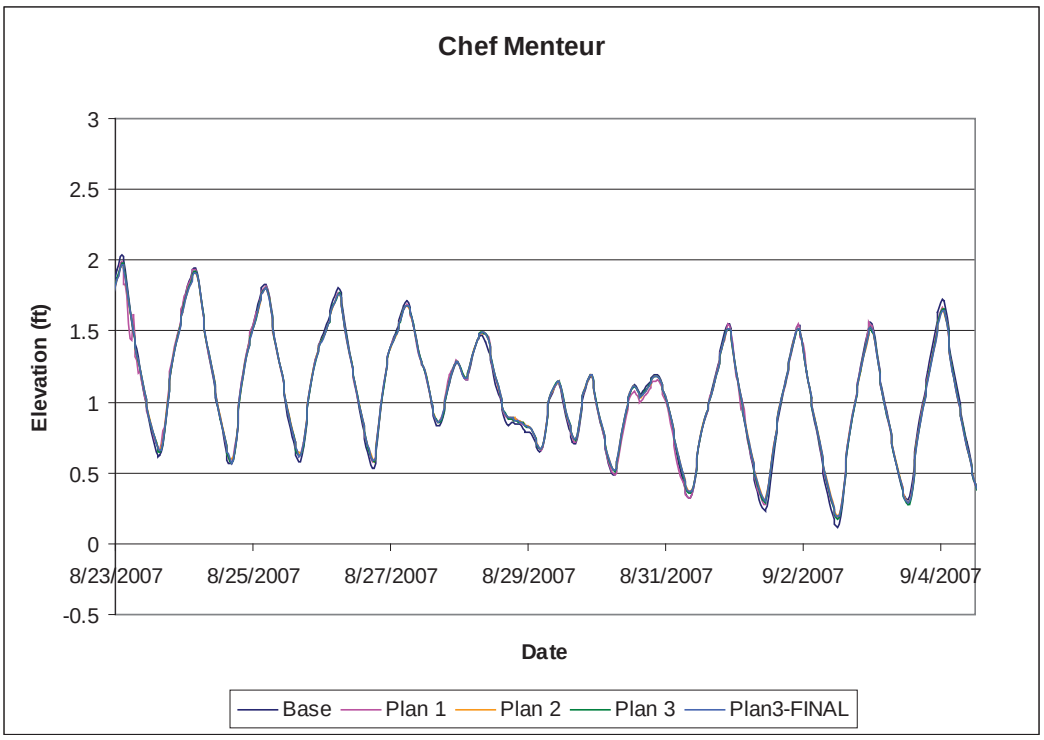

Figure 6-41. Water surface elevation in Chef Menteur (September).

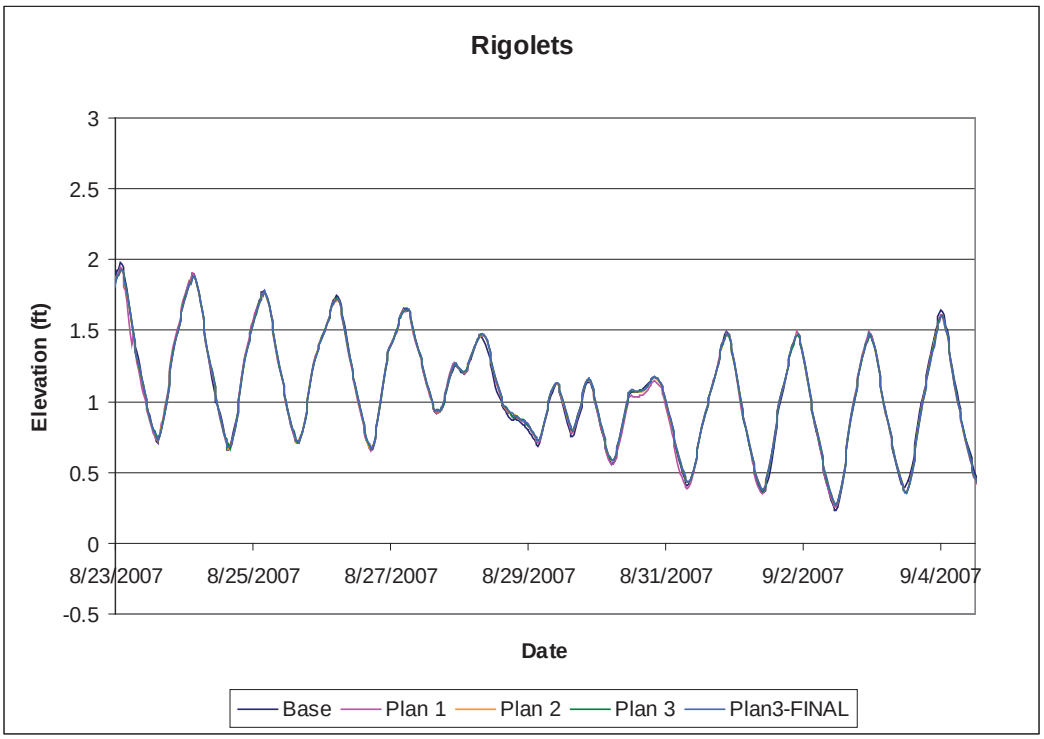

Figure 6-42. Water surface elevation north in Rigolets (September).

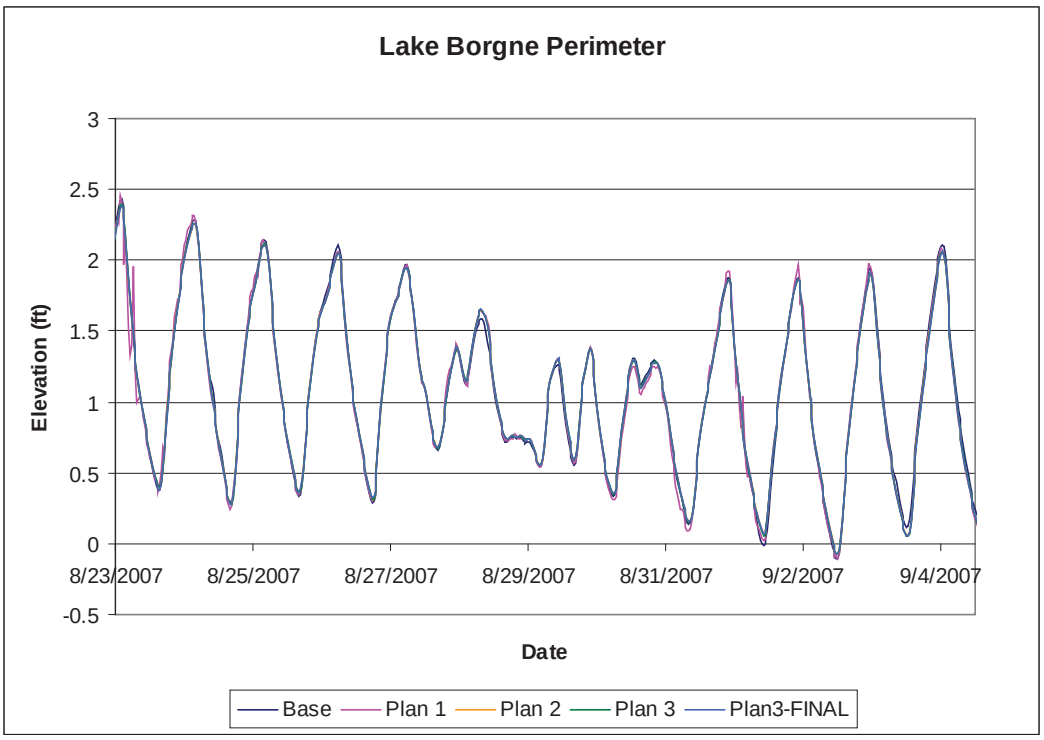

Figure 6-43. Water surface elevation at Lake Borgne perimeter (September).

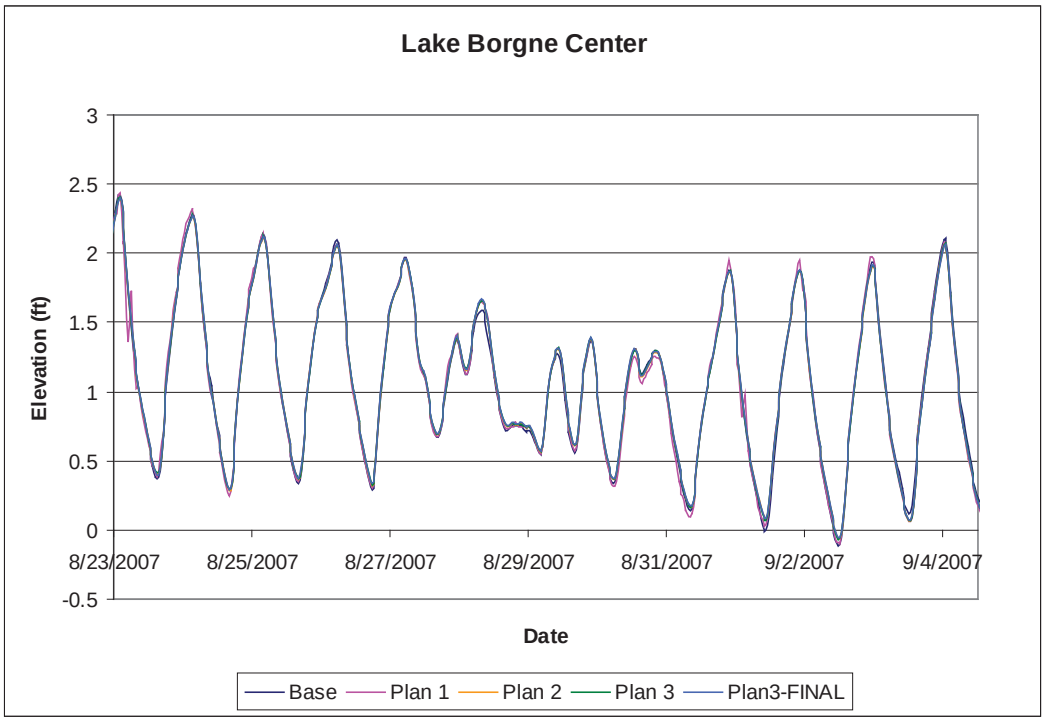

Figure 6-44. Water surface elevation at Lake Borgne center (September).

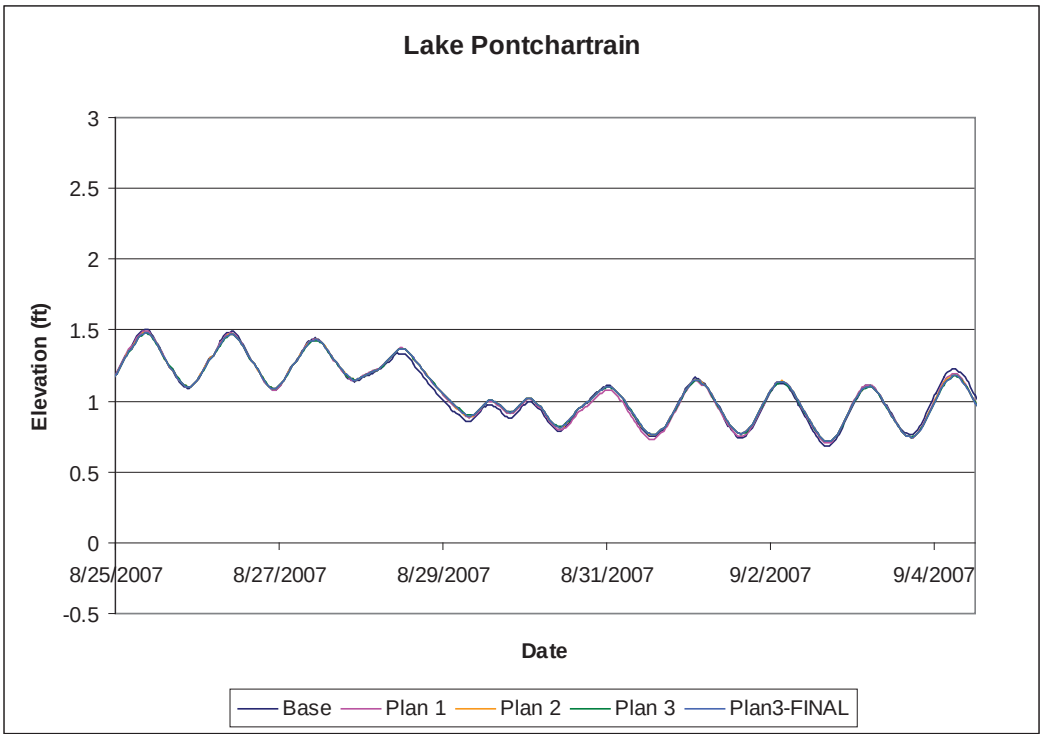

Figure 6-45. Water surface elevation at Lake Pontchartrain (September).

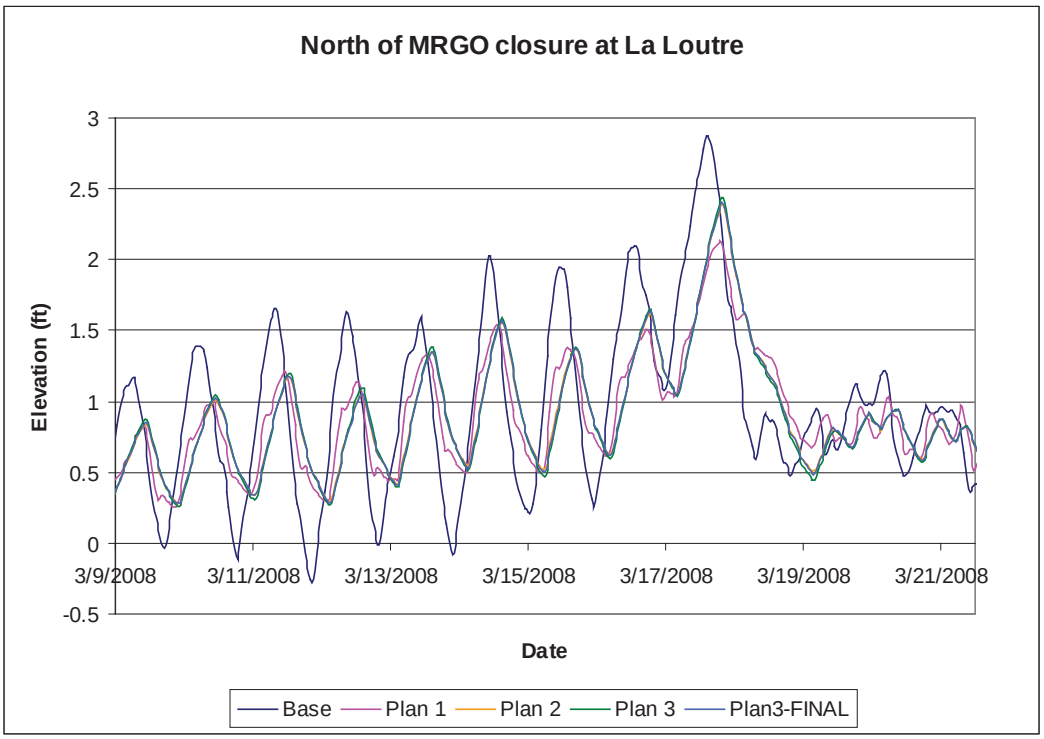

Figure 6-46. Water surface elevation north of MRGO closure at La Loutre (March).

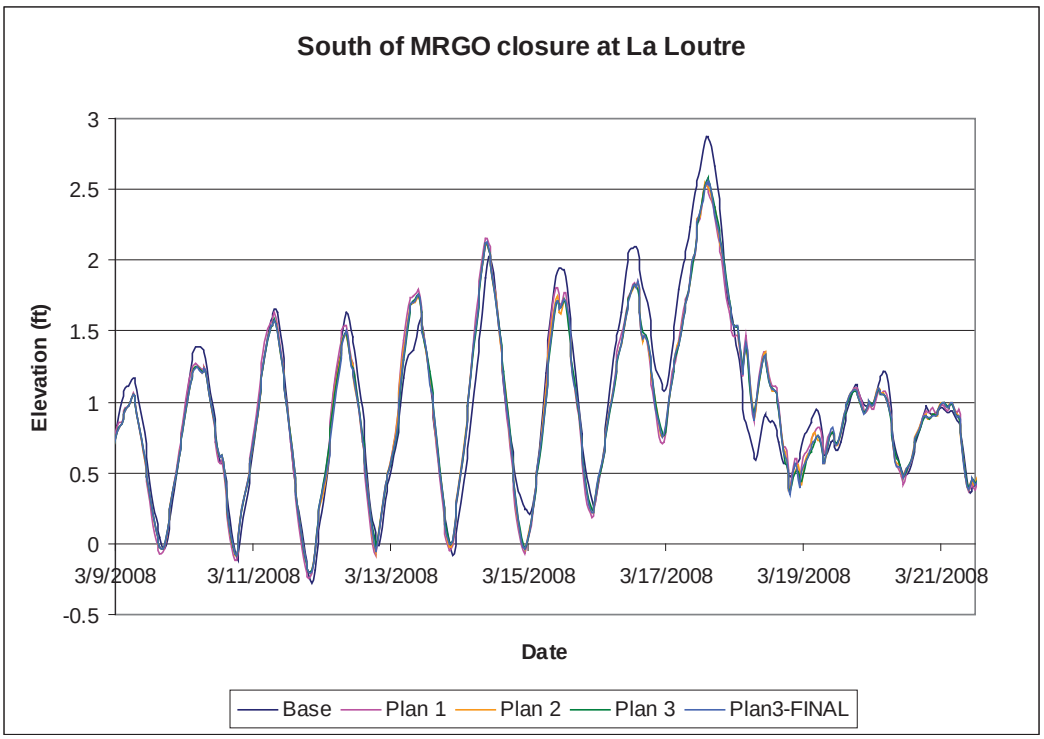

Figure 6-47. Water surface elevation south of MRGO closure at La Loutre (March).

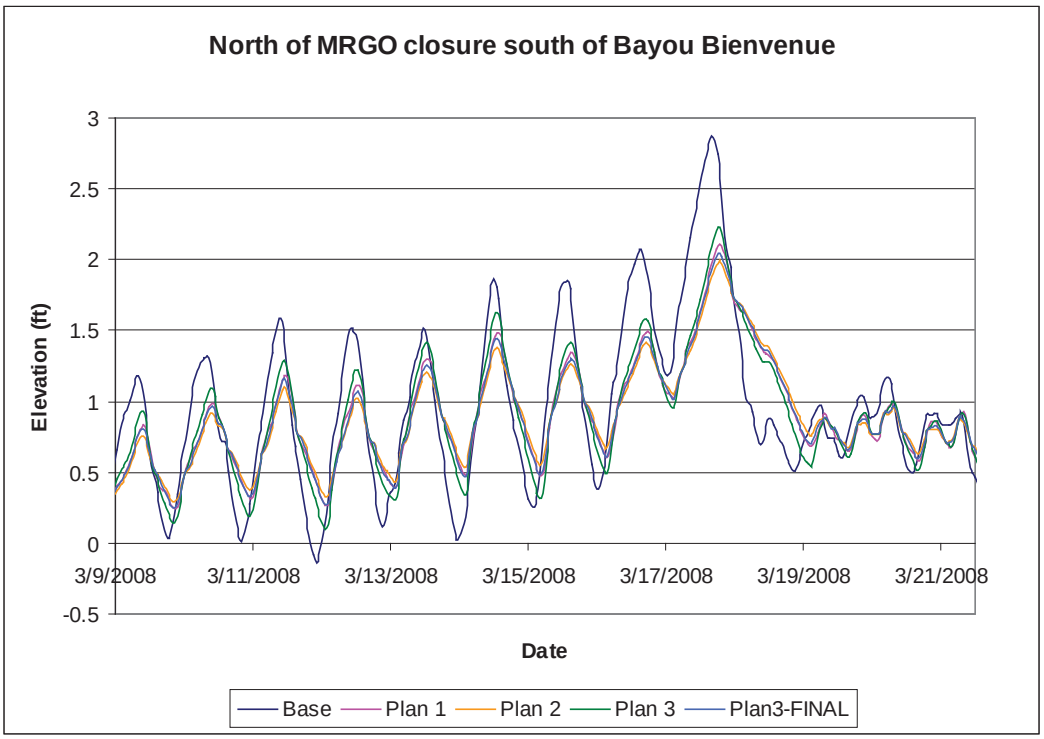

Figure 6-48. Water surface elevation north of MRGO closure at Bayou Bienvenue (March).

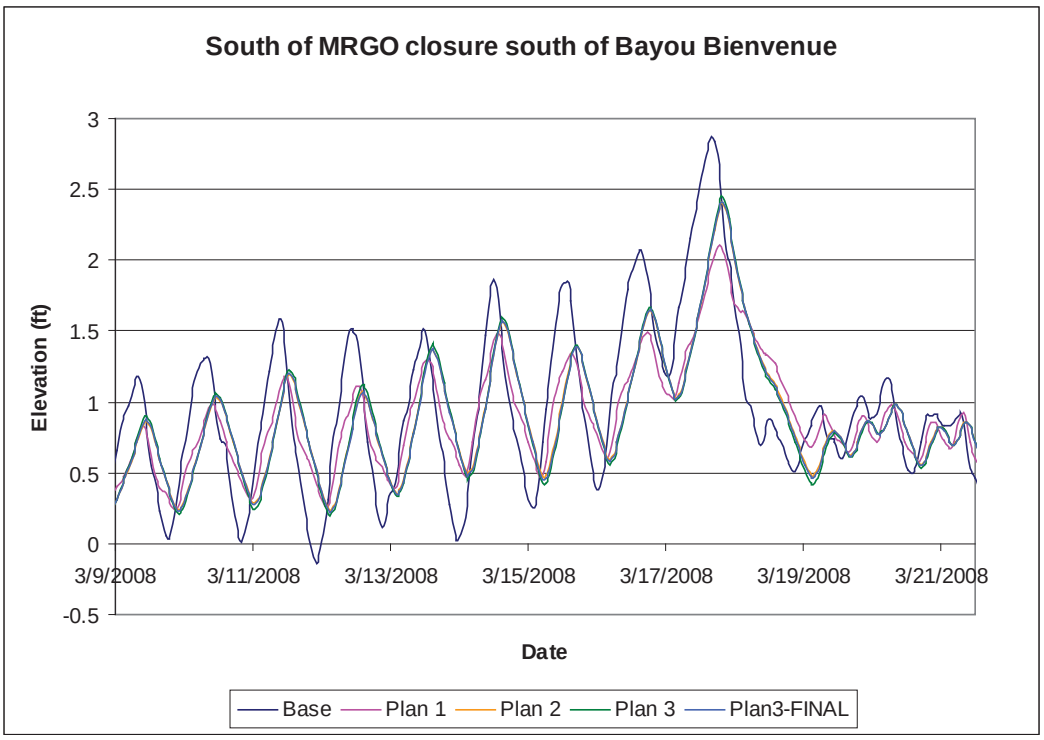

Figure 6-49. Water surface elevation south of MRGO closure at Bayou Bienvenue (March).

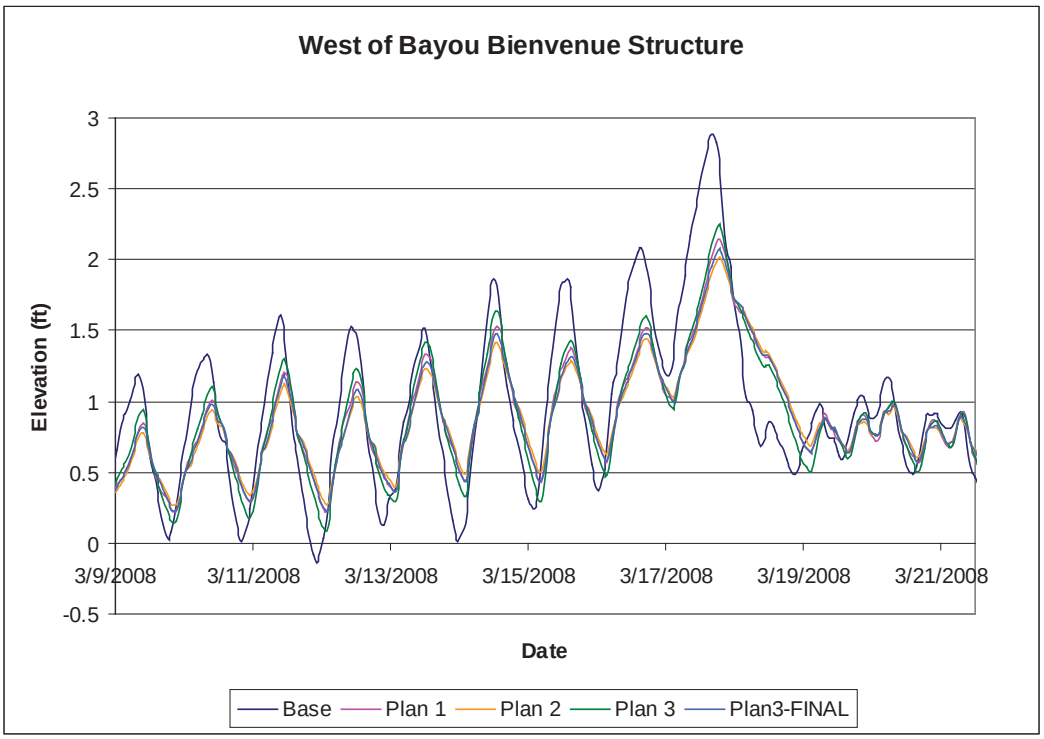

Figure 6-50. Water surface elevation west of Bayou Bienvenue structure (March).

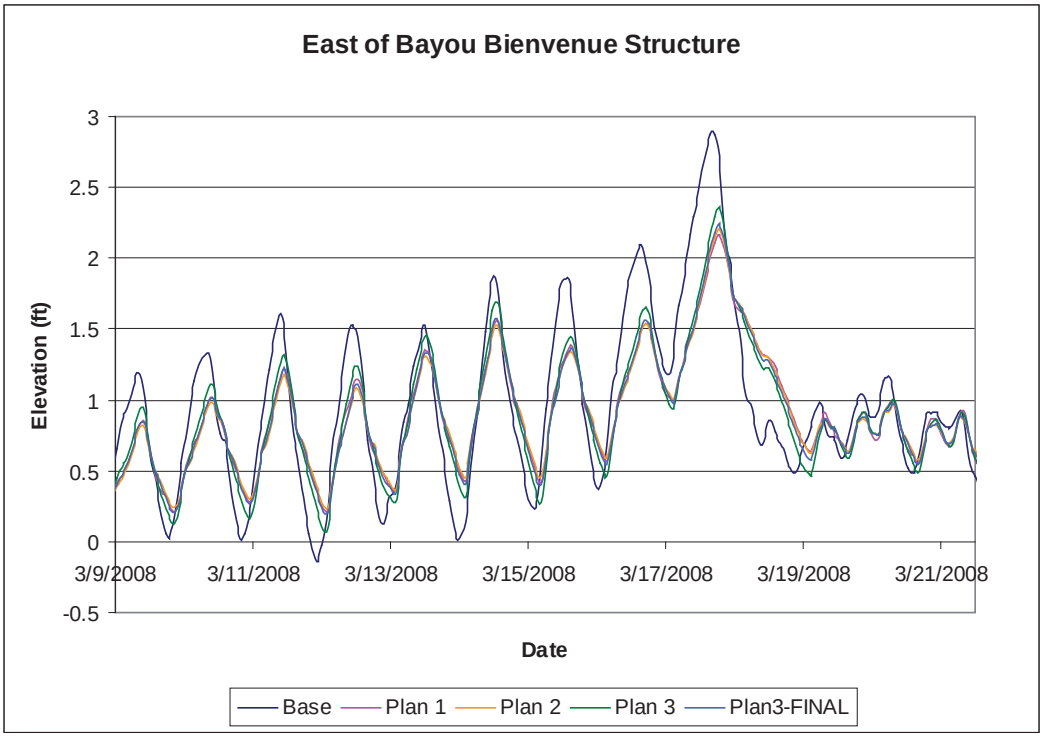

Figure 6-51. Water surface elevation east of Bayou Bienvenue structure (March).

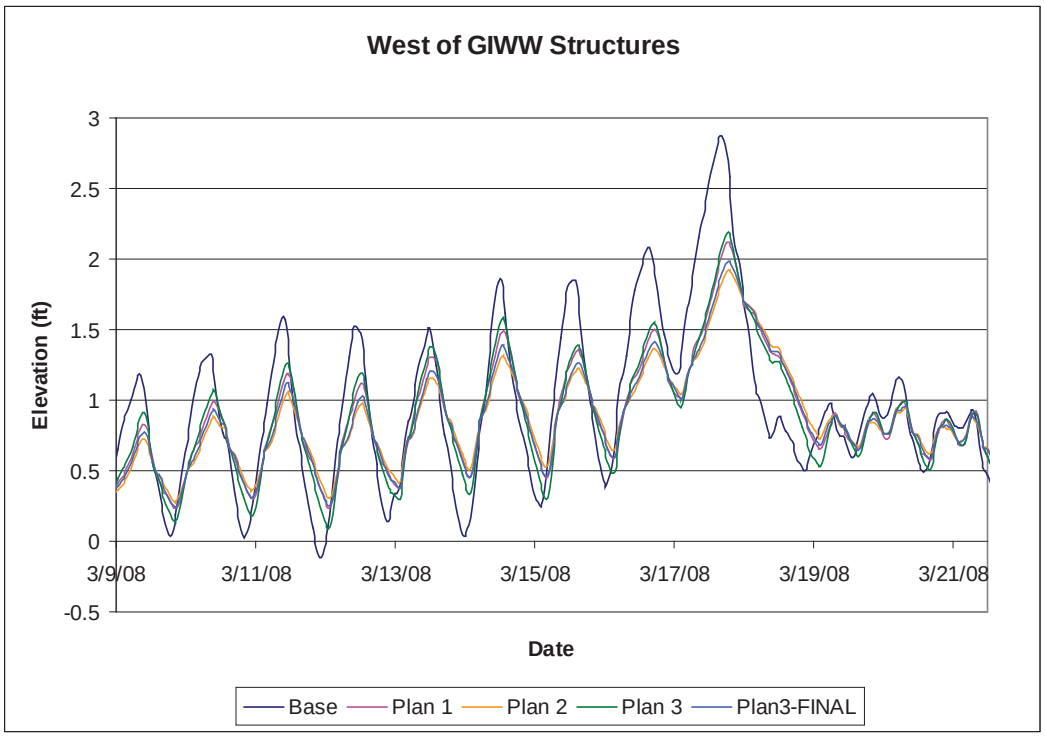

Figure 6-52. Water surface elevation west of GIWW structures (March).

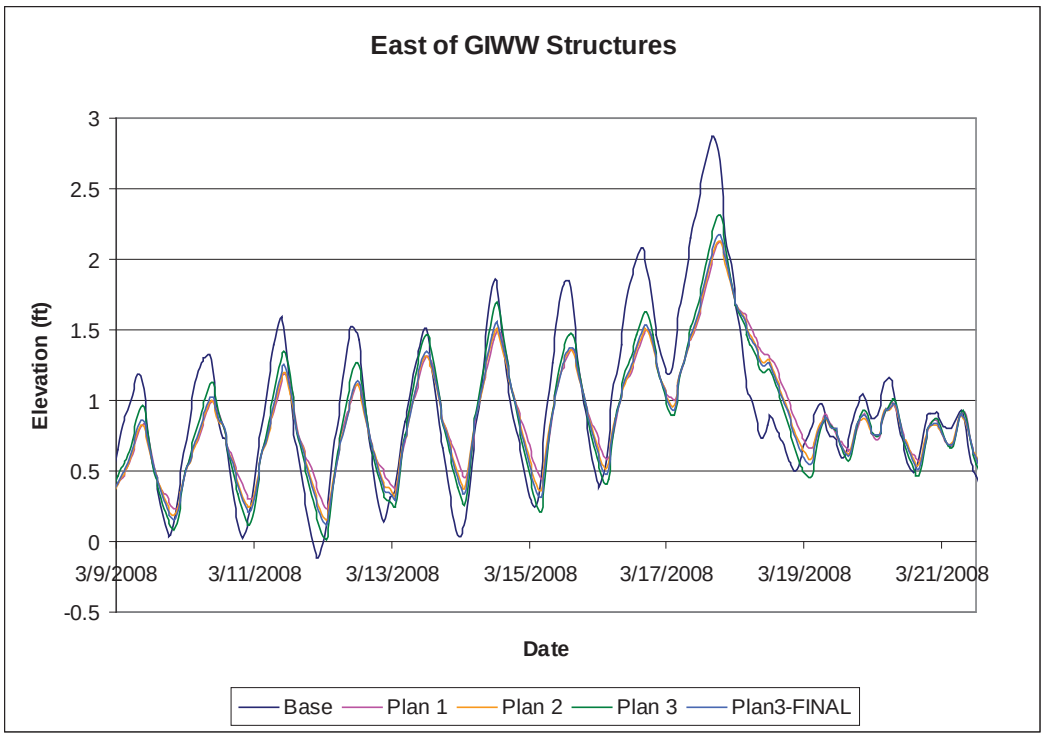

Figure 6-53. Water surface elevation east of GIWW structures (March).

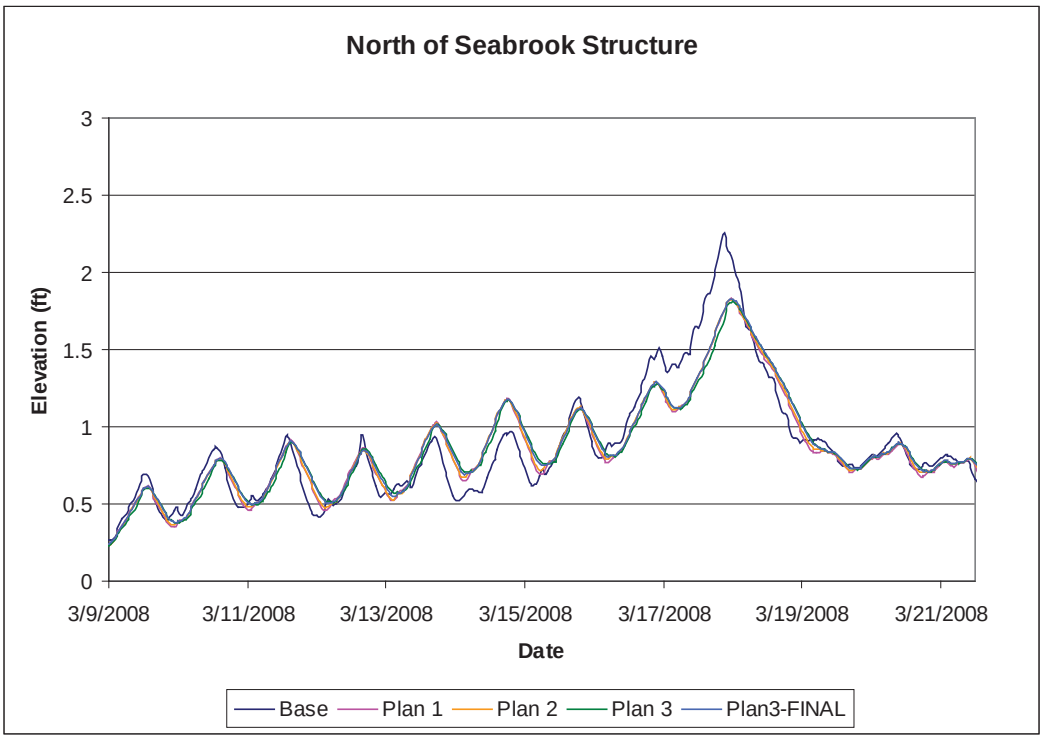

Figure 6-54. Water surface elevation north of Seabrook structure (March).

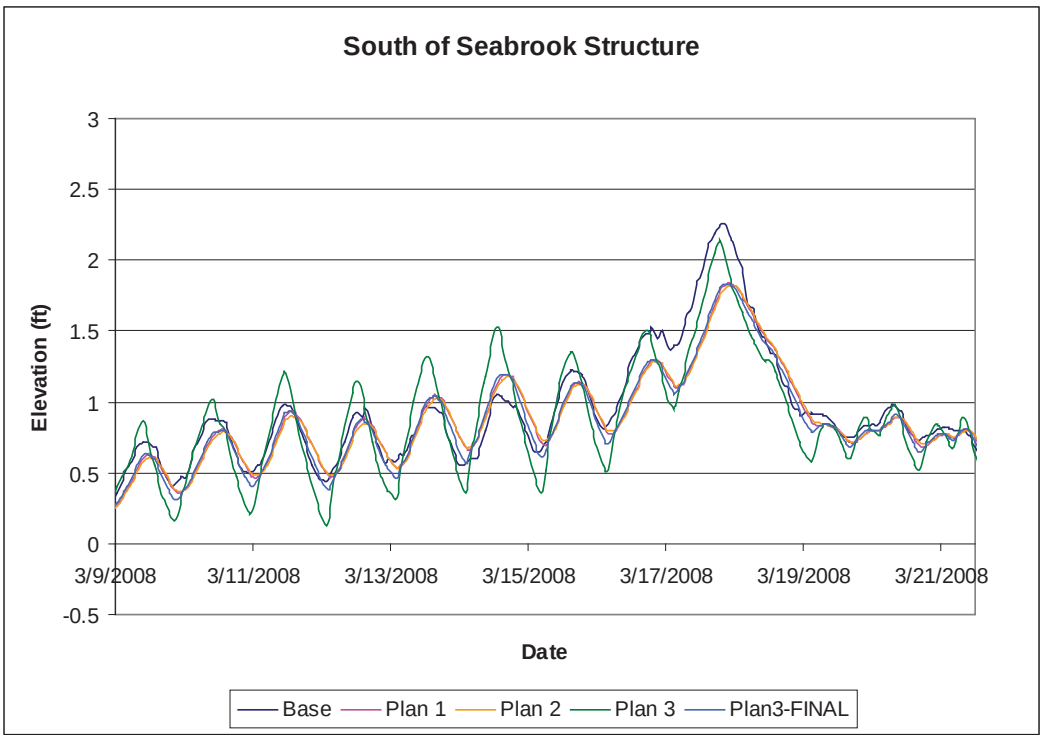

Figure 6-55. Water surface elevation south of MRGO Seabrook structure (March).

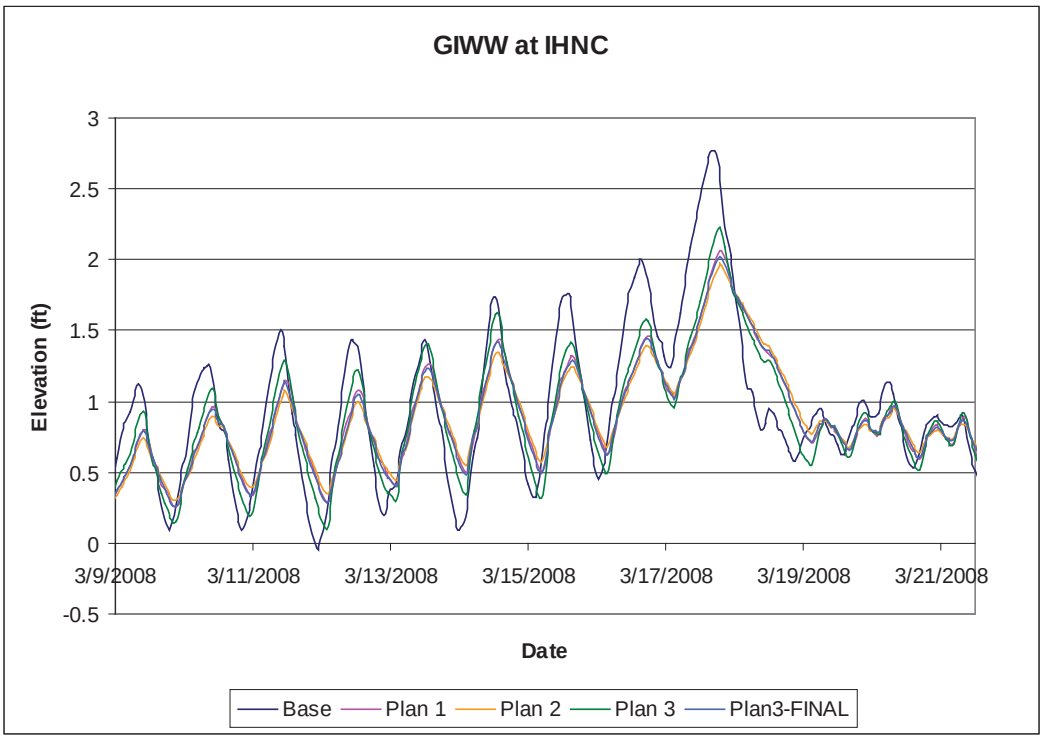

Figure 6-56. Water surface elevation in GIWW at IHNC (March).

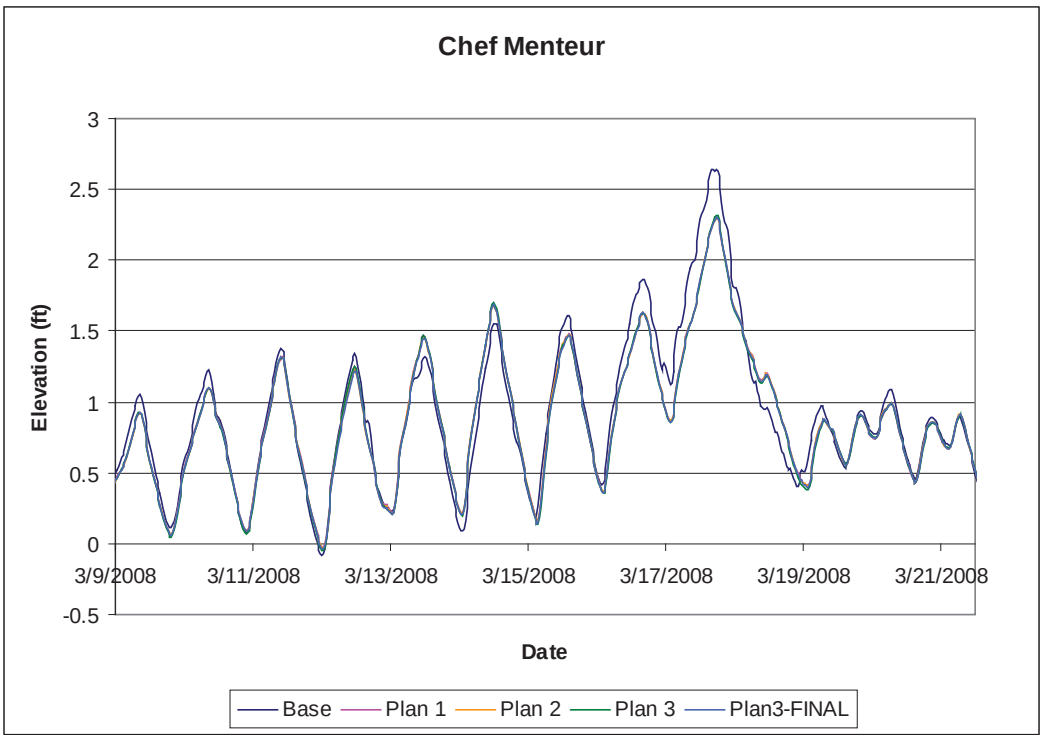

Figure 6-57. Water surface elevation in Chef Menteur (March).

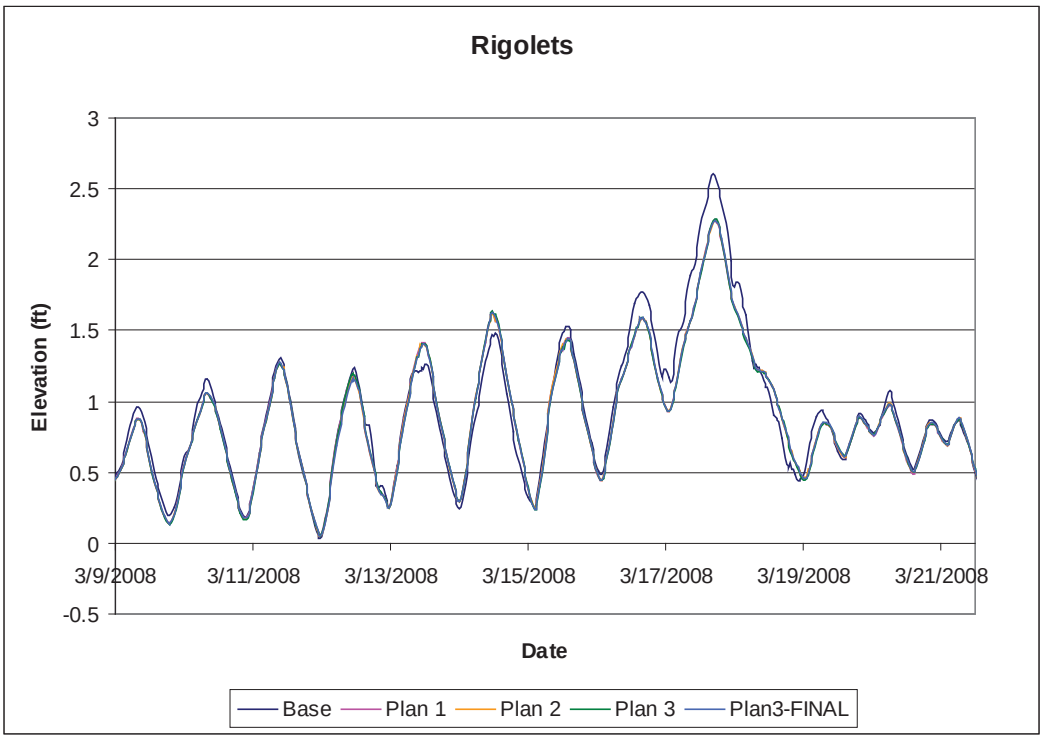

Figure 6-58. Water surface elevation in Rigolets (March).

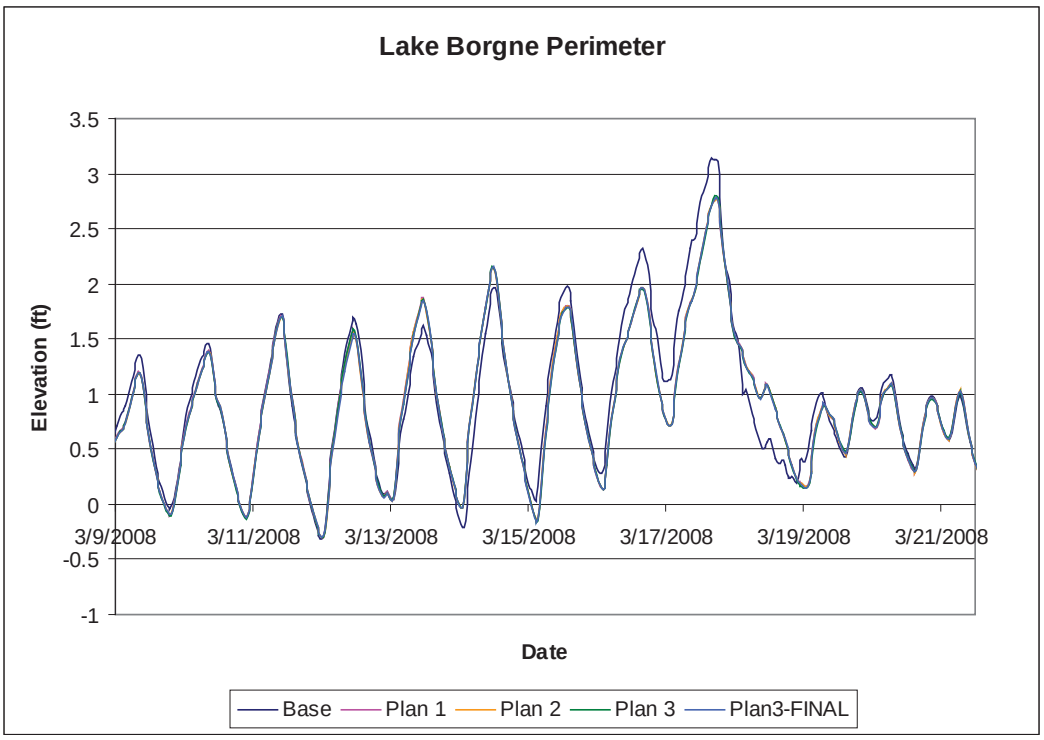

Figure 6-59. Water surface elevation at Lake Borgne perimeter (March).

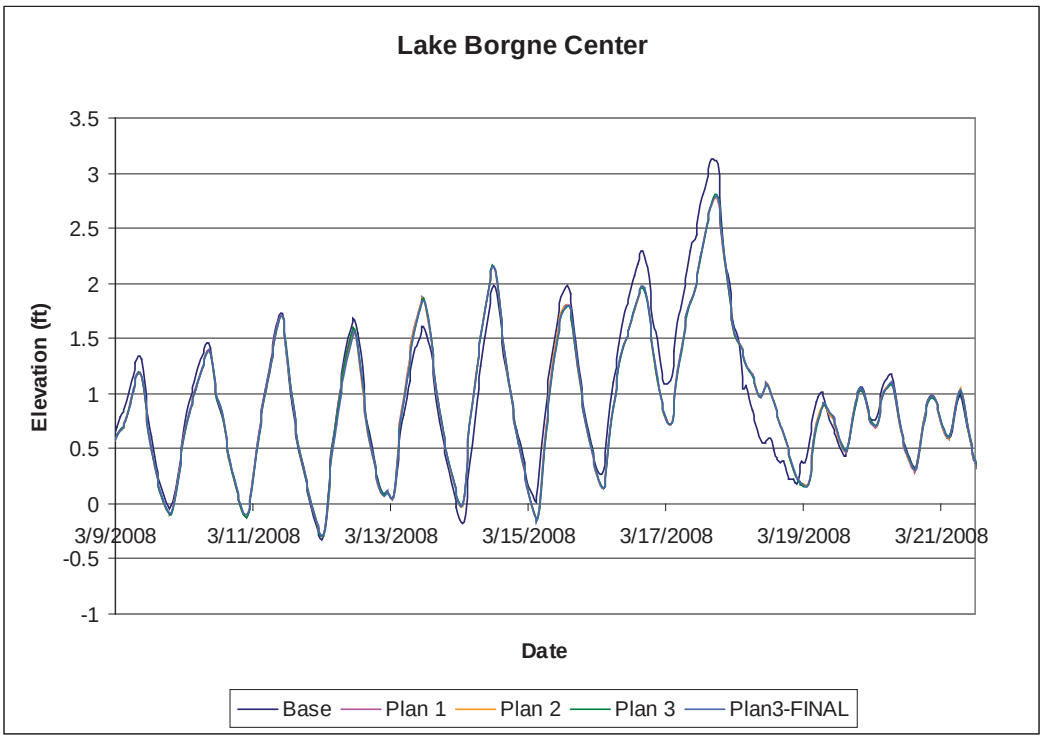

Figure 6-60. Water surface elevation at Lake Borgne center (March).

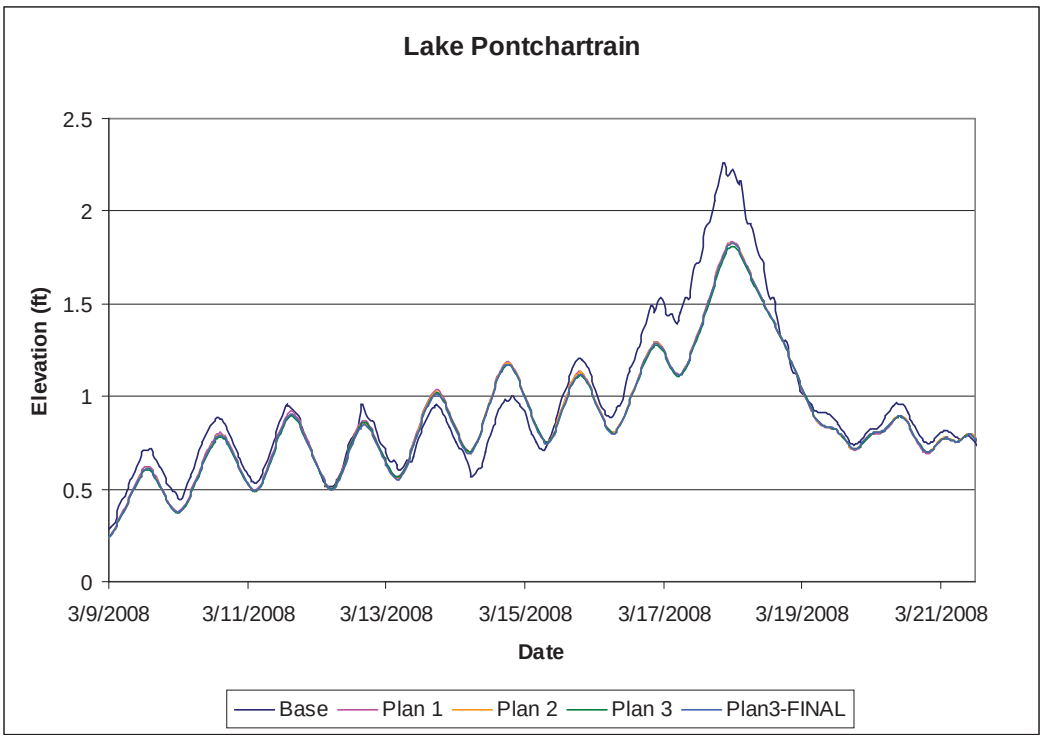

Figure 6-61. Water surface elevation in Lake Pontchartrain (March).

Based on the previous set of figures (Figures 6-30 through 6-61), for almost all of the locations in the area of the plan changes, the greatest change comes with Plan 1, the closure of the MRGO at La Loutre. The differences with each subsequent plan are less extreme. With the second closure and structure implementation of Plan 2, the elevation ranges continue to drop but the phasing generally remains further unchanged. However, once the Seabrook structure is included with Plan 3, the tidal range increases slightly at these locations due to the restriction of flow that it creates within this area of the GIWW and IHNC. Plan 3 Final, though, generates water surface ranges, on the order of Plan 1 and Plan 2, since the flow restriction at Seabrook is less in Plan 3 Final than in Plan 3.

The greatest impact of the Seabrook structure is south of its location (Figures 6-39 and 6-55). North of the structure there is little change due to the wider area and open waters of Lake Pontchartrain (Figures 6-38 and 6-54). To the south, however, the space is confined and the effects are felt in the IHNC. Plan 3 and Plan 3 Final include filling the southern scour hole which is at the location of this comparison point. The filling of this scour hole causes changes in the vicinity beyond just the reduction in cross-section due to the structure. This southward influence extends to the location labeled as "GIWW at IHNC." Here, the changes produced with the addition of Plan 3 (as compared to Plan 2) are larger than those produced with the addition of Plan 2 (as compared to Plan 1) (Figures 6-40 and 6-56). However, at this location, away from the filled hole, the effects are much less than immediately south of the Seabrook structure. For Plan 3 Final, the structure location is further south than for Plan 3 and the impact of the filled scour hole is much less. Plan 3 Final again produces results at this location comparable to those for Plan 1 and Plan 2.

The Chef Menteur location appears unchanged for the September analysis (Figure 6-41) but there is a large effect with Plan 1 that shows up in March (Figure 6-57). It is likely that the higher wind speeds and flows during this time as well as the direction of the wind are ideal for emphasizing effects in this area. This same change is observed at the Rigolets, Lake Borgne, and Lake Pontchartrain (Figures 6-58, 6-59, 6-60, and 6-61). Overall, the effect in March is showing a decline in the range of the water surface elevation during a storm event when compared to the Base condition. Although not included in this research, the exact reason for this decline could be due to the wind direction as well as the direction of the tide at this time. Each of the other plan conditions, however, does not generate further changes.

Circulation Analysis

The analysis of the hydrodynamic model results for both time periods reveals a clear change in circulation once the MRGO is cut off from the Gulf of Mexico. Figure 6-62 shows the direction of flow when the tide is rising for the Base condition. An incoming tide is most important for this project since the goal is to maintain larval fish transport into Lake Pontchartrain. The arrows are not drawn to scale but rather only indicative of flow direction. The flow moves up the MRGO and splits at the GIWW with a portion moving west and up the IHNC and a portion moving east down the GIWW. However, flow also enters the eastern section of the GIWW from Lake Borgne and at times splits to the east and west. Depending on the phase of the wave propagation up the MRGO and that in Lake Borgne, the direction of flow in the central GIWW area (circled in Figure 6-62) can be either to the east or the west for an incoming tide. In other words there is a change in direction as the tidal wave propagates into this area from several locations. Figure 6-63 shows the same information for Plan 1, Plan 2, Plan 3, and Plan 3 Final. Once the MRGO is cut off from the Gulf of Mexico at La Loutre, the tide cannot move up this channel as it did previously. Therefore the flow only enters the GIWW at its connections at Lake Borgne. Flow does move through Bayou Bienvenue but the amount of water it transports is much less than the flows that move up the MRGO or enter through Lake Borgne and has little effect on the overall circulation pattern through the GIWW. These changes show a clear direction of flow along the GIWW as opposed to a direction that may vary at times.

To further support these circulation changes, the velocity signals are compared at two locations along the GIWW, one on the eastern side of the MRGO and one on the western side. Figure 6-64 gives the location of these analysis points. The velocity values (with directions as defined previously) are given in Figure 6-65 for the point west of the MRGO and Figure 6-66 for the point east of the MRGO. Each line represents the Base or one of the plan conditions. For the western location the velocity drops once the MRGO is cut off at La Loutre (Plan 1) and continues to drop with each subsequent plan. It is important to also note that the flow directions indicate the expected diurnal tide signal and the phasing of the tide remains unchanged in this area. At the eastern location the Base case velocity indicates the changing magnitude and direction during the motion of the tide. Once the MRGO is cut off at La Loutre, however, flow along the GIWW comes in from its connection to Lake Borgne and splits east and west. This creates a smooth signal in the eastern GIWW like that observed in the western GIWW.

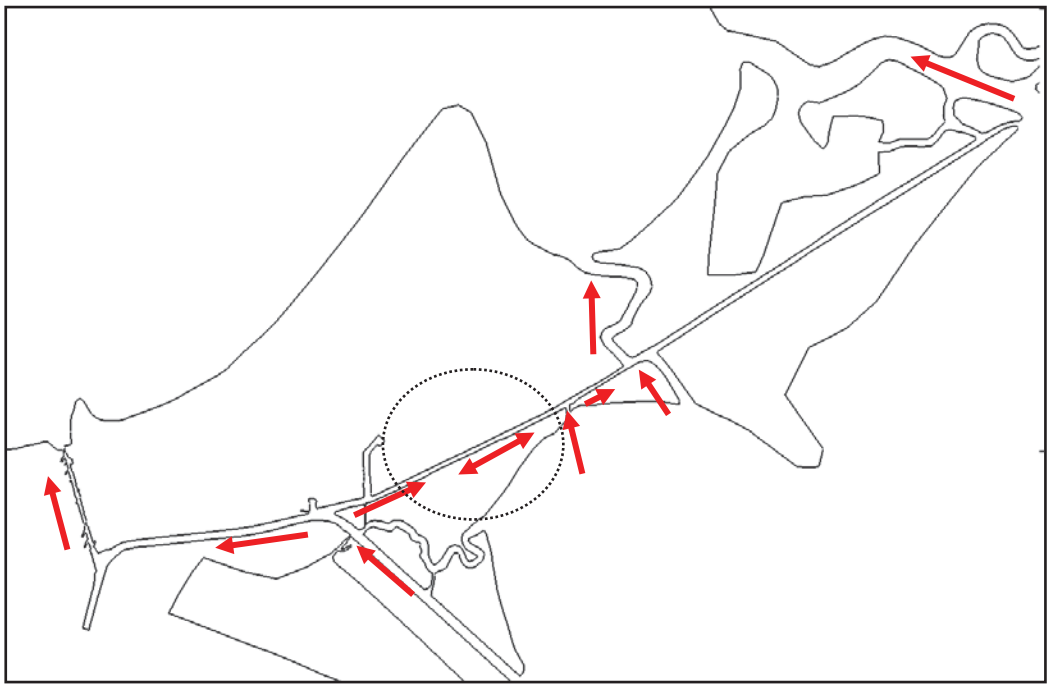

Figure 6-62. Direction of flow for incoming tide in Base case.

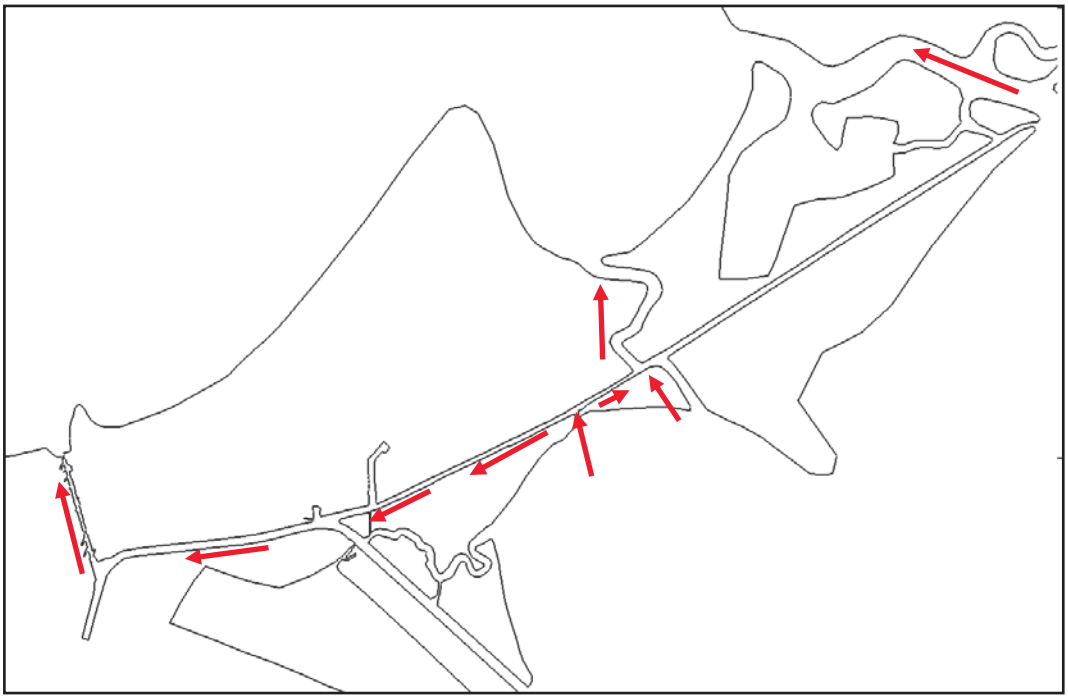

Figure 6-63. Direction of flow for incoming tide for Plan 1, Plan 2, Plan 3, and Plan 3 Final.

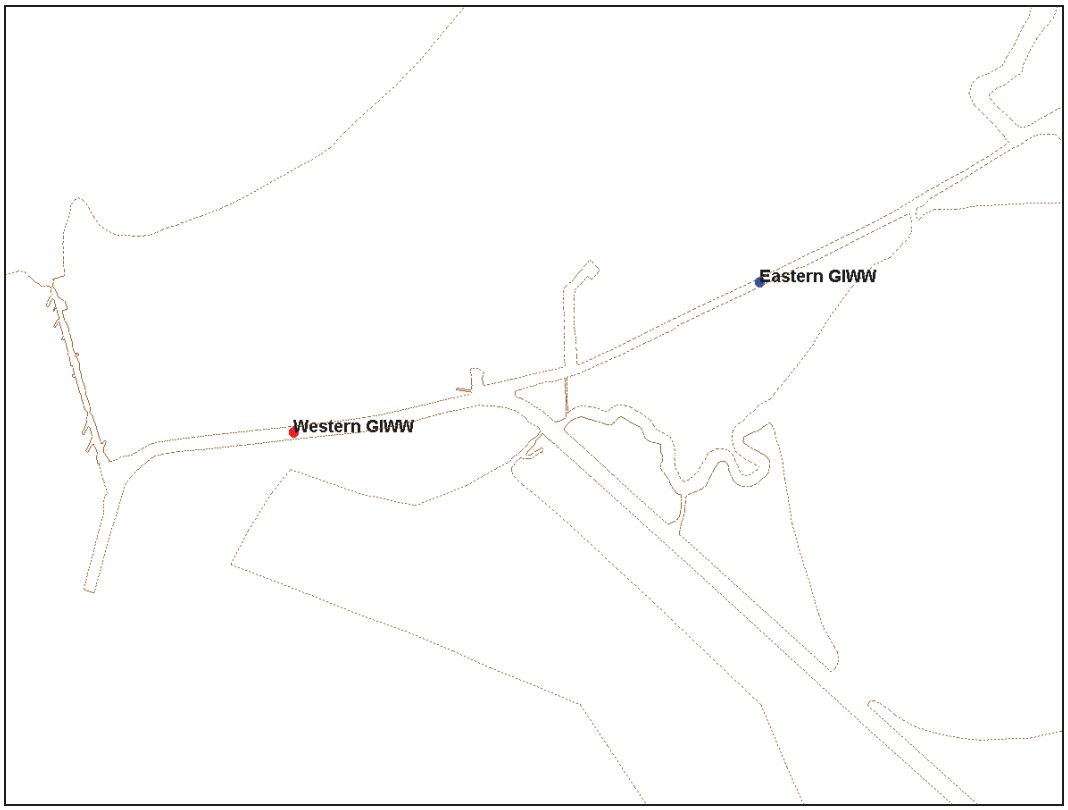

Figure 6-64. GIWW velocity analysis locations.

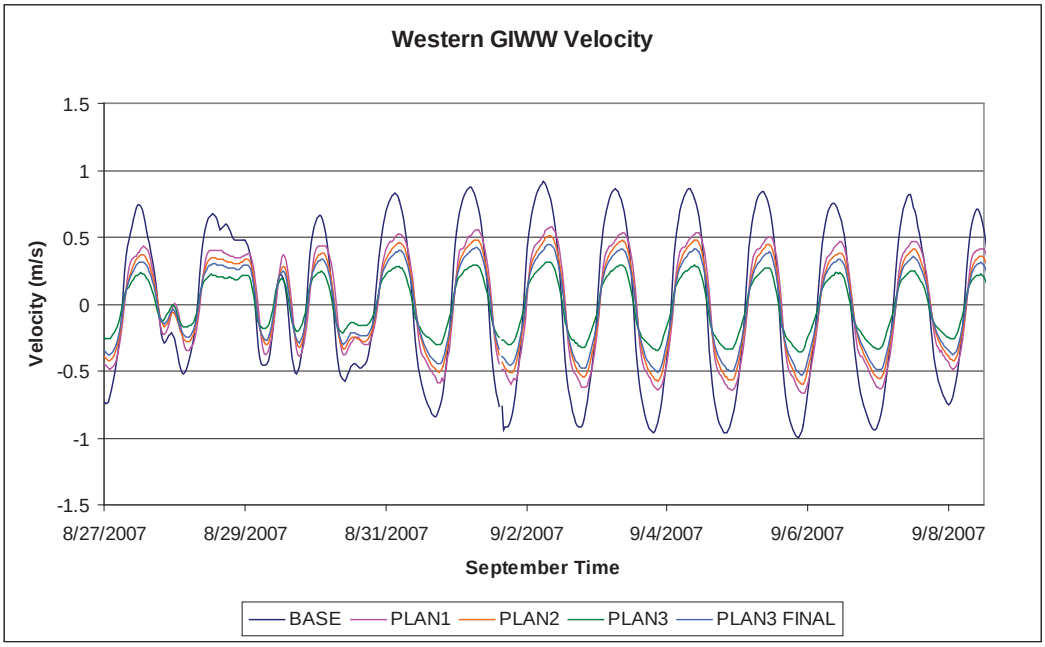

Figure 6-65. Velocity signal in the GIWW west of MRGO, velocities west of the Borgne alignment on the GIWW decrease with the closure of the MRGO at La Loutre.

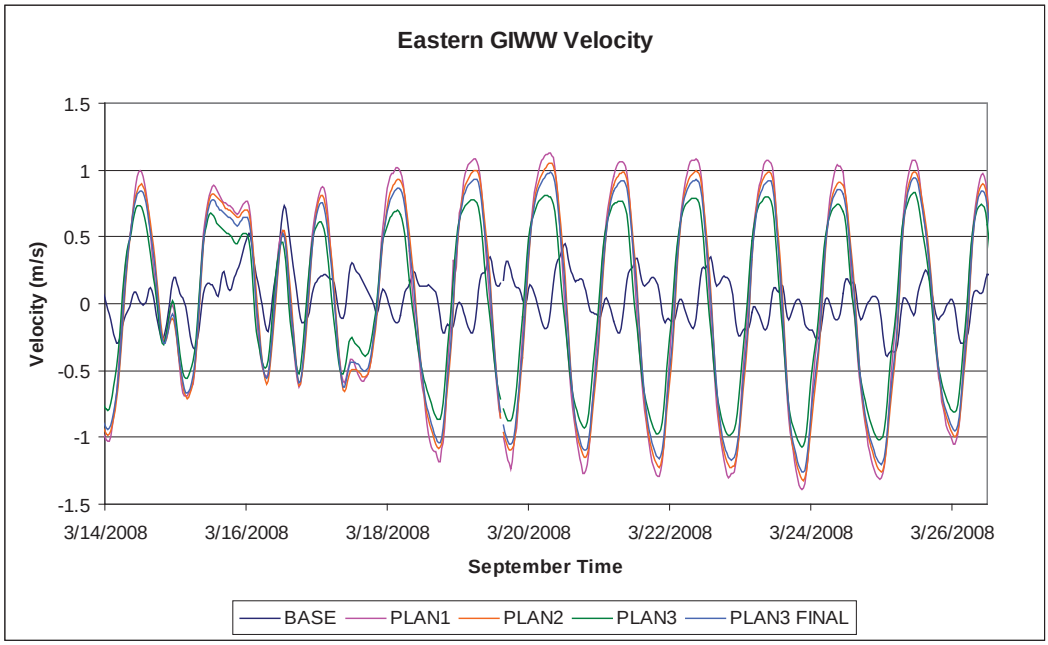

Figure 6-66. Velocity signal in the GIWW east of MRGO, velocities east of the Borgne alignment on the GIWW increase with the closure of the MRGO at La Loutre.

Summary

The results of the hydrodynamic analysis include velocity magnitude and direction, water surface elevation, and overall circulation changes. Comparisons are made to examine how the flow in this area changes from the Base condition with each plan condition. The initial analysis shows that the implementation of Plan 1, closing the MRGO at La Loutre, creates large changes to all of these parameters. These parameters continue to change with the implementation of Plan2, Plan 3, and Plan 3 Final but the changes due to these configurations are less than the initial changes generated with Plan 1. The changes in the circulation through the GIWW are initiated with the Plan 1 closure as well. The velocity magnitudes in the location of the structures rise greatly when the structures are included due to the reduced cross-sectional area at these locations.

7 Particle Tracking Results

The results of the particle tracking modeling for the larval fish transport are addressed in this chapter for the base case as well as design Plans 1-3. The output and analysis of the simulations are separated into Cases 1-3 described in Chapter 5. Case 4 initial conditions are applied in Chapter 8.

Case 1

In this simulation, particles are placed near the MRGO closure at La Loutre. Initial testing of this source revealed several difficulties. For the base case in which there is no construction, particles travel down the path shown in Figure 7-1 which is along the MRGO. However, the transport time for particles to travel down the MRGO to Bayou Bienvenue is approximately 2 weeks for the March 2008 hydrodynamic conditions. The transport time for the September 2007 Base condition is longer. To obtain relevant statistics, it is necessary for particles to have time to reach the recruitment areas within the allotted time frame.

Figure 7-1. Location and transport path for larvae initiated for Case 2. The red circle represents the approximate location of the initial positions.

Transport times for the plan configurations are greater than for the Base. Because all plan configurations include the MRGO closure at La Loutre, the particle pathway becomes obstructed. Alternate pathways around the closure via Lake Borgne are possible; however, the recruitment time for that transport pathway is much too long for the allotted simulation time of this project (4 weeks).

Case 2

Case two particles are initiated both at the GIWW constriction and the MRGO 2nd closure (Figure 5-3). Particles are introduced across the width of the channel for two weeks and then transported for the remaining two weeks of the simulation. Approximately 4800 particles are released.

Figures 7-2 thru 7-5 show “snap shots” of particle positions for the September 2007 hydrodynamic conditions. Each frame (a-c) shows a snap shot of where the particles are at a specified time of one day, one week, and four weeks. The particles are color coded based on their initial position. The red particles are initiated in the region of the GIWW to the east of the constriction. The yellow particles are initiated in the MRGO near the eventual second closure position.

In Figure 7-2, which shows the results of the Base construction phase using the September 2007 hydrodynamics, after one day particles are transported to the union of the MRGO and GIWW. At this time particles are still being introduced into the flow. This is illustrated by the stream of particles that stretch from the initial points towards the MRGO/GIWW connection. After one week some particles have reached the Seabrook recruitment area (R1). Also mixing of particles between the two different initial source locations has occurred. Particles traveling up the MRGO have turned into Bayou Bienvenue and are moving towards Lake Borgne. Some particles are also taking alternate paths into the wetland region to the southwest of the MRGO. After four weeks, the particles appear to be completely mixed as if initial position has no affect on the final position of the representative particles. It is noticeable that a small number of particles end in Lake Borgne.

a)

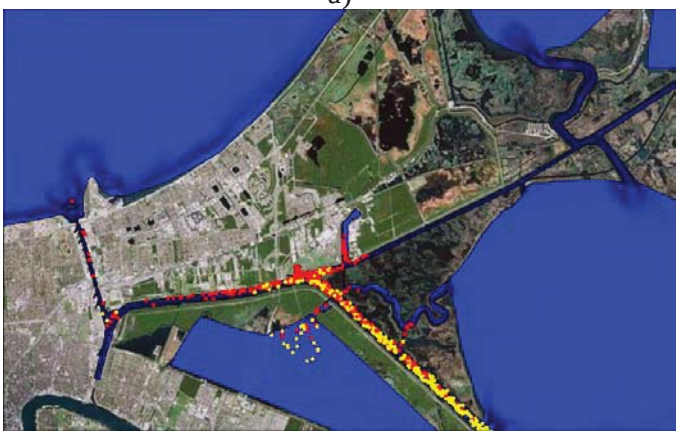

b)

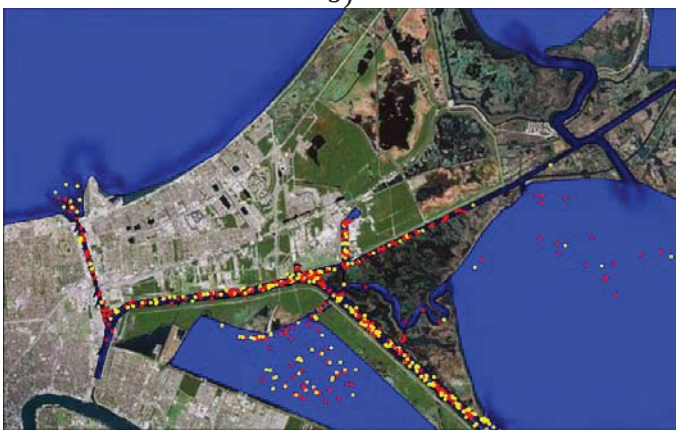

c)

Figure 7-2 September, Base condition larvae positions after a) 1 day, b) 1 week, c) 4 weeks. Red particles are initiated on the GIWW and yellow particles are initiated on the MRGO.

a)

b)

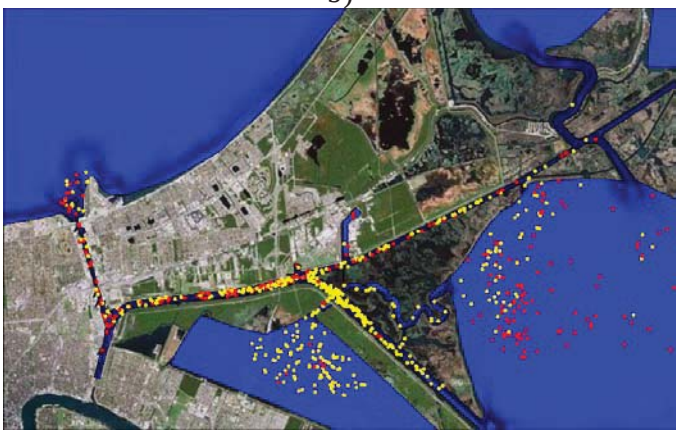

c)

Figure 7-3 September, Plan 1 condition larvae positions after a) 1 day, b) 1 week, c) 4 weeks. Red particles are initiated on the GIWW and yellow particles are initiated on the MRGO.

a)

b)

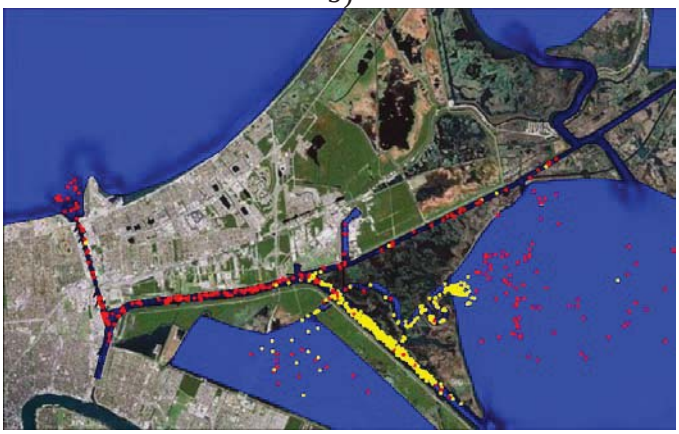

c)

Figure 7-4 September, Plan 2 condition larvae positions after a) 1 day, b) 1 week, c) 4 weeks. Red particles are initiated on the GIWW and yellow particles are initiated on the MRGO.

a)

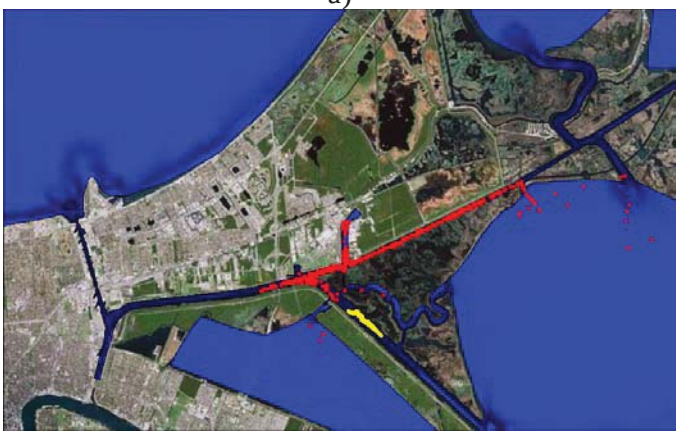

b)

c)

Figure 7-5. September, Plan 3 condition larvae positions after a) 1 day, b) 1 week, c) 4 weeks. Red particles are initiated on the GIWW and yellow particles are initiated on the MRGO.

Figure 7-3 shows the resulting particle positions utilizing September 2007 hydrodynamics with the Plan 1 configuration. At this point, the MRGO closure is in place at La Loutre. The flow along the MRGO is significantly reduced. The effect of this can be seen in Figure 7-3a. The dispersion of the yellow colored particles, initiated in the MRGO to the southeast of the 2nd closure, is smaller after 1 day than the previous Base case. However, the red particles at this same time step appear to have been transported further. After one week this trend is even more obvious. The yellow particles appear significantly less dispersed than the red particles. Due to the reduced flows in the area of the MRGO, the concentration of particles is appreciably higher. Also the number of particles that are transported into Lake Borgne has increased. This is most likely due to the fact that as the flow along the MRGO has decreased, the GIWW velocity has increased. After the full four week period, it is noticeable that the number of remaining yellow particles is greater than the Base case and the distance transported is less.

Plan 2 configuration results are shown in Figure 7-4. Here the 2nd MRGO closure is in place south of Bayou Bienvenue. Particles initiated to the southeast of the closure are initially trapped. The velocity magnitude in this position has decreased drastically. The overall velocity magnitude along the GIWW has decreased, although velocity increases at the GIWW constriction. After 1 week, particles have begun traveling along the GIWW, but the yellow particles (initiated in the MRGO) are still in a very concentrated configuration. Although the number of particles recruited at this point appears to have decreased in comparison with the previous cases, it is also quite visible that the particles that remain are still being transported along the length of the GIWW. Several pathways to Lake Borgne are being utilized/given access due to the velocity decrease. After a four week period, the red particles have traveled along alternate pathways (Bayou Bienvenue and Lake Borgne) to reach the MRGO.

Finally, Figure 7-5 shows the September 2007 results for the Plan 3 configuration. In this phase, the Seabrook construction is added. The velocity magnitude of the flow along the GIWW has been further reduced. The transport of particles decreases, though generally the flow direction and patterns of behavior are very similar to Plan 2 results. The major difference between the particle transport for both of these configurations and the Base and Plan 1 configuration is that particles near the MRGO closure at Bayou Bienvenue are hindered from moving throughout the system.

Figures 7-6 through 7-9 depict the transport results of the March 2008 hydrodynamic conditions. The March 2008 particle transport is similar to the September case. The base configuration shows particles along both the GIWW and the MRGO. The Plan 1 case shows a decrease in transport of particles initiated along the MRGO. The Plan 2 and Plan 3 configurations allow for transport along the GIWW, but the MRGO initiated particles follow pathways to Lake Borgne and Bayou Bienvenue. As shown in the hydrodynamic results section, the March 2008 flow has greater intensity in the tidal conditions. Overall transport is much higher than in the September 2007 conditions.

Data analysis of the simulation results for this work is performed using the recruitment information. As particles pass through the recruitment arcs, the number of particles and some of their characteristics such as their starting position and behavior type are collected.

Figure 7-10 shows the time series of the number of larvae that reach both recruitment points (Figure 5-6) with time given in days for the September 2007 hydrodynamic solution. The total simulation time for these model runs is 28 days. The figure shows Base, Plan1, Plan2, and Plan3 trends. For the September 2007 flow conditions, the maximum number of larvae recruited is approximately 1400 in the Base case. The Plan 1 case recruits approximately 800 representative larvae, 500 for the Plan 2 case, and approximately 100 particles are recruited in the Plan 3 case. This figure also shows the rate at which particles are recruited, represented by the slope of the line. The rise and plateau in the graph are important in understanding the method in which particles are recruited. It is apparent in the graph that for the Plan 1-3 cases, the particles appear to be recruited in much the same way, though the number of recruited particles is different. The rise and plateaus appear in the same places for each case; however the overall slope in the lines decreases as the plan number increases. Plans 1-3 all include the MRGO first closure. This reduces the velocity in the MRGO and therefore subsequent transport. It can, however, be noticed that recruitment values for the Base case are slightly lower than Plan1 and Plan 2 at the beginning of the time series and then abruptly increase at approximately day 20. It is reasonable to assume that Plans 1 and 2 have a larger number of particles recruited initially because these particles are associated with the initial source location in the GIWW. The particles are introduced into the flow to the west of the GIWW structures. As seen in later analysis of the behaviors and recruitment areas, for Plans 1-3, most of the recruitment occurs at Chef

Menteur. Velocity trends and preferred tidal direction in the GIWW change with the MGRO closures. Particles initially move very quickly to the Chef Menteur recruitment position. However, eventually, particles that are initiated in the MRGO reach the Seabrook recruitment area in the Base case and begin to have an effect on the overall number of particles recruited. In addition, more particles in Plans 1-3 are transported into Lake Borgne which decreases the rate of recruitment for those plans. This theory is supported by further analysis later in this section when we remove the MRGO source and consider only the GIWW source. The initial time series (prior to day 20) are generally the same, showing that the MGRO source is insignificant until that point.

The number of larvae that reach both recruitment areas with time given in days for the March 2008 hydrodynamic solution is shown in Figure 7-11. Generally the plot follows the same trends as the September 2007 results. Similar to those results, there is a marked difference between the Base case and the plan cases. The maximum number of recruited particles is approximately 2900 which occur in the Base case. For the Plan 1 case, approximately 750 were recruited, 500 for Plan 2, and 130 for Plan 3. The trends show similarly shaped series, except there is an abrupt increase in the slope of the Base case, representing the increased recruitment rate for that configuration.

A summary of the percentage of particles recruited is shown in Table 7-1. Results show that the largest percentages of particles are recruited in the Base case. Recruitment values decrease as plan numbers increase. These results reflect the trends shown in Figures 7-10 and 7-11.

Table 7-1 Percentage of larvae recruited for each construction phase for simulations in which particles are initiated in the MRGO and GIWW (Case 2 conditions).

Construction Phase	Percent Recruited – September 2007	Percent Recruited – March 2008
Base – September 2007	28.2	60.8
Plan 1– September 2007	16.9	15.6
Plan 2 – September 2007	10.8	10.4
Plan 3 – September 2007	1.2	2.7

a)

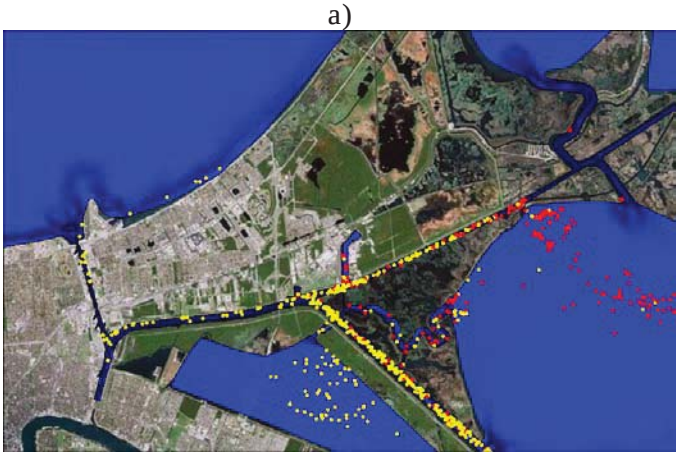

b)

c)

Figure 7-6 March, Base condition larvae positions after a) 1 day, b) 1 week, c) 4 weeks. Red particles are initiated on the GIWW and yellow particles are initiated on the MRGO.

a)

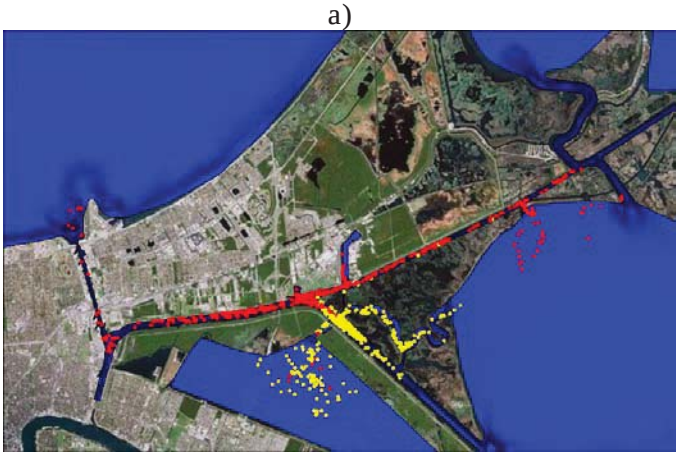

b)

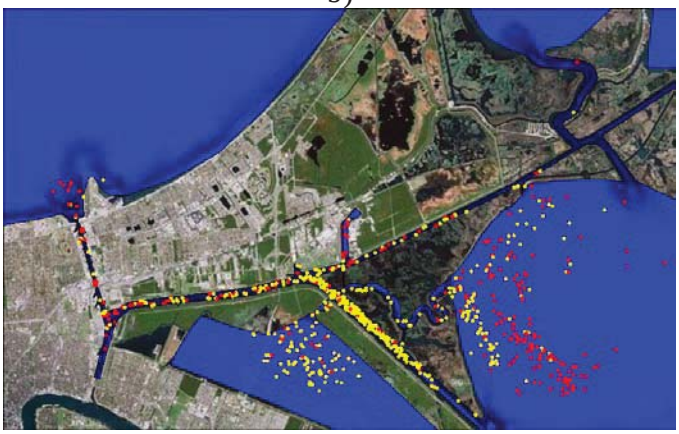

c)

Figure 7-7. March, Plan 1 condition larvae positions after a) 1 day, b) 1 week, c) 4 weeks. Red particles are initiated on the GIWW and yellow particles are initiated on the MRGO.

a)

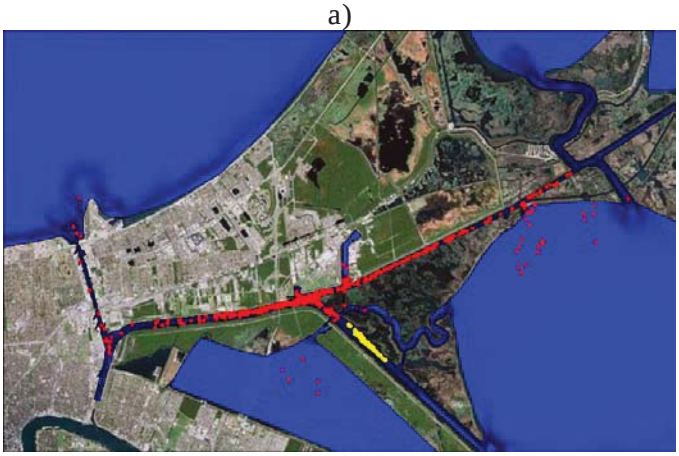

b)

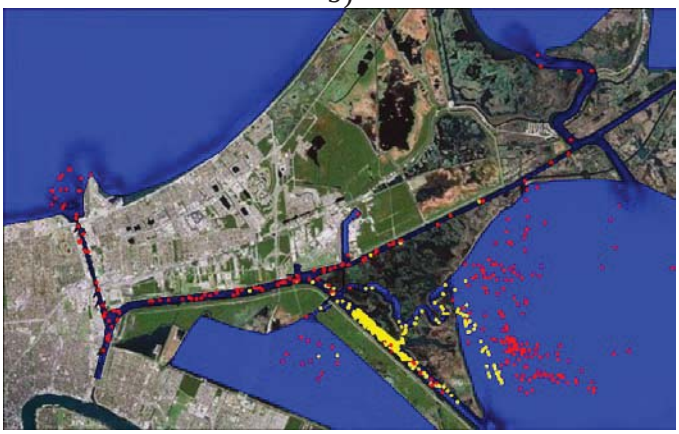

c)

Figure 7-8. March, Plan 2 condition larvae positions after a) 1 day, b) 1 week, c) 4 weeks. Red particles are initiated on the GIWW and yellow particles are initiated on the MRGO.

a)

b)

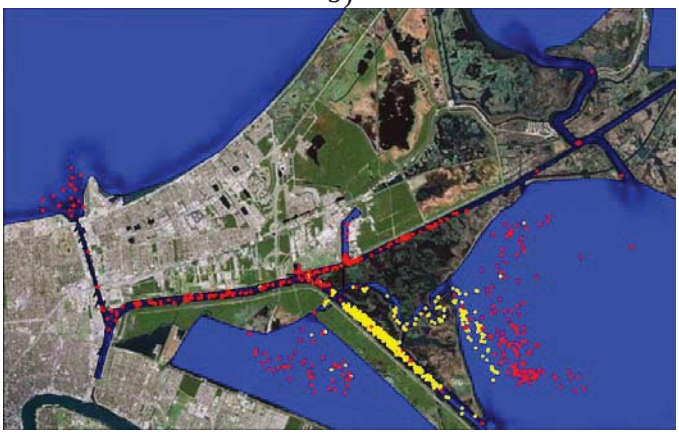

c)

Figure 7-9. March, Plan 3 condition larvae positions after a) 1 day, b) 1 week, c) 4 weeks. Red particles are initiated on the GIWW and yellow particles are initiated on the MRGO.

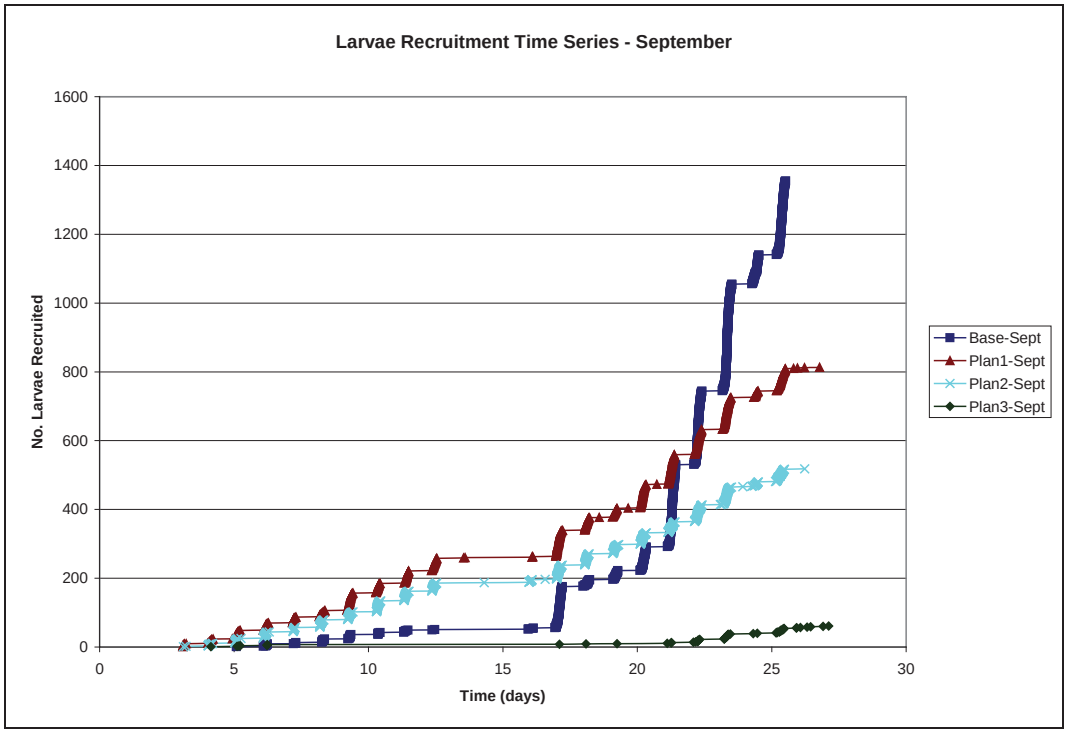

Figure 7-10. Time series of the number of larvae recruited with time for Base, Plan1, Plan2, and Plan3 configurations using September 2007 hydrodynamics. 4800 particles total.

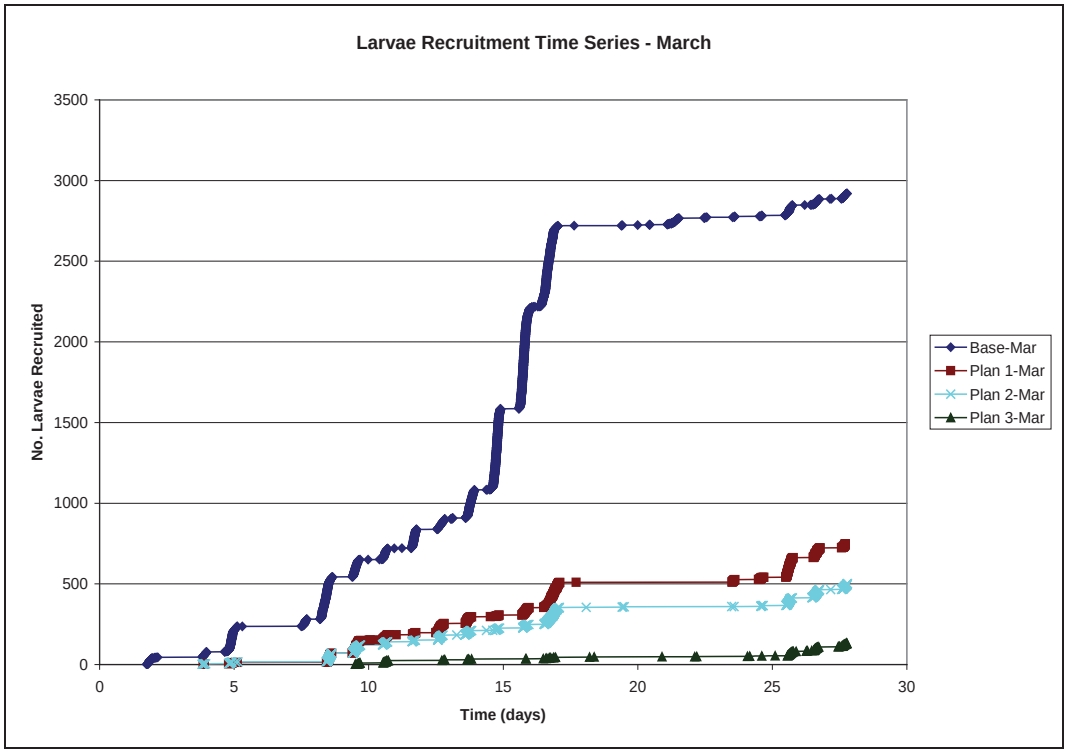

Figure 7-11. Time series of the number of larvae recruited with time for Base, Plan1, Plan2, and Plan3 configurations using March 2008 hydrodynamics. 4800 particles total.

In an effort to understand the results shown in Figures 7-10 and 7-11 a series of tests and sensitivity studies was done on the data. The first consideration was to determine if initiating particles near the MRGO closure might affect the data analysis results. The initial location of the particles released in the MRGO is to the southeast of the 2nd MRGO closure that is included in Plans 2 and 3. In the cases of Plans 2 and 3, particles placed in the MGRO are not able to easily navigate around the 2nd MRGO closure. There will therefore be greater total recruitment for the Base case because of the number of particles released in the MRGO that have a clear pathway to the recruitment areas. It is useful to examine solely the particles which are initiated in the GIWW. Figures 7-12 and 7-13 show these results. It can be seen from these figures that differences in the recruitment values between the plan and Base configurations decrease. In the March case, the previous graph showed that approximately 60 percent of the particles were recruited in the Base case, whereas 15 percent of the particles were recruited in the Plan 1 case. When only the GIWW source is considered, the Base case shows approximately 28 percent of the particles are recruited and the Plan 1 case remains at approximately 15 percent. The September results show similar trends. These results confirm that when the particles which are initiated in the MRGO are not considered, the remaining results are better aligned. It also shows that for the Plan1 and Plan2 configurations, the majority of particles which are recruited come from the GIWW source. This suggests that fish larvae originating in the MRGO may have difficulties determining pathways to the recruitment areas. It is unlikely that many larvae will be transported into these areas due to the MRGO closures.

Another area of interest is the difference between the March 2008 and September 2007 results. Generally, for all simulation cases, the recruitment values within the March 2008 case are larger. This question is addressed by considering the tidal signal (Figure 4-6). The magnitudes of the tidal signal for the March 2008 case seem to have higher peaks. Particle pathways and the recruitment time series illustrate periods where large numbers of particles are recruited over relatively small periods of time. This is indicative of the flushing of particles out of the system. This causes large jumps in the number of recruited particles.

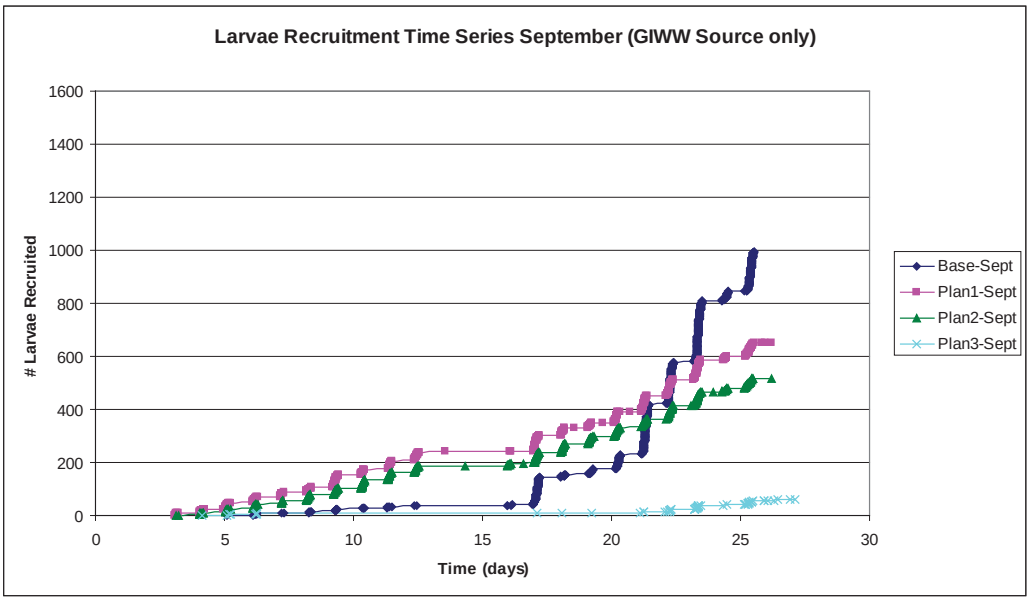

Figure 7-12 Time series of the number of larvae recruited with time for Base, Plan1, Plan2, and Plan3 configurations using March 2008 hydrodynamics for GIWW source only (2195 particles total).

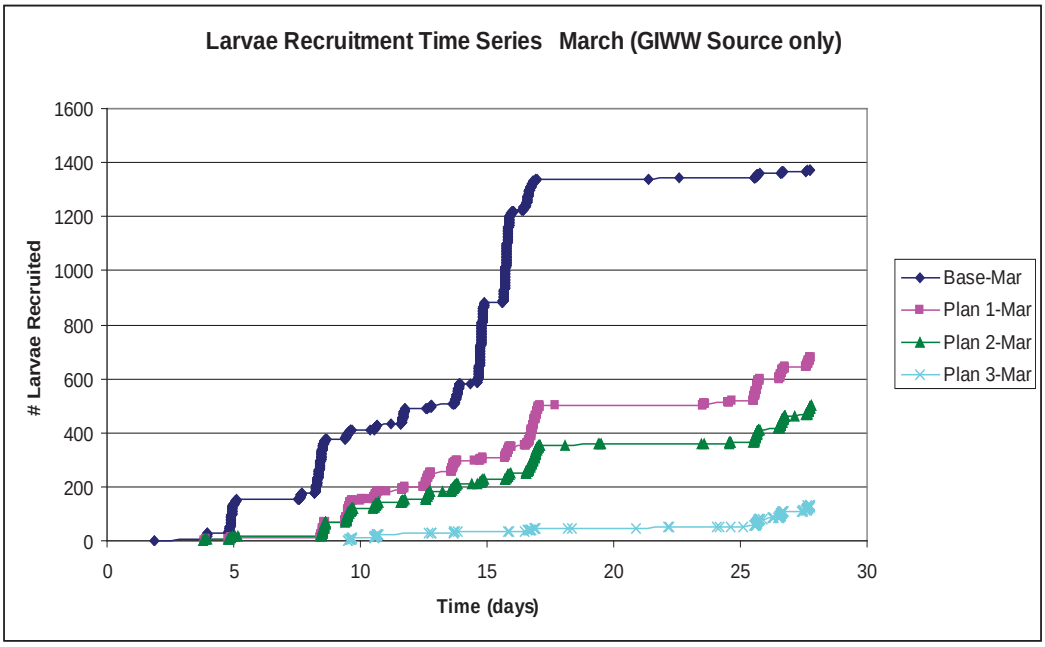

Figure 7-13. Time series of the number of larvae recruited with time for Base, Plan1, Plan2, and Plan3 configurations using March 2008 hydrodynamics for GIWW source only (2195 particles total).

To determine the effect of the tidal peaks on the larvae recruitment time series, a test was done with 80 particles on the March 2008 hydrodynamic, Base configuration (Figure 7-14). The same hydrodynamic results were utilized, except particles were initiated at two different times. One set of

particles was initialized at the beginning of the hydrodynamic period. A second set of particles was initiated after an additional week. The "lagged" series follow the same trends as the "original" series. It can be seen that fewer particles are recruited in the lagged case. This suggests that the timing of particle introduction with regard to the tidal signal is important. If particles are introduced as a large incoming peak in the signal is approached, there is more likelihood that they will be flushed out of the channels and into the recruitment areas.

The peaks of the tidal signals may not be the only reason for the difference between September 2007 and March 2008. Phase differences and flow interaction between the MRGO and GIWW may complicate matters. As seen in the hydrodynamic analysis, there are persistent phase differences between the GIWW and the MRGO. This phase difference may work to the benefit or the detriment of transport. If the flows move in sync, then particles will be quickly washed in one direction, however if they are moving opposed to each other, then it is also possible that transport may be interrupted.

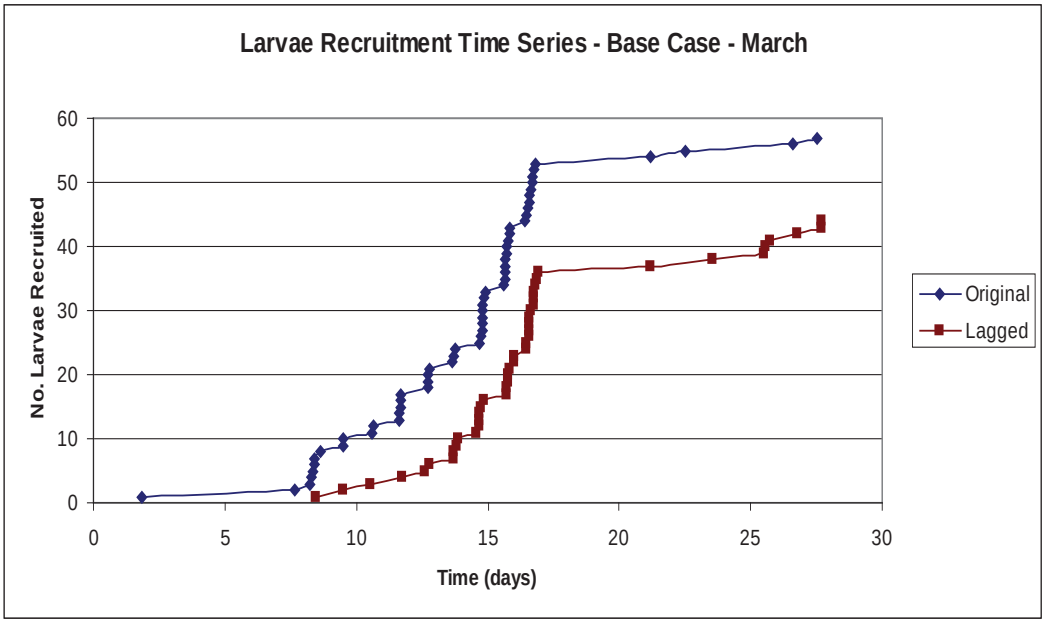

Figure 7-14 Comparison of Larvae Recruitment Time Series for the March 2008 Hydrodynamic, Base configuration.

Finally, the effect of behavior on particle recruitment is studied. The number of larvae (given as a percentage) recruited at both recruitment sites for each type of behavior for the September 2007 period is shown in Figure 7-15. Red zones within the column represent the particles which are

recruited at Chef Menteur. Blue zones within the column represent the number of particles which are recruited at the Seabrook recruitment area. The percentage is based on the total number of particles initiated within the simulation (% recruited = number of particles recruited per behavior/total number of particles of that behavior x 100). The total number of particles is 4800 and so there are 1200 particles for each behavior.

The largest percentages of recruited particles occur in the Base case, as expected from the time series analysis. However, the effects of the behaviors are also apparent. The recruitment for tidal vertical is approximately 42 percent, tidal lateral is 29 percent, passive is 25 percent, and bottom movers is 15 percent. In each plan configuration, it is confirmed that the largest number of particles that are recruited have the tidal vertical behavior and the smallest number of particles recruited have the bottom mover behavior. This trend is reasonable. Bottom movers are affected by only the bottom velocities. Because ADH is a depth averaged flow model, the flow field is assumed to have a logarithmic velocity profile for the PTM analysis. In such a profile, the velocities at the bottom are a small percentage of the average velocity. All things being equal, therefore, particles will have a tendency to be transported at a slower rate on the bottom. It should be reiterated at this time that one of the limitations of the particle tracking model larvae fish movement algorithm is that particles do not currently portray “anchoring” abilities. Results (Chapter 8) suggest that when anchoring is added to the particles, bottom movers have a greater possibility of reaching recruitment zones in an efficient manner.

The trends for the September 2007 case are also seen in the March 2008 data analysis (Figure 7-16). In this case, however, there are greater differences between the Base case and the plan cases. The percent of recruited larvae for all behaviors is above 40 percent for the March Base case and decreases for the plan configurations. It is also evident that for all configurations in the September and March cases, the preference is for recruitment at Chef Menteur.

Case 3

The final set of source conditions for particles are those initiated in Lake Borgne. These particles are representative of larvae that are introduced into the system via the eastern edge of Lake Borgne. Computational testing shows that particles must be initiated along the western edge of the lake to develop statistically relevant results (Figure 5-4). However, it is reasonable

to assume that particles initially introduced into the system through the eastern edge will eventually pass through the western edge of the lake to reach the GIWW and MRGO as this is an established recruitment pathway described by the interagency team. Figure 7-17 shows the computed larvae positions for simulations using the March 2008 hydrodynamics and the Plan 1 configuration. Each figure (a-c) shows a snap shot of where the particles are one day, one week, and four weeks after the simulation begins.

Almost immediately after the simulation begins, particles are flushed into the Chef Menteur recruitment zone. However, not all particles are transported into the GIWW. A large percentage (see Figure 7-17 c) remains within the lake or gets transported towards the east, into the Gulf. Table 7-2 shows the percentage of particles initiated in Lake Borgne, which are subsequently recruited at the recruitment regions. Only the March 2008 hydrodynamic period is utilized for this case. September 2007 hydrodynamic solutions do not show a significant amount of recruited particles. Almost 100 percent of the particles are recruited at the Chef Menteur recruitment area for all configurations. The analysis shows that, for particles initiated in Lake Borgne, there appears to be no real difference between the plan configurations with regard to the percentage of larvae recruited. The Base case is slightly higher than Plans 1-3, but this may be due to the general influx of flow via the MRGO. That is, in the Base case particles that exit Lake Borgne via the south west passage of Bayou Bienvenue into the MRGO may have a greater opportunity for recruitment due to the lack of closures in the MRGO.

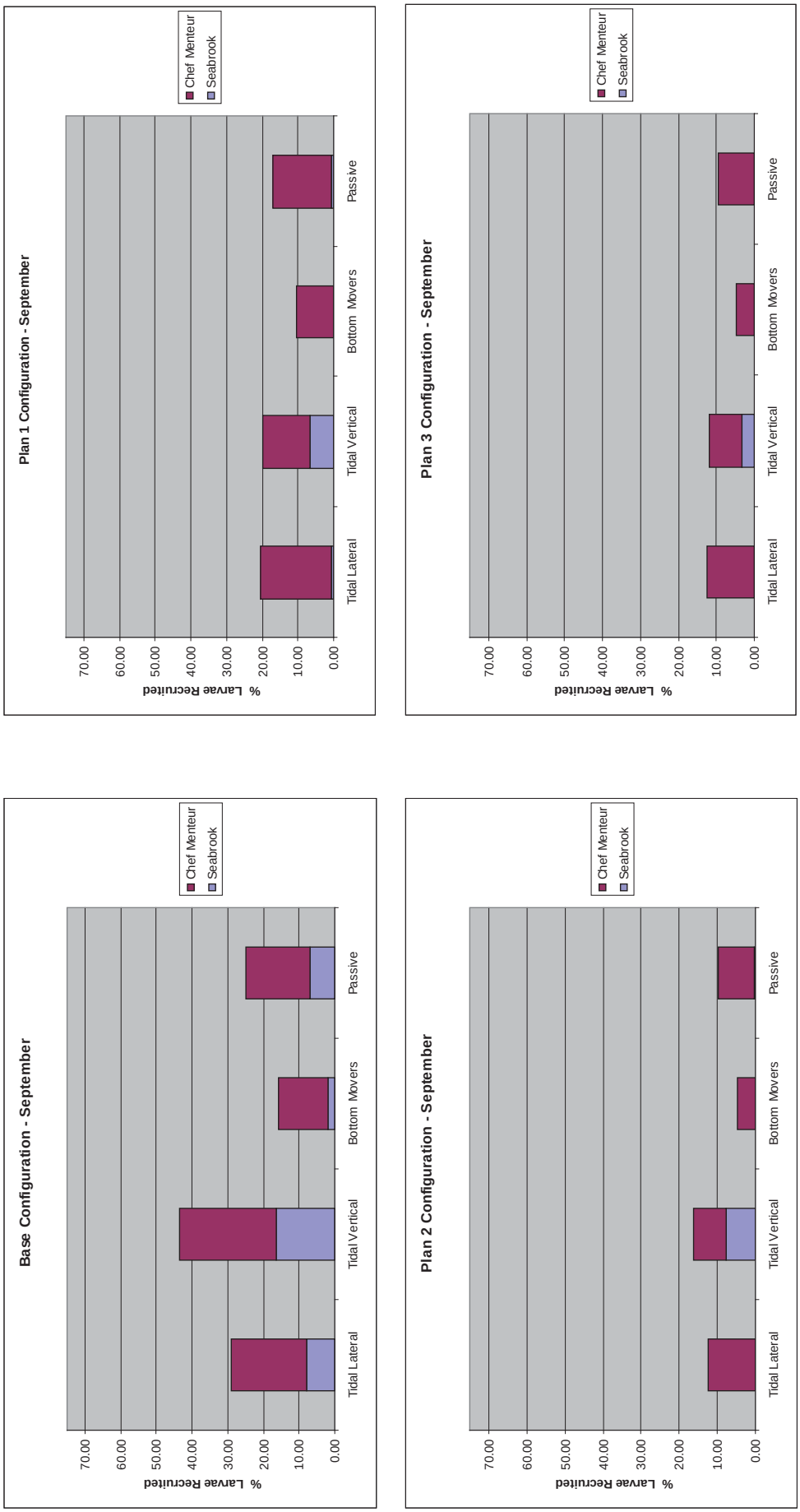

Figure 7-15 Percentage of larvae recruited at Seabrook (blue) and Chef Menteur (red) for Base, Plan1, Plan2, and Plan3 configurations using September 2007 hydrodynamics.

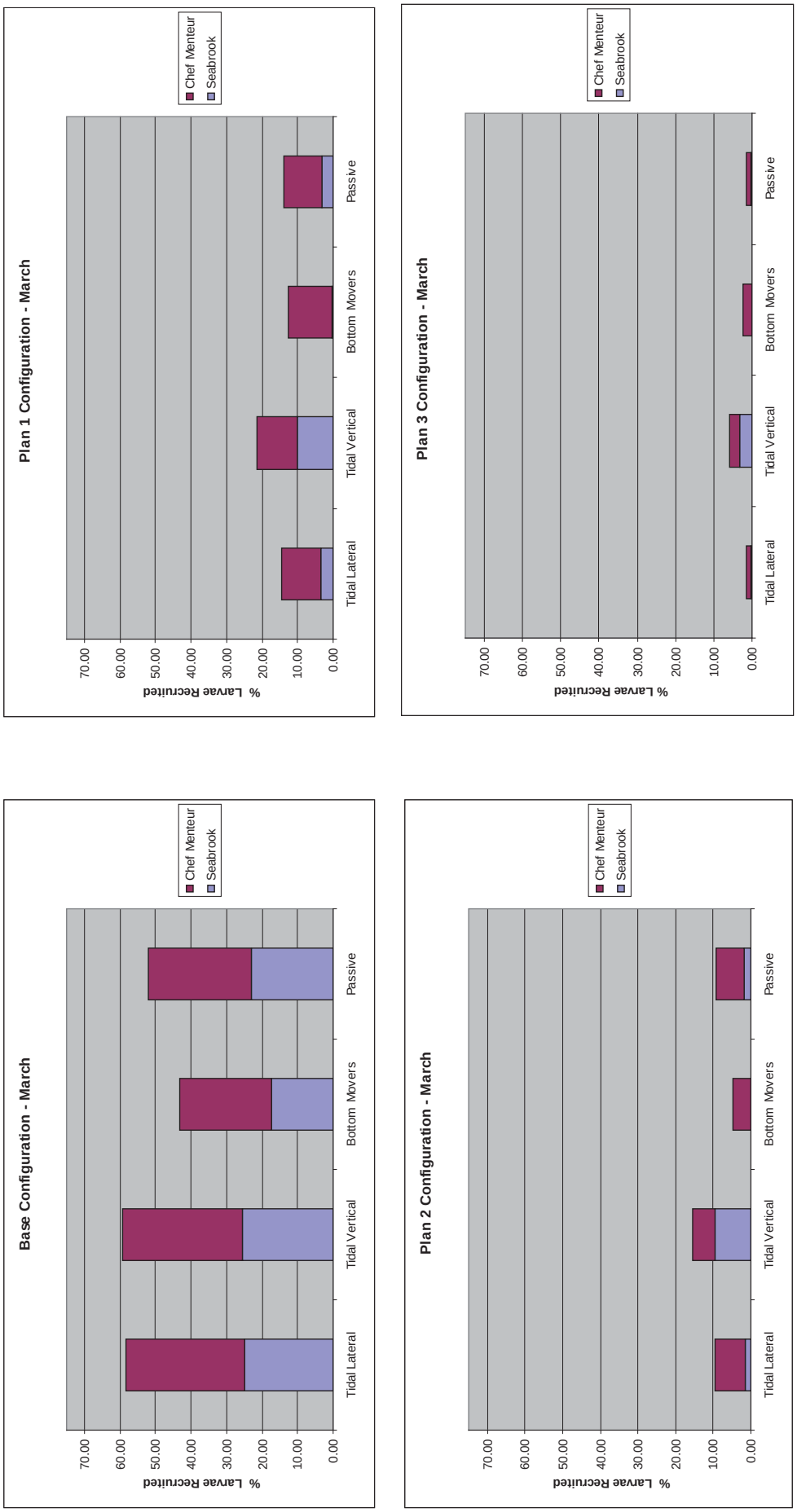

Figure 7-16 Percentage of larvae recruited at Seabrook (blue) and Chef Menteur (red) for Base, Plan1, Plan2, and Plan3 configurations using the March 2008 hydrodynamics.

a)

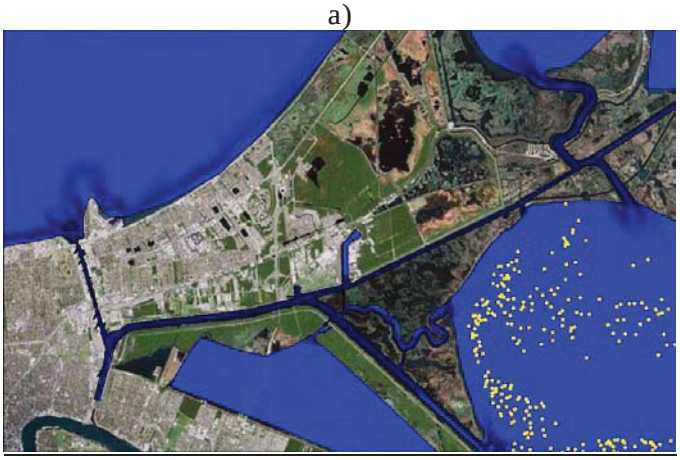

b)

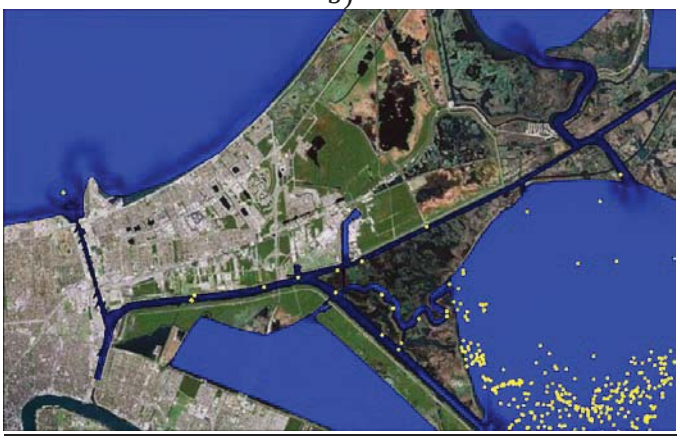

c)

Figure 7-17. March, base condition larvae positions after a) 1 day, b) 1 week, c) 4 weeks. Particles initiated in Lake Borgne.

Table 7-2 Percentage of larvae recruited for each construction phase for simulations in which particles are initiated in Lake Borgne.

Construction Phase	Percent Recruited
Base	21.7
Plan 1	16.4
Plan 2	14.7
Plan 3	16.8

8 Particle Tracking Results – Anchoring Effects and Final Plan

In this chapter, simulation results from the final design plan, Plan 3 - Final, are shown and compared to the Base case and Plans 1-3. In addition, as stated in Chapter 5, a transport characteristic of some larval fish species is the ability to "anchor" to more efficiently reach recruitment areas. This prevents particles from being forced away from recruitment regions due to the hydrodynamics of the tidal system. The addition of this mechanism more accurately represents the behaviors of larval fish during transport. This chapter shows results of simulations which include this characteristic behavior.

The description section of chapter 5 explains that the tidal flag for the rise, fall, and anchoring of particles is determined by the circulation. In an ideal case this would mean that there was always a clear concept of the tidal direction. However, determining the tidal direction can be complicated. Figure 8-1 shows the direction of the flow for the incoming tide for all plan configurations. Based on the configuration, the circulation directions change. In the Base case there is a portion of the flow (circled section within GIWW) in which there is no clear direction of flow for the incoming tide.

If the direction of the tide is ambiguous, such as in the case in which particles are being released in the GIWW, then it is unclear how a preferred path is chosen by larval fish. Therefore, two sets of simulations are performed. In the first case, the preferred direction is to the west. In the second case the preferred direction is to the east. An implicit assumption is that once a larval fish has chosen its preferred direction it operates within a set of rules which requires that it maintain that direction as the incoming tide direction and behaves accordingly. If it is eventually determined how this direction is chosen when the circulation is ambiguous, then the current results can be scaled. It should also be mentioned that, based on Figure 8-1b, it appears that westward is the flow direction for the incoming tide in the circled section for Plans 1-3 and the final plan.

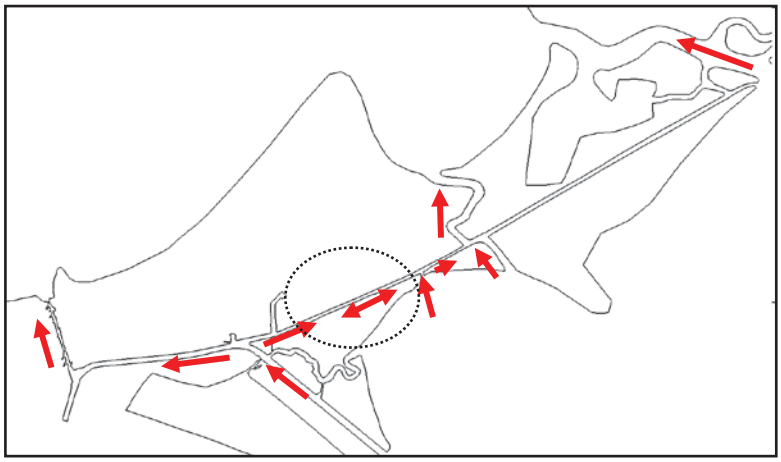

a) Direction of flow for incoming tide in Base case.

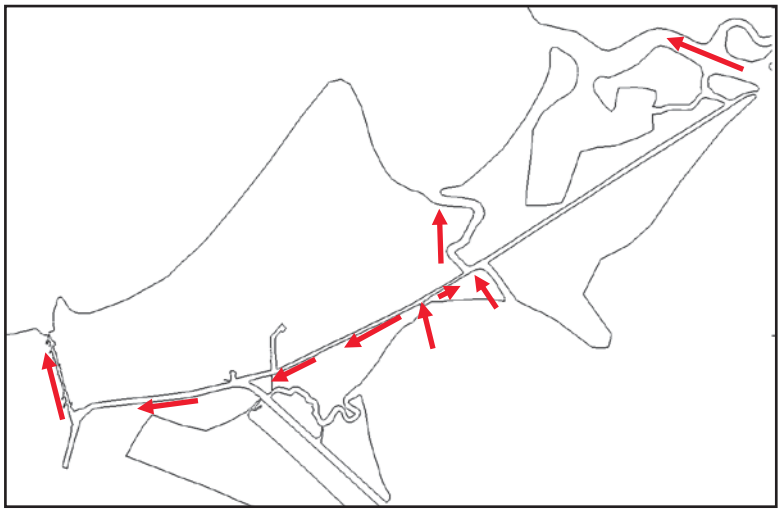

b). Direction of flow for incoming tide for Plan 1, Plan 2, and Plan 3.

Figure 8-1 Circulation Diagram of flow direction for incoming tide for all configurations

Case 2 results (Chapter 7) show that particles released near the second closure in the MRGO have limited transport for the Plan 2 and Plan 3 configurations. The velocity to the southeast of the MRGO closure is very small. When anchoring is added to the other characteristic behavior, the particles take advantage of the higher velocities to reach recruitment regions. However in this case the limited velocities mean that larval fish transport is still extremely slow and the effect is similar to the previous results seen in Figures 7-4, 7-5, 7-8, and 7-9. Subsequent statistics and data analysis which include those particles released near the second closure in the MRGO may skew results slightly. Therefore in this Chapter,

Case 2 initial position of particles is replaced with Case 4 in which particles are initiated only within the GIWW.

Case 1

Results obtained from Case 1 in which particles are initiated near the first MRGO closure are very similar to those results shown in Chapter 7. Particles do not reach the recruitment areas for Plans 1-3 or Plan 3-Final. For the Base case, particles do move along the MRGO faster due to the anchoring. However, very few particles reach the recruitment areas within the given 4 week simulation time period.

Case 3

In this section, particles are initiated within Lake Borgne as shown in Figure 5-4. Two types of simulations are run. In one case particles are anchored with the incoming tide assumed to be towards the west and the second case anchoring is added with the assumption that the incoming tide is towards the east. In subsequent discussion “anchoring to the west” refers to the assumption that the incoming tide is towards the west and “anchoring to the east” refers to the assumption that the incoming tide is towards the east.

Similar to the results shown in Chapter 7, initially particles are transported into the Chef Menteur recruitment zone. However, many particles remain in Lake Borgne. Figures 8-2 (a-c) show snapshots of particle positions during the March 2008 hydrodynamic period after 1 day, 1 week, and 4 weeks for the final plan configuration. Anchoring is to the west. Although anchoring affects particles in the GIWW, IHNC, and MRGO, when particles are in Lake Borgne, anchoring is turned off. This characteristic behavior does not affect particle transport within Lake Borgne because there is no real tidal direction. Once particles exit into the GIWW or the MRGO, particles are transported quickly towards recruitment zones. Tables 8-1 and 8-2 show the percentage of particles recruited within September 2007 and March 2008 hydrodynamic period for particles anchored to the west and east respectively. As expected, fewer particles are recruited in the September 2007 simulations than in the March 2008 simulations because of the smaller velocities during that period. Generally it can be seen that the Base case contains higher recruitment rates. This is most likely due to the transport of flow within the MRGO. Recruitment rates for Plans 1-3 and the Plan 3-Final remain statistically very similar.

a)

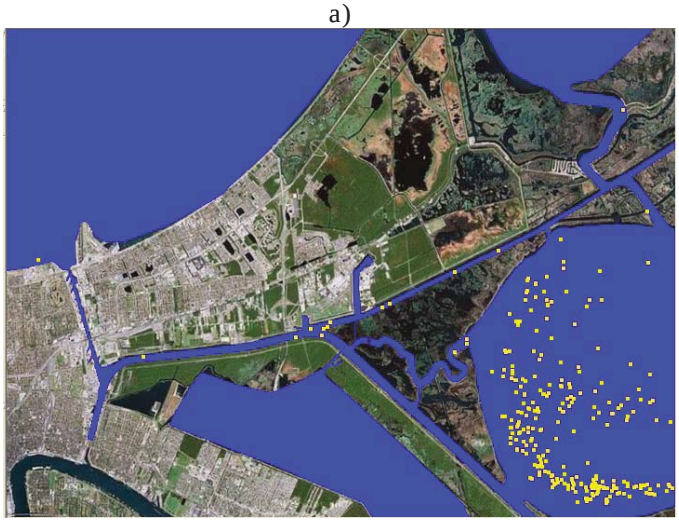

b)

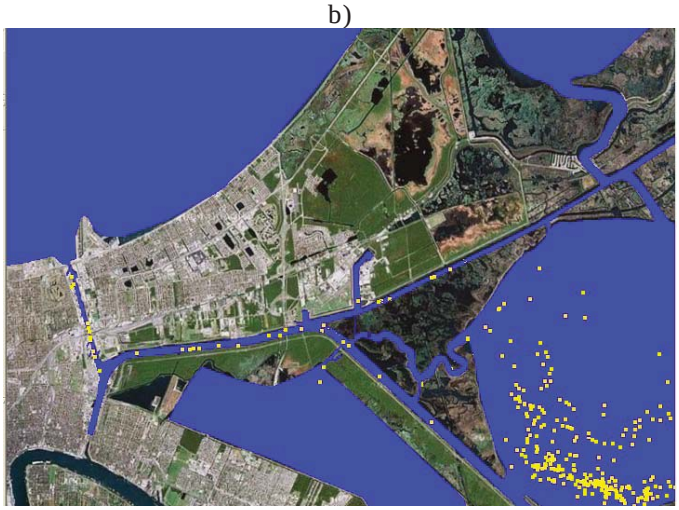

c)

Figure 8-2. March, Base condition larvae positions after a) 1 day, b) 1 week, c) 4 weeks. Particles initiated in Lake Borgne.

Table 8-1 Recruitment Percentages for Case 3 particles – Incoming Tide to the West

Construction Phase	Percent Recruited – September 2007	Percent Recruited – March 2008
Base	10.22%	26.61%
Plan 1	6.99%	17.34%
Plan 2	6.18%	16.53%
Plan 3	6.32%	17.88%
Final Plan	6.72%	16.94%

Table 8-2 Recruitment Percentages for Case 3 particles – Incoming Tide to the East

Construction Phase	Percent Recruited – September 2007	Percent Recruited – March 2008
Base	15.59%	24.87%
Plan 1	10.75%	24.46%
Plan 2	9.95%	19.76%
Plan 3	7.53%	17.61%
Final Plan	9.27%	18.41%

Case 4

Incoming Tide- West

Simulation results for particles which specify the incoming tide as westward within the circled region of Figure 8-1 are shown in Figures 8-3 thru 8-6. These figures display snapshots in time after 1 day, 1 week, and 4 weeks. Particles are color coded based on behavior. Blue particles are tidal lateral, green particles are tidal vertical, yellow particles are bottom movers, and red particles are passive. For the September 2007 Base case, initially particles cluster near the start position in the GIWW. After one week, the particles are dispersed primarily in a westward direction. Some particles have been transported into the MRGO. After four weeks a significant percentage of particles have been recruited, though some particles have made it into Lake Borgne, the MRGO, and the stored water region to the southwest of the MRGO representing the Central Wetlands Area. Similar results are seen in September 2007 of the Plan 3-Final case. However, due to the decrease in flow velocity fewer particles have managed to reach the recruitment region and more particles have made it into Lake Borgne. Based on the color coding, it can be seen that the tidal vertical and bottom

a)

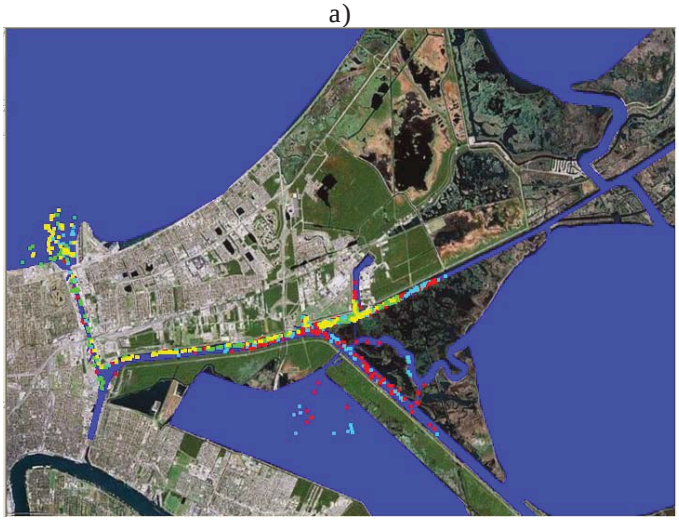

b)

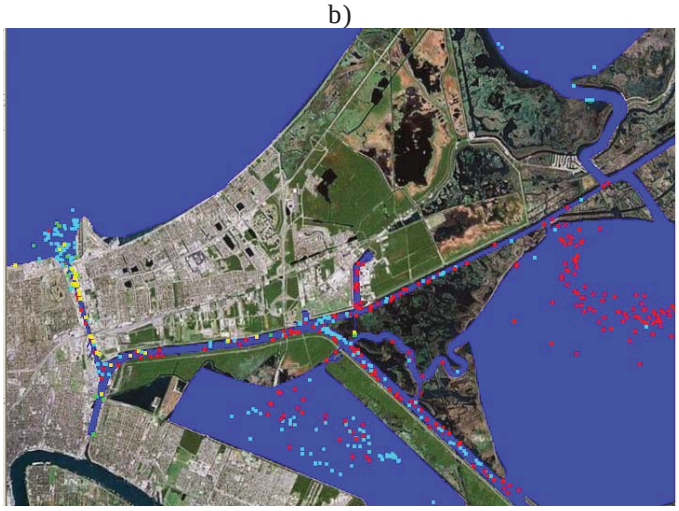

c)

Figure 8-3 September, Base condition larvae positions after a) 1 day, b) 1 week, c) 4 weeks. Particles anchored based on incoming tide to the west and are color coded based on behavior.

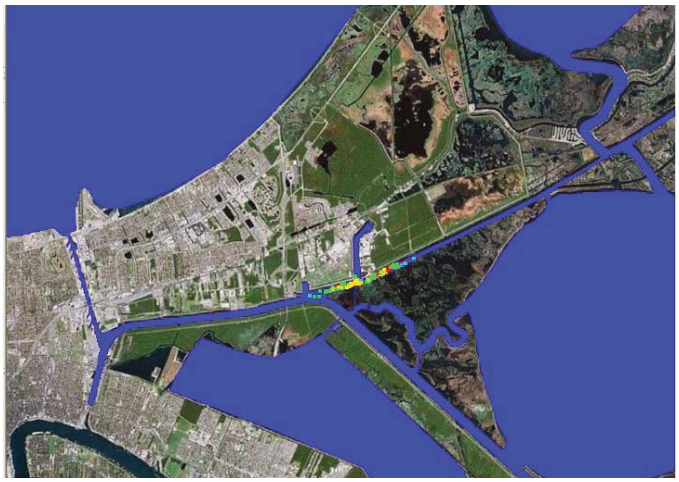

a)

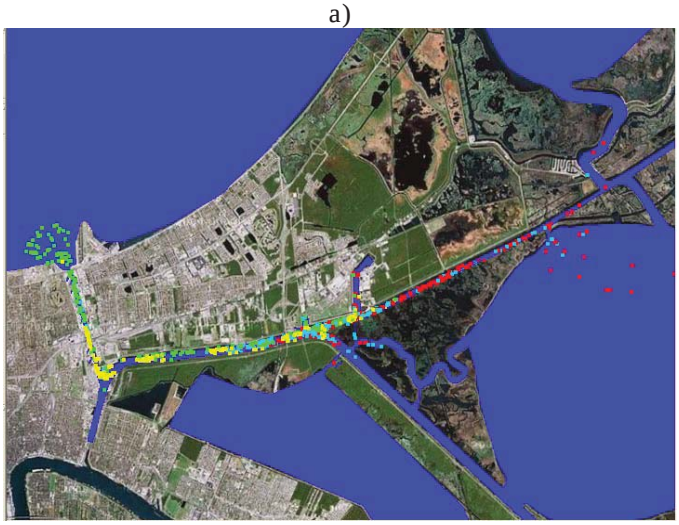

b)

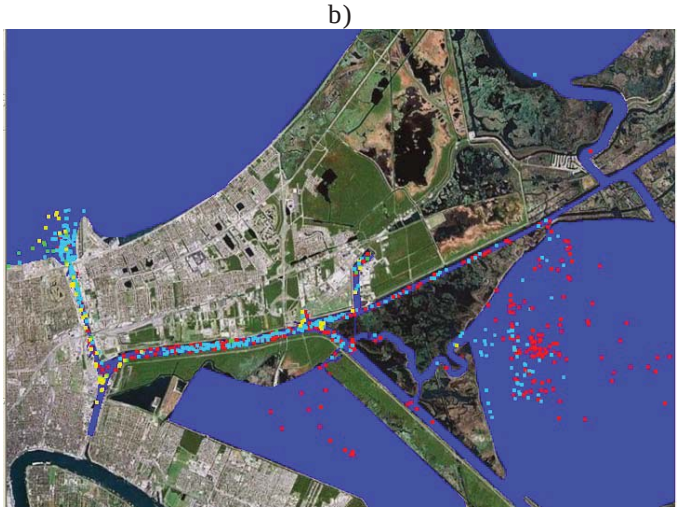

c)

Figure 8-4 September, Final plan condition larvae positions after a) 1 day, b) 1 week, c) 4 weeks. Particles anchored based on incoming tide to the west and color coded based on behavior.

a)

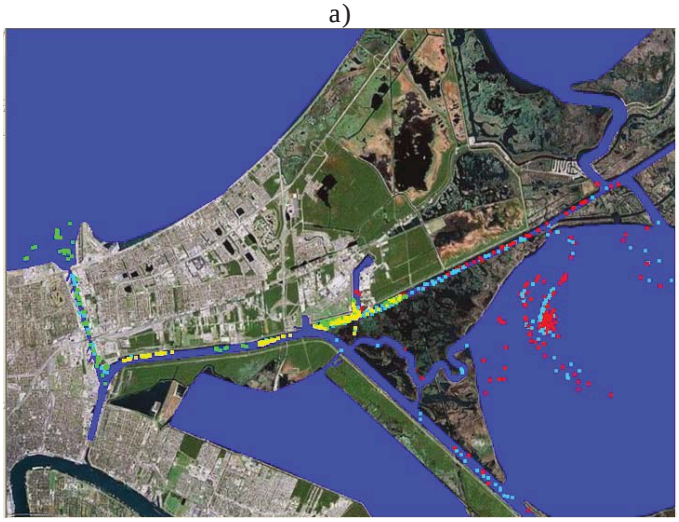

b)

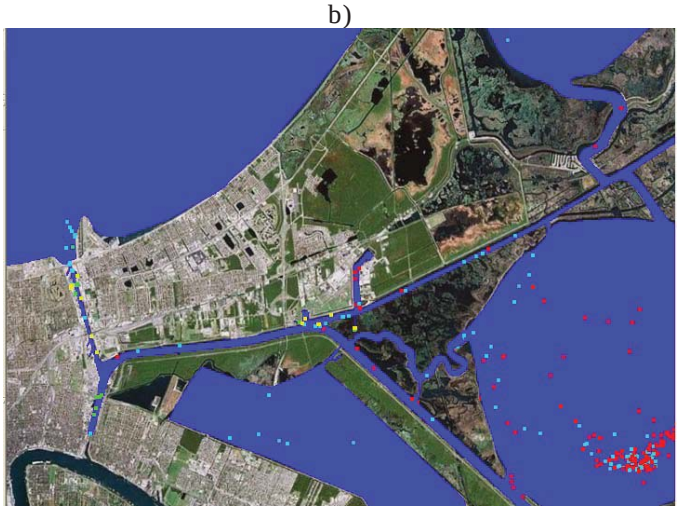

c)

Figure 8-5 March, Base condition larvae positions after a) 1 day, b) 1 week, c) 4 weeks. Particles anchored based on incoming tide to the west. and color coded based on behavior.

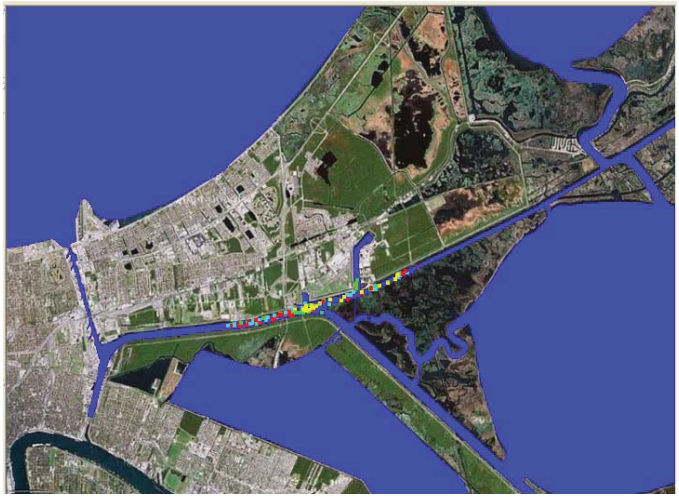

a)

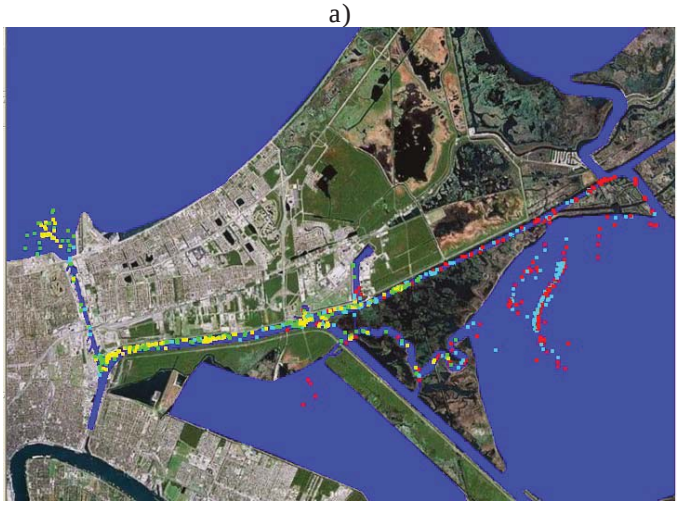

b)

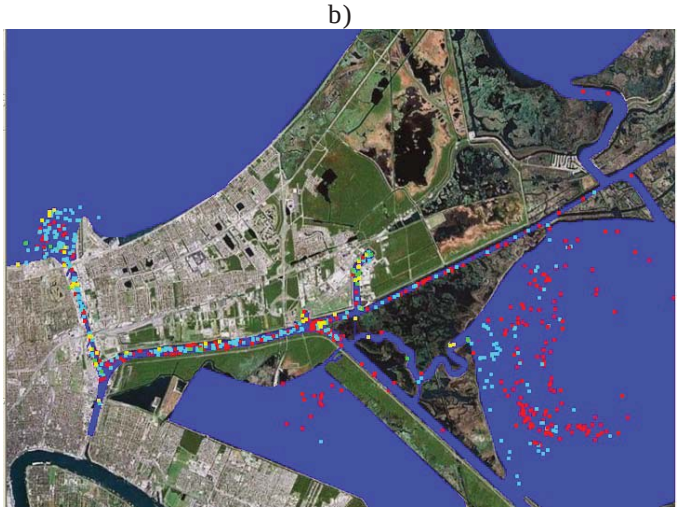

c)

Figure 8-6 March, Final plan condition larvae positions after a) 1 day, b) 1 week, c) 4 weeks. Particles anchored based on incoming tide to the west. and color coded based on behavior.

mover particles are recruiting at a faster rate than the tidal lateral particles or the passive movers. This is most likely because of the anchoring transport mechanism. In the case of the tidal vertical and bottom mover particles, anchoring is applied almost immediately. The tidal lateral particles have anchoring applied after a delay as particles make it to the channel sides. The passive movers have no anchoring at all.

For the March 2008, Base case (Figure 8-5) particles move throughout the system quickly. After one week, particles range along the GIWW from the Seabrook recruitment area to Lake Borgne. The particles seen within Lake Borgne have primarily passive and tidal lateral characteristic behaviors. Within four weeks almost all the particles have been recruited except for those that end in Lake Borgne. These particles may remain there for any length of time before exiting. Figure 8-6 shows similar results to that of Figure 8-4.

Time series of larval recruitment are shown in Figure 8-7 and 8-8 for September 2007 and March 2008 hydrodynamics respectively. Both simulations result in a similar trend. The Base configuration shows the largest recruitment values. There is a decrease in recruitment with respect to increasing plan number for Plans 1-3. This is similar to what was seen in the unanchored particle results shown in Chapter 7. However, there is a great difference in the total number of particles recruited between the previous results and those shown in Figures 8-7 and 8-8. For the Plan 3, September 2007 hydrodynamic condition with particle anchoring more than seven times the number of particles is recruited with the one GIWW source (approximately 550) than the combination of both the GIWW and MRGO sources for the unanchored case (approximately 75). Plan 3-Final shows an increase of recruitment in comparison to Plan 3. In the Final plan, two additional gates are added to the Seabrook area construction, almost doubling the amount of flow allowed through that area. The results shown in the recruitment percentages of Plan 3-Final reflect the increased cross sectional area.

Table 8-3 gives a summary of the total percentage of particles transported to the recruitment areas for both the September 2007 and March 2008 hydrodynamic periods. These results support the observations from the recruitment time series figures. The Base case has the greatest percentage of particles recruited. The percentages decrease as the plan number increases. The final plan values are close to Plan 2 values.

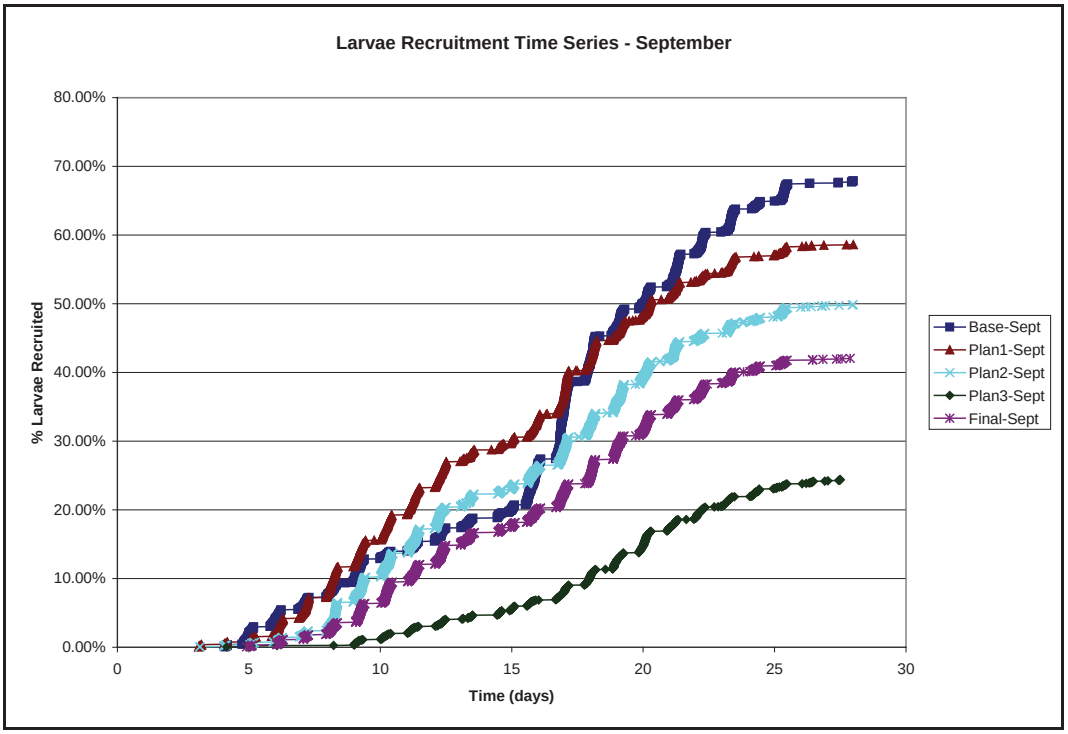

Figure 8-7 Comparison of Larvae Recruitment Time Series for the September 2007 Hydrodynamics, larval fish preferred path to the west. Particles anchored based on incoming tide to the west (2150 particles released).

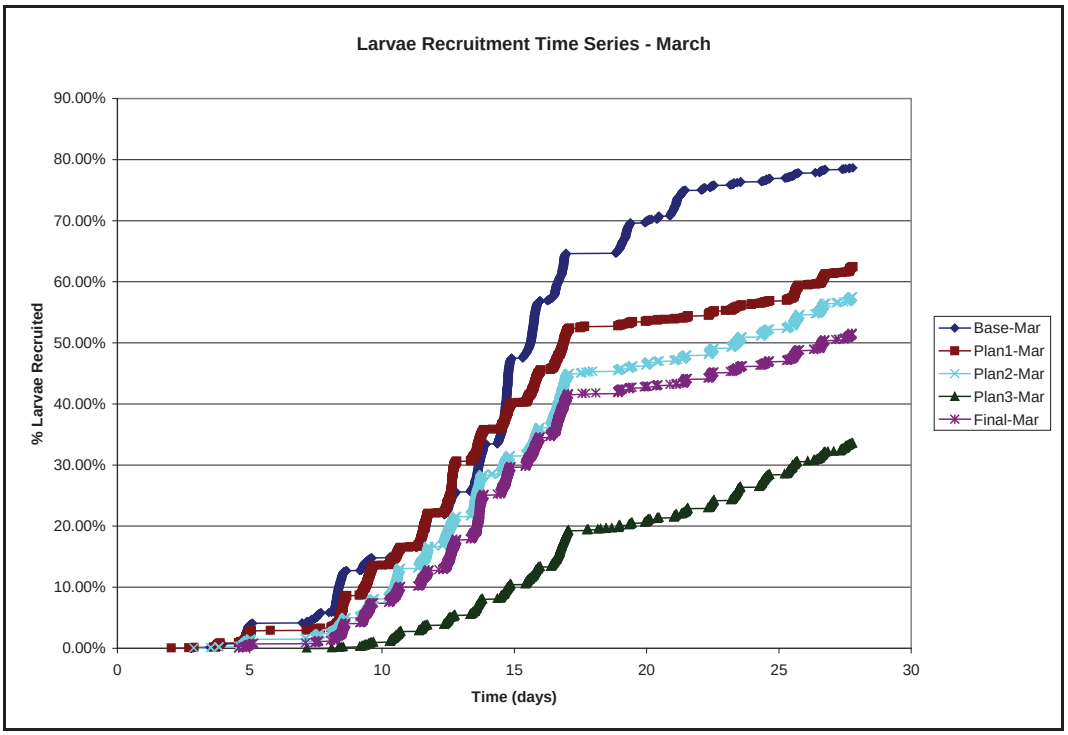

Figure 8-8 Comparison of Larvae Recruitment Time Series for the March 2008 Hydrodynamic, larval fish preferred path to the west. Particles anchored based on incoming tide to the west (2150 particles released).

Table 8-3 Percentage of larvae recruited for each construction phase for simulations in which particles are anchored based on incoming tide to the west (2150 particles released).

Construction Phase	Percent Recruited – September 2007	Percent Recruited – March 2008
Base	67.91	78.5
Plan 1	58.60	62.51
Plan 2	49.86	57.58
Plan 3	24.42	33.63
Final Plan	42.05	51.58

The percentage of particles recruited at the Seabrook and Chef Menteur recruitment regions are presented in Figures 8-9 and 8-10 (% recruited = number of particles recruited per behavior/total number of particles of that behavior x 100). For the September 2007 case the number of particles recruited for the Base plan is largest for the bottom and tidal vertical movers. These two characteristic types both have anchoring added to their behavior, suggesting that anchoring greatly increases the chance that the particle will be recruited. It can also be seen that the greatest number of particles are recruited at Seabrook. Because the direction of the incoming tide within the GIWW is to the west towards Seabrook, this is the logical result. The recruitment percentages decrease slightly for the tidal vertical and bottom movers as the plan number increases from 1 to 3. However, they decrease drastically for the tidal lateral and passive particles. As the particles represented by the passive behavior do not have anchoring, these results show the importance of that characteristic for recruitment. Although the tidal lateral particles do have anchoring, because that behavior is only applied when the particle reaches the side of the channel, there is a lag in the effect of this transport characteristic. Plan 3 final results are extremely close to Plan 2 results as expected. March 2008 results show similar trends, though because of the increased flow velocities a larger amount of passive particles are recruited.

Incoming Tide- East

In this section, the incoming tide within the circled region of Figure 8-1 is specified as eastward. This means that the preferred pathway for particles introduced into the GIWW will be towards the east and the Chef Menteur recruitment region.

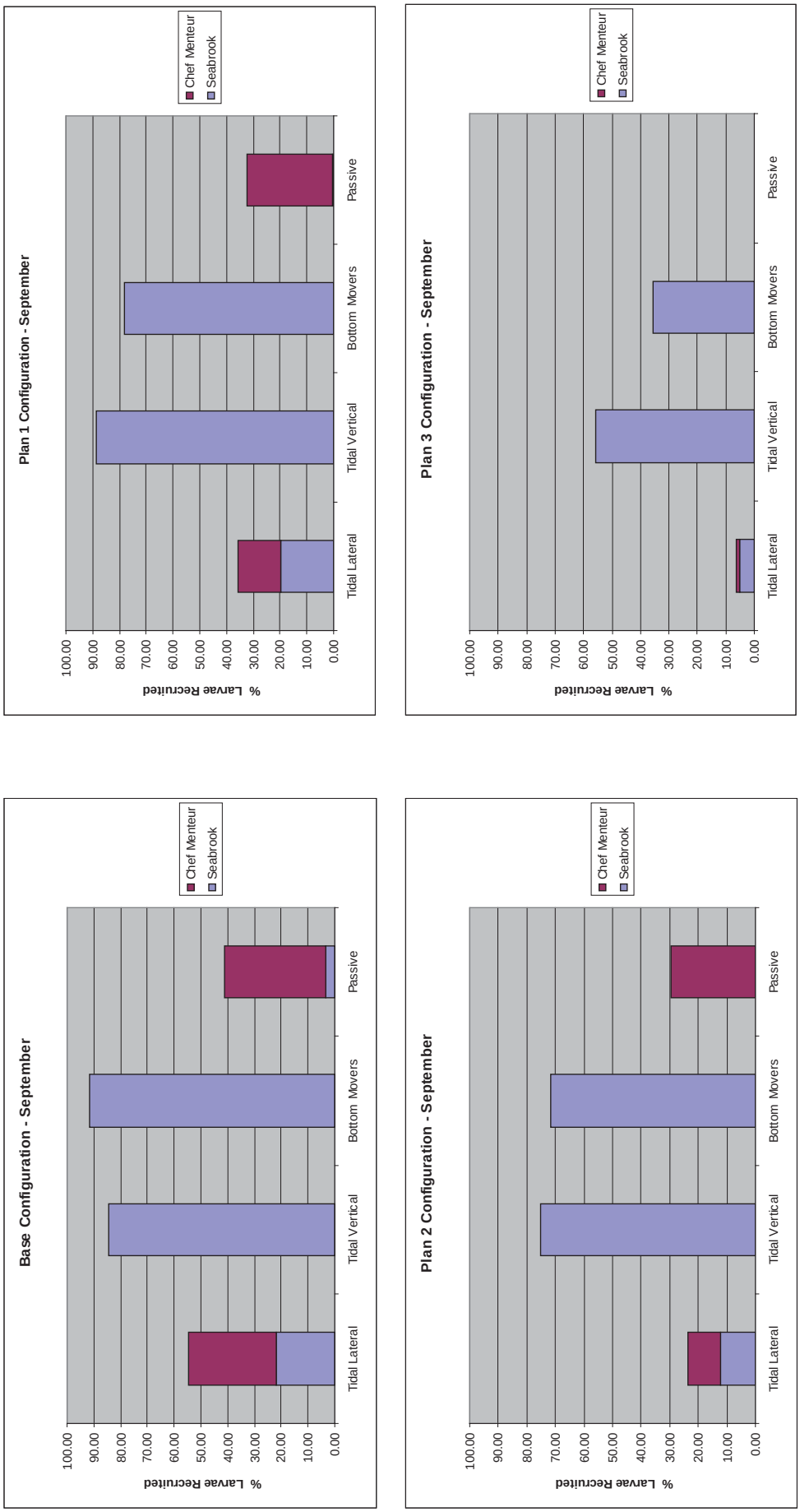

Figure 8-9 Percentage of larvae recruited at Seabrook (blue) and Chef Menteur (red) for Base, Plan1, Plan2, and Plan3 configurations using September 2007 hydrodynamics, larval fish preferred path to the west. Particles anchored based on incoming tide to the west.

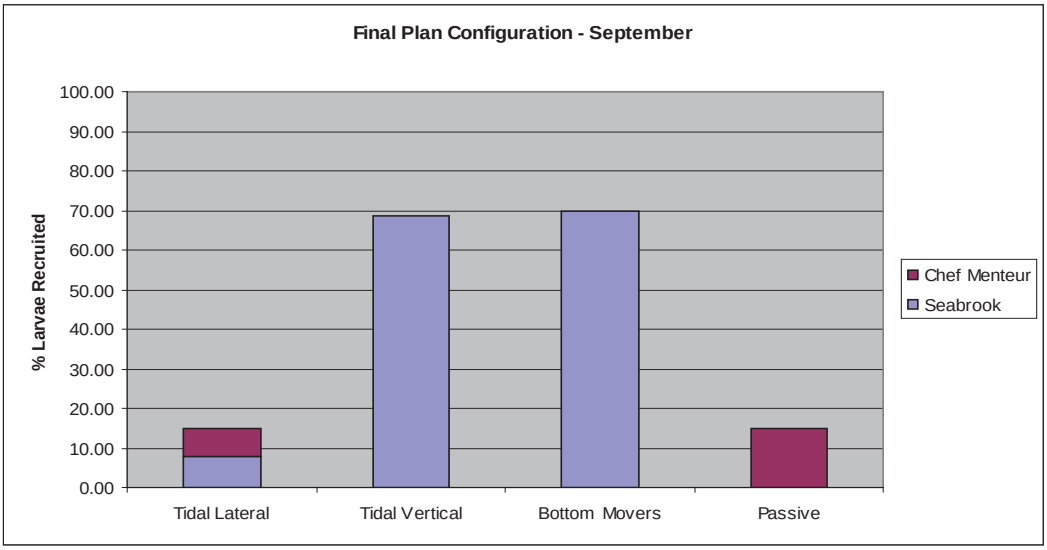

Figure 8-9 (continued) Percentage of larvae recruited at Seabrook (blue) and Chef Menteur (red) for Final Plan configuration using September 2007 hydrodynamics, larval fish preferred path to the west. Particles anchored based on incoming tide to the west.

Figures 8-11 through 8-14 show snapshots in time of the particle positions after 1 day, 1 week, and 4 weeks. Particles are color coded based on behavior. Blue particles are tidal lateral, green particles are tidal vertical, yellow particles are bottom movers, and red particles are passive. Only the Base and Plan 3-Final configurations are displayed. The Base case (Figure 8-11) shows similar results to those seen in the previous section. Initially particles are clustered near the release point. After one week particles have been transported along the GIWW. Some particles have made it to the MGRO. After four weeks, the majority of the particles have been recruited with some remaining in the MRGO and Lake Borgne. Once again, it can be seen that the majority of the particles residing in Lake Borgne are passive and lateral movers. The final plan results illustrate the effect of the slower velocity. Fewer particles appear to have reached the recruitment area. An additional effect is that more particles reach Lake Borgne. Now bottom movers and tidal vertical particles are also in Lake Borgne. This is due in part to the slower velocities near the GIWW entrance to Lake Borgne, which allows for an easily accessible transport pathway into the lake. In addition, there is perhaps a blocking mechanism to transport of particles out of the lake due to phasing of the flows. That is, flow moving along the GIWW prevents the slower moving flow from Lake Borgne from transporting particles into the GIWW. These concepts are supported by the March 2008 particle transport results. Figure 8-13c and 8-14c depict the particle positions for the Base and Plan 3 final configurations respectively. Many more particles exist in Lake Borgne for the final plan design phase.

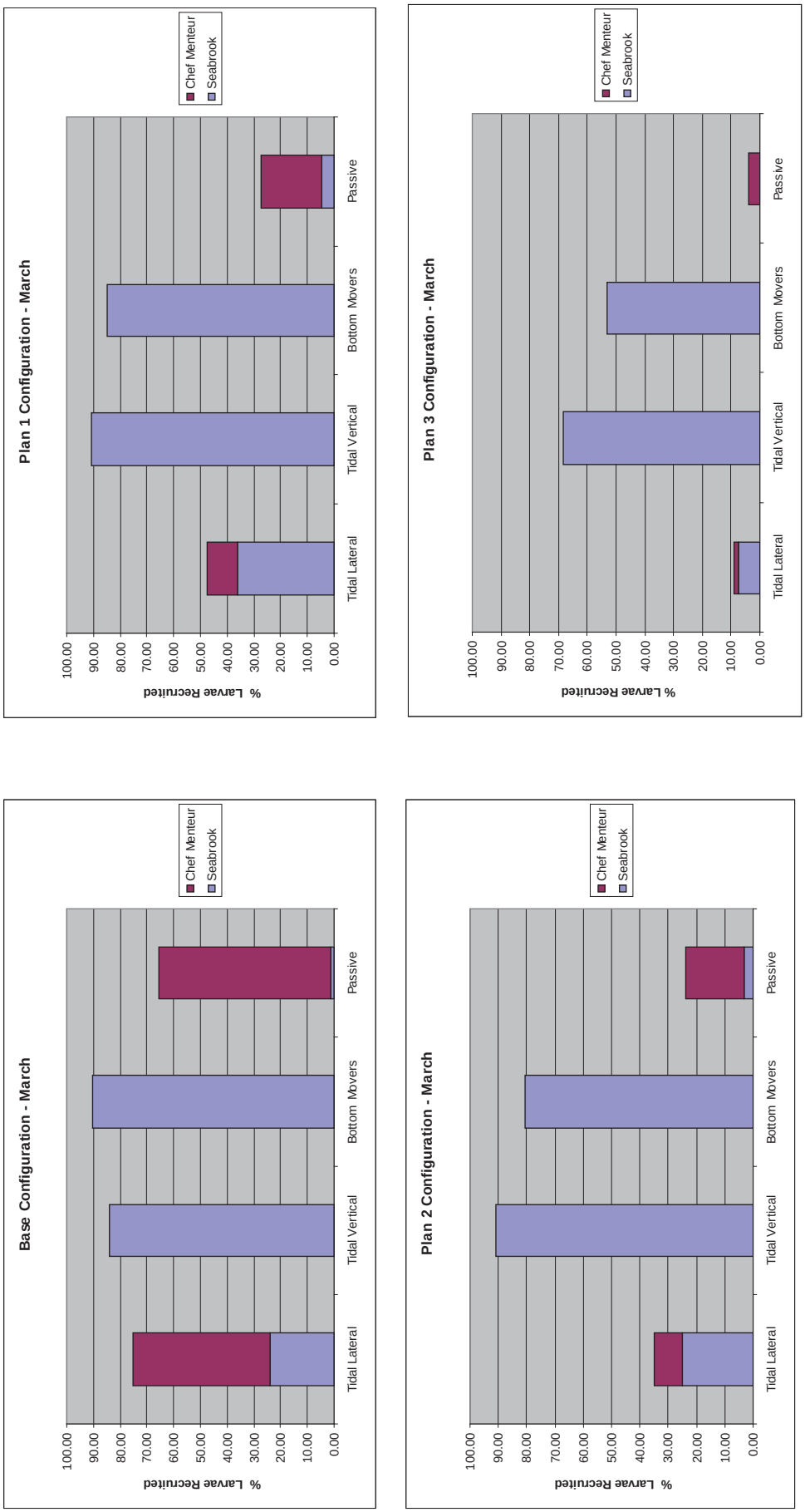

Figure 8-10 Percentage of larvae recruited at Seabrook (blue) and Chef Menteur (red) for Base, Plan1, Plan2, and Plan3 configurations using March 2008 hydrodynamics, larval fish preferred path to the west. Particles anchored based on incoming tide to the west.

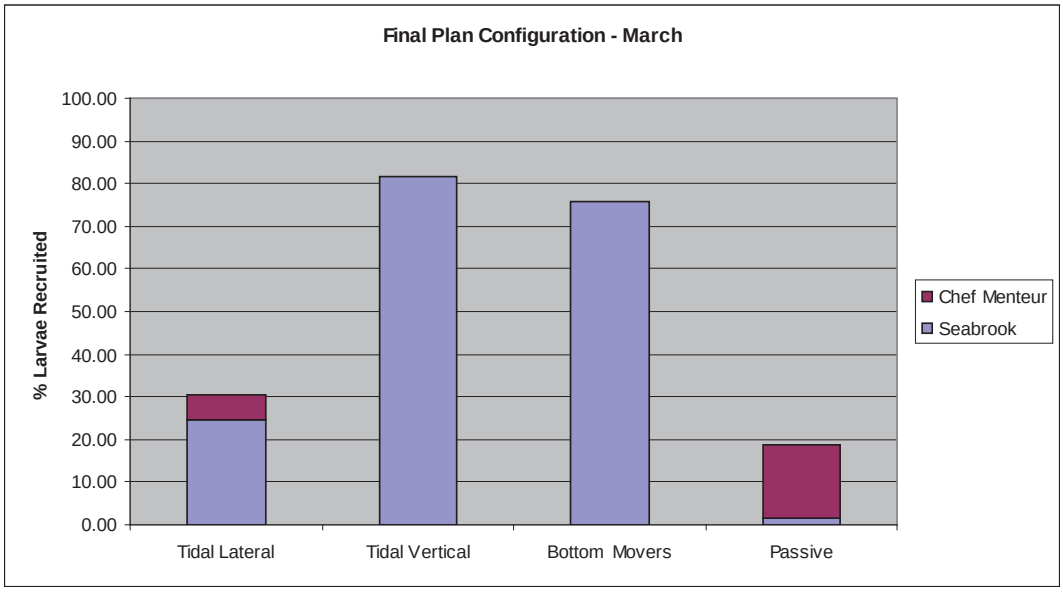

Figure 8-10 continued Percentage of larvae recruited at Seabrook (blue) and Chef Menteur (red) for the final plan configuration using March 2008 hydrodynamics, larval fish preferred path to the west. Particles anchored based on incoming tide to the west.

Recruitment time series (Figures 8-15 and 8-16) present a similar trend as seen in previous simulations. The Base case has the greatest recruitment rates and the Plan 3 case has the lowest. The final plan results show increased recruitment in comparison with Plan 3. This is as expected due to the changes in the Seabrook design changes. There is a great increase in the overall number of particles recruited within the Plan 1-3 design phases in comparison to the unanchored particle cases seen in Chapter 7. An unexpected result is that the Plan 1 and Plan 2 configurations show almost identical time series. The Plan 2 case for the March 2008 hydrodynamics actually has a larger number of particles recruited than the Plan 1 case. The March 2008 Plan 3 case appears to have a greater reduction of particles in comparison to the Base case than the September 2008 conditions. Figure 8-14 shows that a large portion of particles in this case enter Lake Borgne and remain there until the end of the simulation period.

Table 8-4 gives a summary of the total percentage of particles transported to the recruitment areas for both the September 2007 and March 2008 hydrodynamic periods. The values for the Plan 1-3 and Plan 3-Final configurations are lower than those seen in Table 8-3 in which the recruitment direction is towards the west.

a)

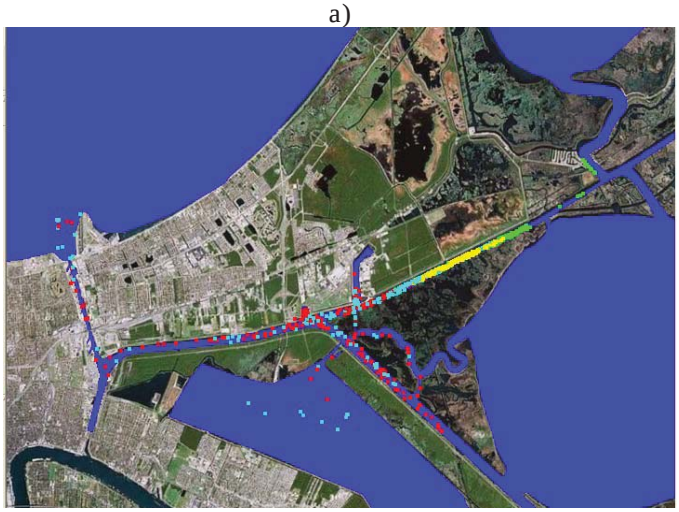

b)

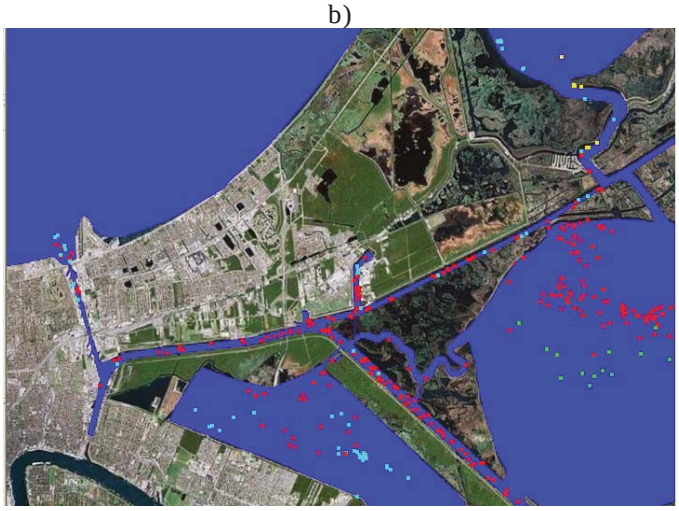

c)

Figure 8-11 September, Base condition larvae positions after a) 1 day, b) 1 week, c) 4 weeks. Particles anchored based on incoming tide to the east and color coded based on behavior.

a)

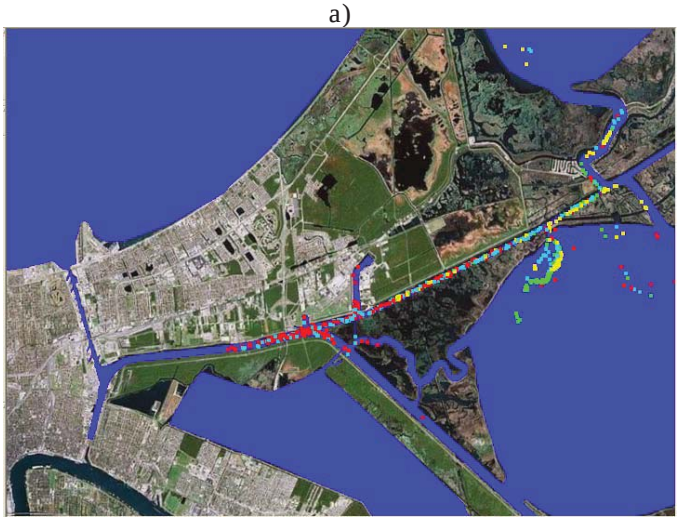

b)

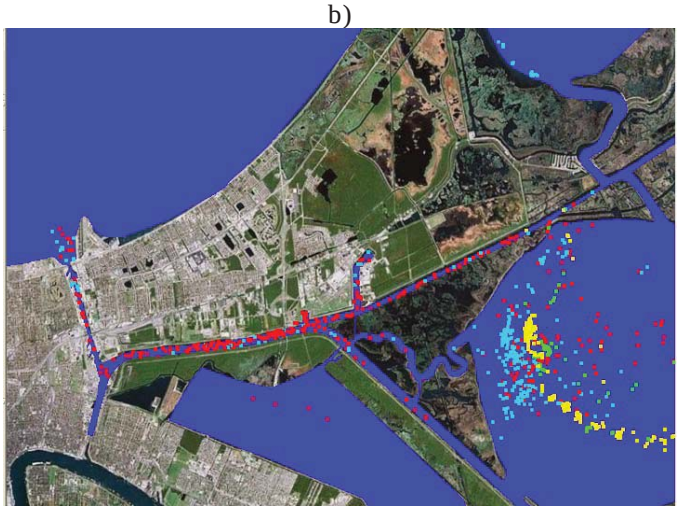

c)

Figure 8-12 September, Final plan condition larvae positions after a) 1 day, b) 1 week, c) 4 weeks. Particles anchored based on incoming tide to the east and color coded based on behavior.

a)

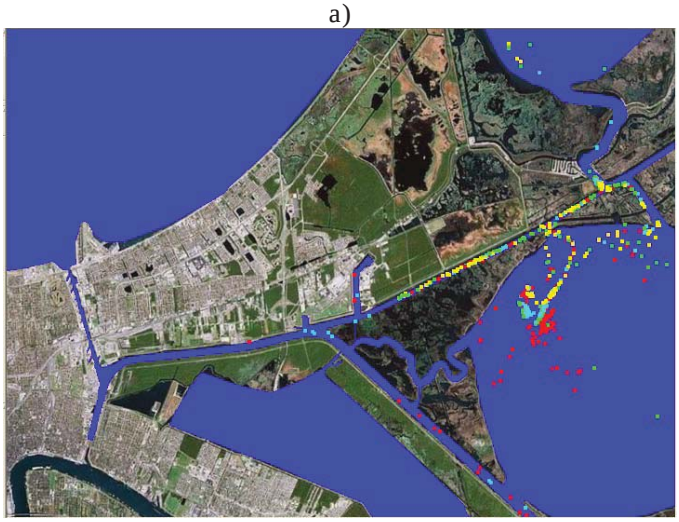

b)

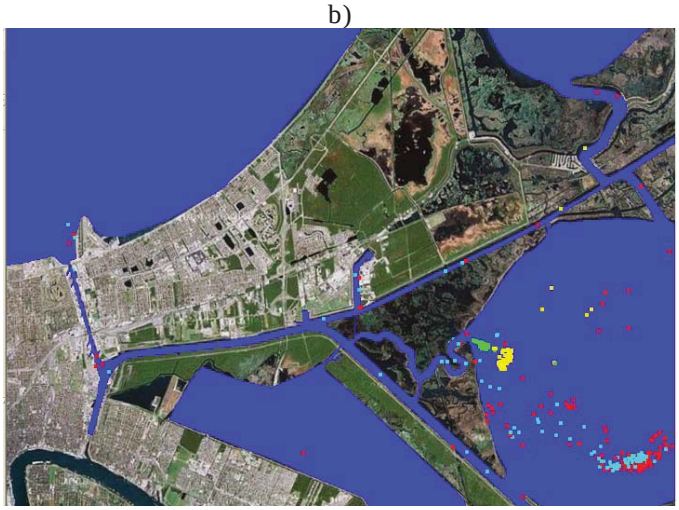

c)

Figure 8-13 March, Base condition larvae positions after a) 1 day, b) 1 week, c) 4 weeks. Particles anchored based on incoming tide to the east and color coded based on behavior.

a)

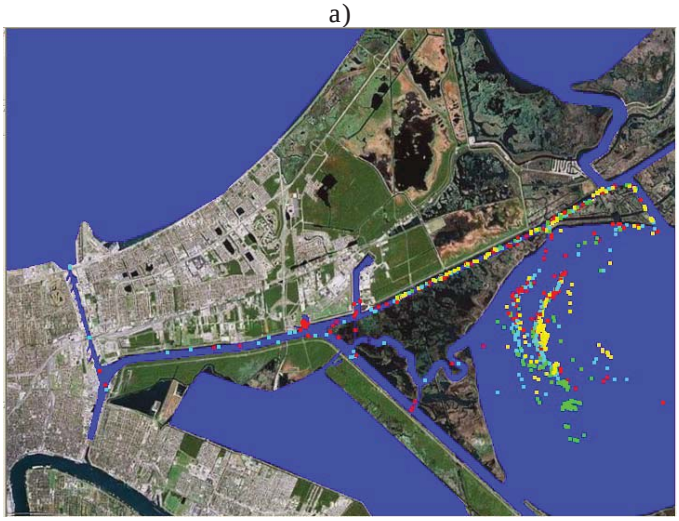

b)

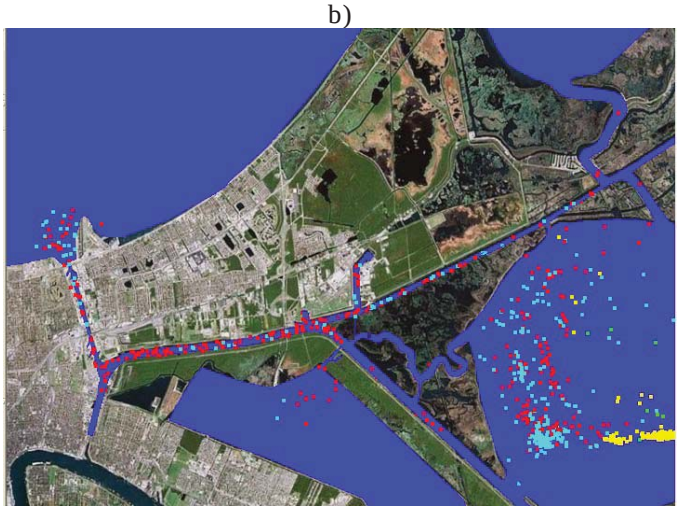

c)

Figure 8-14 March, Final plan condition larvae positions after a) 1 day, b) 1 week, c) 4 weeks. Particles anchored based on incoming tide to the east and color coded based on behavior.

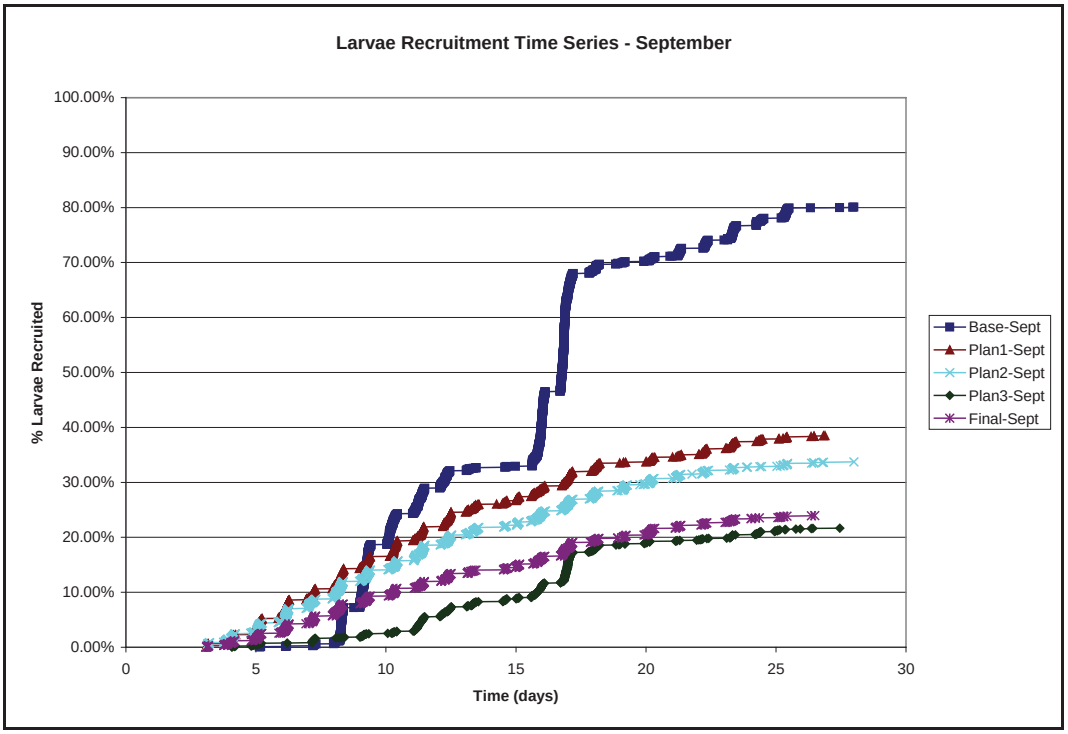

Figure 8-15 Comparison of Larvae Recruitment Time Series for the September 2007 Hydrodynamic, larval fish preferred path to the east. Particles anchored based on incoming tide to the east.

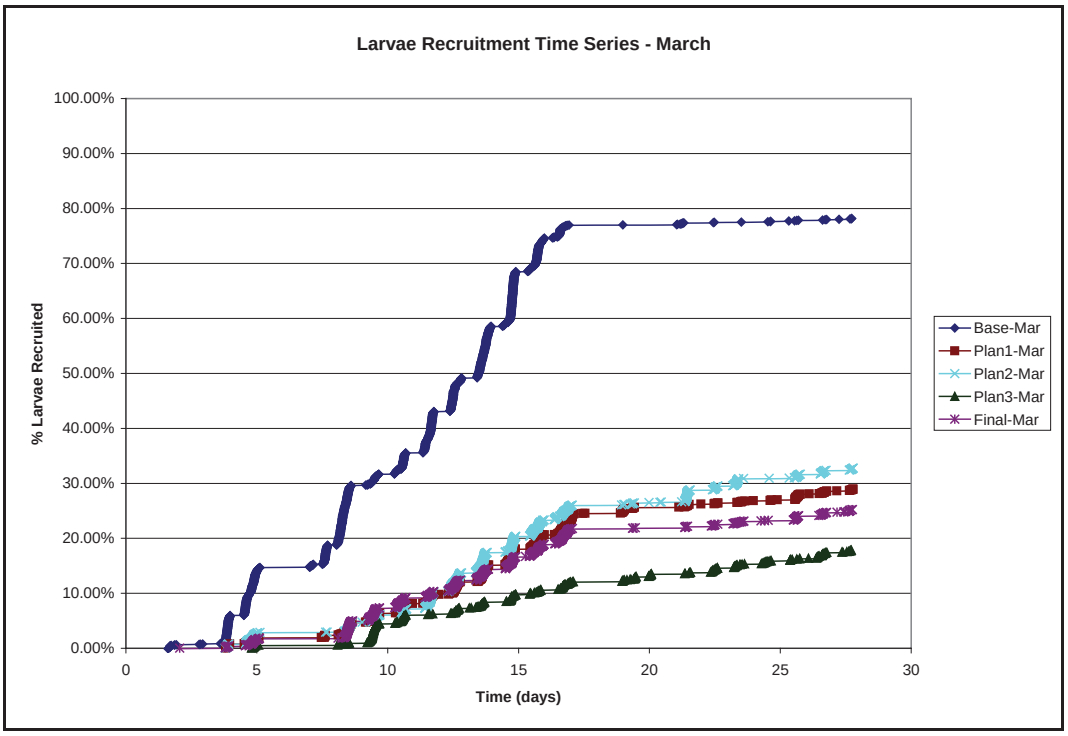

Figure 8-16 Comparison of Larvae Recruitment Time Series for the March 2008 Hydrodynamic, larval fish preferred path to the east. Particles anchored based on incoming tide to the east.

Table 8-4 Percentage of larvae recruited for each construction phase for simulations in which particles are anchored based on incoming tide to the east (2150 particles released).

Construction Phase	Percent Recruited – September 2007	Percent Recruited – March 2008
Base	80.09	78.19
Plan 1	38.51	28.98
Plan 2	33.72	32.79
Plan 3	21.67	17.86
Final Plan	23.95	25.23

Figures 8-17 and 8-18 give comparisons of the percentages of particles recruited into each of the recruitment areas based on behaviors for the September 2007 and March 2008 hydrodynamic conditions. The figures show that most of the particles are recruited at Chef Menteur for these simulations. This is because the preferred pathway in the GIWW is eastwards towards the Chef Menteur recruitment region. The September Base case shows high percentages for the tidal lateral, tidal vertical, and bottom movers. Only about half of the passive particles are recruited. Almost all of these values decrease for the Plan 1 case. The values generally decrease slightly for Plan 2 compared to Plan 1 and then again for Plan 3 compared to Plan 2. The Plan 3-Final values generally increase, to values somewhere between those for Plans 2 and 3. An interesting effect is that particles which have the tidal lateral characteristic behavior appear to be the least affected by the design phase. This is perhaps because a large portion of particles are transported into Lake Borgne. However, due to the lateral movement, these particles may avoid that pathway. The great reduction of particles that are recruited within the Plan1-3 and final case may also be an indication that the westward direction is the “preferred” pathway for particles. That is, that westward is the dominant particle transport pathway. The previous results for the westward incoming tidal direction show the percentage of recruited particles as greater for the plan cases. The current results for the eastward incoming tidal direction may depict the results of particles working counter to the incoming tidal direction, thereby reducing the number of particles which are recruited. The March 2008 results follow similar trends to those seen in the September 2007 case.

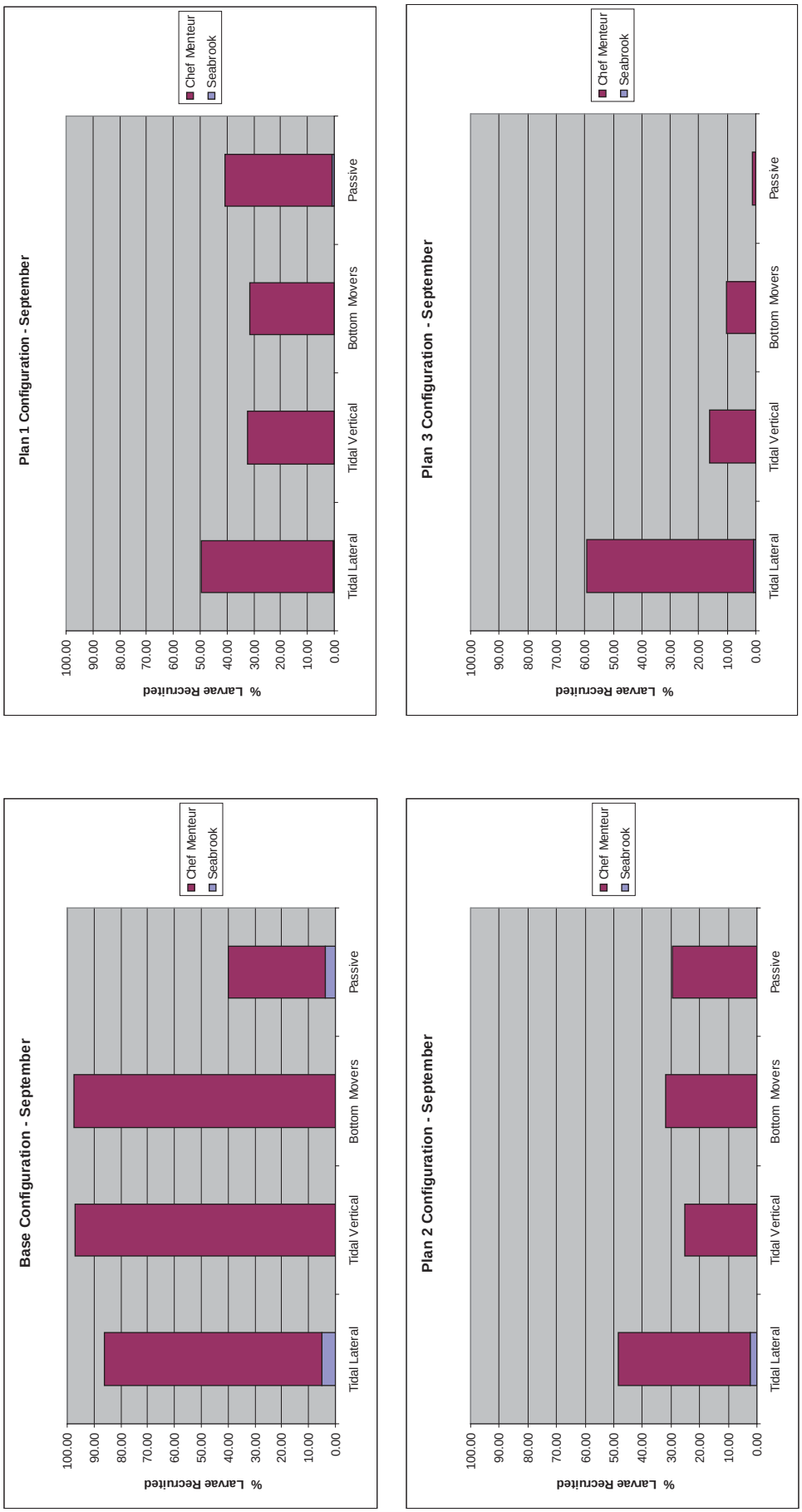

Figure 8-17 Percentage of larvae recruited at Seabrook (blue) and Chef Menteur (red) for Base, Plan1, Plan2, and Plan3 configurations using September 2007 hydrodynamics, larval fish preferred path to the east. Particles anchored based on incoming tide to the east.

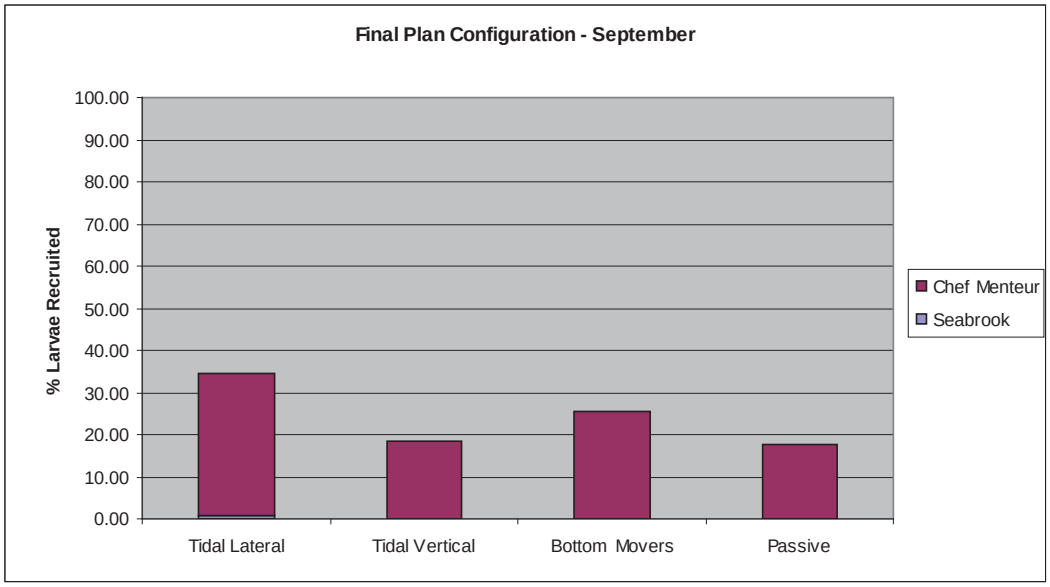

Figure 8-17 (continued) Percentage of larvae recruited at Seabrook (blue) and Chef Menteur (red) for Plan 3-Final configuration using September 2007 hydrodynamics, larval fish preferred path to the east. Particles anchored based on incoming tide to the east.

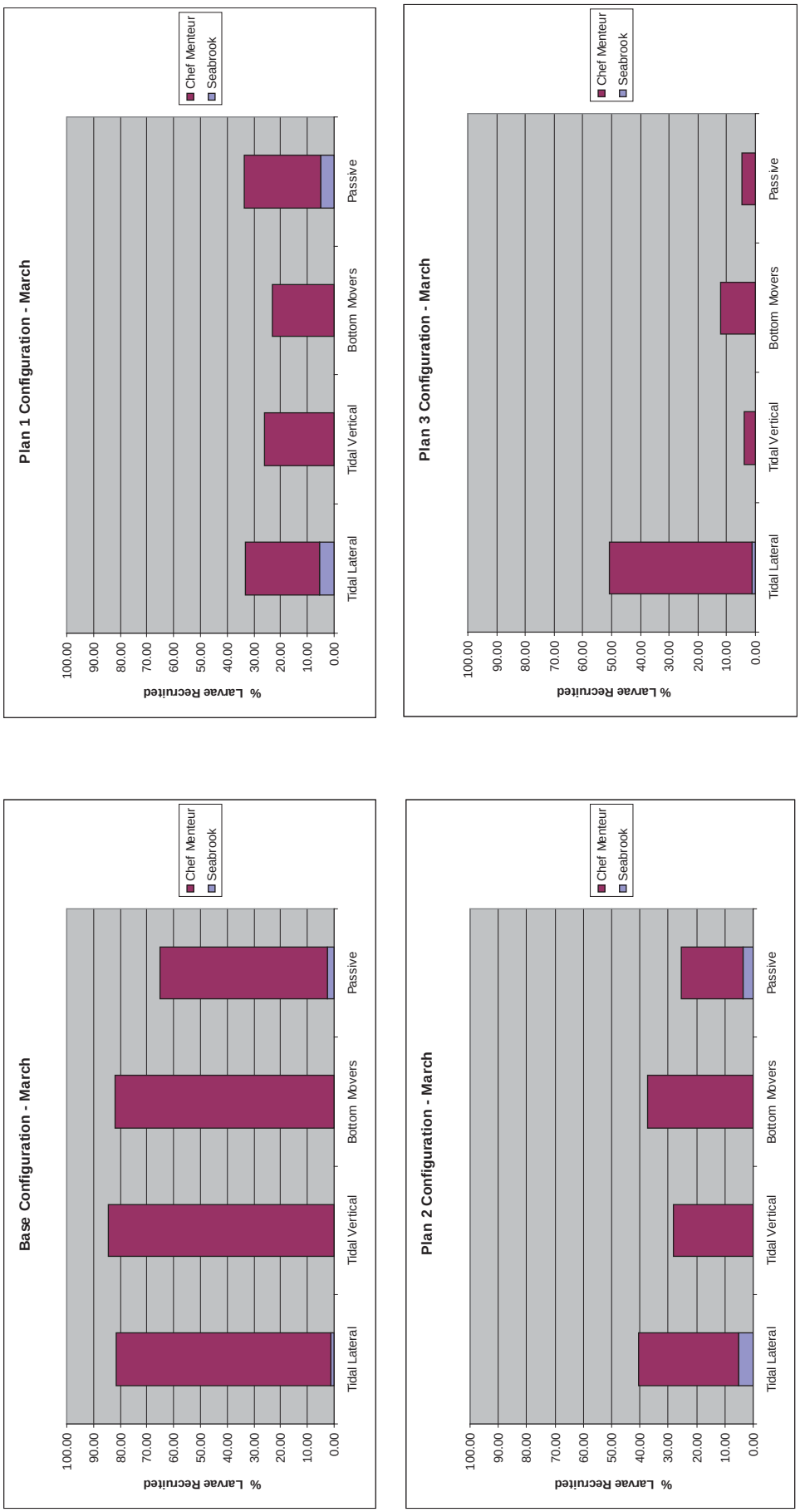

Figure 8-18 Percentage of larvae recruited at Seabrook (blue) and Chef Menteur (red) for Base, Plan1, Plan2, and Plan3 configurations using March 2008 hydrodynamics, larval fish preferred path to the east. Particles anchored based on incoming tide to the east.

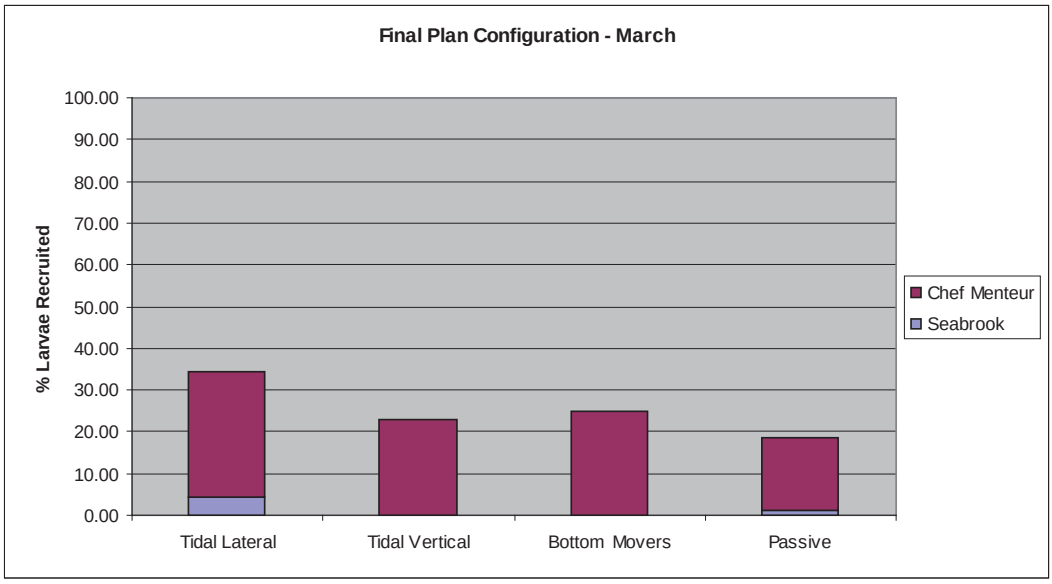

Figure 8-18 continued Percentage of larvae recruited at Seabrook (blue) and Chef Menteur (red) for Plan 3-Final configuration using March 2008 hydrodynamics, larval fish preferred path to the east. Particles anchored based on incoming tide to the east

9 Conclusions

The modeling efforts discussed in this document were performed for analysis of flow and circulation changes in the IHNC, MRGO, and GIWW areas due to several planned hurricane protection structures. The hydrodynamic model was verified to current 2008 conditions and these results are provided. Two analysis periods were then simulated to determine how the flow patterns and velocity magnitudes change within the system due to these structures. The hydrodynamic solutions were then provided to drive the larval fish transport simulations. All of this information can together give insight into how the system changes as well as how certain species will be affected by these changes.

The results of the hydrodynamic simulations show that by cutting off the MRGO, as in Plan 1, the entire circulation pattern within the GIWW/MRGO system changes. The velocities in the GIWW and Bayou Bienvenue increase, but the velocity at Seabrook decreases due to the reduction of flow volume when the MRGO is cut off from the Gulf of Mexico. With Plan 2 the MRGO is blocked in one additional place, further north, and structures are placed on Bayou Bienvenue and the GIWW. The velocities through these structures increase, but again the velocities at Seabrook are reduced due to restricted flow into the system. Plan 3 includes a structure at Seabrook. With this structure in place, the velocities at the GIWW and Bayou Bienvenue structures reduce, although the velocity at the Seabrook structure is increased. The increase when the structures are introduced is likely due to the reduced cross-sectional area. In the western section of the GIWW, the reduction of flow into this area is due to reduced flow associated with each plan configuration. As the GIWW/IHNC area becomes more constricted with structures at each end, the flow through this area is also reduced.

It is a concern of the navigation industry that velocity magnitudes not increase beyond the limit for safe navigation. A percent less than analysis was performed at several locations within the model domain to show how often the velocities reach certain values. Although there are some extreme velocity magnitudes in the structures, these values are not typical and only occur for a small fraction of the time, typically under storm circumstances when flows and winds are well above average.

Larval fish transport within the IHNC, MRGO, GIWW, and Chef Menteur regions was examined using particle tracking analyses for four cases which are differentiated by initial particle release positions. In addition to source changes, the hydrodynamic period and plan configurations are also varied. Particles initiated in the MRGO at La Loutre currently take 1.5 to 2 weeks to reach the Bayou Bienvenue closure area for the Base case. This pathway is not available for Plans 1-3 due to the closure of the MRGO at La Loutre.

Transport of particles within the system is dominated by the hydrodynamics of the system. The tidal intensity and regularity of the tidal signal are a major factor determining transport. Particles released during stronger events, such as those seen in the March 2008 hydrodynamic period, may be recruited into Lake Pontchartrain at a greater rate than a less intense flow condition such as the September 2007 hydrodynamic period. However, recruitment rate is additionally affected by the larval fish characteristic transport behaviors.

Analysis of simulation results show that the rate of particle recruitment of particles released in MRGO and GIWW is affected by the plan configuration for Cases 2-4. The Base configuration shows the highest recruitment values and Plan 3 configuration shows the lowest recruitment values. The Plan 3 Final configuration shows a decrease of particles reaching recruitment areas in comparison to the Base design, Plan 1, and Plan 2. However, recruitment values for the simulations using the Plan 3 Final geometry increase with respect to Plan 3. This is most likely due to the increase of cross sectional area at Seabrook in Plan 3 Final. Results indicate an approximate 10-15 percent recruitment decrease between Plans 1 and Plan 3 Final. Case 3 results, particles released in Lake Borgne, show that there is no real difference between the transport pathways from Lake Borgne to Chef Menteur with respect to Plans 1, 2, and 3 Final. The Base case generally has a slightly higher value of recruited particles; however results for these plans differ within 5 percent.

Characteristic larval fish behavior affects the recruitment rate of particles. When the transport mechanism of anchoring is added to particle transport behavior, recruitment occurs at a much faster rate than without the mechanism. Generally, passive particles have the lowest recruitment values, followed by tidal lateral behavior, bottom movers, and finally tidal vertical movers.

References

Lackey, T. C., and S. J. Smith. 2008. *Application of the Particle Tracking Model To Predict the fate of Dredged Suspended Sediment at the Willamette River*. Proceedings Western Dredging Association Twenty-Eighth Annual Technical Conference, St. Louis, MO.

Lackey, T. C., and N. J. MacDonald. 2007. *The Particle Tracking Model Description and Processes.* Proceedings XVIII World Dredging Congress 2007, WEDA, Lake Buena Vista, Florida.

McAnally, W. H., and R. C. Berger. 1997. *Salinity Changes in Pontchartrain Basin Estuary Resulting from Bonnet Carre` Freshwater Diversion.* Technical Report CHL-97-2. Vicksburg, MS: U.S. Army Waterways Experiment Station.

MacDonald, N. J., M. H. Davies, A. K. Zundel, J. D. Howlett, Z. Demirbilek, J. Z. Gailani, T. C. Lackey, and S. J. Smith. 2006. *PTM: Particle Tracking Model; Report 1: Model Theory, Implementation, and Example Applications.* ERDC/CHL TR-06-02. Vicksburg, MS: U.S. Army Waterways Experiment Station.

Martin, K., D. Webb, G. Savant, and G. Lynch. (In review). *Lake Borgne Surge Barrier Navigation Study.* Technical Report in review, U.S. Army Engineer Research and Development Center, Vicksburg, MS.

Tate, J. N., A. R. Carrillo, R. C. Berger, and B. J. Thibodeaux. 2002. *Salinity Changes in Pontchartrain Basin Estuary, Louisiana, Resulting from Mississippi River-Gulf Outlet Partial Closure Plans with Width Reduction*. CHL-TR-02-12. Vicksburg, MS: U.S. Army Engineer Research and Development Center.

Wu, J. 1969. *Wind Stress and Surface Roughness at Air-Sea Interface.*" Journal of Geophysical Research. 74(2)444-455.

Acknowledgements

We would like to acknowledge the contributions of the interagency team for the Keith Lake Fish Passage study for providing the general description of larval fish transport characteristics. We would also like to acknowledge the Seabrook interagency team for the additional larval fish transport mechanism information concerning anchoring and their discussion of larval fish behavior. We thank Dr. Ionnis Y. Georgiou for his assistance with regard to conceptualizing modifications to tidal flag definitions within PTM and his additional discussion of hydrodynamic transport mechanisms. We appreciate the assistance of Gary Brown, Dr. Joseph Gailani, and Jarrell Smith with regard to conceptualizing modifications to larval fish transport including tidal flag definitions and decay algorithms. We thank Cassandra Ross and Francisco Velez for their general assistance with this work. We acknowledge the contributions of Keith Martin and Dr. Gaurav Savant on the Lake Borgne surge barrier work which preceeded this study.

Research funding for the Particle Tracking Model comes from the Dredging Operations and Environmental Research program (DOER) as well as the Coastal Inlets Research Program (CIRP). Adaptive Hydraulics (ADH) research funding is provided under the System-Wide Water Resources Program (SWWRP).

Appendix A: Hydrodynamic Sensitivity Simulations

This appendix documents three sensitivity studies conducted during the course of this work. They involve a Plan 3 Wide which was a precursor to the Plan 3 Final plan, the effects of a construction cofferdam at the Seabrook location, and the effects of bridge piers near the Seabrook location.

Plan 3 wide

Velocity Magnitudes

The three initial design alternatives, as documented in the main body of the report, are given below. After the initial results were reviewed by HPO, an additional alternative was modeled for hydrodynamics. This alternative is similar to Plan 3 except the dimensions of the Seabrook structure are increased and is referred to as Plan 3 Wide. These analyses, for Plan 3 Wide, were performed prior to the determination of Plan 3 Final, which is not included in the results provided in this appendix.

- Base - condition includes the fully open MRGO, GIWW, and IHNC
- Plan 1 – close the MRGO at La Loutre
- Plan 2 – close the MRGO at La Loutre, include the Borgne alignment (56 ft X 8 ft gate on Bayou Bienvenue, and two 150 ft X 16 ft gates on GIWW)
- Plan 3 – close the MRGO at La Loutre, include the Borgne alignment, include the 95 ft X 16 ft gate at Seabrook structure with southern scour hole filled
- Plan 3-wide – close the MRGO at La Loutre, include the Borgne alignment, include the 115 ft X 30 ft gate at Seabrook structure with southern scour hole filled

After the model was run for the Base and Plan conditions, velocity data were extracted for the location of the structures for the Bayou Bienvenue structure, the GIWW sector gate, the GIWW barge gate, and the Seabrook structure. Figures A-1 and A-2 show these locations. For the Base condition and Plans 1 and 2, data are analyzed at a location north of the Seabrook

structure location where the velocities are highest. The analysis for Plan 3 (original and widened) is at the location in the Seabrook structure where the velocity magnitudes are the greatest. It is important to keep in mind that velocities will increase for a given flux when the cross-sectional area is reduced simply due to continuity. Therefore, once a structure is in place at these locations, it is likely that the velocity magnitudes will rise.

The average velocities for flood and ebb are determined at each location and time period for the Base and three plans, as are the maximum velocities for all conditions. Since there is a circulation within this system through the GIWW, the definition of flood and ebb can be misleading. For this reason a definition of positive and negative or flood and ebb is necessary. Positive (flood) directions are defined as those directed predominantly toward the north or east and negative (ebb) values are defined as those directed predominantly toward the south or west. The arrows in Figures A-1 and A-2 show the positive direction for each location. The results of this analysis are given in Figures A-3 through A-10. A direction arrow is included for each location to help define the flow direction.

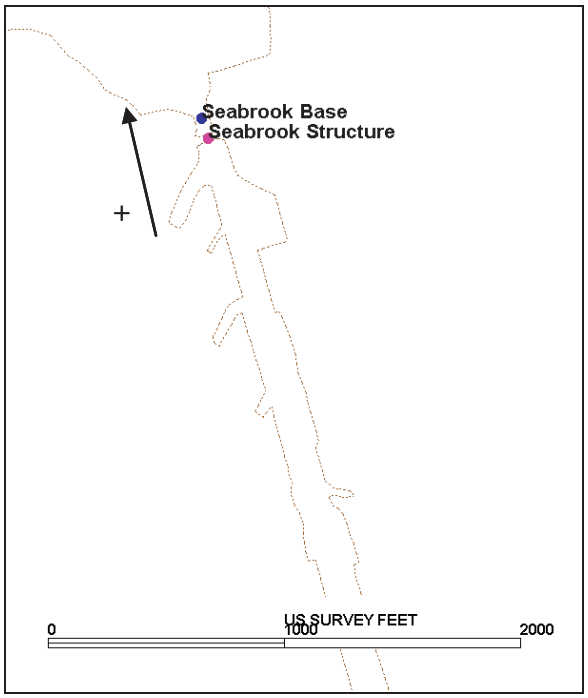

Figure A1. Hydrodynamic analysis locations – Seabrook.

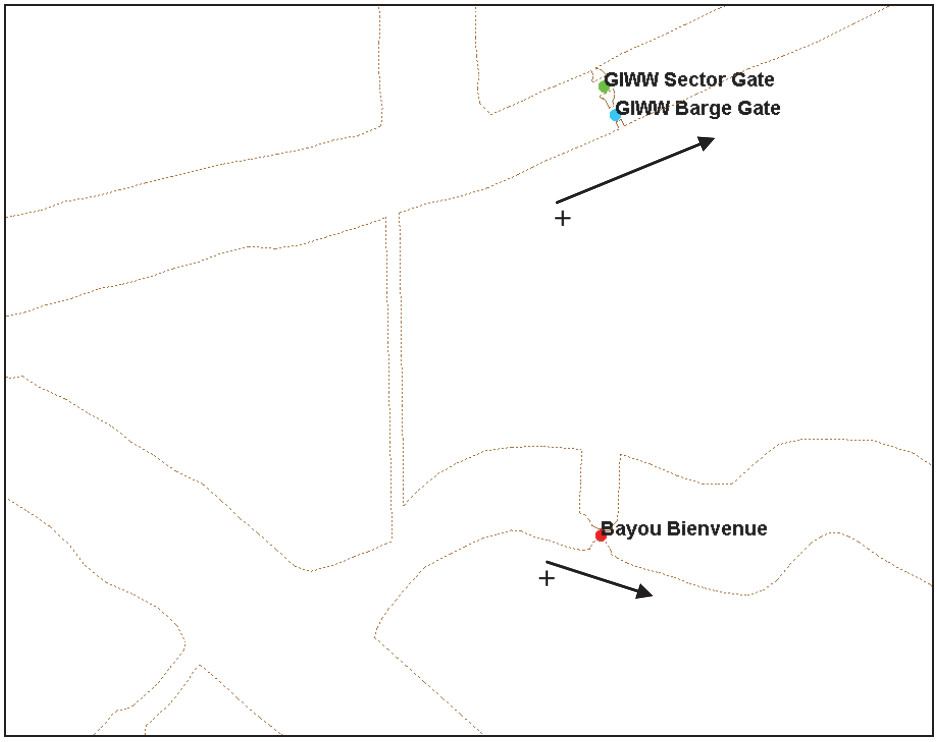

Figure A2. Hydrodynamic analysis locations – Bayou Bienvenue Structure, GIWW Sector Gate, and GIWW Barge Gate.

Figures A-3 to A-10 show that the increase in the opening at Seabrook (Plan 3-wide) results in a reduction of the velocity magnitudes at this location as compared to the original Plan 3. This pattern is produced for both the average and extreme values for both September and March. The velocity magnitudes at this location are actually lower than the values for the Base condition in most of the figures. However, the effect of increasing the size of this opening is propagated throughout the system and changes are visible at the GIWW structures and the Bayou Bienvenue structure. The increased size of the Seabrook opening increases the velocity magnitudes at each of these locations as compared to the original, smaller structure opening. The velocities increase to just under the magnitudes generated with the Plan 2 implementation, which includes no changes to the Seabrook area.

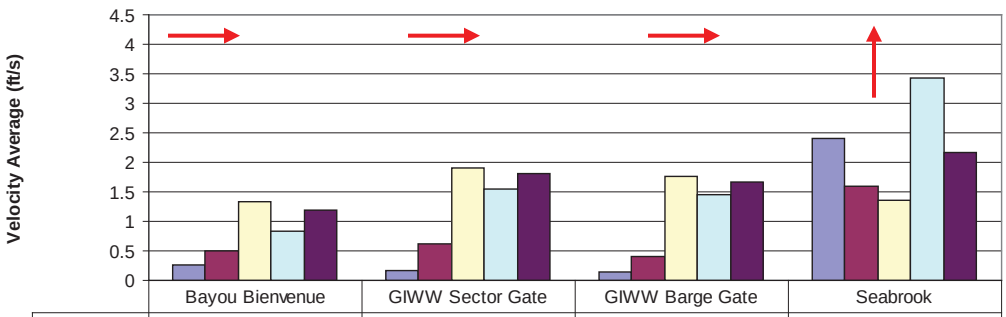

	Bayou Bienvenue	GIWW Sector Gate	GIWW Barge Gate	Seabrook
Base	0.261	0.163	0.145	2.410
Plan 1	0.500	0.628	0.407	1.585
Plan 2	1.332	1.910	1.752	1.368
Plan 3	0.843	1.545	1.460	3.435
Plan3 wide	1.201	1.817	1.669	2.173

Figure A3. Velocity average for September (positive).

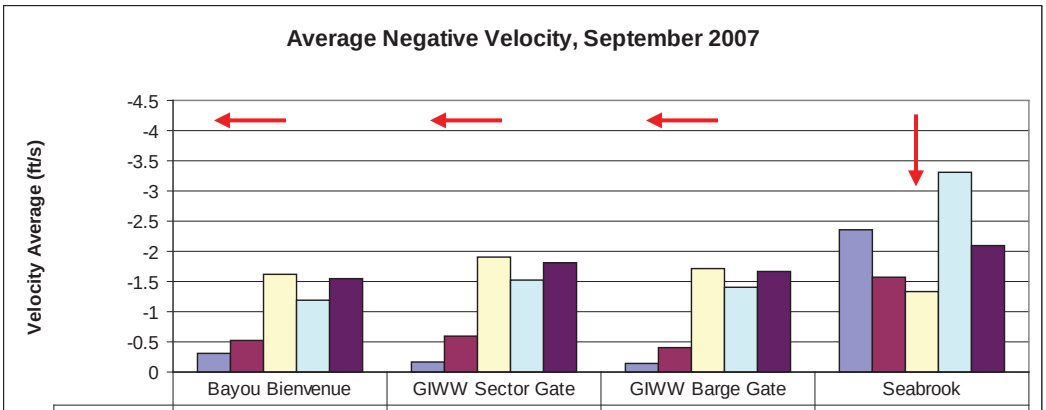

	Bayou Bienvenue	GIWW Sector Gate	GIWW Barge Gate	Seabrook
Base	-0.320	-0.157	-0.146	-2.365
Plan 1	-0.513	-0.601	-0.408	-1.567
Plan 2	-1.619	-1.908	-1.717	-1.322
Plan 3	-1.196	-1.520	-1.403	-3.298
Plan3 wide	-1.538	-1.817	-1.659	-2.085

Figure A4. Velocity average for September (negative).

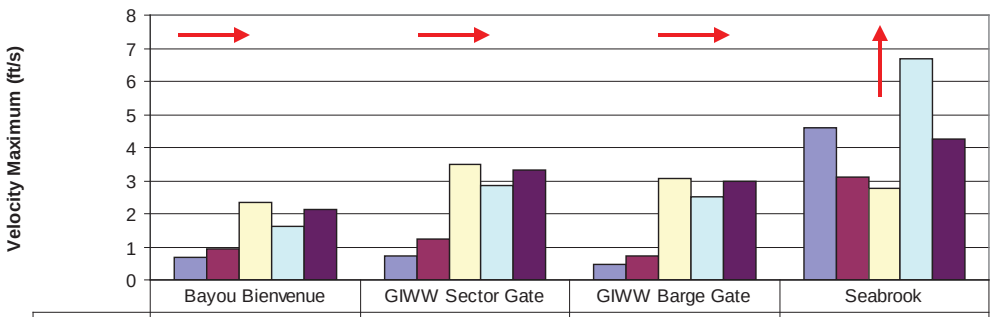

	Bayou Bienvenue	GIWW Sector Gate	GIWW Barge Gate	Seabrook
Base	0.679	0.714	0.473	4.580
Plan 1	0.954	1.215	0.729	3.122
Plan 2	2.327	3.503	3.083	2.765
Plan 3	1.601	2.836	2.524	6.663
Plan3 wide	2.125	3.313	2.969	4.261

Figure A5. Velocity maximum for September (positive).

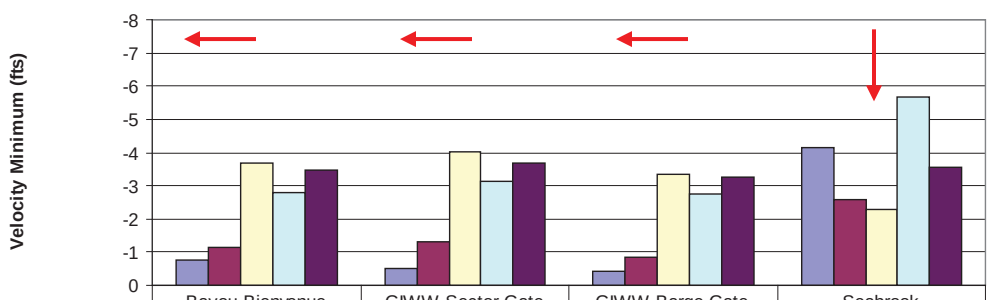

	Bayou Bienvenue	GIWW Sector Gate	GIWW Barge Gate	Seabrook
Base	-0.756	-0.491	-0.409	-4.134
Plan 1	-1.129	-1.311	-0.835	-2.583
Plan 2	-3.685	-4.001	-3.344	-2.279
Plan 3	-2.793	-3.140	-2.761	-5.652
Plan3 wide	-3.457	-3.694	-3.247	-3.560

Figure A6. Velocity minimum for September (negative).

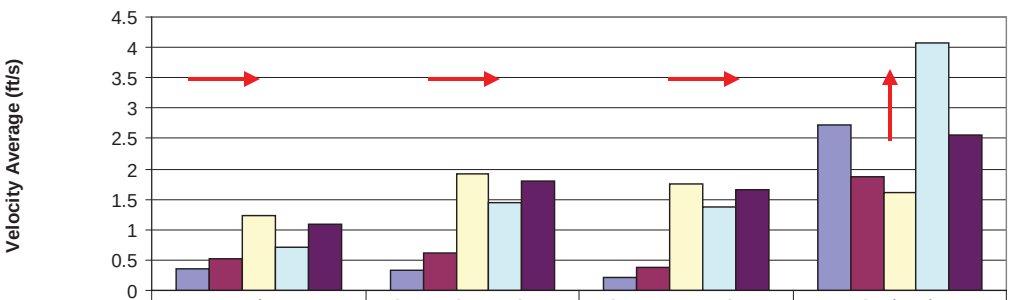

	Bayou Bienvenue	GIWW Sector Gate	GIWW Barge Gate	Seabrook
Base	0.361	0.324	0.213	2.729
Plan 1	0.511	0.614	0.388	1.870
Plan 2	1.231	1.919	1.762	1.618
Plan 3	0.704	1.456	1.382	4.071
Plan3 wide	1.100	1.798	1.661	2.561

Figure A7. Velocity average for March (positive).

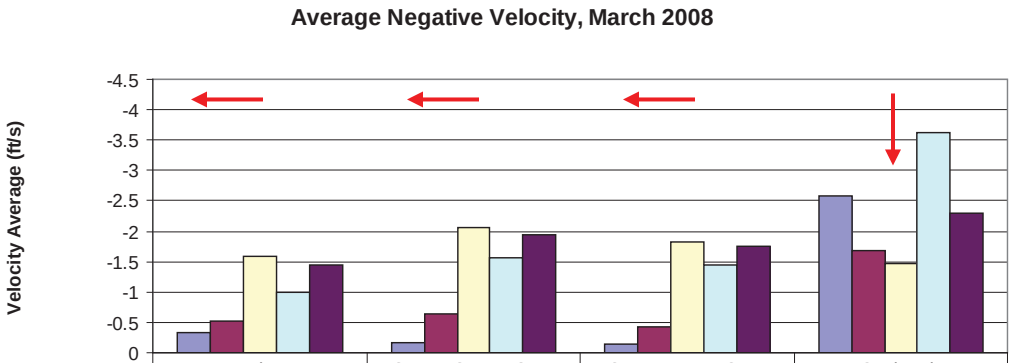

	Bayou Bienvenue	GIWW Sector Gate	GIWW Barge Gate	Seabrook
Base	-0.333	-0.175	-0.143	-2.585
Plan 1	-0.531	-0.648	-0.422	-1.679
Plan 2	-1.581	-2.064	-1.833	-1.460
Plan 3	-1.005	-1.559	-1.446	-3.634
Plan3 wide	-1.450	-1.946	-1.741	-2.302

Figure A8. Velocity average for March (negative).

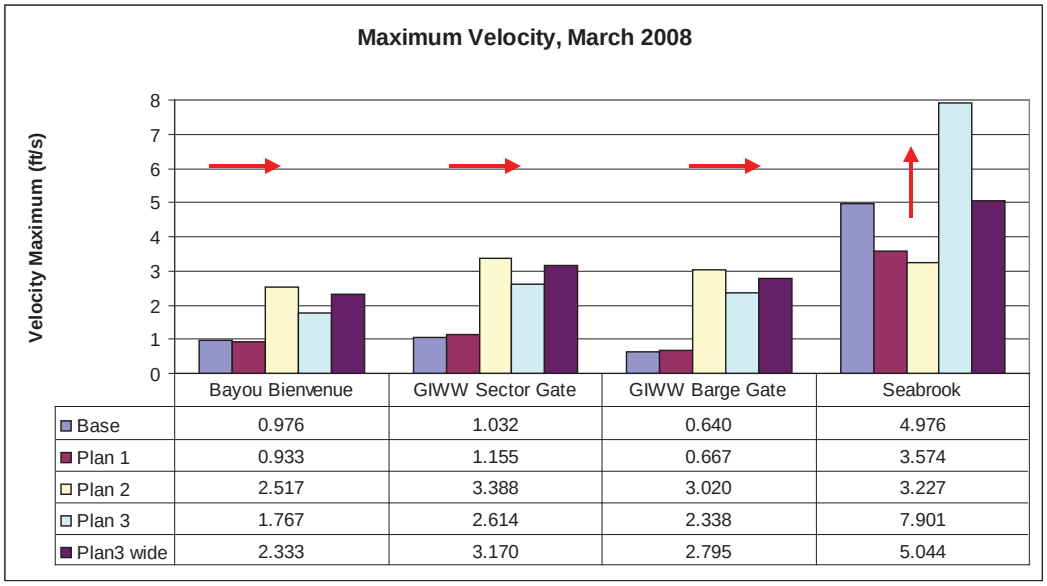

	Bayou Bienvenue	GIWW Sector Gate	GIWW Barge Gate	Seabrook
Base	0.976	1.032	0.640	4.976
Plan 1	0.933	1.155	0.667	3.574
Plan 2	2.517	3.388	3.020	3.227
Plan 3	1.767	2.614	2.338	7.901
Plan3 wide	2.333	3.170	2.795	5.044

Figure A9. Velocity maximum for March (positive).

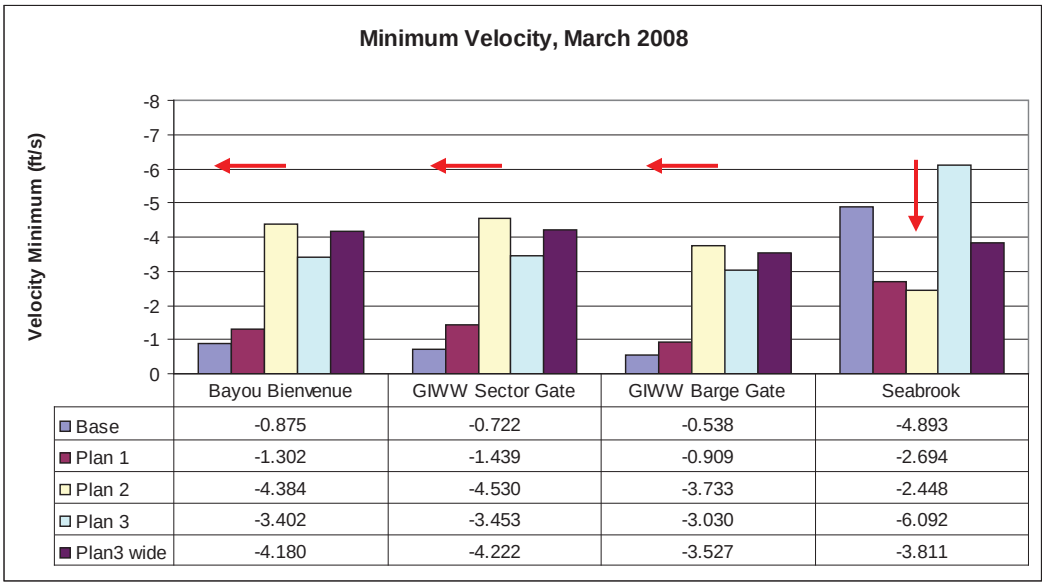

	Bayou Bienvenue	GIWW Sector Gate	GIWW Barge Gate	Seabrook
Base	-0.875	-0.722	-0.538	-4.893
Plan 1	-1.302	-1.439	-0.909	-2.694
Plan 2	-4.384	-4.530	-3.733	-2.448
Plan 3	-3.402	-3.453	-3.030	-6.092
Plan3 wide	-4.180	-4.222	-3.527	-3.811

Figure A10. Velocity minimum for March (negative.)

Velocity less than plots are provided for the locations at the GIWW sector gate and the Seabrook structure in Figures A-11 through A-16. These locations experience the largest velocities when the structures are in place. These figures support the results that, by increasing the opening at Seabrook, the velocities are reduced from those produced by the original Plan 3 structure opening.

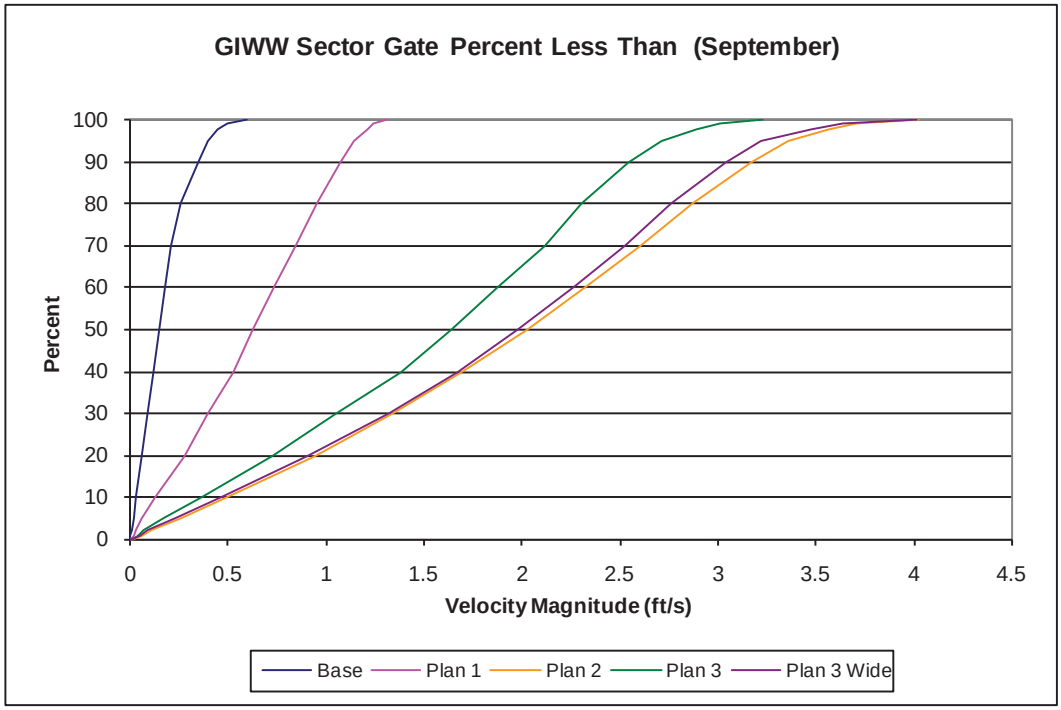

Figure A11. Velocity less than at the GIWW sector gate for September.

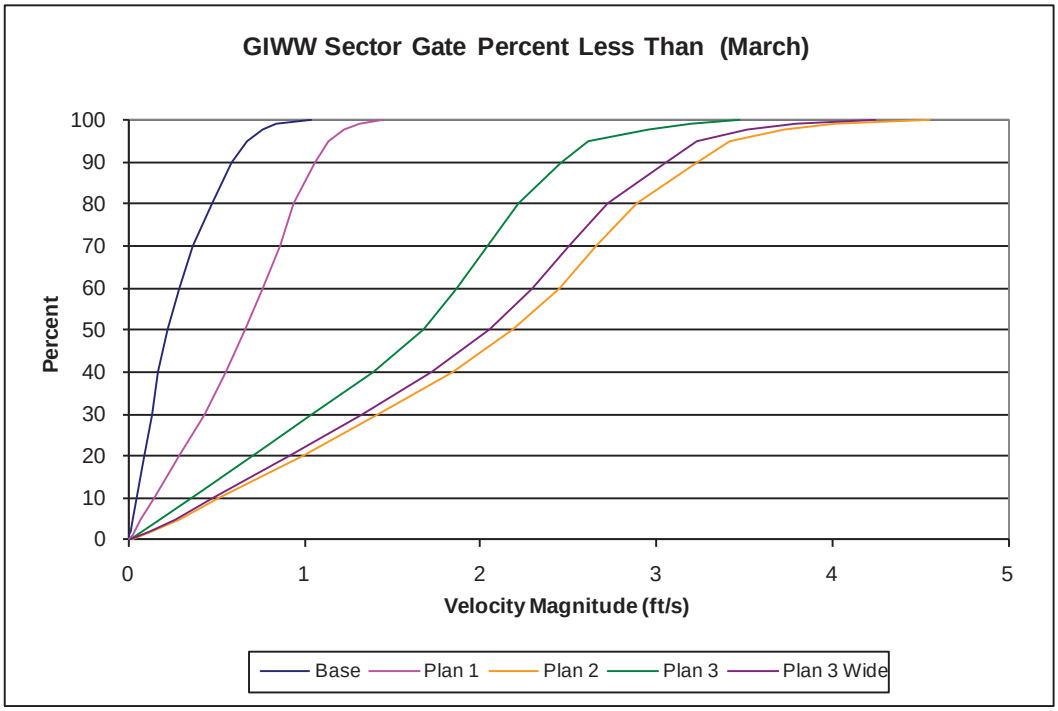

Figure A12. Velocity less than at the GIWW sector gate for March.

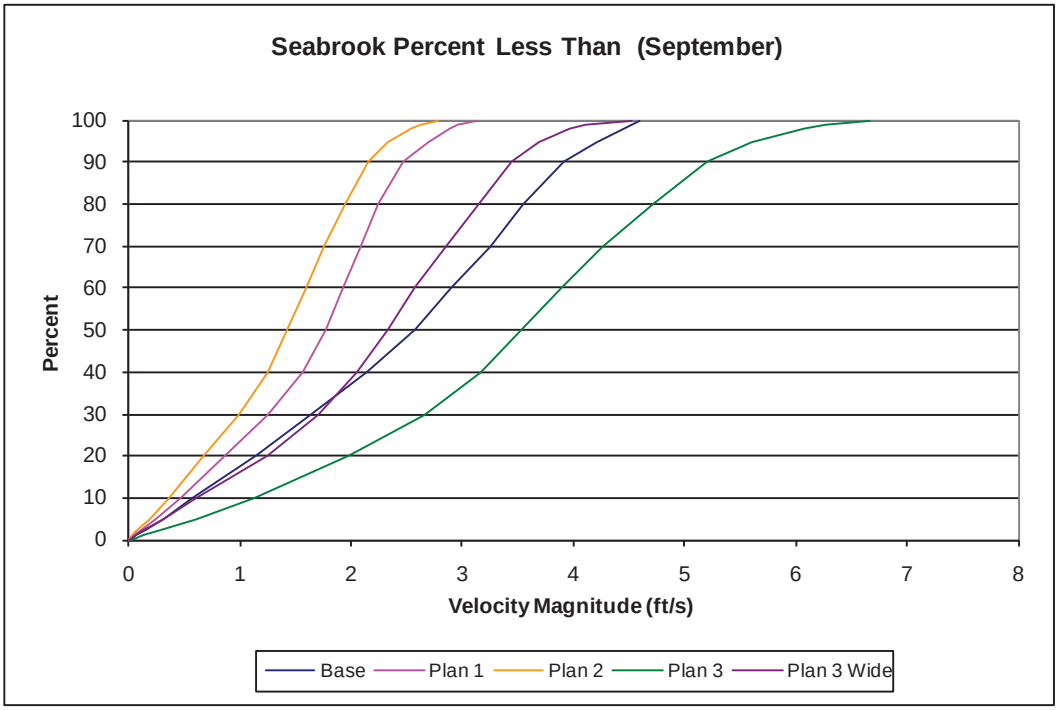

Figure A13. Velocity less than at the Seabrook structure for September.

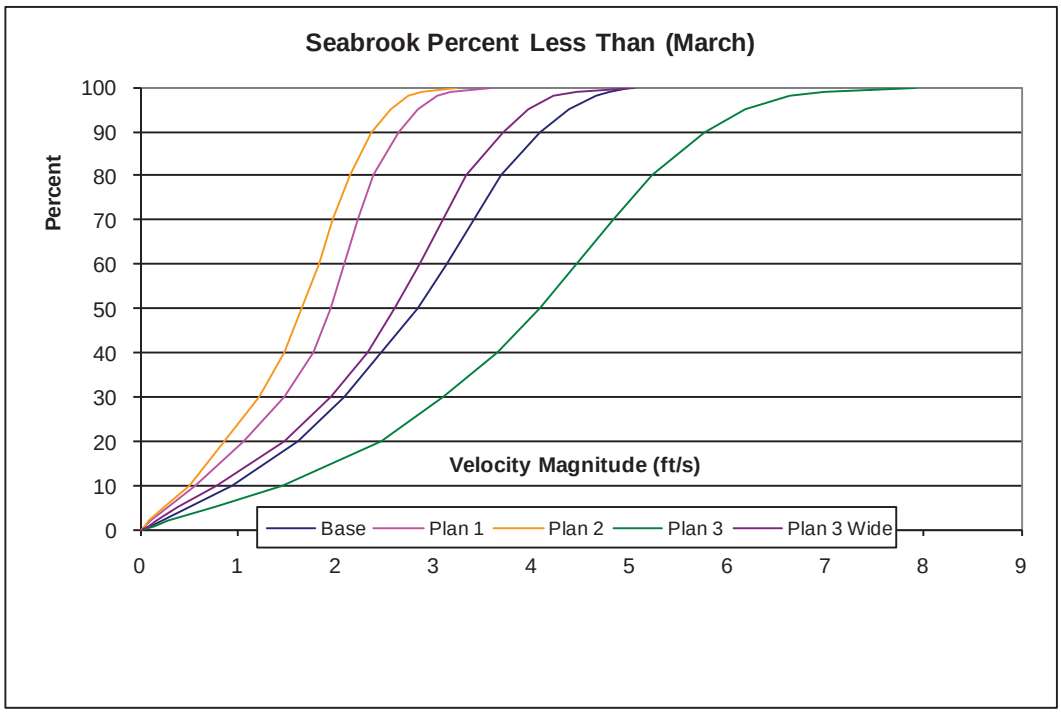

Figure A14. Velocity less than at the Seabrook structure for March.

Water Surface Analysis

An analysis of the water surface elevation as it reacts to the plan conditions is shown in the following figures. An arc was drawn from the east side of the GIWW sector gate, through this structure, along the GIWW, up the IHNC, through the Seabrook structure, and ending in southern Lake Pontchartrain. Figure A-15 shows this arc. The arc is divided into 1000 ft increments for reference such that the GIWW structures are at 1800 ft, the IHNC joins the GIWW at 40,000 ft, and the Seabrook structure is at 56,000 ft. Figures A-16 and A-17 show the water surface elevation along this arc for midnight August 27, 2007 and March 3, 2008. These times were chosen to show a high ebb velocity event from August and a high flood velocity event from March for the Seabrook region such that the water level differences between Lake Borgne and Lake Pontchartrain are large. Figures A-18 and A-19 focus on the GIWW sector gate and Figures A-20 and A-21 focus on the IHNC and Seabrook structure, respectively.

These figures show that there is a change in the water surface elevation as the flow passes through these structures. This concept of elevation changes or head differences on each side of a constriction is supported by basic hydraulic theory due to constriction of flow volume and high velocities through the narrow structure. Since water flows from high to low elevation, the flow will be directed from the higher toward the lower water surface elevation and will move fastest when this difference is greatest.

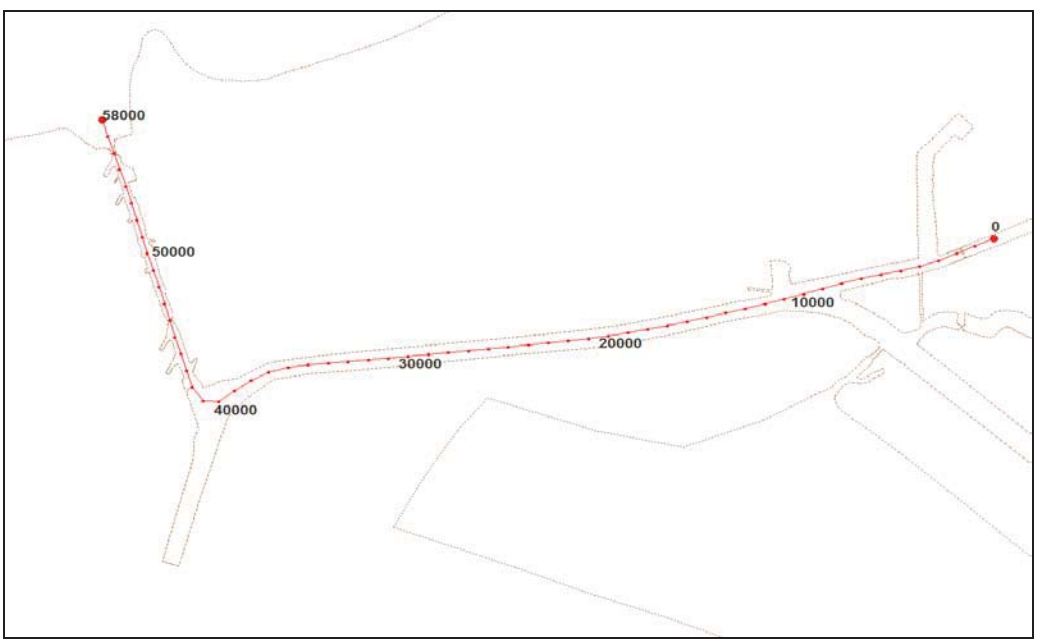

Figure A15. Water surface analysis arc and location reference in 1000 ft increments.

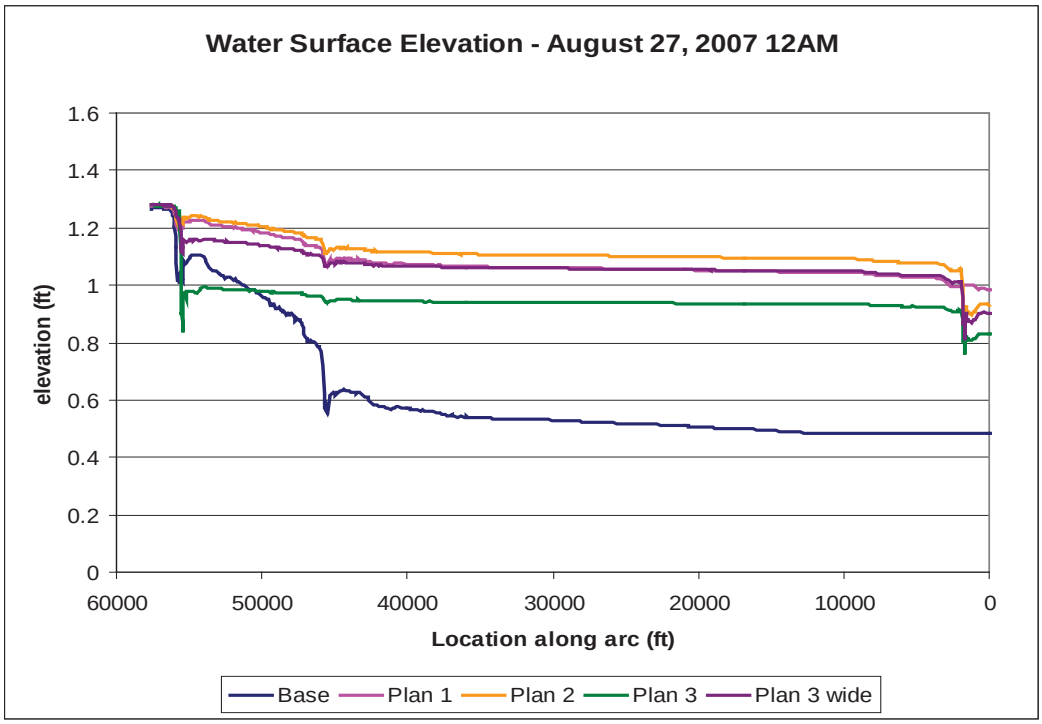

Figure A16. Water surface elevation along arc for Base and all plans for August 27, 2007.

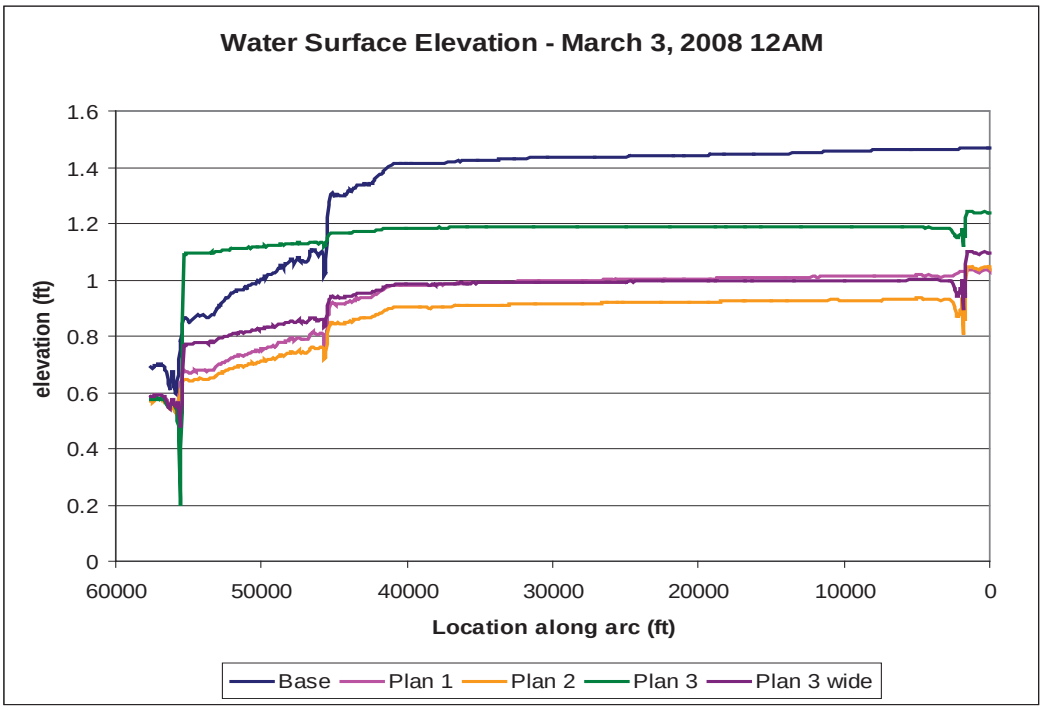

Figure A17. Water surface elevation along arc for Base and all plans for March 3, 2008.

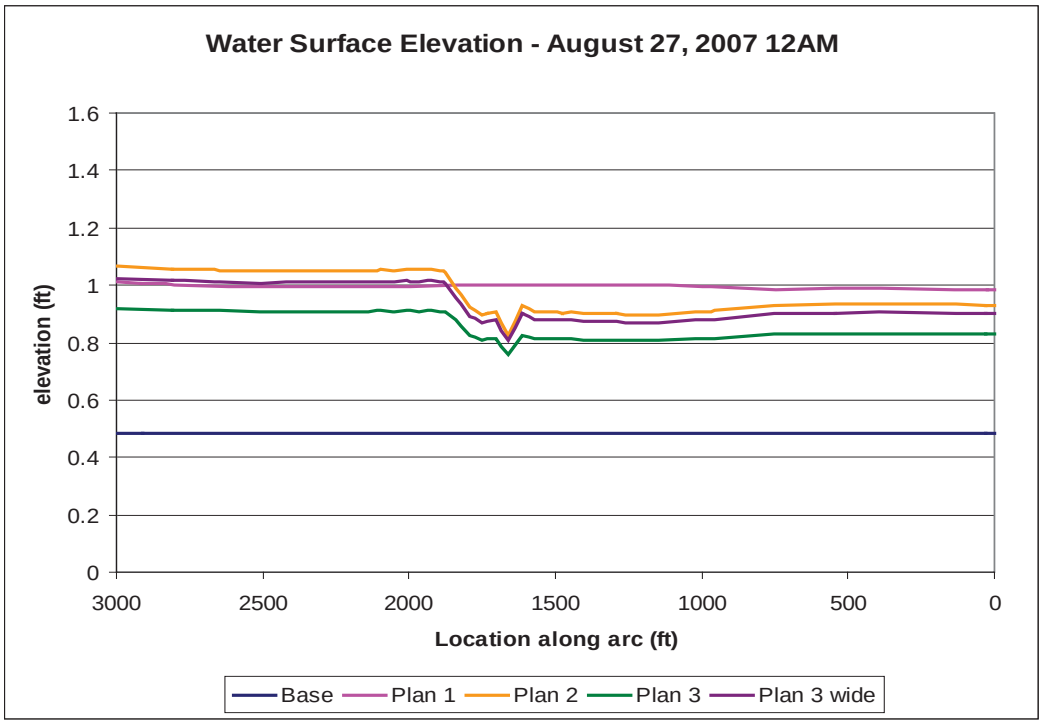

Figure A18. Water surface elevation through GIWW sector gate (August).

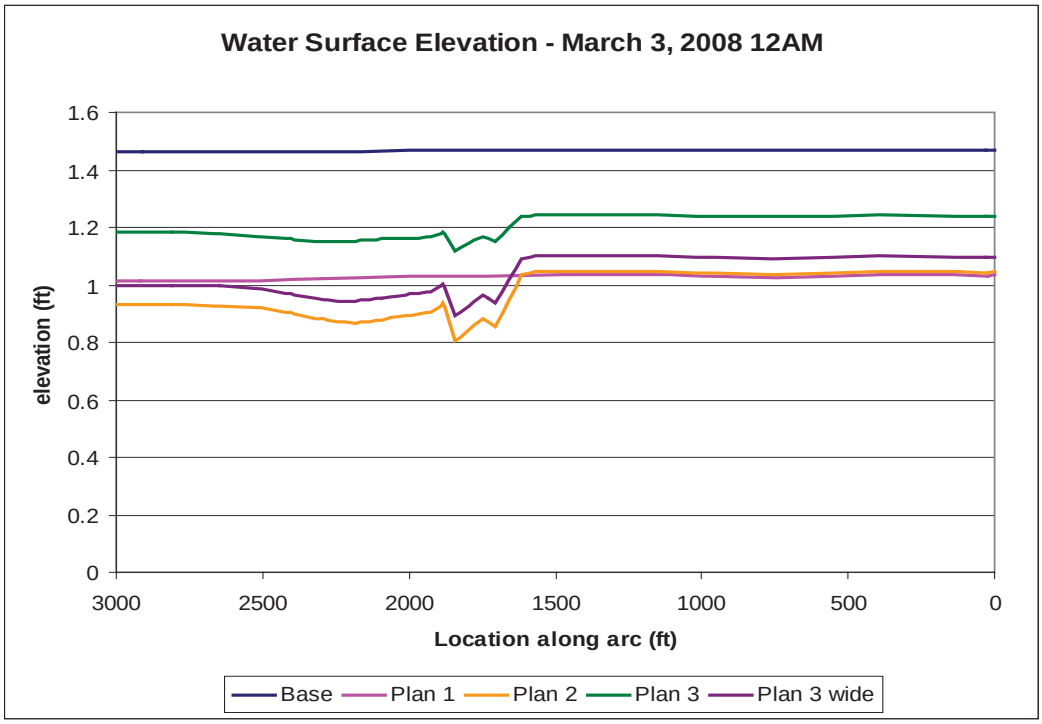

Figure A19. Water surface elevation through GIWW sector gate (March).

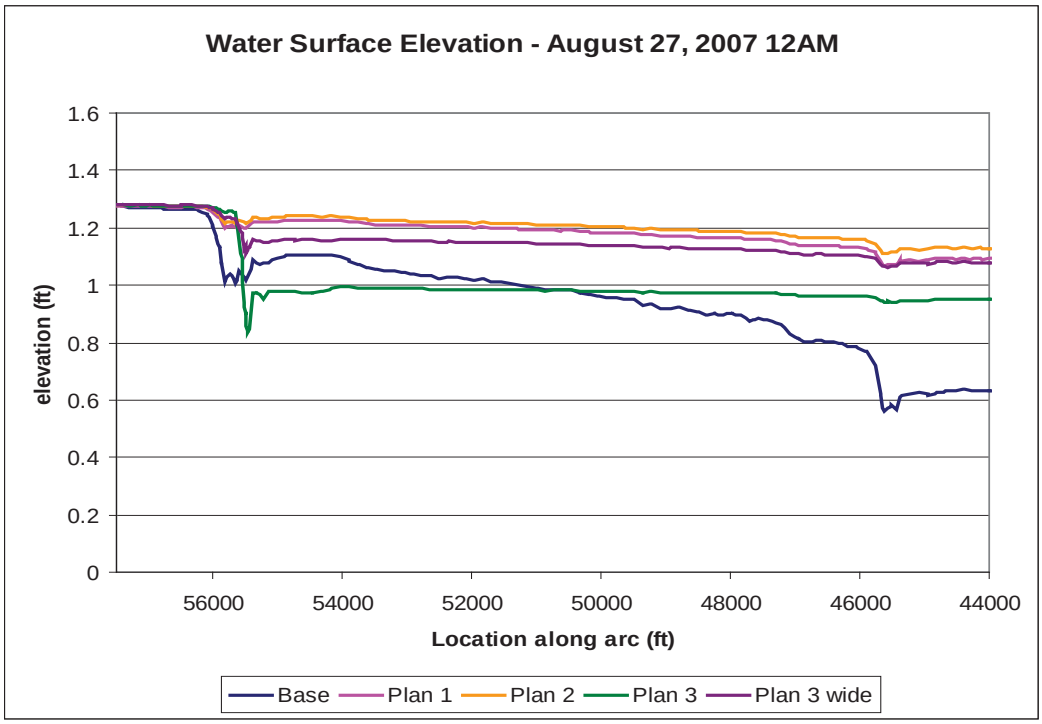

Figure A20. Water surface elevation through IHNC and Seabrook structure (August).

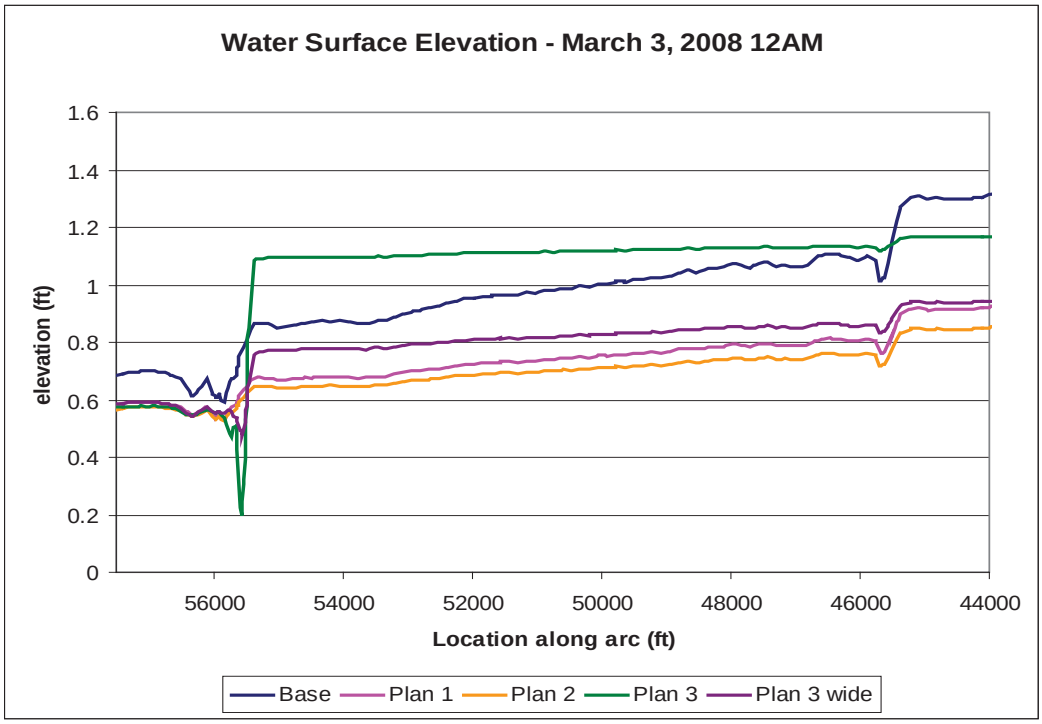

Figure A21. Water surface elevation through IHNC and Seabrook structure (March).

Cofferdam Simulations

During the construction of the Seabrook gate, a cofferdam may be placed in the IHNC as a construction method option. However, flow around this cofferdam may be too large to accommodate any through traffic and possibly may generate erosion problems. The following figures show the analysis of the effect of a 246 X 100 ft cofferdam placed at Seabrook, which can accommodate a 96 ft wide structure. The analysis points are at the Bayou Bienvenue structure, the GIWW barge gate, the GIWW sector gate, and at three locations at Seabrook (north of the structure, at the northwest corner, and at the northeast corner). Figure A-22 shows these additional Seabrook locations. These simulations include all additions through Plan 2 and the fill of the southern scour hole at Seabrook which will be the configuration when the cofferdam is used. Figures A-23 and A-30 show the average and maximum velocity magnitudes at these locations for both the positive (flood) and negative (ebb) flow directions, as defined earlier, over the four week simulation periods. For comparison, the velocity analysis for the Plan 3 Final Seabrook configuration is also provided in the plots.

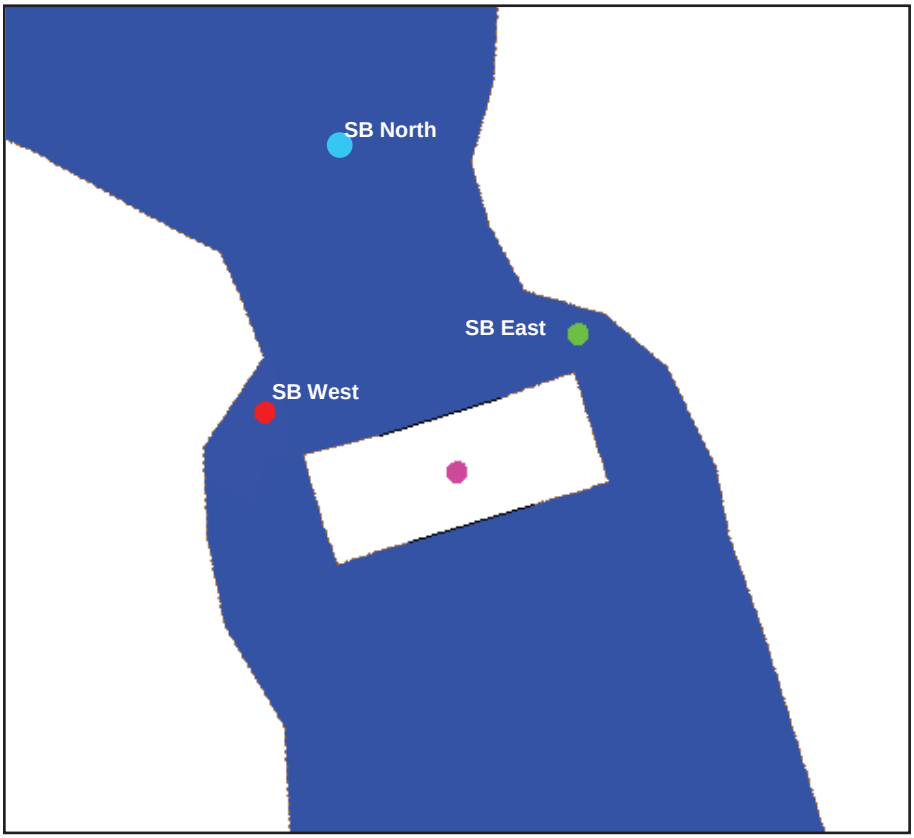

Figure A22. Seabrook analysis locations for cofferdam simulation.

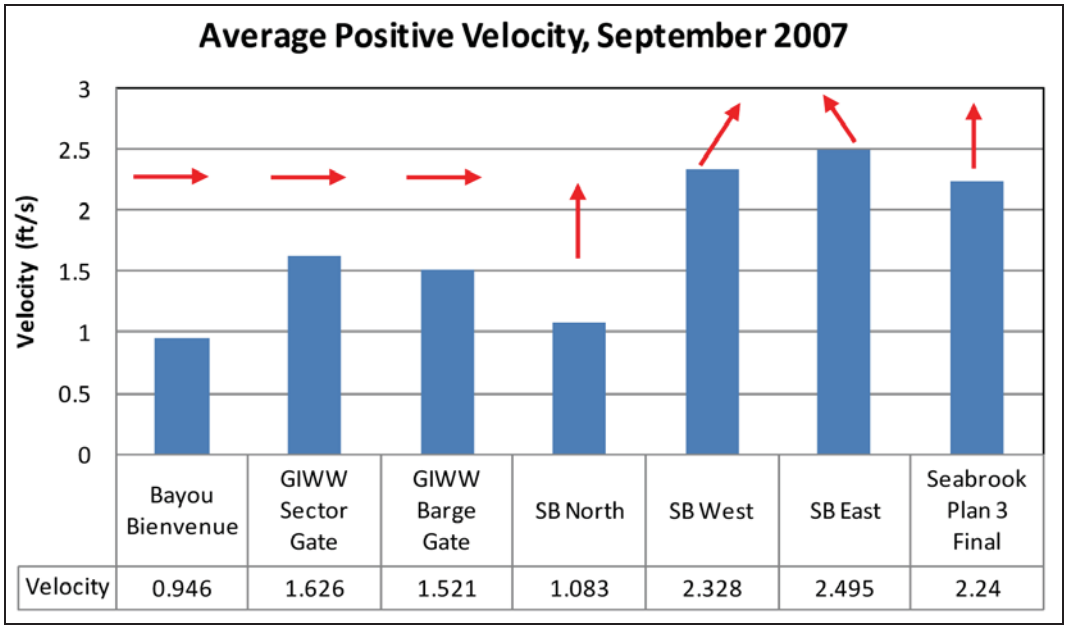

Figure A23. Velocity average for September with cofferdam (positive).

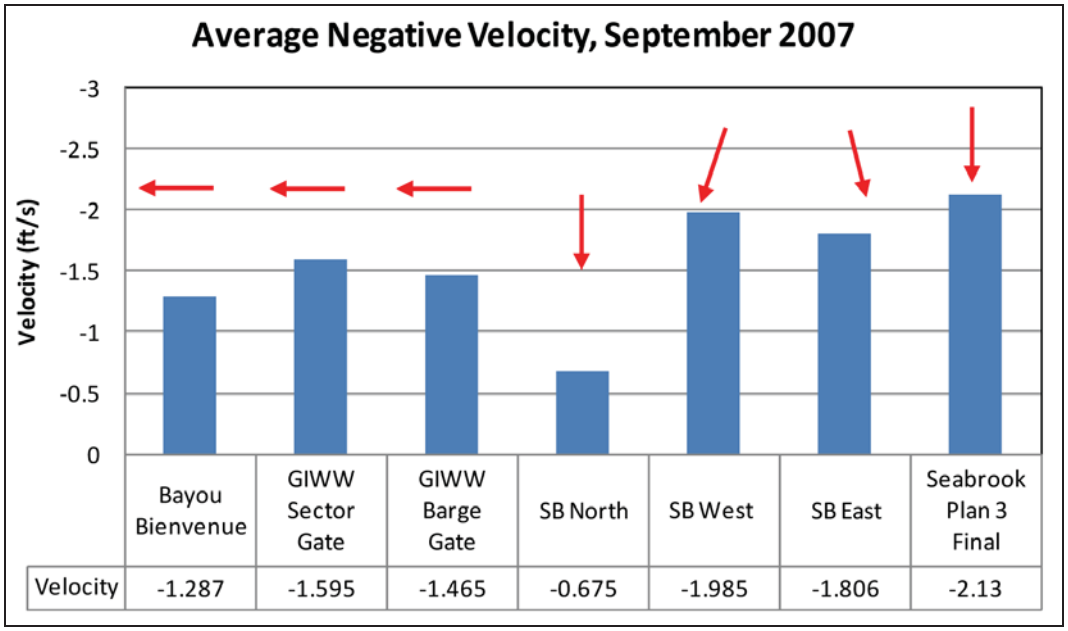

Figure A24. Velocity average for September with cofferdam (negative).

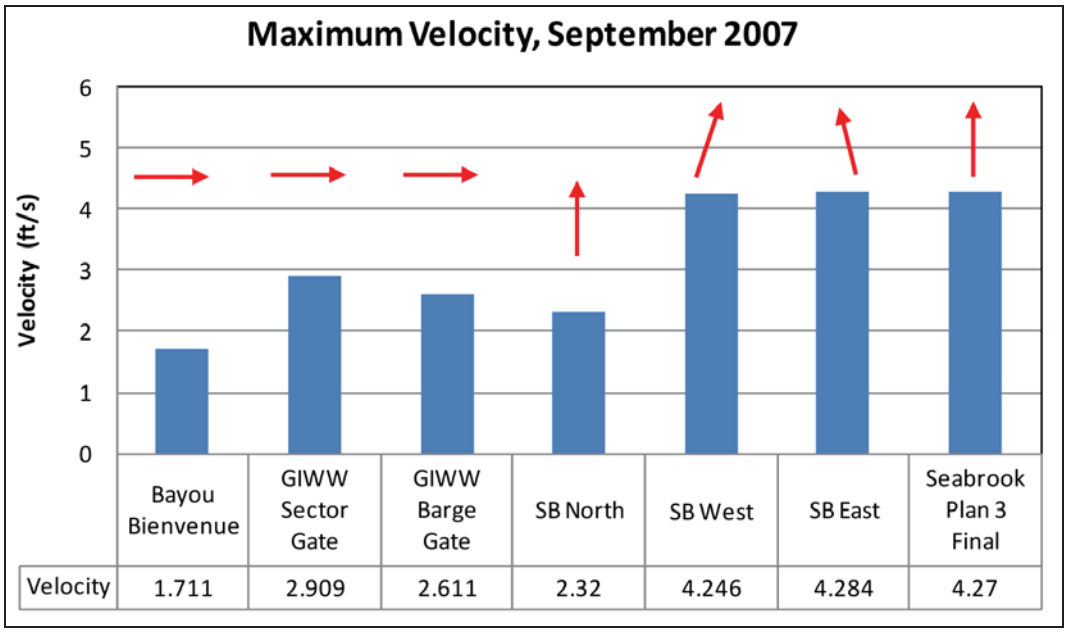

Figure A25. Velocity maximum for September with cofferdam (positive).

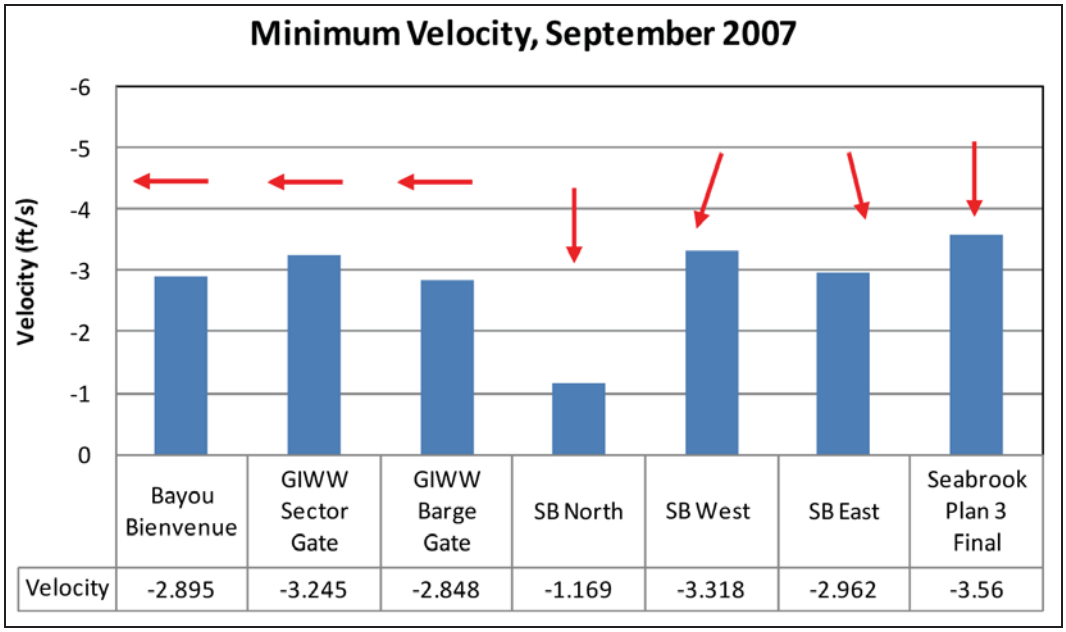

Figure A26. Velocity minimum for September with cofferdam (negative).

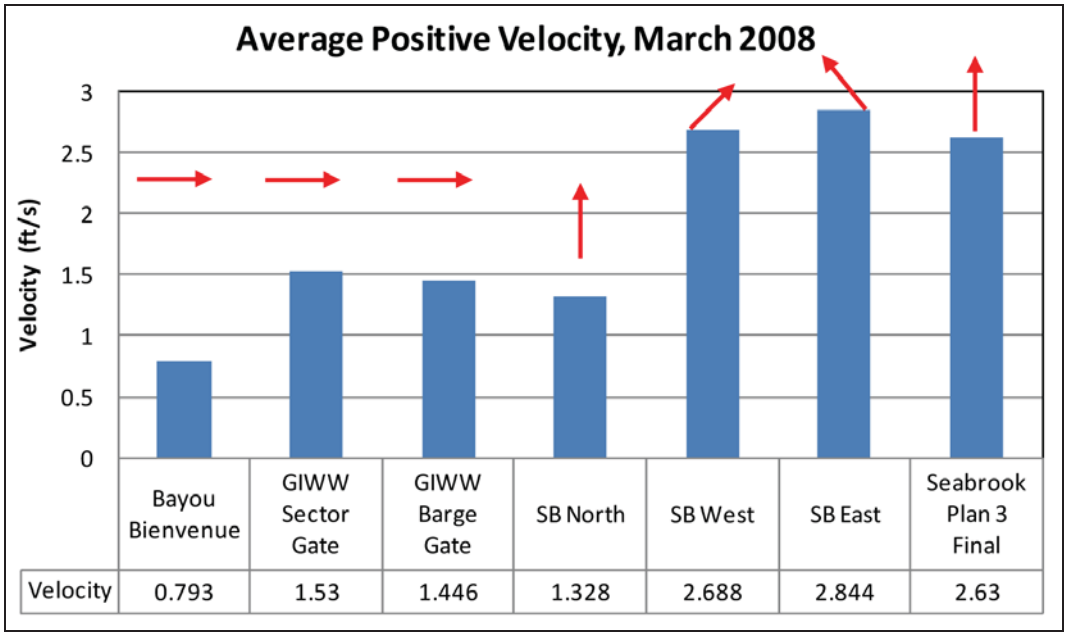

Figure A27. Velocity average for March with cofferdam (positive).

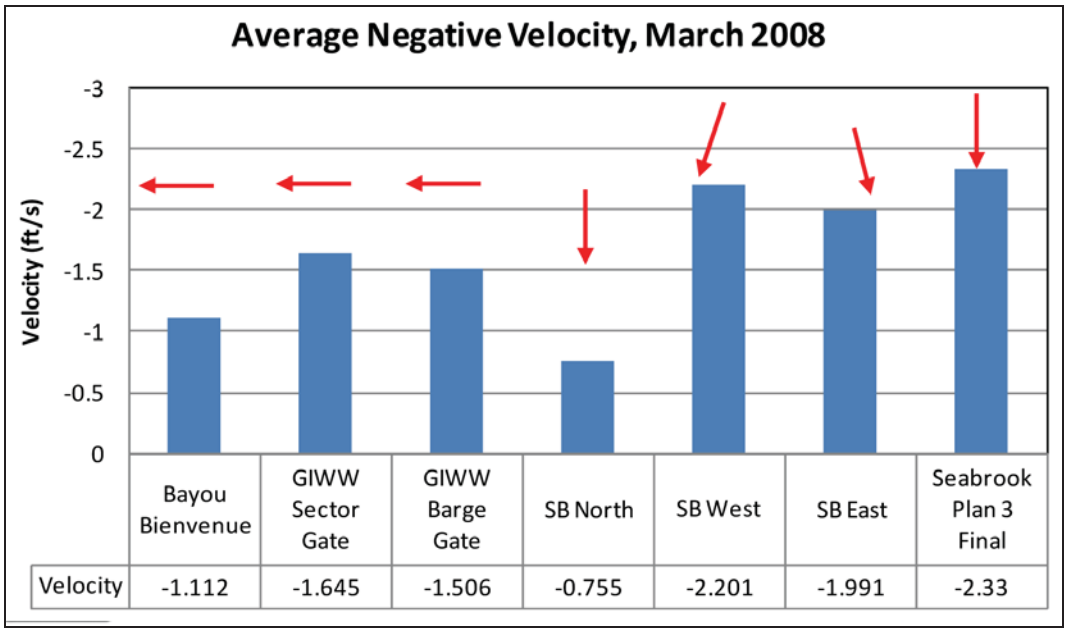

Figure A28. Velocity average for March with cofferdam (negative).

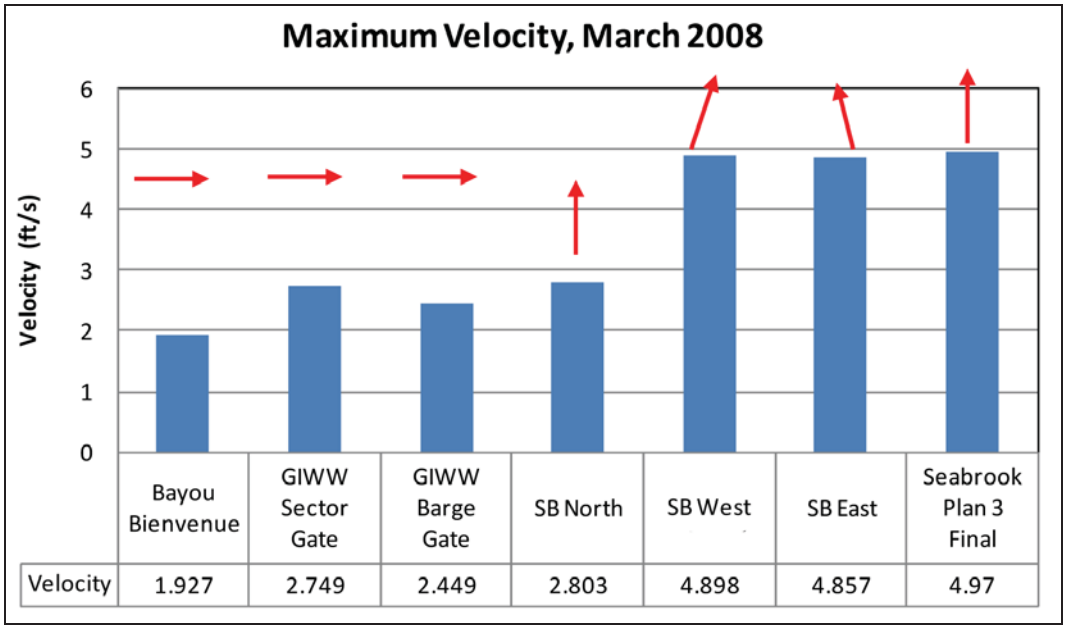

Figure A29. Velocity maximum for March with cofferdam (positive).

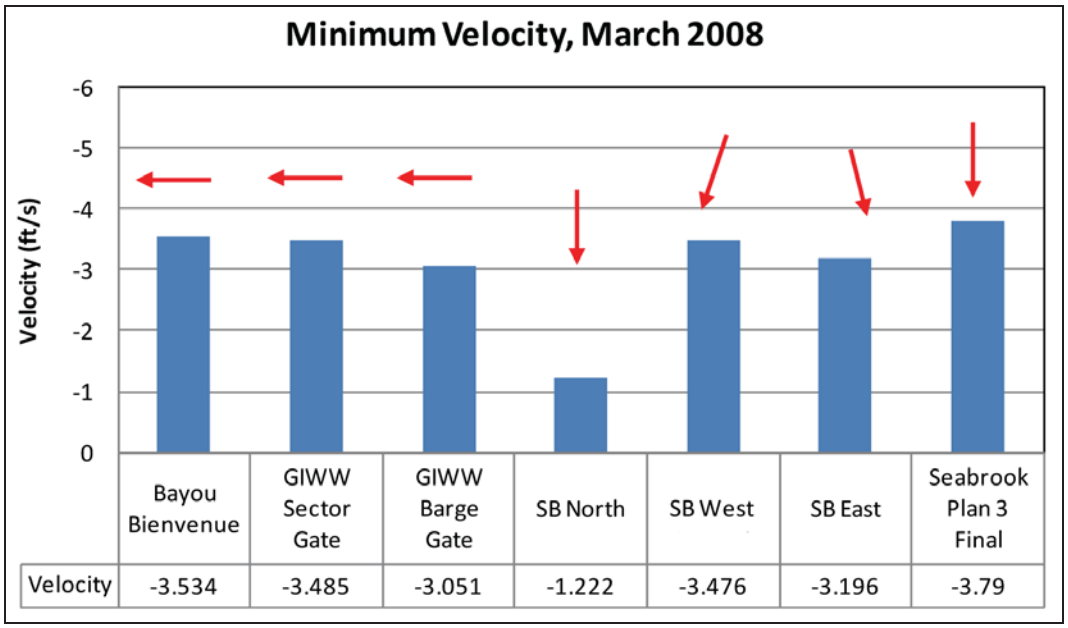

Figure A30. Velocity minimum for March with cofferdam (negative).

Based on the above figures, the velocities with the cofferdam in place during construction of the Seabrook structure (Plan 3/Plan 3 Final) are reduced from those with the structure in place. These values are lower because the total cross-sectional area on each side of the cofferdam (at the narrowest location) is 2570 ft^2 whereas the cross-sectional area for the Plan 3 structure is only 1520 ft^2. Although the discharge through this area will be affected some due to the change in shape and effects of the other structures in the

system, there is enough area on each side of the cofferdam to prevent the velocities from reaching the levels observed due to the implementation of Plan 3. Figures A-31 and A-32 show a snapshot of the velocity magnitude and direction at a time when the flows are large for both an incoming and retreating tide event. The location of highest velocity, as seen in the figures, is closer to the model boundary than the location of the East and West analysis points in Figure A-22. This indicates that the extreme velocities will be slightly higher than the value given in the previous figures, although still not on the order of the values for Plan 3 (maximum positive velocity of 739 ft/s).

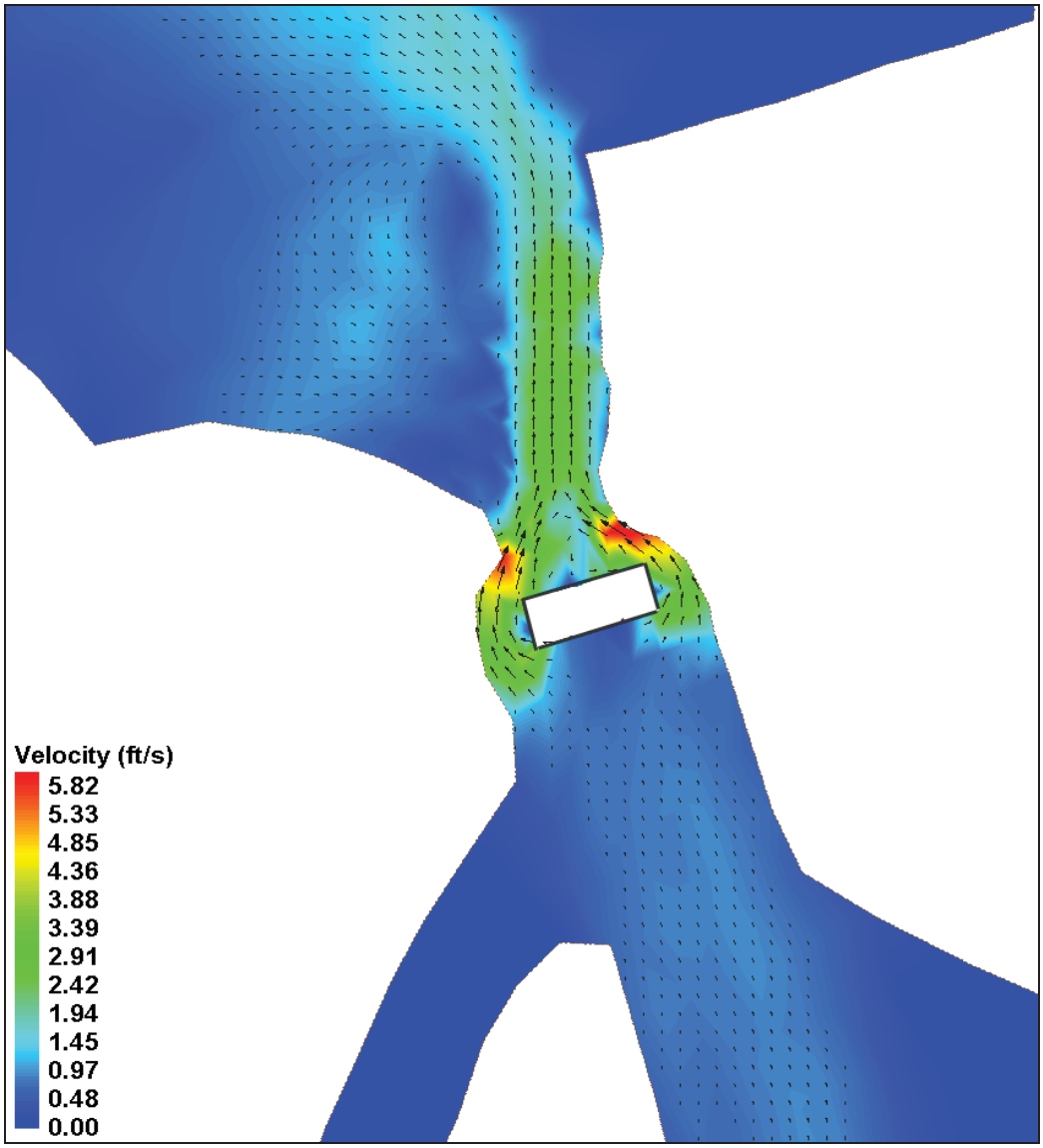

Figure A31. Velocity magnitude and direction at the cofferdam for a high flood flow in March (a single snapshot in time).

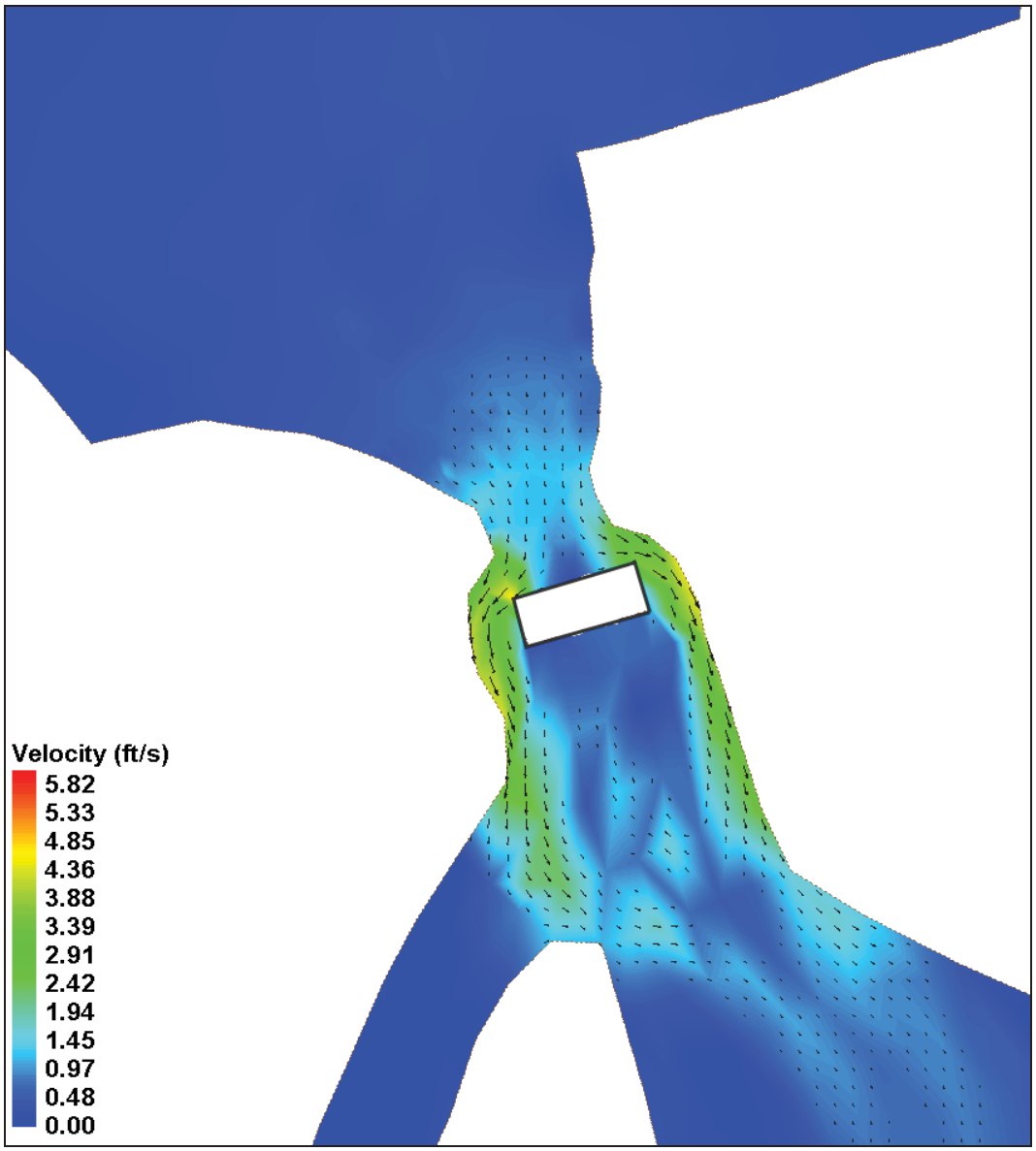

Figure A32. Velocity magnitude and direction at the cofferdam for a high ebb flow in March (a single snapshot in time).

Bridge Pier Sensitivity

A railroad bridge is stationed just north of the proposed location of the Seabrook structure. All previous simulations did not include the bridge piers, so a sensitivity run was made in which the bridge piers are included in the Plan 3 simulations. In this configuration, the Seabrook structure is 95 X 16 ft, the southern scour hole is filled to approximately -39 ft, and the bridge piers are included for the railroad bridge. Figure A-33 shows the geometry for the Seabrook section of the model domain with the bridge piers included. Figures A-34 through A-41 show the average and

maximum velocity magnitudes at various locations within the model domain for the Base and three original plan conditions as well as the condition including the bridge piers. The data locations are the same as those presented Figures A-1 and A-2. Figures A-42 and A-43 show a snapshot of the velocity magnitude and direction at a time when the flows are large for both an incoming and retreating tide event.

From these figures, it is evident that the bridge piers have little effect on the velocity magnitudes in this area. At Seabrook, the bridge piers seem to generate a very small decrease in the velocity magnitudes while at the other locations the effect of the piers may be a little higher or lower than the Plan 3 condition, but still very small.

Since this sensitivity was made using the original dimensions for the Seabrook structure, caution must be used when extrapolating these results to other structure dimensions. However, since the changes to the velocity magnitudes are very small at Seabrook (they actually drop slightly) the effect of the bridge piers will probably be even less with the wider structure because the wider structure has lower velocities in the Seabrook area than the original.

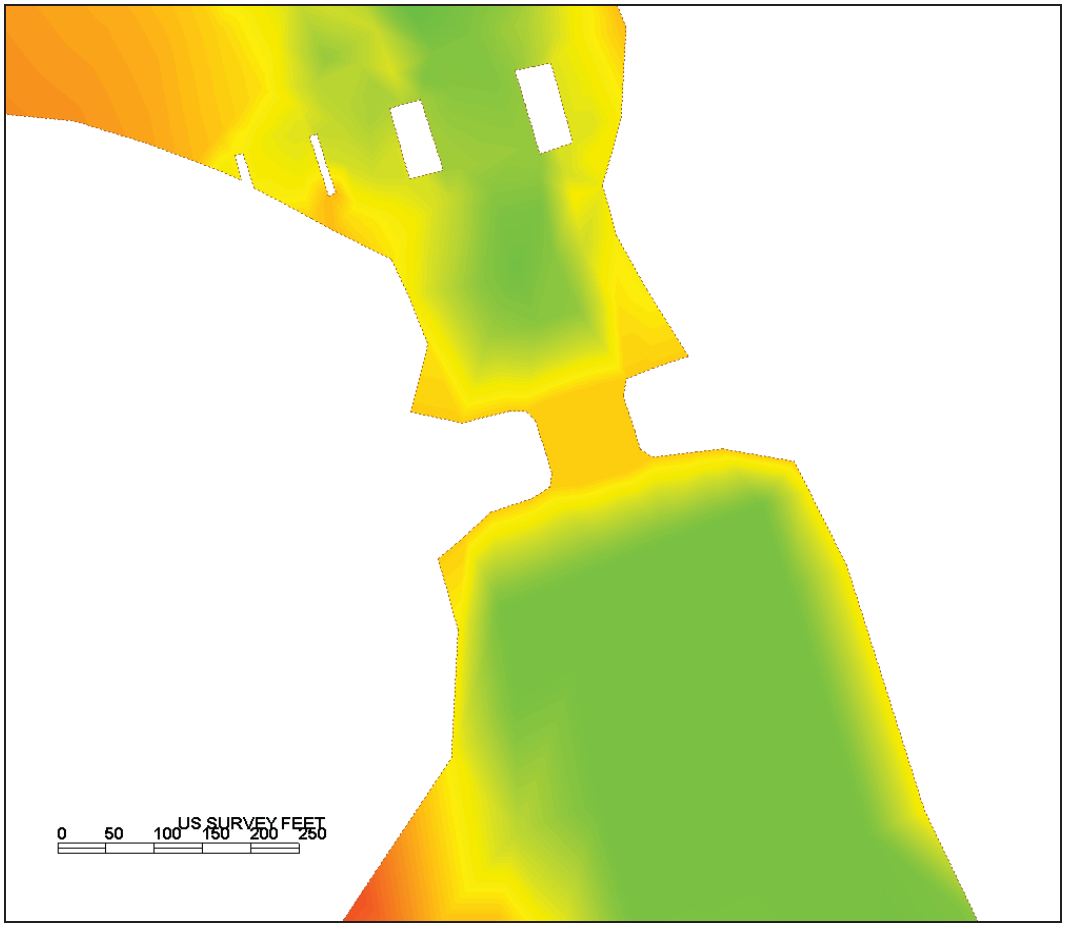

Figure A33. Plan 3 geometry configuration (95 X 16 ft Seabrook structure) with bridge piers (includes MRGO cut at La Loutre and the Borgne alignment).

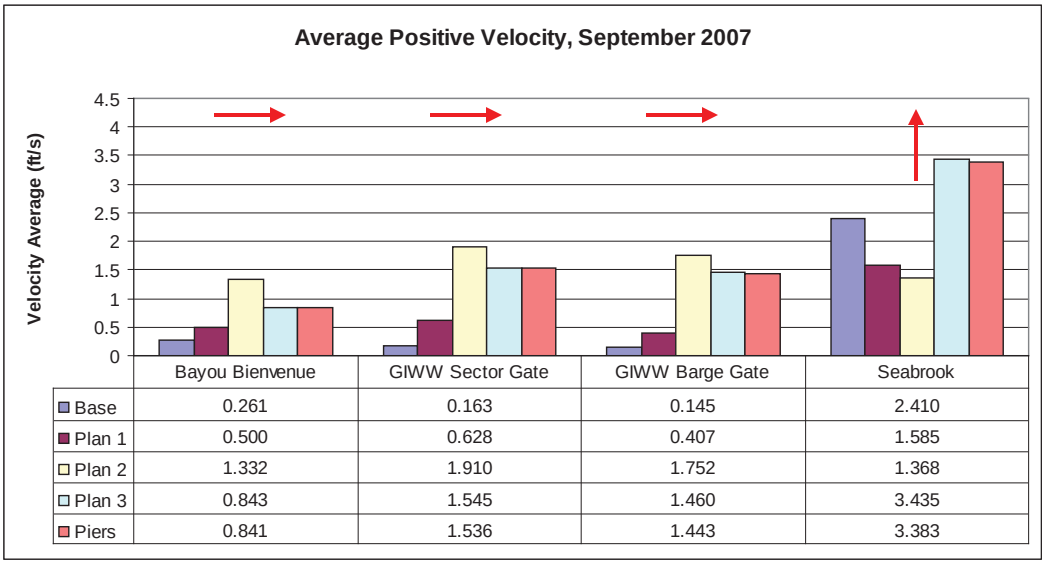

	Bayou Bienvenue	GIWW Sector Gate	GIWW Barge Gate	Seabrook
Base	0.261	0.163	0.145	2.410
Plan 1	0.500	0.628	0.407	1.585
Plan 2	1.332	1.910	1.752	1.368
Plan 3	0.843	1.545	1.460	3.435
Piers	0.841	1.536	1.443	3.383

Figure A34. Velocity average for September (positive).

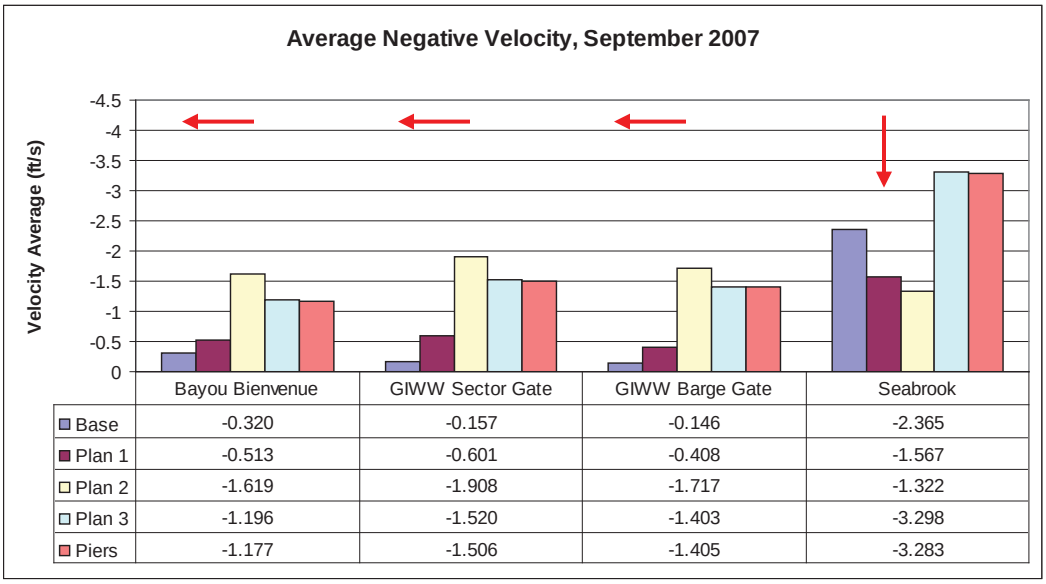

	Bayou Bienvenue	GIWW Sector Gate	GIWW Barge Gate	Seabrook
Base	-0.320	-0.157	-0.146	-2.365
Plan 1	-0.513	-0.601	-0.408	-1.567
Plan 2	-1.619	-1.908	-1.717	-1.322
Plan 3	-1.196	-1.520	-1.403	-3.298
Piers	-1.177	-1.506	-1.405	-3.283

Figure A35. Velocity average for September (negative).

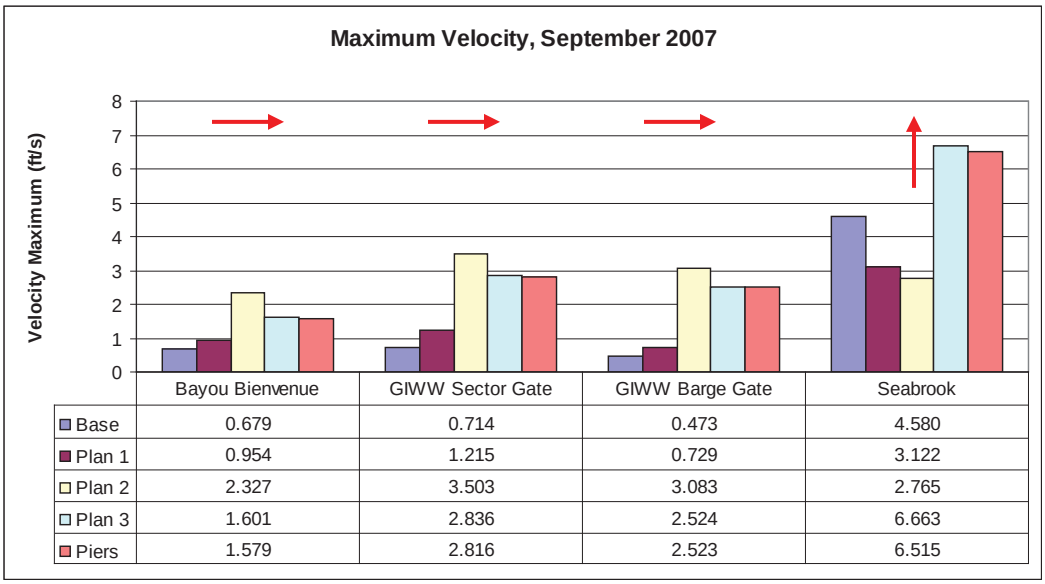

	Bayou Bienvenue	GIWW Sector Gate	GIWW Barge Gate	Seabrook
Base	0.679	0.714	0.473	4.580
Plan 1	0.954	1.215	0.729	3.122
Plan 2	2.327	3.503	3.083	2.765
Plan 3	1.601	2.836	2.524	6.663
Piers	1.579	2.816	2.523	6.515

Figure A36. Velocity maximum for September (positive).

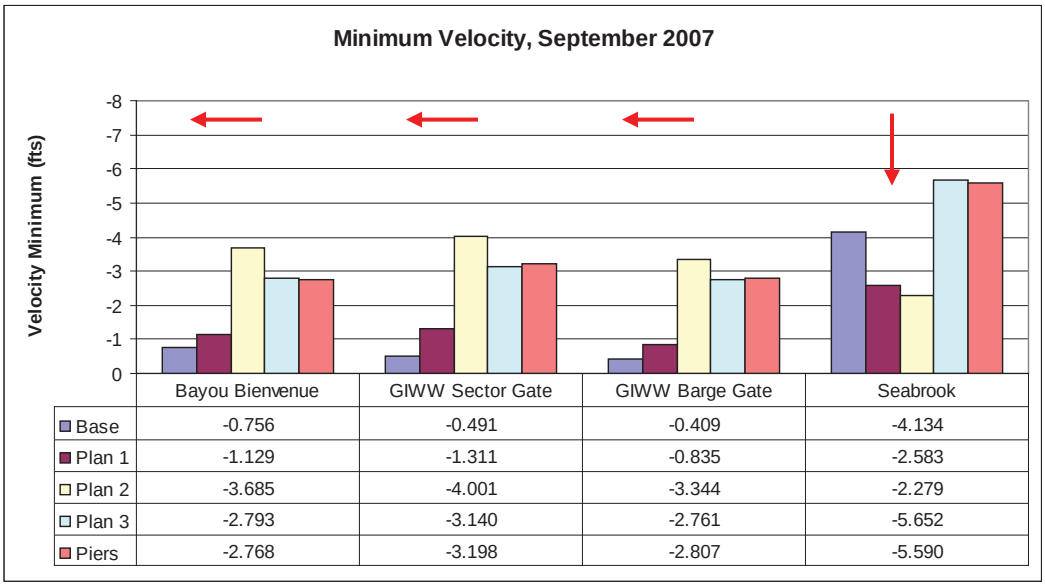

	Bayou Bienvenue	GIWW Sector Gate	GIWW Barge Gate	Seabrook
Base	-0.756	-0.491	-0.409	-4.134
Plan 1	-1.129	-1.311	-0.835	-2.583
Plan 2	-3.685	-4.001	-3.344	-2.279
Plan 3	-2.793	-3.140	-2.761	-5.652
Piers	-2.768	-3.198	-2.807	-5.590

Figure A37. Velocity minimum for September (negative).

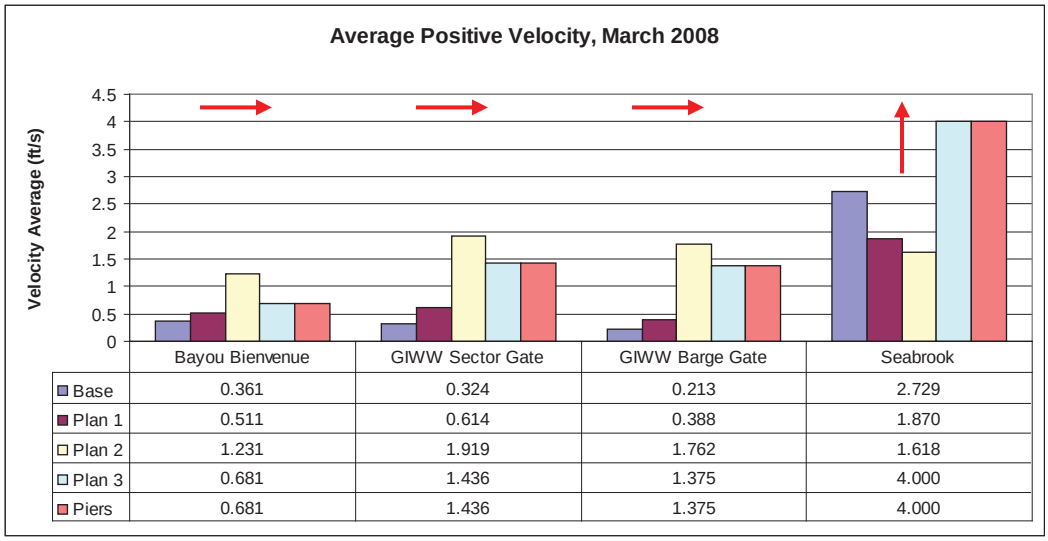

	Bayou Bienvenue	GIWW Sector Gate	GIWW Barge Gate	Seabrook
Base	0.361	0.324	0.213	2.729
Plan 1	0.511	0.614	0.388	1.870
Plan 2	1.231	1.919	1.762	1.618
Plan 3	0.681	1.436	1.375	4.000
Piers	0.681	1.436	1.375	4.000

Figure A38. Velocity average for March (positive).

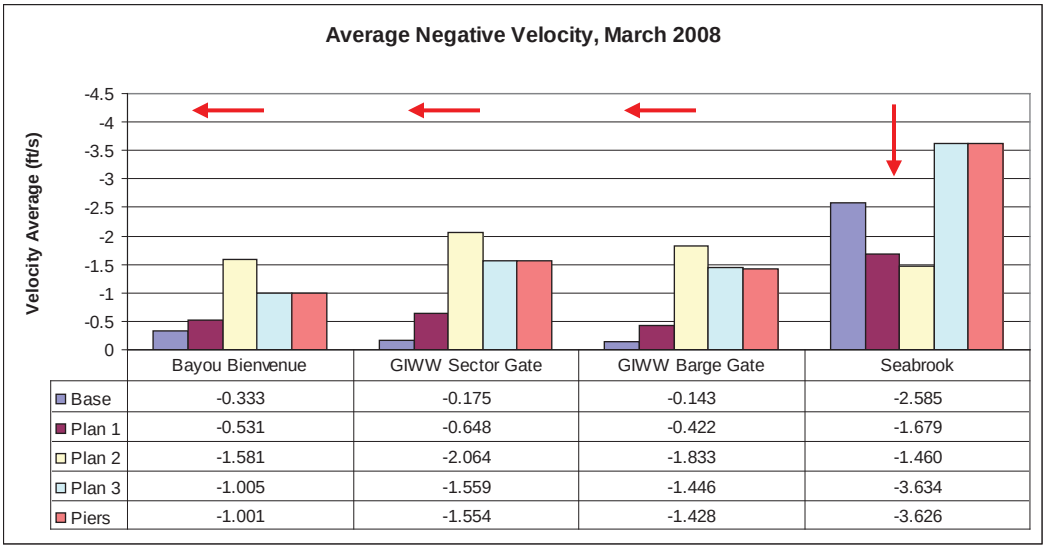

	Bayou Bienvenue	GIWW Sector Gate	GIWW Barge Gate	Seabrook
Base	-0.333	-0.175	-0.143	-2.585
Plan 1	-0.531	-0.648	-0.422	-1.679
Plan 2	-1.581	-2.064	-1.833	-1.460
Plan 3	-1.005	-1.559	-1.446	-3.634
Piers	-1.001	-1.554	-1.428	-3.626

Figure A39. Velocity average for March (negative).

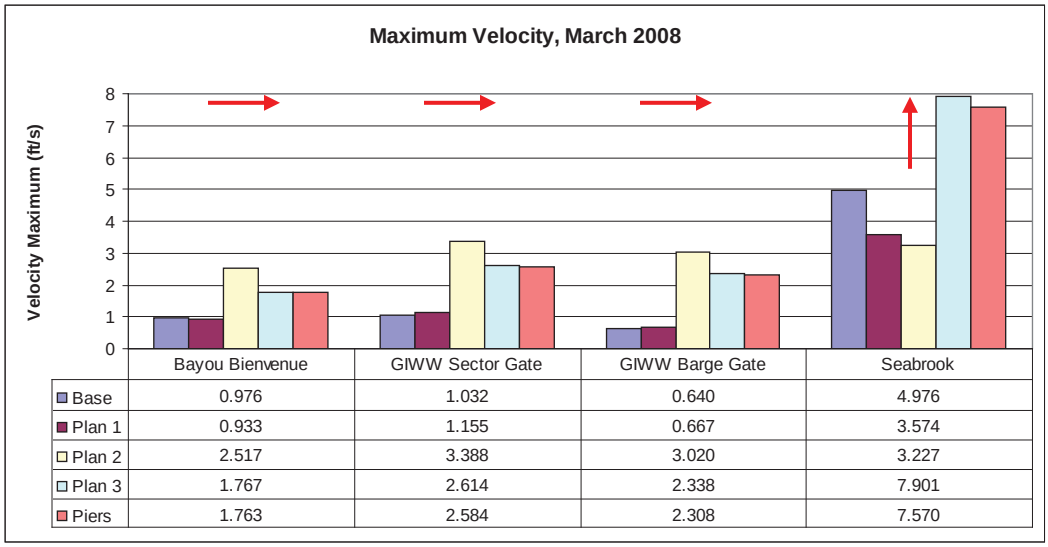

	Bayou Bienvenue	GIWW Sector Gate	GIWW Barge Gate	Seabrook
Base	0.976	1.032	0.640	4.976
Plan 1	0.933	1.155	0.667	3.574
Plan 2	2.517	3.388	3.020	3.227
Plan 3	1.767	2.614	2.338	7.901
Piers	1.763	2.584	2.308	7.570

Figure A40. Velocity maximum for March (positive).

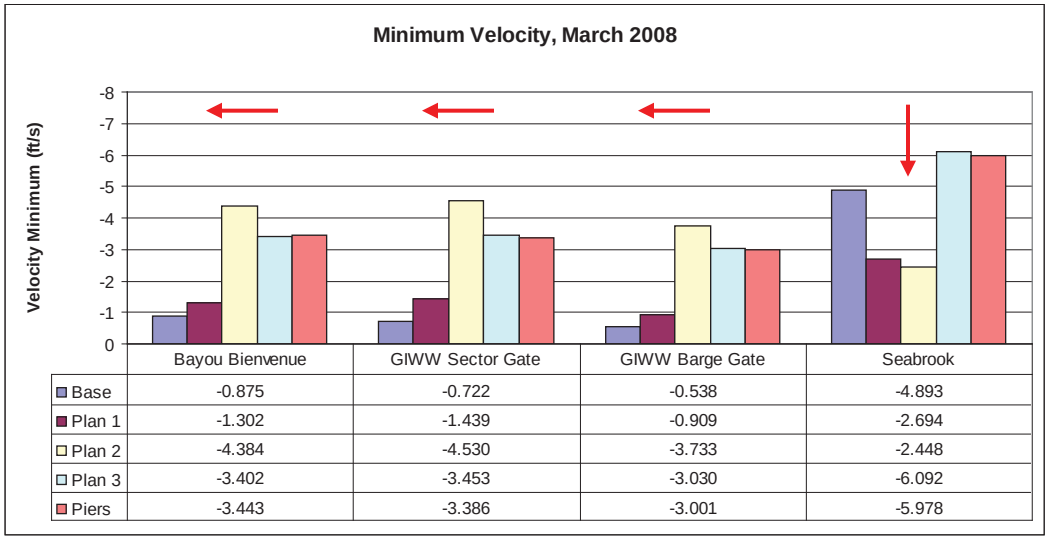

	Bayou Bienvenue	GIWW Sector Gate	GIWW Barge Gate	Seabrook
Base	-0.875	-0.722	-0.538	-4.893
Plan 1	-1.302	-1.439	-0.909	-2.694
Plan 2	-4.384	-4.530	-3.733	-2.448
Plan 3	-3.402	-3.453	-3.030	-6.092
Piers	-3.443	-3.386	-3.001	-5.978

Figure A41. Velocity minimum for March (negative).

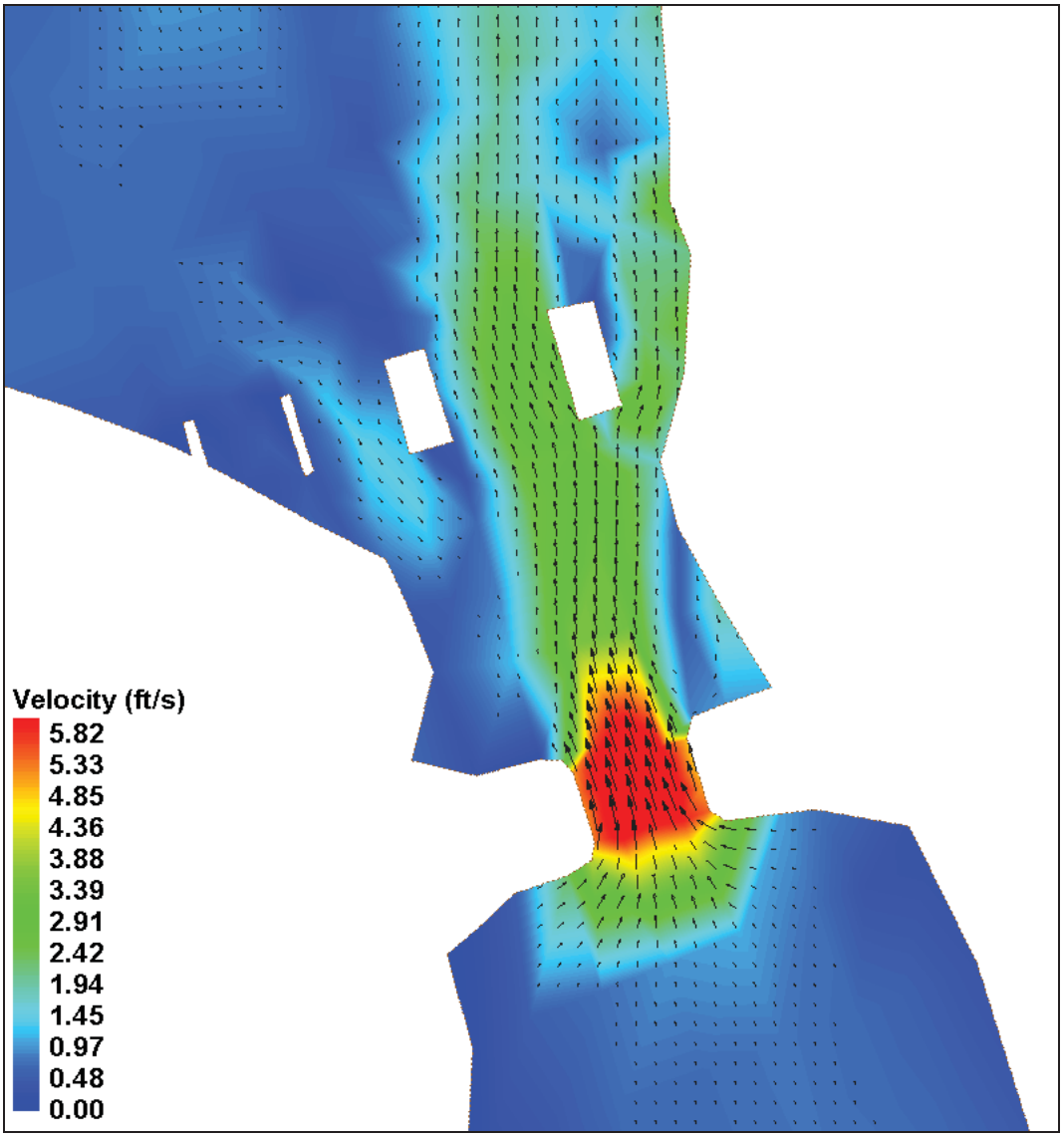

Figure A42. Velocity magnitude and direction with bridge piers for a high flood flow in March (a single snapshot in time).

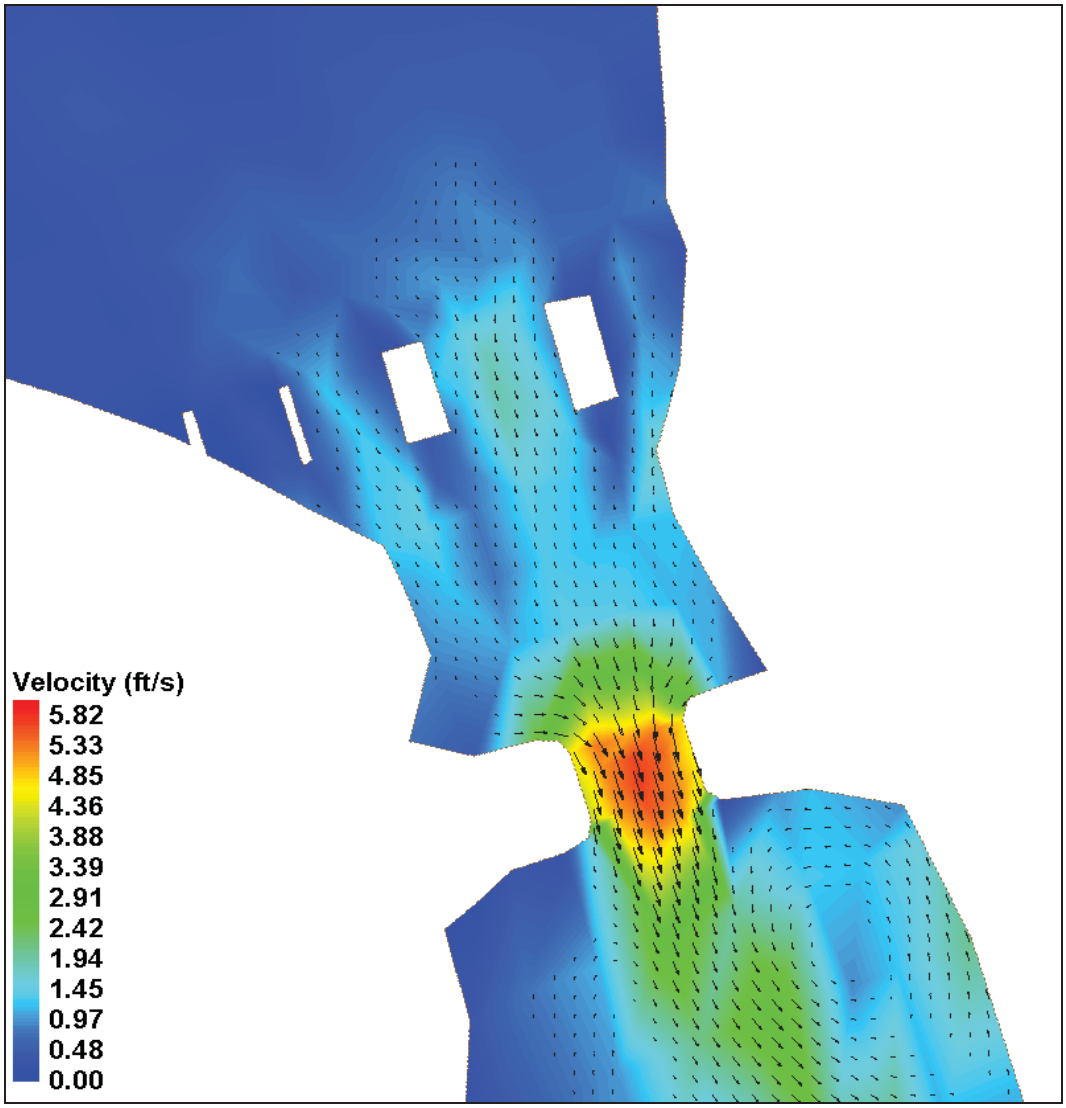

Figure A43. Velocity magnitude and direction with bridge piers for a high ebb flow in March (a single snapshot in time).

Appendix B: Description of the Adaptive Hydraulics Model (ADH)

Adaptive Hydraulics (ADH) is a state-of-the-art modeling system developed by the U.S. Army Corps of Engineers Research and Development Center Coastal and Hydraulics Laboratory. It is capable of simulating both saturated and unsaturated groundwater flow, overland flow, three-dimensional Navier-Stokes flow, and two- or three-dimensional shallow water problems. The current study utilizes the two-dimensional (2D) shallow water module. The 2D shallow-water equations used for this application are a result of the vertical integration of the equations of mass and momentum conservation for incompressible flow under the hydrostatic pressure assumption. Written in conservative form, the 2D shallow water equations are:

$$\frac{\partial U}{\partial t} + \frac{\partial \mathsf{F}}{\partial x} + \frac{\partial \mathsf{G}}{\partial y} + H = 0 \tag{1}$$

where

$$U = \begin{Bmatrix} h \\ uh \\ vh \end{Bmatrix} \tag{2}$$

$$\mathsf{F} = \begin{Bmatrix} uh \\ u^2 h + \frac{1}{2} g h^2 - h \dfrac{\sigma_{xx}}{p} \\ uvh - h \dfrac{\sigma_{yx}}{p} \end{Bmatrix} \tag{3}$$

$$\mathbf{G} = \begin{Bmatrix} vh \\ uvh - h\dfrac{\sigma_{xy}}{p} \\ v^2h + \frac{1}{2}gh^2 - h\dfrac{\sigma_{yy}}{p} \end{Bmatrix} \tag{4}$$

and

$$\mathbf{H} = \begin{Bmatrix} 0 \\ gh\dfrac{\partial z_b}{\partial x} + n^2 gh\dfrac{u\sqrt{u^2+v^2}}{C_0 h^{1/3}} \\ gh\dfrac{\partial z_b}{\partial y} + n^2 gh\dfrac{v\sqrt{u^2+v^2}}{C_0 h^{1/3}} \end{Bmatrix} \tag{5}$$

where:

ρ = fluid density
g = gravitational acceleration
z_b = riverbed elevation
n = Manning's roughness coefficient
h = flow depth
u = x-component of velocity
v = y-component of velocity
C_o = dimensional conversion coefficient (1 for SI units, 1.486 for U.S. customary units)
σ_{ij} = the Reynolds stresses due to turbulence, where the first subscript (i) indicates the direction, and the second (j)indicates the face on which the stress acts.

The Reynolds stresses are determined using the Boussinesq approach to the gradient in the mean currents.

$$\sigma_{xx} = 2p\upsilon_t \frac{\partial u}{\partial x} \tag{6}$$

$$\sigma_{yy} = 2p\upsilon_t \frac{\partial v}{\partial y} \tag{7}$$

and

$$\sigma_{xy} = \sigma_{yx} = 2p\upsilon_t \left(\frac{\partial u}{\partial y} + \frac{\partial v}{\partial x} \right) \tag{8}$$

where ν_t = kinematic eddy viscosity (which varies spatially).

The ADH shallow-water equations are placed in conservative form so that mass balance and the balance of momentum and pressure are identical across an interface. This is important to match the speed and height of a surge or hydraulic jump.

The equations are represented in a finite element approach. The quality of the numerical solution depends on the choice of the basis/trial function and the test function. The trial function determines how the variables are represented and the test function determines the manner in which the differential equation is enforced. In the Galerkin approach the test functions are chosen to be identical with the trial functions. When the flow is advection-dominated, the Galerkin approach produces oscillatory behavior. The Galerkin form of the test function cannot detect the presence of a node-to-node oscillation and so allows this spurious solution. The approach used in ADH is to enrich the standard Galerkin test function with an additional term that can detect and control this spurious solution.

The enriched Galerkin method used here, the Petrov-Galerkin method, is based on elemental constants for coefficients to stabilize these spurious oscillations. This reduces the stabilization to the nonconservative form. This is not a problem for mass or momentum conservation since the stabilization is only applied within the elements and uses the Galerkin test function to enforce “flux” balance across element edges.

For illustration of this technique, consider the shallow-water equations in nonconservative form

$$\frac{\partial u}{\partial t} + A\frac{\partial u}{\partial x} + B\frac{\partial u}{\partial y} + H = 0 \tag{9}$$

where $A = \frac{\partial F}{\partial U}$ and $B = \frac{\partial G}{\partial U}$. The trial functions (or interpolation/basis functions) are the Lagrange polynomials. These are piecewise linear functions that are continuous across element boundaries. Spatial derivatives, however, are not continuous across these element edges. Each of the dependent and independent variables is interpolated via these trial functions. For example,

$$\tilde{u}(x,y) = \sum_{j=1}^{N} u_j(x,y)\,\varphi_j \tag{10}$$

means that the approximate solution is made up of the product of the trial function for node j, ϕ_j, and the nodal value at that location, u_j. The test function is chosen as:

$$\varphi_i^* = \varphi_i I + a\left(\frac{\partial \varphi_i}{\partial x} A + \frac{\partial \varphi_i}{\partial y} B\right) \tag{11}$$

where,

$$a = 0.51\left[\bar{v} \bullet \bar{v} + gh + \left(\frac{l}{\Delta t}\right)^2\right]^{-1/2} \tag{12}$$

l = $(\Omega_e)^{1/2}$, the square of the element area
$\bar{v}$ = $(\bar{u}, \bar{v})$, the element average velocity components
Δt = time step size

The finite element statement becomes:

$$\int_{\Omega}\left(\varphi_i \frac{\partial U_l}{\partial t} - \frac{\partial \varphi_i}{\partial x} F_l - \frac{\partial \varphi_i}{\partial y} G_l + \varphi_i H_l\right) d\Omega +$$

$$\int_{\partial\Omega} \varphi_i \left\{F_l n_x + G_l n_y\right\} ds + \sum_e l_{\Omega e}\, a\left(\frac{\partial \varphi_i}{\partial x} A_l + \frac{\partial \varphi_i}{\partial y} B_l\right)$$

$$\left(\frac{\partial U_l}{\partial t} + A_l \frac{\partial U_l}{\partial x} + B_l \frac{\partial U_l}{\partial y} + H_l\right) = 0 \tag{13}$$

where, the subscript l indicates the finite element approximation. The Petrov-Galerkin contributions are integrated on the interior of the elements, but not across element edges. This contribution stabilizes the Galerkin approach. This scheme utilizes a single scaling factor α. This is different from the scheme reported in Berger and Stockstill (1995). That scheme involved scaling each eigenvalue, but that method does not converge using the iterative solver in ADH. Instead, a single value scaling (Equation 12) is used.

One of the major features of ADH is its ability to automatically adapt the mesh in areas where additional resolution is needed to properly resolve the hydrodynamics and then unresolved the area when the resolution is no longer needed. This feature thus answers the computational burden while allowing adequate resolution for a good simulation. This adaptation process is done by normalizing the results so that an error quantity is determined for each element. If this error exceeds the tolerance set by the user, then the element is refined. ADH contains other essential features such as wetting and drying, completely coupled sediment transport, conservative transport, such as salinity, and wind effects. A series of modularized libraries make it possible for ADH to include vessel movement, friction descriptions, varying turbulence closures and water quality and ecological modeling, among other features. ADH can run in parallel or on a single processor and runs on both Windows systems and UNIX based systems.

Appendix C: Description of the Particle Tracking Model Processes and Algorithms

PTM employs three modes of operation: two-dimensional, Quasi-3-dimensional, and three-dimensional (2D, Quasi-3D, and 3D). The differences in these three modes are determined by the algorithms that are utilized for the calculations. The 2D representation of particle motion is the simplest. It provides a preliminary assessment of particle motions and pathways. A 3D approach is required for applications where interaction with the native bed is significant, or where the vertical movement and settling of sediment particles are concerned. The Quasi-3D mode involves a combination of empirical particle transport functions and a 3D advection, settling, and dispersion routine to mimic some of the key 3D transport processes. The 3D mode performs more comprehensive 3D particle entrainment, deposition, and re-suspension routines, but takes longer computational time due to the requirement of smaller time-steps.

Using the example of sediment particle motion, the internal procedure for PTM follows four steps. First initial particle positions are determined for a time step. This is accomplished either by user source input or (after the first time-step) through output from the previous time-step. The code then goes through a series of mesh based Eulerian Calculations. At each time step of these calculations, framework calculations establish background data such as water depth, flow velocities, frictional information, native (bed) sediment characteristics. Flow velocities and water depths are provided by the particular hydrodynamic model associated with the system. Bed form calculations are performed to predict sub-grid scale bed forms over the domain. Shear and mobility calculations predict the influence of the flow field on the bed sediments over the domain. Transport calculations approximate the potential sediment transport fluxes over the domain and bed change calculations estimate the local instantaneous rates of erosion and deposition of bed materials (expressed as the time rate of bed change, dz/dt) using the potential transport fluxes. The frequency of updating shears, bedforms, and mobility are determined by the user.

Next, Lagrangian computations are performed for each particle. Because hydrodynamic data are most likely available less frequently than that required by Lagrangian calculations, values are interpolated in time. Flow

algorithms are performed which interpolate the local flow and wave conditions spatially at the particle's location. Mobility calculations determine the mobility of the particle and, if deposited, the likelihood of its entrainment in the flow using the flow and wave conditions at the particle's location. The trajectory integration determines the position of the particle at the end of the time-step using an advection-diffusion routine with consideration of settling, deposition, and erosion. Particle inertia is not considered. Particle positions are then checked for violation of boundary conditions. And finally, sediment traps are checked to determine if a particle's destination falls within a sediment trap. These newly calculated positions are the input for the next iteration.

PTM contains algorithms that appropriately represent initiation of motion, transport, settling, deposition, mixing, and resuspension processes in nearshore wave/current conditions. In the next two sections, we discuss the algorithms for both the mesh based Eulerian calculations and the Lagrangian particle transport calculations. As mentioned in the previous section, PTM operates in three different modes (2D, Quasi-3D, and 3D). For simplicity we discuss here only those algorithms which pertain to fully 3D calculations. More detailed information about the other two modes can be found in MacDonald et al (2006).

Eulerian Transport Calculations

Shear Stress

Shear stresses are a function of both the flow and sediment bed conditions. As they play a major role in many of the subsequent calculations, we will begin by describing the methods used to calculate these quantities. First it should be mentioned that there are actually four types of shear stresses calculated in PTM. They are the shear stress due to skin friction and the shear stress due to form drag for both current-induced and wave-induced stresses. In this document we will denote these variables as follows:

1. Current-induced shear stress due to skin friction, τ_c' .
2. Current-induced shear stress due to form drag, τ_c'' .
3. Wave-induced shear stress due to skin friction, τ_w' .
4. Wave-induced shear stress due to form drag, τ_w'' .

PTM implements methods described in van Rijn (1993) to calculate shear stress. The current-induced bed shear stress T_c (Pa) can be calculated from the depth-averaged velocity, $\overline{U}$, as:

$$T_c'' = \frac{\rho \overline{U}^2}{\left(C''\right)^2} \tag{1}$$

Here, ρ is the water density, and C'' is the dimensionless Chézy coefficient, which for rough turbulent flow is approximated by:

$$C'' = 2.5 \ln\left[11 \frac{h}{k_s''}\right] \tag{2}$$

where h = flow depth (m). For the current-induced shear stress due to form drag, τ_c'', the form roughness height, k_s'', is estimated using a combination of the bed form length and steepness. The bed shear velocity, u_* (m/sec), is computed from:

$$u_* = \sqrt{\frac{T_c''}{\rho}} = \frac{\overline{U}}{C''} \tag{3}$$

For rough turbulent flows, the bed shear velocity, u_* is dependent upon the flow depth, h, the characteristic roughness of the flow, k_s'' and $\overline{U}$:

$$u_* = \frac{\overline{U}}{2.5 \ln\left(11 \frac{h}{k_s''}\right)} \tag{4}$$

For the current-induced shear stress due to skin friction, τ_c', a roughness height, k_s' representative of the skin, or grain-size, roughness of the bed is used. In PTM, skin roughness is taken as three times the D_{90} of the bed material for erodible beds, where D_{90} is the grain size that 90 percent of the sediment is finer (by weight). The model interface can override this value with a user-specified value. It should also be noted that the calculations becomes more complicated in the case of combined wave and current flows. Details of these calculations can be found in the technical report (MacDonald et al. 2006).

Initiation of Motion

The initiation of motion for PTM particles located at the bed is dependent on the critical shear stress τ_{cr}. This value is utilized in the critical Shield's parameter. Defined by the Shield's curve, the dimensionless parameter θ (Sheild's parameter) gives the threshold of motion for particles at the bed (see Yalin (1977) for complete discussion).

$$\theta = \frac{\tau}{\rho g(s-1)D} \tag{5}$$

In this equation, D is the characteristic grain size, ρ is the density, g is the gravitational acceleration, and s is the relative density ratio of the particles. The value of θ at which the inception of sediment transport occurs is then called the critical Shield's parameter θ_{cr} and is given by:

$$\theta_{cr} = \frac{\tau_{cr}}{\rho g(s-1)D} \tag{6}$$

PTM uses a analytical representation of this equation based on later work performed by Soulsby and Whitehouse (1997) who developed a relationship based on the dimensionless grain size, D_{gr}.

$$D_{gr} = D_{50}\sqrt[3]{\frac{(s-1)g}{\nu^2}} \tag{7}$$

Here D_{50} is the grain size at which 50 percent of the sediment is finer (by weight) and ν is the kinematic viscosity of the fluid. The resulting new equation determined by Soulsby and Whites for θ_{cr} is:

$$\theta_{cr} = \frac{0.30}{1+1.2D_{gr}} + 0.55\left[1-e^{-0.020D_{gr}}\right] \tag{8}$$

Transport Mobility

The dimensionless mobility, M is the ratio of the skin shear stress acting on the bed, τ' to the critical shear stress, τ_{cr}, and is defined as:

$$M = \frac{T'}{T_{cr}} = \frac{\theta}{\theta_{cr}} \tag{9}$$

The critical shear, τ_{cr} (Pa), can be determined from:

$$\tau_{cr} = \theta_{cr} \rho (s-1) g D \tag{10}$$

The dimensionless transport parameter, T, is also commonly used to assess sediment mobility. It is defined as:

$$T = \frac{\tau' - \tau_{cr}}{\tau_{cr}} = M - 1 \tag{11}$$

From the known distributions of the native (bed surface) sediments and the flow conditions over the domain, the mobility of the bed sediments (and particles on the bed) may be determined.

Bedform Calculation

Estimating bed form geometry is necessary to calculate the shear stress due to form drag, τ'' and the overall flow resistance offered by the bed. The equilibrium dimensions of bed forms under waves and currents are computed using the technique of van Rijn (1984c) for currents and the technique of Mogridge et al. (1994) for combined current and wave conditions. Van Rijn's (1984c) bed form and roughness calculation methodology is as follows. The equilibrium bed form height, η_b is determined on the basis of mobility, flow depth, and grain size as follows:

$$\begin{aligned} n_b &= 0 && M \le 1 \\ n_b &= 0.11h\left(\frac{D_{50}}{h}\right)^{0.3}\left[1 - e^{-0.5(M-1)}\right](24 - M) && 1 < M \le 24 \\ nb &= 0 && M > 24 \end{aligned} \tag{12}$$

These are steady-state equations, predicting no bed forms for conditions where the mobility, M, is less than unity (no transport) and for high flow conditions where bed forms would be washed out ($M > 24$). Bed forms do not develop for very fine materials ($D_{50} < 0.05$ mm). In PTM, it is assumed that if $D_{50} < 0.05$ mm, bed roughness is defined solely by skin friction and is:

$$k_s' = 3D_{90} \tag{13}$$

The above equations compute the equilibrium bed form height. In nature, bed forms continually adjust to changing flow conditions. The rate of change of bed forms is related to the local bed load transport rate (van Rijn 1984a; Nielsen 1992). In PTM, a simple algorithm has been implemented to allow bed forms to gradually adjust from their present height to their new equilibrium height. The rate of change of bed form height is related to the overall transport rate. In this case, PTM uses the transport pickup rate, q_p (m/sec), to estimate the maximum temporal rate of change of the bed. At time t in a simulation, the bed form height, η, existing on the bed is compared to the equilibrium bed form height, η_b, from the predictive equations. If η is less than η_b, then the bed forms are growing; if η is greater than η_b, then the bed forms are decaying. The time rate of change of bed form height is then calculated as:

$$\begin{aligned} \frac{\partial \eta}{\partial t} &= -q_p \quad \eta > \eta_b \\ \frac{\partial \eta}{\partial t} &= q_p \quad \eta < \eta_b \end{aligned} \tag{14}$$

The bed form length is assumed to respond instantly to changes in flow conditions.

Potential Transport Rate

PTM requires potential transport rates over the model domain to compute gradients in transport to estimate the potential for erosion and deposition of the native bed materials. These rates are used to determine the likelihood of burial of a sediment particle once deposited. PTM offers a choice of two techniques, Soulsby-van Rijn (Soulsby 1997) and van Rijn (1993), for the potential total load transport rate under combined wave-current conditions.

Lagrangian Transport Calculations

Transport of particles in PTM is accomplished by three basic steps: 1) Particle location, 2) Particle interpolation, and 3) Particle integration. That is, first particle positions are located within the mesh. Then the Eulerian forcings are interpolated from the surrounding mesh to the particle

position. Finally, a new particle position is calculated by solving the basic equation

$$\frac{d\vec{X}}{dt} = \vec{V} \tag{15}$$

This simple differential equation states that the change in the position ($\vec{X}$) over time dt is equal to the velocity ($\vec{V}$). Therefore, the most basic solution to these equations determine that

$$\vec{X}^{n+1} = \vec{X}^{n} + \vec{V}dt \tag{16}$$

By thus solving this equation, the new particle position $\vec{X}^{n+1}$ can be calculated at each time t. The main difficulties come in calculating the value of $\vec{V}$ which is a function of several quantities that will describe later.

Particle Position Integration

The basic Euler scheme shown in equation 16 is the simplest algorithm to the above differential equation. The scheme is first order accurate and often requires very small time steps as flows become very complex or when dealing with intricate sediment transport such as near bed particle behavior. Therefore a more accurate method must be used to allow for greater accuracy and larger time steps. Testing focused on determining effects of accuracy and efficiency for the PTM integration scheme is currently being performed.

As a first step in this direction, PTM v1.0 utilizes a two step predicator corrector scheme. This scheme is by nature second order accurate. In step 1 of the scheme, the particle position is integrated one half time steps. Then in step 2 this value and the initial particle position are used to calculate the new particle position, $\vec{X}^{n+1}$. In the following equations $\vec{X}'$ is the half time step particle position and $\vec{V}'$ is the velocity of the particle at this time.

$$\text{STEP 1:} \quad \vec{X}' = \vec{X}_n + \frac{1}{2}(\vec{V}dt) \tag{17}$$

$$\text{STEP 2:} \quad \vec{X}^{n+1} = \vec{X}_n + (\vec{V}'dt) \tag{18}$$

Velocity Calculations

As seen in the previous section, the velocity calculations play an important role in determining the particle position at each time step. The particle velocity term V in the previous equations is actually a mixture of various forcing elements. To understand this better, first we separate the particle velocity into the horizontal (U) and vertical (W) components. Within these components we can further compartmentalize the velocity as follows:

In the horizontal directions:

$$U = U_A + U_D \tag{19}$$

where A indicates advective forcing and D indicates diffusion. In the vertical direction we get similar terms

$$W = W_A - W_S + W_D \tag{20}$$

The horizontal velocity of each particle is equal to the fluid velocity at the vertical elevation of the particle added to the velocity due to diffusion. The vertical velocity, however, is determined by the vertical velocity component of the fluid at the point z_p minus the settling velocity, W_s of the particle. The vertical velocity component due to advection from the flow W_A can be determined by an assumed velocity profile if the hydrodynamic input is two-dimensional or obtained exactly from three-dimensional hydrodynamic input. The particle fall velocity, W_S (m/sec), is defined as a function of the dimensionless grain size, D_{gr} and can be approximated by the following equations proposed by Soulsby (1997). They have been adapted for extremely fine grain sizes ($D_{gr} < 0.0672$) for PTM.

$$\frac{W_S D}{\nu} = \begin{cases} \sqrt{107.33 + 1.049 D_{gr}^3} - 10.36 & D_{gr} \geq 0.672 \\ 0.0077 D_{gr}^2 & D_{gr} < 0.672 \end{cases} \tag{21}$$

PTM uses a random walk diffusion model to calculate the velocity due to diffusion. The random walk representation of the horizontal dispersive velocity U_D is computed as:

$$U_D = 2(\Pi - 0.5)\sqrt{\frac{6E_t}{dt}} \tag{22}$$

where Π is a random number uniformly distributed between 0 and 1. Note that the horizontal dispersive velocities are isotropic. The vertical diffusion velocity is:

$$W_D = 2(\Pi - 0.5)\sqrt{\frac{6E_v}{dt}} \tag{23}$$

The turbulent diffusion coefficients in the previous equations are estimated as presented in Fischer et al. (1979) and as applied by Shen et al. (1993) amongst others. The turbulent diffusion coefficient, E_t is estimated to be:

$$E_t = K_{E_t} h u_*'' \tag{24}$$

The empirical coefficient K_{E_t} relates the turbulent diffusion to the local shear velocity and water depth. Typically, K_{E_t} ranges from 0.15 to 0.6. The variable u_*'' is the shear velocity associate with form drag only. Slight modifications have been made to this equation in PTM to account for enhanced mixing due to wave breaking. The vertical diffusion coefficient is modeled using a parabolic-shaped distribution,

$$E_v = M_b K_{E_t} U_x \left[\frac{z_p (h - z_p)^2}{h^3} \right] \tag{25}$$

where M_b is a wave breaking coefficient and h is the flow depth and z_p is the vertical particle location.

Particle-bed Interactions

This section describes the series of algorithms developed to simulate the behavior of particles near the bed. It includes a hiding and exposure function, frequency of entrainment calculations, as well as deposition and re-entrainment algorithms.

Hiding and Exposure Function

On a mixed bed with mean sediment size D_{50}, smaller particles hide behind larger particles and require a larger shear stress for the onset of mobility. Similarly, particles larger than D_{50} are more exposed and require a smaller shear stress for mobility. This is treated in PTM by means of a

hiding and exposure function (Egiazaroff 1965; Kleinhans and van Rijn 2002). The function is a correction factor, and it is applied to the critical shear stress for inception of motion as:

$$\dot{\theta}_{cr} = \xi \theta_{cr} \tag{26}$$

where ξ is a dimensionless hiding and exposure correction factor. The hiding and exposure function is given by (Egiazaroff 1965):

$$\xi = \frac{5}{3}\left[\log\left(19\frac{D}{D_{50}}\right)\right]^{-2} \tag{27}$$

This function is valid for $0.3 < D/D_{50} < 10$, and limits the particle's mobility threshold to be no greater than three times and no less than one-third of the critical Shields parameter of that particle. The hiding and exposure function is only applied to particles that are deposited on the bed.

Frequency of Entrainment

In nature, the behavior of a particle at the bed can be extremely complex. Particles deposit at the bed and can be re-entrained right away or can perhaps mix with the active sediment transport layer and then become entrained some time later. To include this interaction within PTM, a probabilistic approach is used. The frequency of entrainment of a particle from the bed is computed as a function of the potential transport rate for the particle. This is combined with other factors that account for the likelihood of mixing of the particle within an active transport layer and the likelihood of burial of the particle by ambient transport processes.

In PTM, particle entrainment is based on the mean shear stress, critical shear stress for erosion as defined by the Shields curve, and by the following five supplemental considerations:

1. The turbulent fluctuations in the instantaneous shear stress.
2. Modifications to the critical shear stress to account for hiding and exposure effects of graded sediment beds.
3. The transport pickup rate from the bed.
4. The ambient transport conditions on the bed (erosion/deposition), leading to an estimate of the depth of burial of the particle.

5. Mixing of the particles within the active transport layer, which is based on the thickness of the active transport layer.

The details of these calculations are lengthy and can be found in MacDonald et al 2006. Once calculated, these processes have then been implemented in a manner such that the frequency that a particle is picked up from the bed, f_e , is determined as:

$$f_e = K_{burial} K_{mixing} f_p \tag{28}$$

In this equation, f_p is the frequency of pickup based on the estimated particle transport pickup rate for the particle. K_{mixing} is a reduction factor to account for the fact that the particle may lie anywhere within the thickness of the active sediment transport layer at the particle location. K_{burial} is a reduction factor to account for the possible burial of the particle by ambient sediments. The units of f_e are sec^{-1} or Hz.

Particle Deposition and Re-entrainment

Particles are deposited on the bed once they pass below one-quarter of the skin roughness height, k_s'.

$$\text{if} \quad z_p \begin{cases} < \dfrac{k_s'}{4} & deposits \\ \geq \dfrac{k_s'}{4} & active \end{cases} \tag{29}$$

If a particle becomes deposited, it will cease to move until it is re-entrained. The frequency of entrainment, f_e, is computed considering the particle pickup rate, the mixing depth of native sediment in the active transport layer, and the likelihood of burial by native sediments.

The entrainment elevation is computed using a Rouse-type random number generator. This generator will produce random numbers that are distributed according to a Rouse sediment concentration profile for the specific sediment and flow conditions. As a result, the random numbers will be biased towards 0 (taken as the bed) rather than 1 (taken as the surface). The new elevation of a re-entrained particle is taken as:

$$z_p = \Psi h \tag{30}$$

where Ψ is a random number between 0 and 1 distributed according to a Rouse sediment concentration profile.

Boundary Conditions

PTM uses the land and open boundaries given in the mesh file. Particles may pass through an open boundary. If a particle passes through an open boundary, it ceases to be included in the computation. However, a particle may not pass through a land boundary. The particle will be placed alongside the boundary in question. If a particle is driven onto a dry point, it becomes stranded. Wetting and drying are included, if the original hydrodynamic model was run with this capability.

REPORT DOCUMENTATION PAGE

Form Approved
OMB No. 0704-0188

Public reporting burden for this collection of information is estimated to average 1 hour per response, including the time for reviewing instructions, searching existing data sources, gathering and maintaining the data needed, and completing and reviewing this collection of information. Send comments regarding this burden estimate or any other aspect of this collection of information, including suggestions for reducing this burden to Department of Defense, Washington Headquarters Services, Directorate for Information Operations and Reports (0704-0188), 1215 Jefferson Davis Highway, Suite 1204, Arlington, VA 22202-4302. Respondents should be aware that notwithstanding any other provision of law, no person shall be subject to any penalty for failing to comply with a collection of information if it does not display a currently valid OMB control number. **PLEASE DO NOT RETURN YOUR FORM TO THE ABOVE ADDRESS.**

1. REPORT DATE *(DD-MM-YYYY)*
December 2010

2. REPORT TYPE
Final report

3. DATES COVERED *(From - To)*

4. TITLE AND SUBTITLE
Seabrook Fish Larval Transport Study

5a. CONTRACT NUMBER

5b. GRANT NUMBER

5c. PROGRAM ELEMENT NUMBER

6. AUTHOR(S)
Jennifer N. Tate, Tahirih C. Lackey, and Tate O. McAlpin

5d. PROJECT NUMBER

5e. TASK NUMBER

5f. WORK UNIT NUMBER

7. PERFORMING ORGANIZATION NAME(S) AND ADDRESS(ES)
U.S. Army Engineer Research and Development Center
Coastal and Hydraulics Laboratory
3909 Halls Ferry Road
Vicksburg, MS 39180-6199

8. PERFORMING ORGANIZATION REPORT NUMBER
ERDC/CHL TR-10-12

9. SPONSORING / MONITORING AGENCY NAME(S) AND ADDRESS(ES)
U.S. Army Corps of Engineers
New Orleans District, Hurricane Protection Office
7400 Leake Ave., Rm 184
New Orleans, LA 70118

10. SPONSOR/MONITOR'S ACRONYM(S)

11. SPONSOR/MONITOR'S REPORT NUMBER(S)

12. DISTRIBUTION / AVAILABILITY STATEMENT
Approved for public release; distribution is unlimited.

13. SUPPLEMENTARY NOTES

14. ABSTRACT

The U.S. Army Engineer Hurricane Protection Office (HPO) requested that the USACE Engineer Research and Development Center (ERDC) perform a numerical modeling study for the purpose of analyzing the impacts of proposed hurricane and storm damage risk reduction system (HSDRRS) measures to be placed in the Gulf Intracoastal Waterway (GIWW) and the Mississippi River Gulf Outlet (MRGO) on the larval fish transport in the area. This study was requested in addition to separate navigation studies to analyze the impacts the protection measures have on the hydrodynamics and vessel traffic. It is known that larval fish migrate from the Gulf of Mexico into Lake Pontchartrain. A particle tracking simulation can be performed such that the particles are given basic larval fish transport behaviors and released at various locations in the area. The hydrodynamic processes move these particles within the system and the changes to the transport due to the planned changes to the system can be analyzed. The model is validated with field data from 2008 of water surface elevation, discharge, and velocity. Four plan simulations are modeled in addition to the base condition. Transport of particles within the system is dominated by the hydrodynamics of the system. The tidal intensity and regularity of the tidal signal are a main factor of transport. Particles released during stronger events may be recruited at a greater rate than a less intense flow condition. However that is additionally affected by the larval fish characteristic transport behaviors.

15. SUBJECT TERMS
Adaptive Hydraulics (AdH)
Hydrodynamic modeling
Inner Harbor Navigation Canal
Larval Fish Transport Modeling
New Orleans Hurricane Protection
Particle Tracking Model (PTM)
Seabrook

16. SECURITY CLASSIFICATION OF:			**17. LIMITATION OF ABSTRACT**	**18. NUMBER OF PAGES**	**19a. NAME OF RESPONSIBLE PERSON**
a. REPORT	**b. ABSTRACT**	**c. THIS PAGE**			**19b. TELEPHONE NUMBER** *(include area code)*
UNCLASSIFIED	UNCLASSIFIED	UNCLASSIFIED	UNLIMITED	220	

Standard Form 298 (Rev. 8-98)
Prescribed by ANSI Std. 239.18